frontiers | Research Topics

Synaptic plasticity and dysfunction, friend or foe?

Edited by
Fereshteh S. Nugent, Lu Chen and Ka Wan Li

Published in
Frontiers in Synaptic Neuroscience

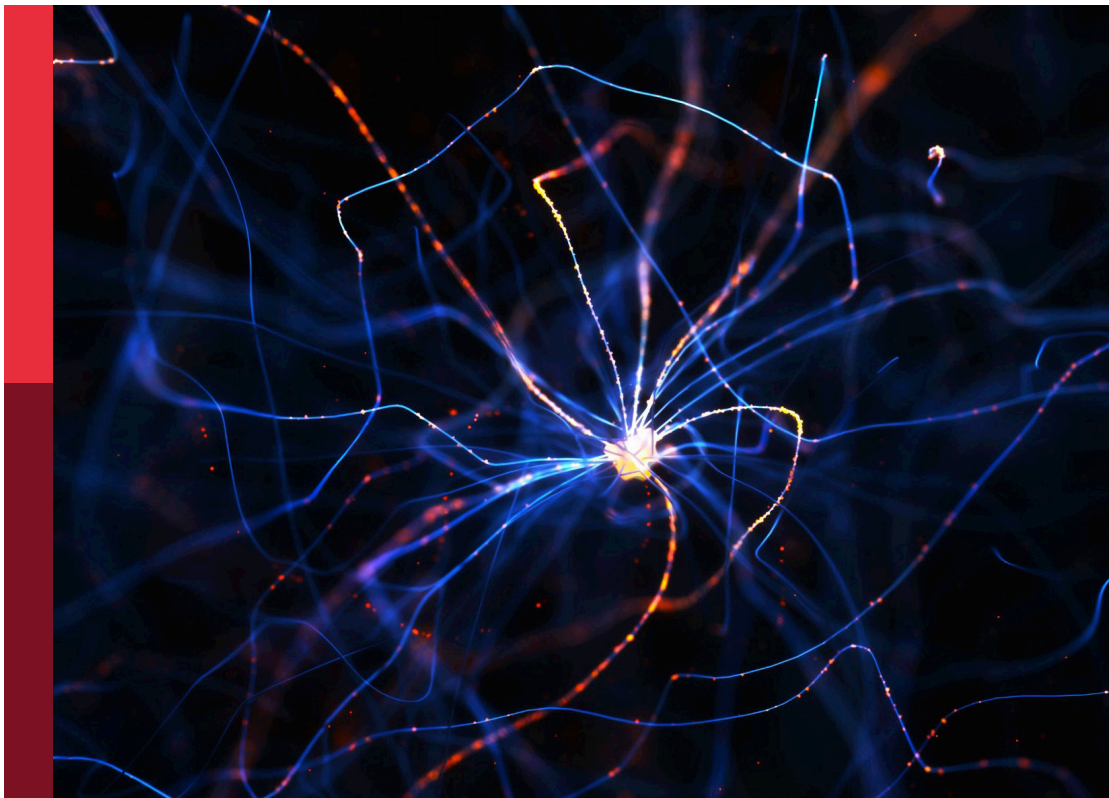

ISSN 1664-8714
ISBN 978-2-8325-2434-3
DOI 10.3389/978-2-8325-2434-3

About Frontiers

Frontiers is more than just an open access publisher of scholarly articles: it is a pioneering approach to the world of academia, radically improving the way scholarly research is managed. The grand vision of Frontiers is a world where all people have an equal opportunity to seek, share and generate knowledge. Frontiers provides immediate and permanent online open access to all its publications, but this alone is not enough to realize our grand goals.

Frontiers journal series

The Frontiers journal series is a multi-tier and interdisciplinary set of open-access, online journals, promising a paradigm shift from the current review, selection and dissemination processes in academic publishing. All Frontiers journals are driven by researchers for researchers; therefore, they constitute a service to the scholarly community. At the same time, the *Frontiers journal series* operates on a revolutionary invention, the tiered publishing system, initially addressing specific communities of scholars, and gradually climbing up to broader public understanding, thus serving the interests of the lay society, too.

Dedication to quality

Each Frontiers article is a landmark of the highest quality, thanks to genuinely collaborative interactions between authors and review editors, who include some of the world's best academicians. Research must be certified by peers before entering a stream of knowledge that may eventually reach the public - and shape society; therefore, Frontiers only applies the most rigorous and unbiased reviews. Frontiers revolutionizes research publishing by freely delivering the most outstanding research, evaluated with no bias from both the academic and social point of view. By applying the most advanced information technologies, Frontiers is catapulting scholarly publishing into a new generation.

What are Frontiers Research Topics?

Frontiers Research Topics are very popular trademarks of the *Frontiers journals series*: they are collections of at least ten articles, all centered on a particular subject. With their unique mix of varied contributions from Original Research to Review Articles, Frontiers Research Topics unify the most influential researchers, the latest key findings and historical advances in a hot research area.

Find out more on how to host your own Frontiers Research Topic or contribute to one as an author by contacting the Frontiers editorial office: frontiersin.org/about/contact

Synaptic plasticity and dysfunction, friend or foe?

Topic editors

Fereshteh S. Nugent — Uniformed Services University, United States

Lu Chen — Stanford University, United States

Ka Wan Li — VU Amsterdam, Netherlands

Citation

Nugent, F. S., Chen, L., Li, K. W., eds. (2023). *Synaptic plasticity and dysfunction, friend or foe?* Lausanne: Frontiers Media SA. doi: 10.3389/978-2-8325-2434-3

Table of contents

04 Editorial: Synaptic plasticity and dysfunction, friend or foe?
Fereshteh S. Nugent, Ka Wan Li and Lu Chen

08 Wnt Signaling Through Nitric Oxide Synthase Promotes the Formation of Multi-Innervated Spines
Faye McLeod, Kieran Boyle, Aude Marzo, Nuria Martin-Flores, Thaw Zin Moe, Ernest Palomer, Alasdair J. Gibb and Patricia C. Salinas

18 GluN2D NMDA Receptors Gate Fear Extinction Learning and Interneuron Plasticity
Christophe J. Dubois and Siqiong June Liu

33 Transsynaptic Long-Term Potentiation in the Hippocampus of Behaving Mice
Maria Teresa Romero-Barragán, Agnes Gruart and José M. Delgado-García

46 Protein phosphatase-1 inhibitor-2 promotes PP1γ positive regulation of synaptic transmission
Karl Foley, Haider Altimimi, Hailong Hou, Yu Zhang, Cody McKee, Makaía M. Papasergi-Scott, Hongtian Yang, Abigail Mayer, Nancy Ward, David M. MacLean, Angus C. Nairn, David Stellwagen and Houhui Xia

55 Metaplasticity framework for cross-modal synaptic plasticity in adults
Hey-Kyoung Lee

64 mGluR-dependent plasticity in rodent models of Alzheimer's disease
Gonzalo Valdivia, Alvaro O. Ardiles, Abimbola Idowu, Claudia Salazar, Hey-Kyoung Lee, Michela Gallagher, Adrian G. Palacios and Alfredo Kirkwood

72 The effect of single-cell knockout of Fragile X Messenger Ribonucleoprotein on synaptic structural plasticity
Marie Gredell, Ju Lu and Yi Zuo

83 Early life adversity impaired dorsal striatal synaptic transmission and behavioral adaptability to appropriate action selection in a sex-dependent manner
Gregory de Carvalho, Sheraz Khoja, Mulatwa T. Haile and Lulu Y. Chen

99 Inhibitory hippocampus-medial septum projection controls locomotion and exploratory behavior
Yuh-Tarng Chen, Rachel Arano, Jun Guo, Uzair Saleem, Ying Li and Wei Xu

frontiers | Frontiers in Synaptic Neuroscience

TYPE Editorial
PUBLISHED 03 May 2023
DOI 10.3389/fnsyn.2023.1204605

OPEN ACCESS

EDITED AND REVIEWED BY
P. Jesper Sjöström,
McGill University, Canada

*CORRESPONDENCE
Fereshteh S. Nugent
✉ fereshteh.nugent@usuhs.edu
Ka Wan Li
✉ k.w.li@vu.nl
Lu Chen
✉ luchen1@stanford.edu

RECEIVED 12 April 2023
ACCEPTED 17 April 2023
PUBLISHED 03 May 2023

CITATION
Nugent FS, Li KW and Chen L (2023) Editorial: Synaptic plasticity and dysfunction, friend or foe? *Front. Synaptic Neurosci.* 15:1204605. doi: 10.3389/fnsyn.2023.1204605

Editorial: Synaptic plasticity and dysfunction, friend or foe?

Fereshteh S. Nugent[1]*, Ka Wan Li[2]* and Lu Chen[3]*

[1]F. Edward Hebert School of Medicine, Uniformed Services University, Bethesda, MD, United States, [2]Department of Molecular and Cellular Neurobiology, Vrije Universiteit Amsterdam, Amsterdam, Netherlands, [3]Departments of Neurosurgery, Neuropsychiatry and Behavioral Sciences, Stanford University School of Medicine, Palo Alto, CA, United States

KEYWORDS

synaptic transmission, synaptic plasticity, early life adversity, long-term potentiation, long-term depression, metaplasticity, behavioral learning, Alzheimer's disease

Editorial on the Research Topic
Synaptic plasticity and dysfunction, friend or foe?

Introduction

Synaptic plasticity defined as the ability of neurons to modify their synaptic strength and connectivity as a function of activity, has long been postulated to mediate experience-dependent remodeling of neural circuits that ultimately underlies memory formation at various timescales. Since the discovery of hippocampal long-term potentiation (LTP), considerable progress has been made in our understanding of structural and mechanistic bases of different forms of synaptic plasticity that drive behavioral adaptation to the changing environment but also may confer our vulnerability or resilience to brain and behavioral pathology in response to adverse environmental factors, aging, and different types of trauma and insult across development (Südhof and Malenka, 2008; Nicoll, 2017; Li et al., 2019; Simmons et al., 2022). In this Research Topic, we highlight several conceptual advances in the field of synaptic plasticity that bridge the gaps between synaptic mechanisms underlying information processing in neuronal circuits of the healthy brain for normal behaviors. These articles provide insights into novel aspects of synaptic plasticity by linking newly identified molecular, synaptic and circuit correlates of synaptic structure, function, and behavioral learning. We also present two examples of dysregulation of synaptic plasticity as synaptic pathophysiological links to maladaptive circuit function that could underlie cognitive deficits and behavioral impairments related to psychiatric disorders using preclinical models of early life adversity and Alzheimer's disease.

Papers in this collection

Molecular signaling in synaptic structure and function

Our ability to adapt to the changing world replies largely on experience-dependent learning and memory formation, a process that requires synaptic plasticity. Synaptic plasticity is initiated by cascades of signal transduction, leading to synaptic structural reorganization and rearrangement of protein nano-machineries that changes synaptic efficacy and connectivity.

One of the main cellular mechanisms that control synaptic efficacy is the dynamic regulation of synaptic protein phosphorylation status by kinases and phosphatases (Feng and Zhang, 2009). Protein phosphatase-1 (PP1) is implicated in the changes of glutamatergic synapse activity and actin reorganization in dendritic spines, both of which are linked to the processes of neuroplasticity. The action of PP1 is regulated by a number of interactors, including neurabin (Munton et al., 2004). Foley et al. described an interesting finding that Inhibitor-2 positively regulates PP1 function in synaptic transmission, which is dictated by the threonine-72 phosphorylation on Inhibitor-2. Furthermore, using Förster resonance energy transfer /Fluorescence lifetime imaging microscopy studies, it was demonstrated that Inhibitor-2 enhances PP1γ interaction with its major synaptic scaffold, neurabin.

Structural plasticity of synapses correlates with changes in synaptic strength. For example, activation of NMDA receptors results in long-term enhancement of both dendritic spine size and synaptic strength (Herring and Nicoll, 2016). McLeod et al. here provide interesting evidence demonstrating that Wnt signaling promotes multi-innervated spines formation through neuronal nitric oxide synthase (nNOS)/NO/ soluble guanylate cyclase (sGC) signaling, leading to enhanced frequency and amplitude of excitatory postsynaptic currents. This finding provides an additional structural plasticity mechanism underlying LTP expression.

Dysfunction in synaptic proteins may lead to impairments in synaptic transmission or plasticity, thus impacting cognitive functions through altered neuronal circuit functions. Fragile X Syndrome (FXS) is a form of inherited intellectual disability caused by the loss-of-function mutations in the FMR1 gene. Key synaptic phenotypes in the FXS include exaggerated long-term synaptic depression (LTD) and impaired homeostatic synaptic plasticity, as well as altered spine density and morphology (Huber et al., 2002; Klemmer et al., 2011; Zhang et al., 2018). Gredell et al. showed that selective deletion of FMRP in a sparse subset of cortical layer 5 pyramidal neurons leads to altered structural dynamics of dendritic spines. Interestingly, although FMRP may operate cell-autonomously in this context during adolescence, additional non-cell-autonomous factors might also be involved in the regulation of synaptic phenotype in adults.

Synaptic and circuit mechanisms underlying behavioral learning

The study by Romero-Barragán et al., examined the development of long-term synaptic plasticity at multiple hippocampal synaptic loci in response to high-frequency perforated path (PP) stimulation in the intact brain of behaving animals. They made the interesting observation that LTP can be induced not only at the ipsilateral PP-CA3 synapses where the presynaptic input received direct stimulation, but also at secondary downstream synapses such as CA3 to contralateral CA1 synapses, thus corroborating previous reports demonstrating polysynaptic "propagation" of LTP at synapses directly downstream of the stimulated ones (Buzsaki, 1988; Krug et al., 2001; Stepan et al., 2012; Taylor et al., 2016). Although the exact mechanism driving polysynaptic LTP induction is yet to be worked out, these studies provide an interesting perspective for studies investigating memory engram formation during behavioral learning.

In addition to LTP of excitatory synapses, inhibitory synaptic connections and their modification are known to be an integral component of circuit remodeling during behavioral learning. For example, in this collection of papers, Chen et al. showed that the inhibitory projections from the hippocampus to the medial septum bidirectionally control the speed of locomotion in mice, thus directly impacting exploratory behavior in mice. This unexpected role of hippocampal inhibitory output adds to the complexity of the hippocampus in cognitive functions.

Beyond the hippocampus, fear conditioning has been shown to induce long-term synaptic changes at both excitatory and inhibitory synapses in multiple brain regions, including the cerebellar cortex (Sacchetti et al., 2004; Scelfo et al., 2008). The study by Dubois and Liu investigated the inhibitory synapse function in the cerebellar cortex in the context of fear memory extinction. They showed that the enhanced spontaneous GABA release from cerebellar molecular layer interneurons after fear condition can be reversed by fear extinction, and that this reversal of learning-induced inhibitory synapse plasticity requires the GluN2D NMDA receptors. It is of note that the fear learning-induced enhancement of GABA release is not affected by GluN2D deletion, suggesting that different signaling pathways are at play in the induction and reversal processes of this form of synaptic plasticity. Reversal of long-term changes at excitatory synapse that occur during fear memory formation has been attributed to fear extinction [e.g., spine elimination and regrowth in the frontal association cortex during fear learning and extinction (Lai et al., 2012)]. Results from the study by Dubois and Liu further demonstrates the significance of inhibitory synapses plasticity in behavioral learning.

The developing and adult primary cortical areas are able to exhibit a form of widespread plasticity; i.e., cross-modal plasticity, that is triggered by the deprivation of input in one sensory modality (for example, deafness or blindness). The cross-modal plasticity increases the capabilities and performance of spared modalities in the affected individual that is dependent on the remaining senses in their everyday life (Bavelier and Neville, 2002; Ewall et al., 2021). In a mini review appearing in this collection, Lee describes the two components of adult cross-modal plasticity when a sensory loss results in cross-modal recruitment of the deprived primary sensory area for processing of the remaining senses as well as inducing a compensatory plasticity within the spared primary sensory cortices to enhance and refine the spared senses. She proposes the sliding threshold metaplasticity model as the mechanism that can account for synaptic plasticity related to both cross-modal recruitment and compensatory plasticity.

Developmental-and aging-related synaptic dysfunction

Converging evidence from human and preclinical studies of early life stress/adversity (ELS/ELA) suggest that exposure to severe stress and adverse experiences during sensitive early developmental

periods confer considerable risk for vulnerability to substance use disorder, depressive and anxiety phenotypes by triggering/altering synaptic plasticity in brain regions and neural circuits that are critical for cognitive functioning, mood regulation and motivated behavior (Lippard and Nemeroff, 2020; Simmons et al., 2022; Spadoni et al., 2022). In this collection, de Carvalho et al. used the limited bedding and nesting (LBN) model of ELA, which causes fragmented and unpredictable maternal care and neglect of pups (Molet et al., 2016). They found that LBN induced behavioral inflexibility in a reversal learning paradigm in both sexes, whereas LBN impaired goal-directed action strategies in male but not female mice. They also found sex-specific differences in the effects of LBN on synaptic transmission from cortical inputs to the dorsomedial or dorsolateral striatum ((DMS/DLS) where glutamatergic transmission was reduced in both DMS and DLS of male LBN mice while corticostriatal synaptic transmission was only affected in DMS of female LBN mice. Overall, this study provides sexually dimorphic synaptic and circuit mechanisms within the dorsal striatum with implications in ELA-induced impairments in goal directed behaviors.

Hippocampal LTP and LTD at Schaffer collateral-CA1 synapses can be elicited by activation of either NMDA or metabotropic glutamate (mGluR5) receptor activation (Palmer et al., 1997; Popkirov and Manahan-Vaughan, 2011; Wang et al., 2016). While the role of NMDA receptor-dependent hippocampal plasticity have been extensively studied for age- and Alzheimer's disease (AD)-related decline in cognitive functioning and learning and memory, less is known about the involvement of mGluR5-dependent hippocampal plasticity in this context. In this collection, Valdivia et al. used the APP/PS1 mouse model of AD (Lok et al., 2013) and the Chilean rodent model of natural AD (Octodon degus) (Tan et al., 2022) and found that while mGluR5-dependent plasticity was intact in young animals, it was lost with parallel cognitive deficits as animals aged. Given the conflicting result of a recent study demonstrating the potentiation of mGluR LTD in the APP/PS1 mouse model (Privitera et al., 2022), validation of loss of mGluR LTD in aging APP/PS1 mice and Octodon degus in this study is of interest for future investigations using preclinical AD models that exhibit natural age-related neurodegenerative processes common to the AD such as in Octodon degus AD model.

Concluding remarks

The collection in this Research Topic serves as a vignette of the current efforts in the field of synaptic plasticity. These discoveries will continue to deepen our understanding of normal and pathological synaptic plasticity and we hope they fuel enthusiasm for future synaptic-based research on causal mechanistic links between structural and functional synaptic plasticity within brain circuits and networks influencing learning, reward and motivated behaviors in health and disease.

Author contributions

FN, KL, and LC equally contributed to writing the article and approved the submitted version. All authors contributed to the article and approved the submitted version.

Funding

FN was supported by the National Institutes of Health (NIH)—National Institute of Neurological Disorders and Stroke (NIH/NINDS) Grant#R21 NS120628 and LC by the NIH/NINDS Grant#NS11566001.

Conflict of interest

The authors declare that the research was conducted in the absence of any commercial or financial relationships that could be construed as a potential conflict of interest.

The handling editor PS declared a past collaboration (https://doi.org/10.3389/fnsyn.2022.1043480) with the author FN.

Publisher's note

Author disclaimer

The opinions and assertions contained herein are the private opinions of the authors and are not to be construed as official or reflecting the views of the Uniformed Services University of the Health Sciences or the Department of Defense or the Government of the United States.

References

Bavelier, D., and Neville, H. J. (2002). Cross-modal plasticity: where and how? *Nature Rev. Nurosci.* 3, 443–52. doi: 10.1038/nrn848

Buzsaki, G. (1988). Polysynaptic long-term potentiation: a physiological role of the perforant path-CA3/CA1 pyramidal cell synapse. *Brain Res.* 455, 192–5. doi: 10.1016/0006-8993(88)90133-3

Ewall, G., Parkins, S., Lin, A., Jaoui, Y., and Lee, H. K. (2021). Cortical and subcortical circuits for cross-modal plasticity induced by

loss of vision. *Front. Neural. Circuits*. 15, 665009. doi: 10.3389/fncir.2021.665009

Feng, W., and Zhang, M. (2009). Organization and dynamics of PDZ-domain-related supramodules in the postsynaptic density. *Nat. Rev. Neurosci*. 10, 87–99. doi: 10.1038/nrn254

Herring, B. E., and Nicoll, R. A. (2016). Long-term potentiation: from CaMKII to AMPA receptor trafficking. *Annu. Rev. Physiol*. 78, 351–65. doi: 10.1146/annurev-physiol-021014-071753

Huber, K. M., Gallagher, S. M., Warren, S. T., and Bear, M. F. (2002). Altered synaptic plasticity in a mouse model of fragile X mental retardation. *Proc. Nat. Acad. Sci*. 99, 7746–50. doi: 10.1073/pnas.122205699

Klemmer, P., Meredith, R. M., Holmgren, C. D., Klychnikov, O. I., Stahl-Zeng, J., Loos, M., et al. (2011). Proteomics, ultrastructure, and physiology of hippocampal synapses in a fragile X syndrome mouse model reveal presynaptic phenotype. *J. Biol. Chem*. 286, 25495–504. doi: 10.1074/jbc.M110.210260

Krug, M., Brödemann, R., Matthies, R., Rüthrich, H., and Wagner, M. (2001). Activation of the dentate gyrus by stimulation of the contralateral perforant pathway: evoked potentials and long-term potentiation after ipsi-and contralateral induction. *Hippocampus*. 11, 157–67. doi: 10.1002/hipo.1033

Lai, C. S., Franke, T. F., and Gan, W. B. (2012). Opposite effects of fear conditioning and extinction on dendritic spine remodelling. *Nature* 483, 87–91. doi: 10.1038/nature10792

Li, J., Park, E., Zhong, L. R., and Chen, L. (2019). Homeostatic synaptic plasticity as a metaplasticity mechanism—A molecular and cellular perspective. *Curr Opin. Eurobiol*. 54, 44–53. doi: 10.1016/j.conb.08010

Lippard, E. T., and Nemeroff, C. B. (2020). The devastating clinical consequences of child abuse and neglect: increased disease vulnerability and poor treatment response in mood disorders. *Am. J. Psychiatry*. 177, 20–36. doi: 10.1176/appi.ajp.2019.19010020

Lok, K., Zhao, H., Shen, H., Wang, Z., Gao, X., Zhao, W., et al. (2013). Characterization of the APP/PS1 mouse model of Alzheimer's disease in senescence accelerated background. *Neurosci. Lett*. 557, 84–9. doi: 10.1016/j.neulet.10051

Molet, J., Heins, K., Zhuo, X., Mei, Y. T., Regev, L., Baram, T. Z., et al. (2016). Fragmentation and high entropy of neonatal experience predict adolescent emotional outcome. *Transl. Psychiatry*. 6, e702. doi: 10.1038/tp.2015.200

Munton, R. P., Vizi, S., and Mansuy, I. M. (2004). The role of protein phosphatase-1 in the modulation of synaptic and structural plasticity. *FEBS. Lett*. 567, 121–8. doi: 10.1016/j.febslet.0321

Nicoll, R. A. (2017). A brief history of long-term potentiation. *Neuron*. 93, 281–90. doi: 10.1016/j.neuron.2016.12.015

Palmer, M. J., Irving, A. J., Seabrook, G. R., Jane, D. E., and Collingridge, G. L. (1997). The group I mGlu receptor agonist DHPG induces a novel form of LTD in the CA1 region of the hippocampus. *Neuropharmacology* 36, 1517–32. doi: 10.1016/S0028-3908(97)00181-0

Popkirov, S. G., and Manahan-Vaughan, D. (2011). Involvement of the metabotropic glutamate receptor mGluR5 in NMDA receptor-dependent, learning-facilitated long-term depression in CA1 synapses. *Cereb. Cortex*. 21, 501–9. doi: 10.1093/cercor/bhq093

Privitera, L., Hogg, E. L., Lopes, M., Domingos, L. B., Gaestel, M., Müller, J., et al. (2022). The MK2 cascade mediates transient alteration in mGlu R-LTD and spatial learning in a murine model of Alzheimer's disease. *Aging Cell*. 21, e13717. doi: 10.1111/acel.13717

Sacchetti, B., Scelfo, B., Tempia, F., and Strata, P. (2004). Long-term synaptic changes induced in the cerebellar cortex by fear conditioning. *Neuron*. 42, 973–82. doi: 10.1016/j.neuron.05012

Scelfo, B., Sacchetti, B., and Strata, P. (2008). Learning-related long-term potentiation of inhibitory synapses in the cerebellar cortex. *Proc. Nat. Acad. Sci*. 105, 769–74. doi: 10.1073/pnas.0706342105

Simmons, S. C., Grecco, G. G., Atwood, B. K., and Nugent, F. S. (2022). Effects of prenatal opioid exposure on synaptic adaptations and behaviors across development. *Neuropharmacology*. 2, 109312. doi: 10.1016/j.neuropharm.2022.109312

Spadoni, A. D., Vinograd, M., Cuccurazzu, B., Torres, K., Glynn, L. M., Davis, E. P., et al. (2022). Contribution of early-life unpredictability to neuropsychiatric symptom patterns in adulthood. *Depress. Anxiety*. 39, 706–17. doi: 10.1002/da.23277

Stepan, J., Dine, J., Fenzl, T., Polta, S. A., von Wolff, G., Wotjak, C. T., et al. (2012). Entorhinal theta-frequency input to the dentate gyrus trisynaptically evokes hippocampal CA1LTP. *Front. Neural. Circ*. 6, 64. doi: 10.3389/fncir.2012.00064

Südhof, T. C., and Malenka, R. C. (2008). Understanding synapses: past, present, and future. *Neuron*. 60, 469–76. doi: 10.1016/j.neuron.10011

Tan, Z., Garduño, B. M., Aburto, P. F., Chen, L., Ha, N., Cogram, P., et al. (2022). Cognitively impaired aged Octodon degus recapitulate major neuropathological features of sporadic Alzheimer's disease. *Acta. Neuropathol. Commun*. 10, 182. doi: 10.1186/s40478-022-01481-x

Taylor, C. J., Ohline, S. M., Moss, T., Ulrich, K., and Abraham, W. C. (2016). The persistence of long-term potentiation in the projection from ventral hippocampus to medial prefrontal cortex in awake rats. *Eur. J. Neurosci*. 43, 811–22. doi: 10.1111/ejn.13167

Wang, H., Ardiles, A. O., Yang, S., Tran, T., Posada-Duque, R., Valdivia, G., et al. (2016). Metabotropic glutamate receptors induce a form of LTP controlled by translation and arc signaling in the hippocampus. *J. Neurosci*. 36, 1723–9. doi: 10.1523/JNEUROSCI.0878-15.2016

Zhang, Z., Marro, S. G., Zhang, Y., Arendt, K. L., Patzke, C., Zhou, B., et al. (2018). The fragile X mutation impairs homeostatic plasticity in human neurons by blocking synaptic retinoic acid signaling. *Sci. Translat. Med*. 10, eaar4338. doi: 10.1126./scitranslmed.aar4338

frontiers in Synaptic Neuroscience

BRIEF RESEARCH REPORT
published: 04 September 2020
doi: 10.3389/fnsyn.2020.575863

Wnt Signaling Through Nitric Oxide Synthase Promotes the Formation of Multi-Innervated Spines

Faye McLeod[1†], Kieran Boyle[1†], Aude Marzo[1], Nuria Martin-Flores[1], Thaw Zin Moe[1], Ernest Palomer[1], Alasdair J. Gibb[2] and Patricia C. Salinas[1]*

[1] Department of Cell and Developmental Biology, University College London, London, United Kingdom, [2] Department of Neuroscience, Physiology and Pharmacology, University College London, London, United Kingdom

Structural plasticity of synapses correlates with changes in synaptic strength. Dynamic modifications in dendritic spine number and size are crucial for long-term potentiation (LTP), the cellular correlate of learning and memory. Recent studies have suggested the generation of multi-innervated spines (MIS), in the form of several excitatory presynaptic inputs onto one spine, are crucial for hippocampal memory storage. However, little is known about the molecular mechanisms underlying MIS formation and their contribution to LTP. Using 3D enhanced resolution confocal images, we examined the contribution of Wnt synaptic modulators in MIS formation in the context of LTP. We show that blockage of endogenous Wnts with specific Wnt antagonists supresses the formation of MIS upon chemical LTP induction in cultured hippocampal neurons. Gain- and loss-of-function studies demonstrate that Wnt7a signaling promotes MIS formation through the postsynaptic Wnt scaffold protein Disheveled 1 (Dvl1) by stimulating neuronal nitric oxide (NO) synthase (nNOS). Subsequently, NO activates soluble guanylyl cyclase (sGC) to increase MIS formation. Consistently, we observed an enhanced frequency and amplitude of excitatory postsynaptic currents. Collectively, our findings identify a unique role for Wnt secreted proteins through nNOS/NO/sGC signaling to modulate MIS formation during LTP.

Keywords: multi-innervated spines, structural plasticity, LTP, Wnt signaling, nitric oxide

OPEN ACCESS

Edited by:
Ka Wan Li,
Vrije Universiteit Amsterdam, Netherlands

Reviewed by:
Thomas Mittmann,
Johannes Gutenberg University of Mainz, Germany
Elizabeth Hernández-Echeagaray,
National Autonomous University of Mexico, Mexico

****Correspondence:***
Patricia C. Salinas
p.salinas@ucl.ac.uk

† These authors share first authorship

Received: *24 June 2020*
Accepted: *13 August 2020*
Published: *04 September 2020*

Citation:
McLeod F, Boyle K, Marzo A, Martin-Flores N, Moe TZ, Palomer E, Gibb AJ and Salinas PC (2020) Wnt Signaling Through Nitric Oxide Synthase Promotes the Formation of Multi-Innervated Spines. Front. Synaptic Neurosci. 12:575863. doi: 10.3389/fnsyn.2020.575863

INTRODUCTION

Neuronal activity plays a crucial role in the establishment and refinement of neuronal networks (West and Greenberg, 2011). Activity induces functional and structural changes at the synapse through a process known as synaptic plasticity. In the mammalian brain, one of the main forms of synaptic plasticity is long-term potentiation (LTP), thought to underlie experience-dependent learning and memory. It is well established that activation of N-methyl-D-aspartate receptors (NMDARs) can induce LTP through the CaMKII cascade resulting in increased dendritic spine size and synaptic strength (Malenka and Bear, 2004; Herring and Nicoll, 2016). Interestingly, LTP induction also increases the formation of spines innervated by two or more presynaptic boutons, called multi-innervated spines (MIS) (Nikonenko et al., 2003). However, little is known about mechanisms controlling MIS formation during LTP induction.

Recent studies show that MIS generation facilitates long-term memory (Radwanska et al., 2011; Giese et al., 2015; Aziz et al., 2019). In the hippocampus, multi-synaptic filopodia/atypical spines are common immature synaptic structures during early development but the formation of MIS is rare, representing less than 1% of the total excitatory synapses under basal conditions in the adult (Fiala et al., 1998; Petrak et al., 2005; Radwanska et al., 2011). In organotypic hippocampal cultures, activation of postsynaptic NMDARs or expression of the postsynaptic scaffold proteins PSD-95 or SAP-97 induces the formation of MIS (Nikonenko et al., 2003, 2008; Poglia et al., 2011). Importantly, the generation of MIS requires nitric oxide (NO) signaling. PSD-95 binds to neuronal NO synthase (nNOS), resulting in NO messenger generation at the postsynaptic side. NO can then act retrogradely on presynaptic bouton(s) to activate soluble guanylyl cyclase (sGC) and induce the formation of multiple boutons in contact with one dendritic spine, thus promoting the formation of MIS (Nikonenko et al., 2008). Crucially, recent *in vivo* evidence suggests that MIS generation in the hippocampus may facilitate long-term memory formation (Radwanska et al., 2011; Giese et al., 2015; Aziz et al., 2019). Although findings have begun to decipher the role of MIS on hippocampal-mediated memory, the exact molecular mechanisms that trigger MIS formation during experience-dependent learning and memory have not been fully established.

Wnt secreted proteins are a family of synaptic modulators that play a crucial role in synapse assembly and function in the developing and mature brain. In the hippocampus, Wnts regulate neurotransmitter release at the presynaptic level (Cerpa et al., 2008; Ciani et al., 2015), whereas Wnts at the postsynaptic level increase synaptic NMDAR and α-amino-3-hydroxy-5-methyl-4-isoxazolepropionic acid receptor (AMPAR) levels, dendritic spine growth and synaptic transmission (Cerpa et al., 2011, 2015; Ciani et al., 2011; McQuate et al., 2017; McLeod and Salinas, 2018). Moreover, Wnt expression and/or release is increased by synaptic activity in hippocampal neurons (Chen et al., 2006; Wayman et al., 2006; Gogolla et al., 2009; McLeod et al., 2018). Importantly, LTP induction rapidly increases synaptic Wnt7a/b protein levels which are required for LTP-associated spine growth and synaptic strength (McLeod et al., 2018). Given that Wnt proteins modulate structural and functional plasticity, the Wnt signaling cascade could contribute to activity-mediated generation of MIS.

Here, we investigated whether Wnt signaling contributes to activity-dependent MIS formation. Our results show that LTP induces the formation of MIS through Wnt signaling in hippocampal neurons as LTP-induced MIS formation is blocked by acute blockade of Wnts with a specific Wnt antagonist. Moreover, we show that Wnt7a, which strongly promotes spine growth and is regulated by chemical LTP induction in the hippocampus, acts postsynaptically through the specific Wnt scaffold protein Disheveled 1 (Dvl1) to induce the formation of MIS. Importantly, we demonstrate that Wnt-Dvl1 signaling promotes MIS formation through activation of nNOS at the postsynaptic side and subsequent stimulation of sGC, most likely through NO diffusion to the presynaptic side. Altogether, our results demonstrate for the first time that Wnt signaling acts through NO to retrogradely promote the formation of multiple presynaptic inputs on spines during synaptic plasticity.

RESULTS

Chemical LTP Increases the Number of MIS Through Wnts

Previous studies have shown that Wnt signaling promotes synaptic strength and spine growth during LTP (McLeod et al., 2018) and that LTP induction increases the number of MIS (Nikonenko et al., 2003). These findings led us to hypothesize that Wnt signaling could contribute to LTP-mediated formation of MIS in hippocampal neurons. To test this idea, NMDAR-mediated chemical LTP (cLTP) was induced in hippocampal cultures. We found that cLTP increased the number (control = 31.45 ± 0.7 spines/100 μm; cLTP = 44.45 ± 1.3 spines/100 μm; Student's *t*-test $P < 0.001$) and width (Control = 0.65 ± 0.01 μm; Glycine = 0.8 ± 0.02 μm; Student's *t*-test $P < 0.001$) of dendritic spines, in agreement with previous publications (Fortin et al., 2010; McLeod et al., 2018). Under basal conditions, MIS accounted for approximately 2% of all spines (as determined by the number of spines contacted by more than one vGlut1 puncta in three-dimensional (3-D) reconstructions of confocal z-stacks), whereas cLTP induction increased the proportion of MIS to approximately 5% (**Figures 1A,B**). We next investigated whether Wnts, which are elevated by LTP (Chen et al., 2006; McLeod et al., 2018), contribute to this cLTP-mediated structural plasticity. To block endogenous Wnts, we used the specific Wnt antagonist Sfrp3, a secreted protein that we have previously shown can block the function of Wnts at synapses (Sahores et al., 2010). Exposure to Sfrp3 during cLTP induction completely blocked the increase in MIS number induced by the potentiating stimulus (**Figures 1A,B**). These results demonstrate that endogenous Wnts are required for activity-induced formation of MIS.

Wnt7a Promotes the Formation of MIS Through Postsynaptic Activation of Wnt Signaling

We have recently shown that synaptic activity increases the levels of Wnt7a/b protein at dendritic spines and that Wnt7a signals postsynaptically to regulate LTP-mediated spine growth and AMPAR recruitment (McLeod et al., 2018). We therefore examined if Wnt7a could induce MIS formation. We found that exposure to Wnt7a significantly increased the number of MIS (**Figures 2A,B**).

To address whether postsynaptic activation of the Wnt pathway was required to promote MIS formation, we specifically blocked Wnt signaling on the postsynaptic side. Wnt7a is known to promote spine growth and synaptic strength through Dvl1 at the postsynaptic compartment (Ciani et al., 2011). Dvl1 is a cytoplasmic scaffold protein that is required for Wnt signaling (Gao and Chen, 2010). Importantly, expression of Dvl1 activates the Wnt signaling pathway in a cell autonomous manner (Boutros and Mlodzik, 1999). Indeed, expression of Dvl1 results

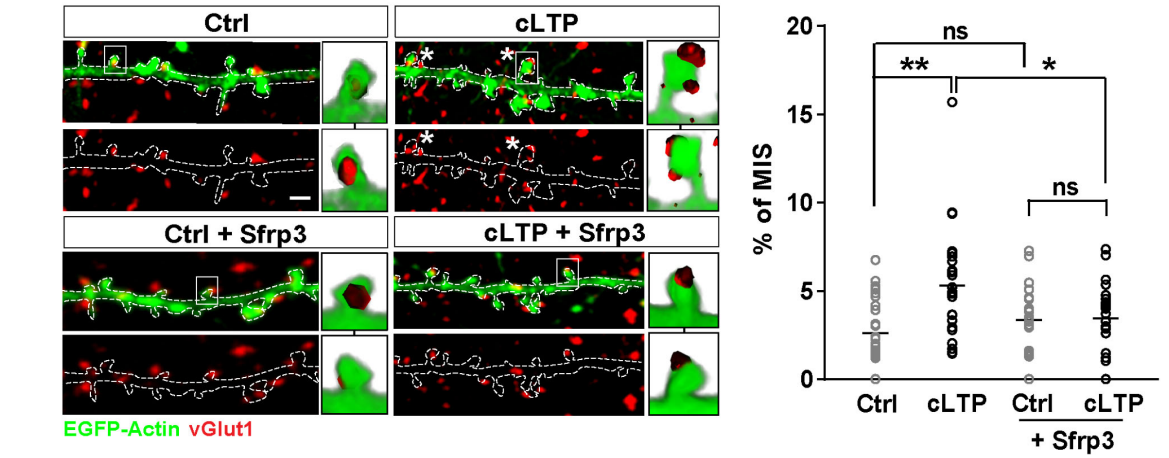

FIGURE 1 | LTP-mediated increase in MIS number requires endogenous Wnts. **(A)** EGFP-actin-expressing cultured neurons (13–14 DIV) (in green) exposed to control (Ctrl) or cLTP conditions, with or without the specific Wnt antagonist Sfrp3 and immunostained for vGlut1 (in red). cLTP induction increased the proportion of spines contacted by more than one vGlut1 puncta (MIS; asterisks). However, this effect was blocked by Sfrp3. Three-dimensional zoomed-in images display front (top) and back (bottom) representations of innervated spines with single or multiple vGlut1 puncta. Scale bar = 1 μm. **(B)** Quantification of mean percentage of MIS in each condition (n = 25–31 cells/condition from 3 independent cultures, $^{*}P < 0.05$ and $^{**}P < 0.01$ by two-way ANOVA followed by Tukey *post hoc* test).

in dendritic spine enlargement and increased innervation of spines, with a concomitant increase in mEPSC amplitude and frequency as observed with gain-of-function of Wnt7a (Ciani et al., 2011). We therefore examined whether knock-down of Dvl1 affects Wnt7a-induced formation of MIS.

We first generated two different short hairpin RNA (shRNA) sequences against Dvl1. Dvl1 shRNAs were validated in normal rat kidney (NRK) epithelial cells by quantitative PCR (qPCR), which revealed a 20% reduction in endogenous Dvl1 mRNA levels using clone 1 and a 50% reduction using clone 2 (**Supplementary Figure S1**). Dvl1 shRNA clone 2 was used for subsequent experiments in primary hippocampal neurons and was co-transfected with EGFP-actin to allow identification and assessment of transfected dendrites contacted by non-transfected axons. We found that loss of postsynaptic Dvl1 function had no significant effect on basal conditions (**Figures 2A,B**). However, MIS formation was completely abolished following addition of recombinant Wnt7a (**Figures 2A,B**), suggesting that postsynaptic Wnt signaling is required for Wnt7a-induced MIS formation.

Next, to investigate whether postsynaptic activation of the Wnt pathway enhances the formation of MIS, we performed gain-of-function studies on Dvl1. We therefore expressed Dvl1 in cultured hippocampal neurons co-transfected with EGFP-actin. We found that under control conditions, 45% of innervated spines are contacted by a single vGlut1-labeled presynaptic bouton and 45% are non-innervated. In contrast, expression of Dvl1 decreased the number of non-innervated spines (to 20%), did not affect the number of single innervated spines but increased the proportion of MIS containing two, three or more vGlut1-labeled boutons (**Figures 3A,B**). The presence of MIS in dendritic spines expressing Dvl1 compared to controls was further demonstrated in 3D movies (**Supplementary Movies S1**, **S2**). We also examined the impact of Dvl1 gain-of-function on the number of spines containing the postsynaptic marker PSD-95, which has been shown to modulate MIS formation (Nikonenko et al., 2008). We previously showed that Dvl1 gain-of-function increases the number of spines containing PSD-95 and the volume of PSD-95 per spine (Ciani et al., 2011). Consistently, we found a similar increase in the proportion of spines containing more than one PSD-95 puncta (**Figures 3A,B**). Our studies demonstrate that even though Dvl1-expressing dendrites were contacted by axons with basal Dvl1 levels, postsynaptic gain- of- function of Dvl1 was able to promote the formation of MIS, implying that the presynaptic side responds to signals from the postsynaptic side by assembling new synaptic boutons.

Postsynaptic Activation of the Wnt Pathway Requires Nitric Oxide Signaling to Regulate MIS Formation

How does postsynaptic Dvl1 promote the formation of new presynaptic boutons? One possible explanation is that retrograde signals like NO could mediate this effect. The enzyme essential for NO synthesis in neurons, nNOS, is localized at the PSD in dendritic spines of hippocampal neurons (Burette et al., 2001). In contrast, the NO receptor, soluble guanylyl cyclase (sGC), has two isoforms (NO-GC1 and NO-GC2) located at both the pre- and the postsynaptic terminals, with NO-GC1 found predominantly presynaptically (Aoki et al., 1998; Burette et al., 2001, 2002; Neitz et al., 2014). Importantly, MIS formation following postsynaptic expression of PSD-95 or SAP97 is blocked by inhibition of NO signaling, whereas the NO donor DETA increases MIS formation in hippocampal slices (Nikonenko et al., 2008; Poglia et al., 2011). Therefore, we hypothesized that postsynaptic activation of Wnt signaling could utilize retrograde NO signaling to promote the

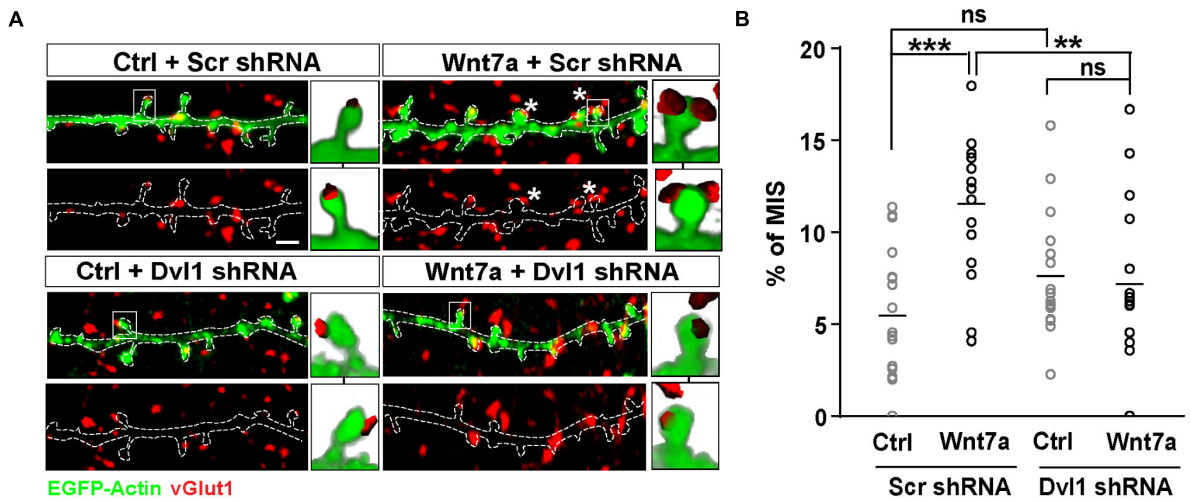

FIGURE 2 | Wnt7a-Dvl1 signaling is required postsynaptically to promote MIS formation. **(A)** Scrambled (Scr) control or Dvl1 shRNA expressing neurons (13–14 DIV) exposed to control (Ctrl) or Wnt7a conditions for 3 h (scale bar: 1 μm). Wnt7a-mediated increase in MIS (asterisks) requires Dvl1. Representative images of EGFP-actin dendrites (in green) and vGlut1 (in red) are shown. Three-dimensional zoomed-in images display front (top) and back (bottom) representations of innervated spines with single or multiple vGlut1 puncta. **(B)** Quantification of mean percentage of MIS in each condition (n = 16–18 cells/condition from 3 cultures, $^{**}P < 0.01$ and $^{***}P < 0.001$ by two-way ANOVA followed by Tukey *post hoc* test).

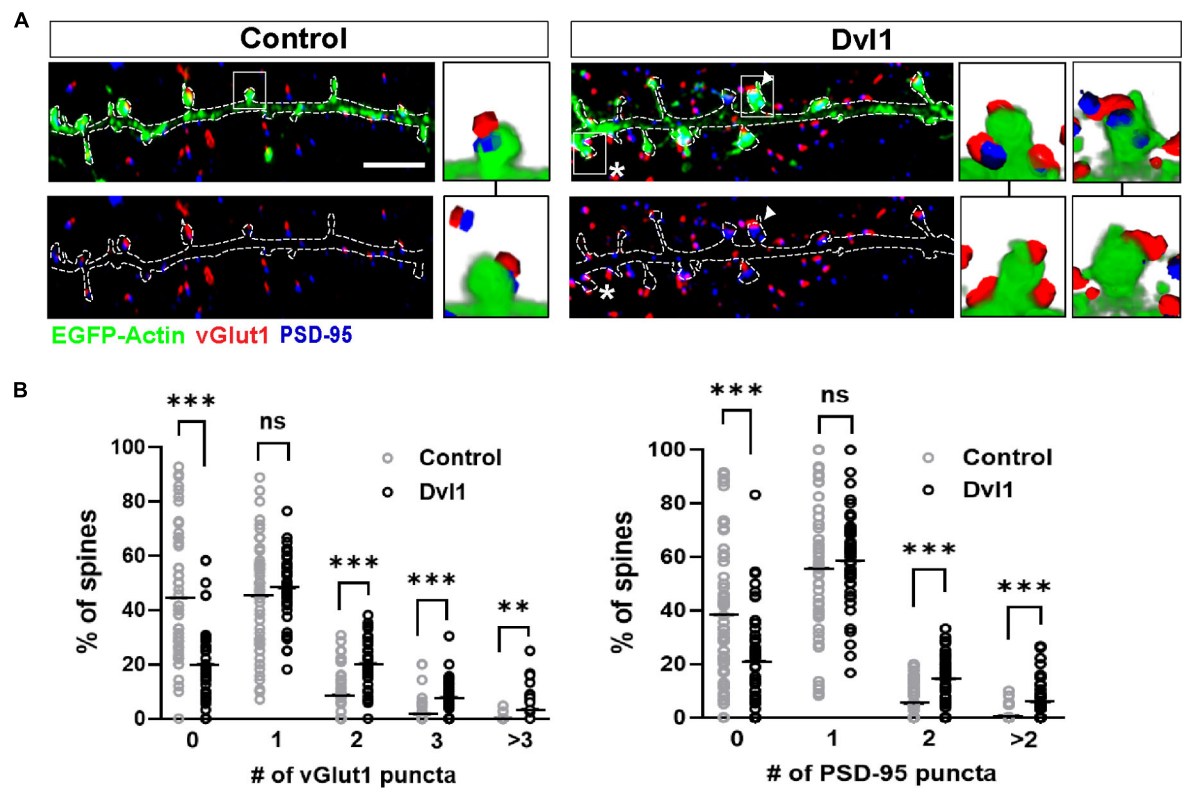

FIGURE 3 | Postsynaptic Dvl1 gain of function increases the innervation of spines and the formation of MIS. **(A)** Representative images of dendrites expressing EGFP-actin (green) and empty vector (control) or Dvl1-HA and immunostained for vGlut1 (red) and PSD-95 (blue). Dvl1 expression increases the proportion of spines contacted by more than one vGlut1 (asterisks) puncta and spines containing more than one discrete PSD-95 puncta (multiple PSDs; arrowhead) when compared to control neurons. Scale bar = 5μm. Three-dimensional zoomed-in images display front (top) and back (bottom) representations of spines with one or more vGlut1 and PSD95 puncta. **(B)** Quantification of the distribution of number of vGlut1 and PSD-95 puncta per spine (n = 37–42 cells from 3 independent cultures, $^{**}P < 0.01$, $^{***}P < 0.001$, Mann-Whitney test).

formation of MIS by stimulating the assembly of new synaptic boutons onto spines.

To assess this, we applied the nNOS inhibitor NG-nitro-L-arginine (L-NNA) or the sGC inhibitor 1H-[1,2,4] oxadiazolo[4,3-a]quinoxalin-1-one (ODQ) onto control EGFP-actin expressing neurons or neurons co-expressing EGFP-actin and Dvl1. Under basal conditions, inhibition of nNOS by L-NNA had no effect on MIS formation and on spines with multiple PSDs (**Figures 4A–C**). As described above (**Figure 3**), Dvl1 gain-of-function increased the percentage of MIS and spines with multiple PSDs (**Figures 4A–C**). Crucially, inhibition of NO-sGC signaling by either L-NNA or ODQ blocked the effect of Dvl1 on both the number of MIS and multiple PSDs (**Figures 4A–C**). Importantly, inhibition of nNOS did not affect spine number and size under basal conditions or block Dvl1-induced spine enlargement (**Supplementary Figure S2A**). Similarly, inhibition of sGC by ODQ did not affect Dvl1-associated spine size enhancement (**Supplementary Figure S2A**). In contrast, NO-sGC signaling inhibition blocked Dvl1-mediated increase in the percentage of excitatory synapses as determined by colocalization of vGlut1 and PSD-95 (**Supplementary Figure S2B**). Moreover, L-NNA also reduced the number of excitatory synapses (**Supplementary Figure S2B**) under basal conditions suggesting that NO signaling plays a role in excitatory synapse formation in hippocampal neurons. Collectively, these results demonstrate that activation of postsynaptic Wnt signaling promotes MIS formation and synaptic connectivity through NO-sGC signaling.

Given the profound effect of NO-sGC signaling blockade on Wnt mediated MIS formation, we investigated the impact of this pathway at the functional level by performing electrophysiological recordings. Previous studies have shown that Dvl1-induced changes in spine innervation and morphology have functional correlates, as the frequency and amplitude of miniature excitatory postsynaptic currents (mEPSC) are increased by gain of function of Dvl1 on the postsynaptic side (Ciani et al., 2011). We therefore tested whether inhibition of NO signaling blocks these synaptic functional changes. Under control conditions in primary hippocampal neurons (**Supplementary Figure S2B**), L-NNA did not affect either the frequency or amplitude of mEPSCs suggesting preserved basal transmission properties with inhibition of NO production (**Figures 4D,E**). In contrast, L-NNA completely blocked the ability of Dvl1 to increase mEPSC frequency and amplitude (**Figures 4D,E**), suggesting that NO signaling is required for Dvl1-mediated functional changes at excitatory synapses.

DISCUSSION

Neuronal activity induces long lasting structural modifications in synapses to promote changes in synaptic strength. For example, LTP induction results in the enlargement of dendritic spines and the formation of multi-contact synapses (Hruska et al., 2018; Zaccard et al., 2020), including MIS, a unique form of structural synaptic plasticity. Indeed, formation of MIS is associated with NMDAR-dependent LTP (Nikonenko et al., 2003; Hruska et al., 2018). Here, we have uncovered a novel role for Wnt signaling in MIS generation. We demonstrate that enhanced MIS formation during NMDAR-mediated cLTP requires Wnt signaling. Specifically, Wnt7a, which is expressed in the hippocampus, promotes the formation of MIS through postsynaptic activation of the Wnt pathway. This results in activation of NO signaling and a retrograde modulation of presynaptic inputs and mEPSC frequency and amplitude. Our findings unravel a molecular mechanism by which Wnt signaling acts through the NO-sGC cascade to trigger activity-induced MIS formation.

Wnts are required for the formation of MIS during NMDAR-mediated cLTP in hippocampal neurons. Previous studies have demonstrated that LTP-dependent activation of NMDAR increases MIS number in hippocampal organotypic cultures (Nikonenko et al., 2003). However, the initial signal(s) that triggers LTP-mediated MIS formation has not been demonstrated. We focused our attention on Wnts for several reasons. First, Wnt proteins are required for synapse formation, spine enlargement and synaptic strengthening (Sahores et al., 2010; Ciani et al., 2011; McLeod et al., 2018). Second, activation of Wnt signaling postsynaptically increases the content of PSD-95 in dendritic spines (Ciani et al., 2011). Third, we have shown that endogenous Wnt7a/b levels are elevated upon induction of LTP and that Wnt7a signals postsynaptically to regulate LTP-mediated spine growth and AMPAR recruitment (McLeod et al., 2018). Here we demonstrate that Wnt7a also increases MIS formation and the number of spines with multiple PSD-95 puncta. These results are consistent with the finding that PSD-95 is required for dendritic spine stabilization during LTP (Stein et al., 2003; Ehrlich et al., 2007) and MIS formation (Nikonenko et al., 2008; Radwanska et al., 2011). To date, no studies have examined how stable these structural changes are over time. Nonetheless, together our results suggest that the elevation of Wnt7a protein following LTP induction is important for dynamic pre- and postsynaptic structural plasticity.

Specific activation of the Wnt pathway on the postsynaptic side promotes MIS formation. Previous studies have shown that gain of function of Dvl1, which is enriched at dendritic spines in hippocampal neurons, can activate the Wnt pathway in a cell autonomous manner (Ciani et al., 2011). Notably, we found that Dvl1 gain-of-function on the postsynaptic side is sufficient to induce MIS formation. Conversely, postsynaptic loss-of-function of Dvl1 blocks the ability of Wnt7a to promote MIS formation. These results suggest that activation of the Wnt pathway on the postsynaptic dendrite/spine triggers a signal that acts retrogradely to promote the assembly of several synaptic boutons on a single spine.

Consistent with the generation of a retrograde signal, our studies identify NO as the retrograde messenger required for Wnt-induced MIS formation. Under basal conditions, inhibition of nNOS (located postsynaptically) had no effect on MIS formation or on the number of spines with multiple PSDs. In contrast, postsynaptic gain of function of Dvl1, that activates the Wnt pathway in a cell autonomous manner on the postsynaptic side, promoted MIS formation, an effect that was blocked by NO-sGC inhibition. Based on these results, we propose that activation of the Wnt pathway on the postsynaptic side triggers

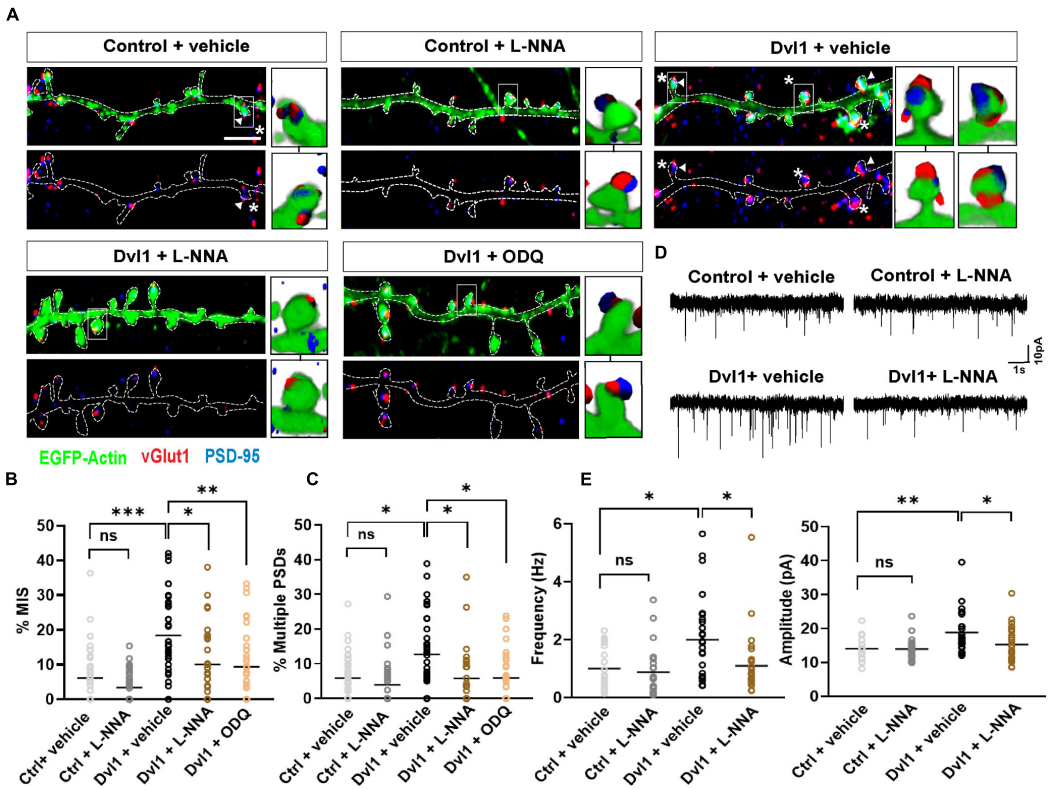

FIGURE 4 | Dvl1 promotes the formation of MIS through NO signaling. **(A)** Representative images of dendrites expressing EGFP-actin (green), or EGFP-actin and Dvl1 and immunostained for vGlut1 (red) and PSD-95 (blue). Following Dvl1 expression, neurons were treated with vehicle, the NOS inhibitor L-NNA or the sGC inhibitor ODQ. NO inhibition blocks the Dvl1 mediated formation of MIS (asterisks) and multiple PSDs (arrowhead). Scale bar = 5 μm. Three-dimensional zoomed-in images display front (top) and back (bottom) representations of spines with one or more vGlut1 and PSD95 puncta. **(B,C)** Quantification of mean percentage of MIS **(B)** and spines **(C)** with multiple PSDs (n = 37–42 cells from 3 independent cultures, $^{*}P < 0.05$, $^{**}P < 0.01$, $^{***}P < 0.001$, n.s. = non-significant by Kruskal-Wallis test followed by Dunn's *post hoc* test). **(D)** Representative 10 s traces of mEPSCs recorded from neurons, co-transfected with EGFP-actin and empty vector (control) or Dvl1-HA and treated with vehicle or the NOS inhibitor L-NNA. Dvl1 increases mEPSC frequency and amplitude, both of which are blocked by L-NNA. **(E)** Quantification of mean mEPSC frequency and amplitude [n = 21–29 cells/condition from 3 independent cultures $^{*}P < 0.05$, $^{**}P < 0.01$ by Kruskal-Wallis test followed by Dunn's *post hoc* test in (frequency) and two-way ANOVA followed by Tukey *post hoc* test in (amplitude)].

NO synthesis through nNOS. NO then diffuses retrogradely to the presynaptic site to promote the formation of several boutons innervating a single spine through sGC activation. This effect is likely mediated through the NO-GC1 isoform, which is predominantly located on the presynaptic terminal (Neitz et al., 2014). These findings are in agreement with previous studies showing that MIS formation requires NO signaling (Nikonenko et al., 2003, 2008; Poglia et al., 2011). Indeed, expression of PSD-95 is sufficient to promote MIS formation through production of NO (Nikonenko et al., 2008). Therefore, it is reasonable to assume Wnt7a through Dvl1 increases PSD-95 levels in spines promoting MIS formation through nNOS/NO/sGC signaling. Importantly, these structural modifications are accompanied by an increase in mEPSC frequency with no changes in spine number, suggesting a functional correlate in response to MIS formation. Interestingly, increasing evidence indicates that Wnts modulate NO signaling in several contexts. For example, Wnt5a regulates NMDAR trafficking and potassium voltage-gated currents through NO production in the hippocampus (Munoz et al., 2014; Parodi et al., 2015). Our studies also highlight a key role for NO production in hippocampal excitatory synapse formation without affecting mEPSC frequency under basal conditions. Similar findings are observed when blockade of NO production occurs in hippocampal organotypic slices (Nikonenko et al., 2013). Overall, these results demonstrate a dynamic interplay between multiple Wnts and NO under basal and synaptic plasticity conditions to regulate pre- and postsynaptic function.

What is the cognitive impact of MIS formation? MIS generation has been associated with learning and long-term memory. Indeed, complex motor learning increases MIS number in layer II/III of the motor cortex (Jones et al., 1999). Other memory tasks, including auditory fear conditioning, also lead to MIS generation in the auditory cortex (Yang et al., 2018). Recent *in vivo* studies have demonstrated that MIS formation is increased at CA1 hippocampal neurons after contextual fear memory formation (Aziz et al., 2019). These findings suggest that MIS generation is an efficient mechanism to increase connectivity and/or strengthen connections on existing synapses during learning. Furthermore, in neurological disorders characterized by increased cortical connectivity and disrupted network function

such as Fragile X syndrome (Bureau et al., 2008; Zhang et al., 2014), the number of MIS are also significantly increased (Booker et al., 2019). This structural plasticity mechanism could be driven by differences in cortical network activity. Interestingly, experience-driven neuronal activity induces structural changes at the synapse through Wnts. Environmental enrichment causes Wnt7a/b upregulation in the CA3 hippocampal region, which promotes the formation of multiple mossy fiber terminals and increases the density of synapses per mossy fiber terminal (Gogolla et al., 2009). Furthermore, *in vivo* studies show that Wnt7a loss of function delays the maturation of glomerular rosettes, complex multisynaptic structures formed between a mossy fiber axon and dendrites from numerous granule cells in the cerebellum (Hall et al., 2000). *In vivo,* structural synaptic plasticity, LTP and memory formation also require Wnts (Marzo et al., 2016). Thus, Wnt signaling is required for activity- or experience-mediated formation of complex synaptic structures. Here we uncover a novel role for Wnt7a-Dvl1 signaling in LTP-mediated MIS formation. We demonstrate that the Wnt cascade modulates NO signaling to regulate structural plasticity at both sides of the synapse in a coordinated manner thus contributing to increased synaptic connectivity.

MATERIALS AND METHODS

Hippocampal Cultures, Cell Transfection, and Treatments

Primary hippocampal neurons (250 cells/mm^2) were isolated from embryonic day 18 Sprague-Dawley rat embryos and cultured as previously described (Dotti et al., 1988). To overexpress Dvl1, cultures were co-transfected at 7-8 DIV with EGFP-actin and Dvl1-HA or empty vector (PCS2) using calcium phosphate. To knockdown Dvl1, cultures were co-transfected using calcium phosphate with EGFP-actin (0.5 μg) and scrambled or Dvl1 shRNA (0.05 μg). Scrambled (5′-GGCGTTACGTCCTAACATGCG-3′) and two Dvl1 shRNA (clone #1: 5′-GGGTCTAACTTACTTATTTAT-3′; clone #2: 5′-CTTGAATCTAGCAGCTTTATT-3′) target sequences were cloned into an AAV-U6 vector expressing mCherry. Dvl1 shRNA clone #2 was used for experiments. Purified recombinant Wnt7a (150 ng/mL; PeproTech) was applied to neurons at 37°C for 3 h. Bovine serum albumin (BSA) was used as a control. 100 μM L-NNA or 10 μM ODQ were added to cultures at 9 DIV and re-added at 11 DIV. Vehicles for L-NNA and ODQ were equimolar HCl and DMSO, respectively, as previously described (Bartus et al., 2013). After appropriate treatment, 12 DIV neurons were fixed for immunofluorescence or used for electrophysiological experiments.

Real-Time PCR

NRK cells were transfected with scrambled or Dvl1 shRNA clones as described above using electroporation and Nucleofector (Lonza). After 24 h, cells were washed in cold PBS and homogenized using Trizol Reagent (Life Technologies). Total RNA was then extracted using Direct-zol columns (ZymoResearch). RNA concentration was quantified using a NanoDrop ND-100 (Thermo Scientific). Up to 2000 ng of RNA were used for cDNA synthesis using RevertAid H Minus First Strand cDNA Synthesis kit (Themo Fisher Scientific). Five nanogram of original RNA was used to perform fast qPCR using GoTaq qPCR Master Mix (Promega) in a LighterCycler® 480 (Roche). Primers for Dvl1 and three housekeeping genes (Gapdh, Actb and Rps18) were designed using OligoPerfect design (Thermo Fisher Scientific) and validated using *in silico* PCR (UCSC genome Browser) and Ensembl BLAST[1]. Primers (*Dvl1* Fw: 5′-GCTGAAGCATGGTTTCCTGC-3′; *Dvl1* Rv: 5′-GTTGAGGTTCAGGGATGCGA-3′; *Actb* Fw 5′-GGCTCCTAGCACCATGAAGA-3′; *Actb* Rv: 5′- CTGGAA GGTGGACAGTGAGG-3′; *Gapdh* Fw 5′-AGACAGCCGCATC TTCTTGT-3′; *Gapdh* Rv: 5′-CTTGCCGTGGGTAGAGTCAT-3′; *Rps18* Fw 5′-CTTCCACAGGAGGCCTACAC-3′; *Rps18* Rv: 5′-GTACTCGCAGGATGTGCTGA-3′) were used at 0.5 μM (Sigma Aldrich).

Chemical Long-Term Potentiation (cLTP)

LTP was induced in 13–14 DIV hippocampal cultures using an NMDAR mediated chemical LTP (cLTP) protocol as previously described (Fortin et al., 2010; McLeod et al., 2018). Briefly, hippocampal neurons were kept at room temperature (RT) for 20–30 min in control solution (125 mM NaCl, 2.5 mM KCl, 1 mM $MgCl_2$, 2 mM $CaCl_2$, 33 mM D-glucose, 5 mM HEPES, 20 μM D-APV, 3 μM strychnine, 20 μM bicuculline and 0.5 μM TTX; pH 7.4). After cLTP induction (addition of glycine 200 μM for 10 min in the absence of Mg^{2+}, D-APV and TTX) cultures were returned to control solution for 1 h prior to fixation (all performed at RT). To block endogenous Wnt proteins, recombinant Sfrp3 (250 ng/mL; R&D Systems) was used only throughout the induction of cLTP and after.

Immunofluorescence, Image Acquisition, and Analyses

Dissociated neurons were fixed with cold 100% methanol or 4% paraformaldehyde (PFA)/4% sucrose in PBS for 20 min at RT, permeabilized with 0.025% Triton, blocked with 5% BSA and then incubated with primary antibodies overnight at 4°C. Primary antibodies against GFP (1:500; Millipore), vGlut1 (1:10,000; Chemicon) and PSD-95 (1:500; Affinity Bioreagents) were used. Secondary antibodies were Alexa 488, 568, and 647 (1:600 dilution, Molecular Probes). Fluorescence images of pyramidal neurons were captured with a Leica TCS SP1 Confocal microscope using a 63x oil objective (NA = 1.32), producing image stacks of 157.8 × 157.8 μm with an average z-depth of ∼5 μm. Six to twelve images were taken per condition per experiment and analyzed blind to the experimental condition using Volocity (Improvision). For each EGFP-actin-transfected cell, 2–3 regions of interest containing ∼50–100 μm of secondary dendrite were cropped from maximum projections. The number of spines were counted, and the spine head/size width determined with a line tool. Finally, the number of spines containing PSD-95, vGlut1 and multiple PSD-95 and/or vGlut1 puncta was counted.

[1]http://ensemble.org/

The 3D visualization tool on Volocity was used to confirm if synaptic puncta were in the same focal plane as spines. MIS were defined as EGFP-actin spines contacted by more than one vGlut1 puncta. To ensure our MIS quantification did not include vGlut1 that could feasibly come from the same presynaptic terminal, we excluded vGlut1 within ∼0.2–0.3 μm of each other. For each condition, approximately 1000 spines were analyzed in total from all three repeats of each experiment.

The 3D images and movies (.avi files) of individual spines were obtained from stacks of confocal images (as above), cropped and then processed using the animation function in Imaris software to zoom and navigate around the spines.

Electrophysiology

Whole-cell patch clamp recordings were performed on primary hippocampal neuron cultures co-transfected with EGFP-actin (1 μg) and Dvl1-HA (1 μg) or empty vector. Most neurons co-express EGFP-actin and Dvl1-HA. Coverslips were placed on an upright microscope and continuously perfused at RT with recording solution containing (in mM): NaCl (125), $NaHCO_3$ (25), KCl (2.5), $NaHPO_4$ (1.25), $CaCl_2$ (1), $MgCl_2$ (1), D-glucose (25) bicuculine (0.01), and TTX (0.0001). Cells were voltage-clamped at -60 mV in the whole cell configuration using borosilicate glass microelectrodes (resistance 5–8 MΩ) filled with a pipette solution containing (in mM): D-gluconic acid lactone (139), HEPES (10), EGTA (10), NaCl (10), $CaCl_2$ (0.5), $MgCl_2$ (1), ATP (1) and GTP (1) adjusted to pH 7.2 with CsOH. mEPSCs were recorded using an Axopatch 200B amplifier, filtered at 1 kHz and digitized at 10 kHz using WinEDR. Currents were analyzed blind using a combination of WinEDR and WinWCP (freely available at http://spider.science.strath.ac.uk/sipbs/software_ses.htm).

Statistical Analyses

All data are represented as mean ± SEM from at least three independent experiments (unless otherwise stated). Statistical analyses were performed on GraphPrism and Origin with data normality assessed using Kolmogorov-Smirnov tests. Normally distributed data were analyzed using an unpaired Student's *t*-test, one-way or two-way ANOVA with Tukey's *post hoc* correction for multiple comparisons. Mann-Whitney and Kruskal-Wallis tests with Dunn's post-test were used for non-parametric data.

DATA AVAILABILITY STATEMENT

The raw data supporting the conclusions of this article will be made available by the authors, without undue reservation, to any qualified researcher.

ETHICS STATEMENT

The animal study was reviewed and approved by the UCL Animal Welfare and Ethical Review Body (Bloomsbury Campus).

AUTHOR CONTRIBUTIONS

PS conceived the overall project, guided the project, and provided the funding. AG contributed to the design and analyses of the electrophysiology experiments. FM and AM performed the cell biology experiments. KB performed the cell biology and electrophysiology experiments. NM-F evaluated the results. TM evaluated the results presented in **Figure 1**. EP performed the qPCR experiments. All authors participated in the design of experiments, interpretation of data, and in the writing of the manuscript.

FUNDING

The MRC (MRC/M024083/1), the Wellcome Trust (075064/Z/04/Z), the Alzheimer's Research UK (ARUK-PG2018A-002), the Alzheimer's Society (AS-PG-18-008), and European Commission Horizon 2020 (H2020 MSCA-IF 749209) supported this work.

ACKNOWLEDGMENTS

We would like to thank members of our lab for insightful discussions on the results and comments on our manuscript.

SUPPLEMENTARY MATERIAL

The Supplementary Material for this article can be found online at: https://www.frontiersin.org/articles/10.3389/fnsyn.2020.575863/full#supplementary-material

FIGURE S1 | Validation of Dvl1 shRNA knockdown constructs. Dvl1 mRNA levels in NRK cells transfected with scrambled or two different Dvl1 shRNA clones were evaluated. Graph represents fold change in mRNA levels relative to scrambled shRNA control. Dvl1 shRNA clone #2 was used for experiments ($n = 4$ independent cultures, $^{**}P < 0.01$ by One-way ANOVA). Related to **Figure 2**.

FIGURE S2 | Postsynaptic Dvl1-mediated increase in excitatory innervation but not spine size is blocked by inhibition of NO signaling. **(A)** Quantification shows that Dvl1 does not affect spine number and this is not affected by inhibition of NO signaling. In addition, the effect of Dvl1 on increased spine head width is unaffected by inhibition of NO signaling. **(B)** Quantification shows that inhibition of NO signaling blocks the effect of Dvl1 on the proportion of spines contacted by vGlut1 puncta, containing PSD-95 puncta, or both. L-NNA also reduces basal innervation ($n = 37$–42 cells from 3 independent experiments, $^{*}P < 0.05$, $^{**}P < 0.01$, $^{***}P < 0.001$, n.s. = non-significant, Kruskal-Wallis test followed by Dunn's *post hoc* test). Related to **Figure 3**.

MOVIE S1 | Single innervation of a spine in a control neuron expressing EGFP-actin (green). Representative 3D reconstruction of a dendritic spine where presynaptic boutons are labeled with vGlut1 (red) and the PSD with PSD-95 (blue). Related to **Figure 3**.

MOVIE S2 | Postsynaptic Dvl1 expression increases the number of MIS. Representative 3D reconstruction of a dendritic spine expressing EGFP-actin (green) and Dvl1-HA. Presynaptic boutons and PSD were labeled with vGlut1 (red) and PSD-95 (blue) respectively. Related to **Figure 3**.

REFERENCES

Aoki, C., Bredt, D. S., Fenstemaker, S., and Lubin, M. (1998). The subcellular distribution of nitric oxide synthase relative to the NR1 subunit of NMDA receptors in the cerebral cortex. *Prog. Brain Res.* 118, 83–97. doi: 10.1016/s0079-6123(08)63202-1

Aziz, W., Kraev, I., Mizuno, K., Kirby, A., Fang, T., Rupawala, H., et al. (2019). Multi-input synapses, but not LTP-strengthened synapses, correlate with hippocampal memory storage in aged mice. *Curr. Biol.* 29, 3600.e4–3610.e4. doi: 10.1016/j.cub.2019.08.064

Bartus, K., Pigott, B., and Garthwaite, J. (2013). Cellular targets of nitric oxide in the hippocampus. *PLoS One* 8:e57292. doi: 10.1371/journal.pone.0057292

Booker, S. A., Domanski, A. P. F., Dando, O. R., Jackson, A. D., Isaac, J. T. R., Hardingham, G. E., et al. (2019). Altered dendritic spine function and integration in a mouse model of fragile X syndrome. *Nat. Commun.* 10:4813. doi: 10.1038/s41467-019-11891-6

Boutros, M., and Mlodzik, M. (1999). Dishevelled: at the crossroads of divergent intracellular signaling pathways. *Mech. Dev.* 83, 27–37. doi: 10.1016/s0925-4773(99)00046-5

Bureau, I., Shepherd, G. M., and Svoboda, K. (2008). Circuit and plasticity defects in the developing somatosensory cortex of FMR1 knock-out mice. *J. Neurosci.* 28, 5178–5188. doi: 10.1523/JNEUROSCI.1076-08.2008

Burette, A., Petrusz, P., Schmidt, H. H., and Weinberg, R. J. (2001). Immunohistochemical localization of nitric oxide synthase and soluble guanylyl cyclase in the ventral cochlear nucleus of the rat. *J. Comp. Neurol.* 431, 1–10.

Burette, A., Zabel, U., Weinberg, R. J., Schmidt, H. H., and Valtschanoff, J. G. (2002). Synaptic localization of nitric oxide synthase and soluble guanylyl cyclase in the hippocampus. *J. Neurosci.* 22, 8961–8970.

Cerpa, W., Gambrill, A., Inestrosa, N. C., and Barria, A. (2011). Regulation of NMDA-receptor synaptic transmission by Wnt signaling. *J. Neurosci.* 31, 9466–9471. doi: 10.1523/JNEUROSCI.6311-10.2011

Cerpa, W., Godoy, J. A., Alfaro, I., Farias, G. G., Metcalfe, M. J., Fuentealba, R., et al. (2008). Wnt-7a modulates the synaptic vesicle cycle and synaptic transmission in hippocampal neurons. *J. Biol. Chem.* 283, 5918–5927. doi: 10.1074/jbc.M705943200

Cerpa, W., Latorre-Esteves, E., and Barria, A. (2015). RoR2 functions as a noncanonical Wnt receptor that regulates NMDAR-mediated synaptic transmission. *Proc. Natl. Acad. Sci. U.S.A.* 112, 4797–4802. doi: 10.1073/pnas.1417053112

Chen, J., Park, C. S., and Tang, S. J. (2006). Activity-dependent synaptic Wnt release regulates hippocampal long term potentiation. *J. Biol. Chem.* 281, 11910–11916. doi: 10.1074/jbc.M511920200

Ciani, L., Boyle, K. A., Dickins, E., Sahores, M., Anane, D., Lopes, D. M., et al. (2011). Wnt7a signaling promotes dendritic spine growth and synaptic strength through Ca(2)(+)/Calmodulin-dependent protein kinase II. *Proc. Natl. Acad. Sci. U.S.A.* 108, 10732–10737. doi: 10.1073/pnas.1018132108

Ciani, L., Marzo, A., Boyle, K., Stamatakou, E., Lopes, D. M., Anane, D., et al. (2015). Wnt signalling tunes neurotransmitter release by directly targeting Synaptotagmin-1. *Nat. Commun.* 6:8302. doi: 10.1038/ncomms9302

Dotti, C. G., Sullivan, C. A., and Banker, G. A. (1988). The establishment of polarity by hippocampal neurons in culture. *J. Neurosci.* 8, 1454–1468.

Ehrlich, I., Klein, M., Rumpel, S., and Malinow, R. (2007). PSD-95 is required for activity-driven synapse stabilization. *Proc. Natl. Acad. Sci. U.S.A.* 104, 4176–4181. doi: 10.1073/pnas.0609307104

Fiala, J. C., Feinberg, M., Popov, V., and Harris, K. M. (1998). Synaptogenesis via dendritic filopodia in developing hippocampal area CA1. *J. Neurosci.* 18, 8900–8911.

Fortin, D. A., Davare, M. A., Srivastava, T., Brady, J. D., Nygaard, S., Derkach, V. A., et al. (2010). Long-term potentiation-dependent spine enlargement requires synaptic Ca2+-permeable AMPA receptors recruited by CaM-kinase I. *J. Neurosci.* 30, 11565–11575. doi: 10.1523/JNEUROSCI.1746-10.2010

Gao, C., and Chen, Y. G. (2010). Dishevelled: the hub of Wnt signaling. *Cell. Signal.* 22, 717–727. doi: 10.1016/j.cellsig.2009.11.021

Giese, K. P., Aziz, W., Kraev, I., and Stewart, M. G. (2015). Generation of multi-innervated dendritic spines as a novel mechanism of long-term memory formation. *Neurobiol. Learn. Mem.* 124, 48–51. doi: 10.1016/j.nlm.2015.04.009

Gogolla, N., Galimberti, I., Deguchi, Y., and Caroni, P. (2009). Wnt signaling mediates experience-related regulation of synapse numbers and mossy fiber connectivities in the adult hippocampus. *Neuron* 62, 510–525. doi: 10.1016/j.neuron.2009.04.022

Hall, A. C., Lucas, F. R., and Salinas, P. C. (2000). Axonal remodeling and synaptic differentiation in the cerebellum is regulated by WNT-7a signaling. *Cell* 100, 525–535. doi: 10.1016/s0092-8674(00)80689-3

Herring, B. E., and Nicoll, R. A. (2016). Long-term potentiation: from CaMKII to AMPA receptor trafficking. *Annu. Rev. Physiol.* 78, 351–365. doi: 10.1146/annurev-physiol-021014-071753

Hruska, M., Henderson, N., Le Marchand, S. J., Jafri, H., and Dalva, M. B. (2018). Synaptic nanomodules underlie the organization and plasticity of spine synapses. *Nat. Neurosci.* 21, 671–682. doi: 10.1038/s41593-018-0138-9

Jones, T. A., Chu, C. J., Grande, L. A., and Gregory, A. D. (1999). Motor skills training enhances lesion-induced structural plasticity in the motor cortex of adult rats. *J. Neurosci.* 19, 10153–10163.

Malenka, R. C., and Bear, M. F. (2004). LTP and LTD: an embarrassment of riches. *Neuron* 44, 5–21. doi: 10.1016/j.neuron.2004.09.012

Marzo, A., Galli, S., Lopes, D., McLeod, F., Podpolny, M., Segovia-Roldan, M., et al. (2016). Reversal of synapse degeneration by restoring wnt signaling in the adult hippocampus. *Curr. Biol.* 26, 2551–2561. doi: 10.1016/j.cub.2016.07.024

McLeod, F., Bossio, A., Marzo, A., Ciani, L., Sibilla, S., Hannan, S., et al. (2018). Wnt signaling mediates LTP-dependent spine plasticity and AMPAR localization through frizzled-7 receptors. *Cell. Rep.* 23, 1060–1071. doi: 10.1016/j.celrep.2018.03.119

McLeod, F., and Salinas, P. C. (2018). Wnt proteins as modulators of synaptic plasticity. *Curr. Opin. Neurobiol.* 53, 90–95. doi: 10.1016/j.conb.2018.06.003

McQuate, A., Latorre-Esteves, E., and Barria, A. (2017). A Wnt/calcium signaling cascade regulates neuronal excitability and trafficking of NMDARs. *Cell. Rep.* 21, 60–69. doi: 10.1016/j.celrep.2017.09.023

Munoz, F. J., Godoy, J. A., Cerpa, W., Poblete, I. M., Huidobro-Toro, J. P., and Inestrosa, N. C. (2014). Wnt-5a increases NO and modulates NMDA receptor in rat hippocampal neurons. *Biochem. Biophys. Res. Commun.* 444, 189–194. doi: 10.1016/j.bbrc.2014.01.031

Neitz, A., Mergia, E., Imbrosci, B., Petrasch-Parwez, E., Eysel, U. T., Koesling, D., et al. (2014). Postsynaptic NO/cGMP increases NMDA receptor currents via hyperpolarization-activated cyclic nucleotide-gated channels in the hippocampus. *Cereb. Cortex* 24, 1923–1936. doi: 10.1093/cercor/bht048

Nikonenko, I., Boda, B., Steen, S., Knott, G., Welker, E., and Muller, D. (2008). PSD-95 promotes synaptogenesis and multiinnervated spine formation through nitric oxide signaling. *J. Cell Biol.* 183, 1115–1127. doi: 10.1083/jcb.200805132

Nikonenko, I., Jourdain, P., and Muller, D. (2003). Presynaptic remodeling contributes to activity-dependent synaptogenesis. *J. Neurosci.* 23, 8498–8505.

Nikonenko, I., Nikonenko, A., Mendez, P., Michurina, T. V., Enikolopov, G., and Muller, D. (2013). Nitric oxide mediates local activity-dependent excitatory synapse development. *Proc. Natl. Acad. Sci. U.S.A.* 110, E4142–E4151. doi: 10.1073/pnas.1311927110

Parodi, J., Montecinos-Oliva, C., Varas, R., Alfaro, I. E., Serrano, F. G., Varas-Godoy, M., et al. (2015). Wnt5a inhibits K(+) currents in hippocampal synapses through nitric oxide production. *Mol. Cell. Neurosci.* 68, 314–322. doi: 10.1016/j.mcn.2015.08.011

Petrak, L. J., Harris, K. M., and Kirov, S. A. (2005). Synaptogenesis on mature hippocampal dendrites occurs via filopodia and immature spines during blocked synaptic transmission. *J. Comp. Neurol.* 484, 183–190. doi: 10.1002/cne.20468

Poglia, L., Muller, D., and Nikonenko, I. (2011). Ultrastructural modifications of spine and synapse morphology by SAP97. *Hippocampus* 21, 990–998. doi: 10.1002/hipo.20811

Radwanska, K., Medvedev, N. I., Pereira, G. S., Engmann, O., Thiede, N., Moraes, M. F., et al. (2011). Mechanism for long-term memory formation when synaptic strengthening is impaired. *Proc. Natl. Acad. Sci. U.S.A.* 108, 18471–18475. doi: 10.1073/pnas.1109680108

Sahores, M., Gibb, A., and Salinas, P. C. (2010). Frizzled-5, a receptor for the synaptic organizer Wnt7a, regulates activity-mediated synaptogenesis. *Development* 137, 2215–2225. doi: 10.1242/dev.046722

Stein, V., House, D. R., Bredt, D. S., and Nicoll, R. A. (2003). Postsynaptic density-95 mimics and occludes hippocampal long-term potentiation and enhances long-term depression. *J. Neurosci.* 23, 5503–5506.

Wayman, G. A., Impey, S., Marks, D., Saneyoshi, T., Grant, W. F., Derkach, V., et al. (2006). Activity-dependent dendritic arborization mediated by CaM-kinase I activation and enhanced CREB-dependent transcription of Wnt-2. *Neuron* 50, 897–909. doi: 10.1016/j.neuron.2006.05.008

West, A. E., and Greenberg, M. E. (2011). Neuronal activity-regulated gene transcription in synapse development and cognitive function. *Cold Spring Harb. Perspect. Biol.* 3:a005744. doi: 10.1101/cshperspect.a005744

Yang, Y., Liu, D. Q., Huang, W., Deng, J., Sun, Y., Zuo, Y., et al. (2018). Author correction: selective synaptic remodeling of amygdalocortical connections associated with fear memory. *Nat. Neurosci.* 21:1137. doi: 10.1038/s41593-018-0180-7

Zaccard, C. R., Shapiro, L., Martin-De-Saavedra, M. D., Pratt, C., Myczek, K., Song, A., et al. (2020). Rapid 3D enhanced resolution microscopy reveals diversity in dendritic spinule dynamics, regulation, and function. *Neuron* 107, 522.e6–537.e6. doi: 10.1016/j.neuron.2020.04.025

Zhang, Y., Bonnan, A., Bony, G., Ferezou, I., Pietropaolo, S., Ginger, M., et al. (2014). Dendritic channelopathies contribute to neocortical and sensory hyperexcitability in Fmr1(-/y) mice. *Nat. Neurosci.* 17, 1701–1709. doi: 10.1038/nn.3864

Conflict of Interest: The authors declare that the research was conducted in the absence of any commercial or financial relationships that could be construed as a potential conflict of interest.

frontiers in Synaptic Neuroscience

ORIGINAL RESEARCH
published: 24 May 2021
doi: 10.3389/fnsyn.2021.681068

GluN2D NMDA Receptors Gate Fear Extinction Learning and Interneuron Plasticity

Christophe J. Dubois[1†] *and Siqiong June Liu*[1,2*]

[1] Department of Cell Biology and Anatomy, LSU Health Sciences Center New Orleans, New Orleans, LA, United States,
[2] Southeast Louisiana VA Healthcare System, New Orleans, LA, United States

The cerebellum is critically involved in the formation of associative fear memory and in subsequent extinction learning. Fear conditioning is associated with a long-term potentiation at both excitatory and inhibitory synapses onto Purkinje cells. We therefore tested whether fear conditioning unmasks novel forms of synaptic plasticity, which enable subsequent extinction learning to reset cerebellar circuitry. We found that fear learning enhanced GABA release from molecular layer interneurons and this was reversed after fear extinction learning. Importantly an extinction-like stimulation of parallel fibers after fear learning is sufficient to induce a lasting decrease in inhibitory transmission (I-LTD$_{stim}$) in the cerebellar cortex, a form of plasticity that is absent in naïve animals. While NMDA (N-methyl-D-aspartate) receptors are required for the formation and extinction of associative memory, the role of GluN2D, one of the four major NMDA receptor subunits, in learning and memory has not been determined. We found that fear conditioning elevates spontaneous GABA release in GluN2D KO as shown in WT mice. Deletion of GluN2D, however, abolished the I-LTD$_{stim}$ induced by parallel fiber stimulation after learning. At the behavioral level, genetic deletion of GluN2D subunits did not affect associative learning and memory retention, but impaired subsequent fear extinction learning. D-cycloserine, a partial NMDA receptor (NMDAR) agonist, failed to rescue extinction learning in mutant mice. Our results identify GluN2D as a critical NMDAR subunit for extinction learning and reveal a form of GluN2D-dependent metaplasticity that is associated with extinction in the cerebellum.

Keywords: GluN2D NMDA receptor, fear conditioning, extinction learning, metaplasticity, long-term depression, inhibitory synapses, D-cycloserine, cerebellar molecular layer interneurons

OPEN ACCESS

Edited by:
Lu Chen,
Stanford University, United States

Reviewed by:
Christian Hansel,
University of Chicago, United States
Zhiping P. Pang,
Rutgers, The State University of New Jersey, United States

***Correspondence:**
Siqiong June Liu
sliu@lsuhsc.edu

[†]***Present address:***
Christophe J. Dubois,
CNRS, RMSB, UMR 5536, University of Bordeaux, Bordeaux, France

Received: *15 March 2021*
Accepted: *14 April 2021*
Published: *24 May 2021*

Citation:
Dubois CJ and Liu SJ (2021) GluN2D NMDA Receptors Gate Fear Extinction Learning and Interneuron Plasticity. Front. Synaptic Neurosci. 13:681068. doi: 10.3389/fnsyn.2021.681068

INTRODUCTION

Pavlovian fear learning is one of the best-characterized model systems of emotional memory in which an individual learns to associate a neutral stimulus with an aversive event. This form of associative memory can be attenuated following repetitive exposures to the neutral stimulus, producing extinction learning (Dunsmoor et al., 2015), a strategy that has been used for the treatment of anxiety and post-traumatic stress disorders (Bowers and Ressler, 2015). Our understanding of the molecular mechanism and the neuronal basis of extinction of fear memory is therefore of prime importance, but remains incomplete at present.

Fear conditioning alters synaptic transmission in a number of brain regions that are important for memory consolidation (Izquierdo et al., 2016; Bocchio et al., 2017), including the prefrontal cortex, hippocampus, and the amygdala (Apps and Strata, 2015; Tovote et al., 2015). In addition to these extensively studied neuronal circuits, clinical studies implicate the cerebellum in emotional regulation and fear memory extinction (Timmann et al., 2010; Linnman et al., 2011; Lange et al., 2015; Utz et al., 2015; Ernst et al., 2019). The cerebellum is required for associative fear memory formation, as reversible inhibition of neuronal activity or release endocannabinoids from Purkinje cells after learning disrupts memory consolidation (Sacchetti et al., 2002; Dubois et al., 2020). Associative fear learning enhances both excitatory (Sacchetti et al., 2004) and inhibitory (Scelfo et al., 2008) transmission to Purkinje cells, and reduces endocannabinoid signaling, increasing GABA release (Dubois et al., 2020). Molecular layer interneurons (MLIs) in the cerebellar cortex control the activity of Purkinje cells and thus a learning-induced enhancement of GABA release from MLIs can alter the activity and output of cerebellar circuitry (Scelfo et al., 2008). A recent study shows that the cerebellum to the ventrolateral periaqueductal gray projection regulates extinction learning (Frontera et al., 2020), indicating that the cerebellum is involved in both fear memory formation and subsequent extinction learning. We hypothesize that learning experience allows the cerebellar circuit to undergo novel form of synaptic plasticity that is absent in the naive animals, and thereby to engage in new extinction learning.

Learning-induced changes in synaptic transmission and plasticity are cellular mechanisms that underlie the formation and subsequent extinction of fear memory. Considerable evidence suggest that NMDA-dependent plasticity is a key component of the extinction learning processes (Sotres-Bayon et al., 2007; Davis, 2011; Ogden et al., 2014). NMDA receptors are tetrameric glutamate receptors composed of two GluN1 subunits associated with GluN2/3 (GluN2A–2D; GluN3A–3B) subunits. Of the four GluN2 subunits, GluN2D subunits are expressed at high levels in inhibitory interneurons and exhibit two distinct properties, very high affinity for glutamate and exceedingly slow deactivation time course (Cull-Candy and Leszkiewicz, 2004). Thus these receptors are capable of detecting low levels of spillover glutamate and play an important role in the plasticity of interneurons (Hunt and Castillo, 2012; Paoletti et al., 2013). D-cycloserine, a partial NMDAR agonist has been shown to promote extinction in rodents (Walker et al., 2002; Ledgerwood et al., 2005; Mao et al., 2006) and has a higher binding affinity for receptors that contain GluN2C and GluN2D subunits than other subunits (Sheinin et al., 2001; Dravid et al., 2010). This is important because potentiation of GluN2C/2D-containing NMDARs with CIQ ((3-Chlorophenyl) [3,4-dihydro-6,7-dimethoxy-1-[(4-methoxyphenoxy)methyl]-2(1H)-isoquinolinyl]methanone) is sufficient to promote extinction learning (Ogden et al., 2014). While deletion of GluN2C leads to a deficit in associative fear learning (Hillman et al., 2011), inhibition of GluN2B-containing receptors impairs extinction of fear memory (Sotres-Bayon et al., 2007). Surprisingly, GluN2D function in behavior remains unknown, largely due to the lack of selective inhibitors. Given the unusual high sensitivity of GluN2D-containing NMDA receptors for glutamate and D-cycloserine and their unique involvement in synaptic plasticity, we tested the hypothesis that GluN2D-containing NMDARs are required for the extinction of fear memory and extinction learning-induced synaptic plasticity in cerebellar interneurons.

Here we show that fear conditioning induced a lasting increase in GABA release from cerebellar MLIs and extinction learning reduced inhibitory transmission. After fear conditioning, stimulation of cerebellar parallel fibers (the axons of granule cells, PFs) using a protocol that mimics extinction learning, induced a lasting suppression of GABA release (I-LTD$_{stim}$), and genetic deletion of GluN2D abolished I-LTD$_{stim}$. This form of plasticity occurs only in conditioned mice and requires GluN2D-containing NMDARs. At behavioral level GluN2D knockout mice exhibited impaired extinction learning and memory. Furthermore, D-cycloserine and retrieval session, which accelerated extinction learning in wildtype mice, no longer enhanced extinction in GluN2D knockout mice. Therefore GluN2D is crucial for extinction learning and associated synaptic plasticity.

MATERIALS AND METHODS

Animals

Male mice on a C57Bl/6J background were used for this study. These animals were either wildtype (Jackson laboratory Bar Harbor, ME, United States) or GluN2D KO mice (Ikeda et al., 1995; Dubois et al., 2016). Breeding colonies were maintained in our animal facility on a 12h light/dark cycle, with *ad libitum* food and water. Genotyping was performed by Mouse Genotype[1], using a common forward sequence GCAGGCCCCTGCCTCCTCGCTC, a reverse GluN2D KO primer sequence TGGATTGCACGCAGGTTCTC, and a reverse wild-type primer sequence CTGACCTCATCCTCAGATGAG generating a PCR product of 982 bp for GluN2D KO, and 281 bp for GluN2D wildtype. Experimental procedures were in accordance with the US National Research Council's Guide for the Care and Use of Laboratory Animals and approved by the Louisiana State University Health Sciences Center guidelines for care and use of laboratory animals (IACUC).

Fear Conditioning Apparatus

Context A Fear conditioning experiments were conducted in a non-reflective black box with 28 × 28 × 30 cm dimensions. Stainless steel rods (spaced at 0.5 cm) delivered a 0.75 mA foot-shock (unconditioned stimulus, United States) via a shock delivery apparatus (Model H13–15, Coulbourn Instruments, Holliston, MA, United States). The conditioned stimulus (CS) was a 3.5 kHz sound at 75 dB delivered through a 75 mm speaker. The conditioning apparatus was placed in a sound–reducing chamber (typical background noise was 65 dB). The timing and

[1]http://mousegenotype.com

length of both the CS and US were set using custom software written by Dr. Iaroslav Savtchouk (Marquette University).

Context B The memory retention test and extinction training were conducted in a plastic chamber (20 × 35 × 40 cm) with off-white color walls and white paper bedding covering the floor. The speaker was positioned at a different location relative to context A to deliver the CS. The apparatus was placed in the sound–reducing chamber.

Fear Conditioning Procedure

Experiments took place at the beginning of the dark phase. The experimenter was blind to the genotype of the animals at the time of the test. All animals were identified by marks on the tail and weighed 1 h before the conditioning session on both days. All experiments were video-recorded (Windows Media Encoder, Microsoft) and stored on a computer for off-line analysis.

Fear Conditioning (Context A)

On day one, 2–3 months-old males were positioned in the center of the arena and allowed to explore for 2 min. Conditioning consisted of two or eight pairings of a 10 s sound (CS) co-terminated with a 1 s foot-shock (US). Each pairing started 30 s apart. After a 2 min recovery period, animals were returned to their home cage until the next day.

Drug Injections

In some experiments, mice were injected i.p 30 min prior to cued memory retention and extinction learning testing. After saline injections all tested parameters were identical to non-injected animals. Therefore, results from saline-injected and non-injected animals were pooled for presentation of D-cycloserine experiments.

Cued Memory Retention and Extinction Learning (Context B)

These procedures were conducted on day 2 in Context B and mice were positioned in the center of the arena. When conditioned with two pairings of US/CS, after a 2 min habituation period, 8 CS of 10 s were presented every 30 s. When conditioned with eight pairings, mice were first exposed to a retrieval CS in context B, following a 2 min acclimation period, and then returned to their home cage for 30 min. Mice were then exposed to a series of twenty 10 s CS every 30 s and a second extinction session of 20 CS, 30 min later.

Extinction Retention (Context B)

Following two extinction sessions, mice were tested for extinction retention with 4 CS exposure every 30 s on day 3.

Behavioral Quantification

A freezing (immobility) episode was defined as a complete absence of movement apart from respiratory activity for at least 1 s. This was characterized by the amount of motion that occurred between two successive video frames, using a custom-written program previously described (Liu et al., 2010). The duration of freezing responses was determined during the 2 min of habituation and during the first 9 s of each tone.

Behavioral Procedures for Electrophysiology

All conditioning procedures were conducted during the dark phase of the light/dark cycle, about 15 h before slice preparation. Male mice were submitted to a conditioning procedure that was identical to the one described for behavioral testing, with eight pairings of CS/US. To ensure a slice quality that would allow us to conduct stable patch-clamp recordings for over an hour, 3–5 weeks old mice were used for electrophysiology experiments. Although at this age mice were less spontaneously active, they exhibited fear learning (41% increase from basal freezing; n = 45, data not shown) and extinction (36% decrease, from tone 1 to tone 8, n = 17, data not shown). Furthermore, the frequency of IPSCs and synaptic plasticity in stellate cells was not different from 2 to 3 months old mice (18–33 days-old mice IPSC frequency 5.3 ± 0.6 Hz, n = 17; 46–90 days-old mice IPSC frequency 5.3 ± 1.7 Hz, n = 5; two-sided P value of the Mann–Whitney test is 0.959, data not shown).

Cerebellar Slice Preparation and Electrophysiology

Cerebellar slices were prepared as previously described (Liu and Cull-Candy, 2000; Dubois et al., 2016). Briefly, the cerebellum was isolated and horizontal slices (400 μm) were cut using a vibratome (Leica VT1200) in ice cold artificial CSF (containing in mM: 81.2 NaCl, 2.4 KCl, 23.4 $NaHCO_3$, 1.4 NaH_2PO_4, 6.7 $MgCl_2$, 0.5 $CaCl_2$, 23.3 glucose, 69.9 sucrose, and pH 7.4). Slices were then maintained in aCSF (in mM: 125 NaCl, 2.5 KCl, 26 $NaHCO_3$, 1.25 NaH_2PO_4, 1 $MgCl_2$, 2 $CaCl_2$, 25 glucose, and pH 7.4) saturated with 95% O_2, 5% CO_2 at room temperature for at least 30 min before recording.

Whole cell patch clamp recordings were obtained at near physiological temperature (35–37°C) from cerebellar stellate cells in an O_2/CO_2-saturated aCSF. Stellate cells were identified by their location in the outer two thirds of the molecular layer and by the presence of spontaneous action potentials in the cell-attached mode. Analog signals were filtered at 6 kHz and digitized at 20 kHz (Multiclamp 700A, Axon Instruments). Series resistance was monitored throughout the recordings. Recordings were terminated if series resistance changed by more than 20%.

Long-Term Depression of Inhibitory Transmission

Miniature inhibitory synaptic currents (mIPSCs) were recorded in stellate cells in the presence of 0.5 μM TTX (Tetrodotoxin) in aCSF, using borosilicate electrodes (6–8 MΩ) filled with a low chloride pipette solution (in mM: 120 Cs acetate, 0.4 $MgCl_2$, 0.1 $CaCl_2$, 2.5 MgATP, 0.4 Na_2GTP, 1.5 Na_2ATP, 10 Cs-EGTA, 5 QX-314 and 10 HEPES, and pH 7.3). Using this internal solution, when putative stellate cells were voltage-clamped at –30 mV, the chloride-mediated mIPSCs were recorded as outward currents (blue events on **Figure 1B**) whereas cation-mediated mEPSCs appeared as inward currents (green events in **Figure 1B**), allowing for separation of IPSCs from EPSCs without the use of pharmacological agents. Indeed,

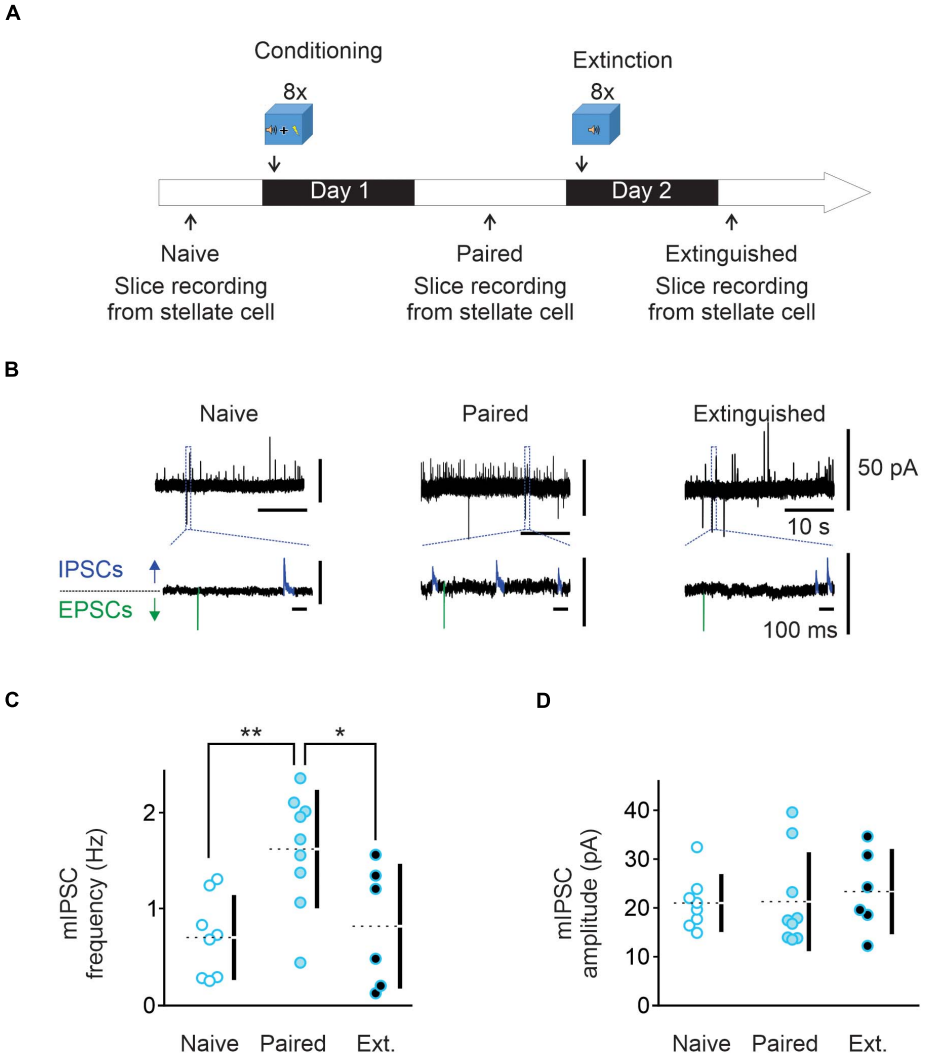

FIGURE 1 | Fear conditioning enhances and extinction learning reduces spontaneous GABA release from cerebellar molecular layer interneurons. **(A)** Conditioning protocol. Male mice (n = 9) were habituated for 2 min in the conditioning chamber (context A) and exposed to eight pairings of a 10 s tone that co-terminated with a 1 s foot-shock (paired animals). Mice were left in the conditioning chamber for another 2 min before being returned to their home cage. Cerebellar slices were prepared and electrophysiology experiments were performed 15 h later. A subset of Extinguished mice (n = 6) were exposed to eight tones alone 24 h after fear conditioning protocol. Cerebellar slices were prepared and electrophysiology experiments were performed 15 h later. **(B)** Representative traces recorded in putative stellate cells from the three behavioral groups at -30 mV. The *bottom* traces are enlargements of regions designated by the dashed lines. In these traces, outward IPSCs are highlighted in blue while inward EPSCs are shown in green. **(C,D)** Individual frequency and amplitude of the recorded mIPSCs from the three behavioral groups. Mean values are represented as doted lines. *$P < 0.05$; **$P < 0.01$. Statistical analysis values can be found in the **Supplementary Table 1**.

pharmacologically blocking glutamatergic neurotransmission to isolate mIPSC would interfere with activation of NMDA receptors during the parallel fiber stimulation. After at least 15 min of stable recording (control period), TTX was washed out for 20 min. Parallel fibers were then stimulated using a parallel bipolar electrode (150 μm branch spacing, 200 μm from the recording electrode). The stimulation strength was adjusted to evoke NMDA receptor currents at +40 mV in response to a single burst stimulation (four stimuli at 100 Hz) and ranged from 5 to 45 V (200 μs duration). I-LTD$_{stim}$ was then induced using 15 trains of burst stimulation (four stimuli at 100 Hz repeated every second for 15 s). The postsynaptic cell was voltage-clamped at –60 mV during the parallel fiber stimulation. TTX was re-introduced into the aCSF and recordings of mIPSCs were resumed within 2 min and lasted for 30–50 min.

Data Analysis

Clampfit 9.0 (Axon Instruments) was used for mIPSCs analysis using an event detection template. The average frequency and amplitude were calculated over periods of 5 min. Miniature EPSC frequency was very low as granule cells were not spontaneously active, and therefore was not quantified.

No statistical method was used to predetermine sample sizes, but they are similar to previous studies (Liu and Cull-Candy, 2000; Lachamp et al., 2009; Dubois et al., 2016, 2020). Each data set was obtained from mice from at least three different litters. Statistical analyses were performed using the estimation statistics webpage[2]. Mann–Whitney test was used to test for significance between the means of two independent groups. Comparison between the means of three or more independent groups of normally distributed data was conducted using a one-way analysis of variance (ANOVA). A two-way ANOVA was used to test for an interaction between two independent variables and the dependent variable. The paired-sample Wilcoxon test was used to test for significance between the amplitude and frequency of miniature inhibitory currents recorded before and after synaptic stimulation. All values are represented as mean ± SEM and a P value of 0.05 was considered as significant. All tests were performed on primary data (not normalized). For detailed statistical analysis, see the **Supplementary Table 1**. Data will be available upon request from the corresponding author.

RESULTS

Fear Conditioning Increases Spontaneous GABA Release, and This Is Reversed by Extinction Training

Fear conditioning has been shown to induce a lasting increase in spontaneous GABA release onto Purkinje and MLIs (Scelfo et al., 2008; Dubois et al., 2020). We determined the effects of learning and extinction paradigms on GABA release from MLIs to synaptic connected MLIs. Animals were subject to eight pairs of a tone co-terminated with a mild electric footshock (paired group). Cerebellar slices were prepared from naïve and conditioned mice next day (**Figure 1A**). Miniature IPCSs were recorded at –30 mV in the presence of 0.5 μM TTX in putative stellate cells in the vermal lobules V/VI, where nociceptive and acoustic stimuli converge in the cerebellum. Using a low chloride pipette solution, mIPSCs were recorded as outward currents (blue in **Figure 1B**) and mEPSCs as inward currents (green in **Figure 1B**). In MLIs from naïve mice, the average mIPSC frequency was 0.69 ± 0.15 Hz and amplitude was 20 ± 2 pA (n = 8, **Figures 1B–D**). After fear conditioning, the average mIPSC frequency was increased to 1.62 ± 0.2 Hz (n = 9, **Figures 1B,C**) while the amplitude remained unchanged at 21 ± 3 pA (**Figures 1B,D**). These results suggest that fear conditioning increases spontaneous GABA release, but not the postsynaptic response, consistent with previous observation in Purkinje cells (Scelfo et al., 2008).

Next, a group of animals were exposed to a series of eight tones without footshock in a novel environment one day after fear conditioning paradigm (Extinction group) as depicted in **Figure 1A**. Cerebellar slices were prepared 15 h later. We found that mIPSC frequency was markedly reduced compared to the paired group (I-LTD$_{ext}$, 0.81 ± 0.25 Hz, n = 6; **Figures 1B,C**), and was comparable to that obtained in naïve animals. The amplitude of mIPSCs was unchanged compared to naïve and paired groups, with an average value of 23 ± 3 pA (**Figure 1D**). Therefore, extinction learning reverts the learning-induced increase in spontaneous GABA release to a level indistinguishable from the naïve state.

[2]https://www.estimationstats.com

An Extinction-Like Stimulus After Fear Conditioning Induces a Lasting Decrease in GABA Release, I-LTD$_{stim}$

In the cerebellar cortex, acoustic stimulation activates parallel fibers (Aitkin and Boyd, 1978), and therefore the CS (*i.e.*, tones) during the extinction protocol, is expected to stimulate these excitatory inputs. We tested whether stimulation of parallel fibers in slices prepared from conditioned mice can induce a lasting decrease in GABA release, to account for the reduction observed after *in vivo* extinction learning.

Slices were obtained 15 h after fear conditioning (**Figure 2A**). We recorded mIPSCs in stellate cells in the presence of 0.5 μM TTX to assess spontaneous GABA release in lobules V/VI. After obtaining a stable baseline, TTX was washed out for 20 min and we stimulated parallel fibers with 15 trains of four stimulations at 100 Hz repeated at 1 Hz (**Figure 2B**). TTX was then re-introduced and recording of mIPSCs was resumed for 30 min or longer. We found that parallel fiber stimulation induced a rapid decrease in the mIPSC frequency from 1.5 ± 0.15 to 1.04 ± 0.14 Hz (n = 5, **Figures 2C,D**), a level that is comparable with the one observed after *in vivo* extinction learning. This reduction in mIPSC frequency was observed in all cells recorded and lasted for at least 30–50 min after stimulation without changing the mIPSC amplitude. These results suggest that stimulation of parallel fibers in slices from conditioned animals triggers a lasting decrease in GABA release from MLIs (I-LTD$_{stim}$, parallel fiber stimulation-induced long-term depression at inhibitory synapses) that mimics the I-LTD$_{ext}$ observed after extinction of associative fear learning.

Learning can unmask novel forms of synaptic plasticity that are absent in naïve animals, inducing a form of metaplasticity, that enables subsequent experience such as extinction to reset synaptic transmission (Hulme et al., 2013). Our previous work has shown that stimulation of parallel fibers induces a lasting increase in GABA release from stellate cells in naïve mice (I-LTP, Dubois et al., 2016). However, after fear conditioning it induced a sustained decrease in GABA release from cerebellar interneurons (I-LTD$_{stim}$). Therefore, fear conditioning enables the parallel fiber stimulation to induce I-LTD$_{stim}$, a stimulus that produces I-LTP in naïve mice, giving rise to a form of metaplasticity.

I-LTD$_{stim}$ Requires GluN2D-Containing NMDA Receptors

We have previously shown that MLIs, like many other inhibitory interneurons, express GluN2D subunits. In naïve mice GluN2D and GluN2B subunits form tri-heteromeric receptors (GluN1/2B/2D) and activation of these receptors induces I-LTP (Dubois et al., 2016). Extinction learning is known to require activation of NMDA receptors, but the role of GluN2D in

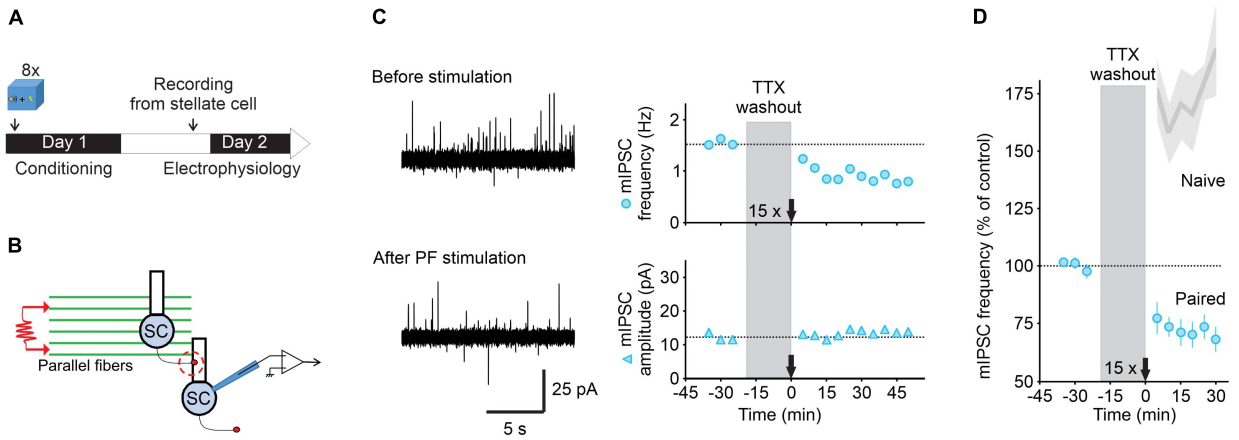

FIGURE 2 | Parallel fiber stimulation triggers a long-lasting decrease in GABA release after fear learning. **(A)** Fear conditioning protocol for electrophysiology experiments. **(B)** Schematic of the experimental procedure. **(C)** Left, representative traces of mIPSCs recorded in a stellate cell at -30 mV (outward currents) before (top) and after (bottom) PF stimulation (15 trains of four pulses at 100 Hz). Right, corresponding time course of mIPSC frequency (top) and amplitude (bottom). **(D)** While this protocol triggered I-LTP in naïve wildtype animals [Shaded gray represent data from Dubois et al. (2016)], after fear conditioning burst activation of parallel fibers induced I-LTD$_{stim}$ (n = 5). Values are mean ± SEM. Statistical analysis values can be found in the **Supplementary Table 1**.

extinction is not known. We therefore tested the role of GluN2D in I-LTD$_{stim}$ induced by the extinction-like stimulus after fear conditioning.

We used homozygous GluN2D knockout mice in which no GluN2D protein was detected (Ikeda et al., 1995). Deletion of GluN2D abolished characteristic low conductance currents in single channel recording and reduced NMDAR-current decay time, indicating a loss of functional GluN2D subunits in these neurons (Dubois et al., 2016). We have previously shown that deletion of GluN2D did not alter glutamate release from parallel fibers, nor spontaneous GABA release from MLIs in naïve mice (Dubois et al., 2016). First, we tested whether learning still can increase GABA release in GluN2D KO mice. The average mIPSC frequency in naïve GluN2D KO mice was 0.68 ± 0.16 Hz with an amplitude of 24 ± 2 pA (n = 10, **Figures 3A,B**), comparable with that in naïve wildtype mice. One day after fear conditioning acquisition mIPSCs frequency in MILs rose to 1.96 ± 0.44 Hz (n = 11, **Figures 3A,B**) while the amplitude remained unaltered (22 ± 2 pA). This increase in spontaneous mIPSC frequency was similar to that observed in wildtype mice after conditioning. Thus deletion of GluN2D did not affect basal and learning-induced change inhibitory transmission.

We next investigated the role of GluN2D-containing receptors in I-LTD$_{stim}$ after fear conditioning using GluN2D KO mice (**Figures 3C,D**). In contrast to wildtype mice, activating parallel fibers with 15 trains of stimuli after fear conditioning failed to reduce the frequency (1.42 ± 0.56 Hz, n = 6, **Figures 3E–G**) or amplitude of mIPSCs recorded in MLIs (24 ± 2 pA, **Figures 3E–G**). The failure to induce I-LTD$_{stim}$ in GluN2D KO mice is unlikely to be due to a change in GABA release since deletion of GluN2D did not alter GABA release in naïve and conditioned mice (Dubois et al., 2016 and **Figures 1C, 2B**). Therefore, GluN2D-containing NMDA receptors are critical for the induction of I-LTD$_{stim}$. Because the 15 train-parallel fiber stimulation induced I-LTP in naïve mutant animals (Dubois et al., 2016), learning unmasks a novel role of GluN2D in regulating GABA release from MLIs.

Genetic Deletion of GluN2D-Containing NMDA Receptors Abolishes Fear Extinction Learning

NMDA receptor-dependent neuronal plasticity is a key component of the extinction learning process (Sotres-Bayon et al., 2007; Davis, 2011; Ogden et al., 2014). We confirmed NMDA receptors mediates extinction learning as administration of memantine (5 mg/kg, i.p.), an NMDAR inhibitor (Bresink et al., 1996), 30 min before extinction abolished extinction learning in wildtype mice (**Supplementary Figures 3A–C**) without a change in learning acquisition (**Supplementary Figures 1A,C**). Thus activation of NMDA receptors is required for fear extinction learning in our paradigm. While GluN2B-containing receptors contribute to extinction of fear memory (Sotres-Bayon et al., 2007), the role of GluN2D in learning and memory remains unknown. Our results so far show that fear conditioning increases GABA release from MLIs. When exposed *in vivo* to an extinction protocol, GABA release returns to pre-conditioning levels (I-LTD$_{ext}$). This LTD of inhibitory synapses can be mimicked *in vitro* with an extinction-like stimulation of the parallel fibers (I-LTD$_{stim}$). This form of plasticity requires the activation of NMDA receptors that contain GluN2D subunits. We therefore determined whether the GluN2D subunits of NMDA receptors are also required for extinction of fear memory.

We assessed whether the genetic deletion of GluN2D affected associative fear learning using a paradigm that consists of eight pairings of a tone (CS) co-terminated with an electric foot shock (US, **Figure 4A**) in context A. Both wildtype (n = 15) and GluN2D KO mice (n = 7) exhibited low freezing during the acclimation period (**Figure 4B**), and a

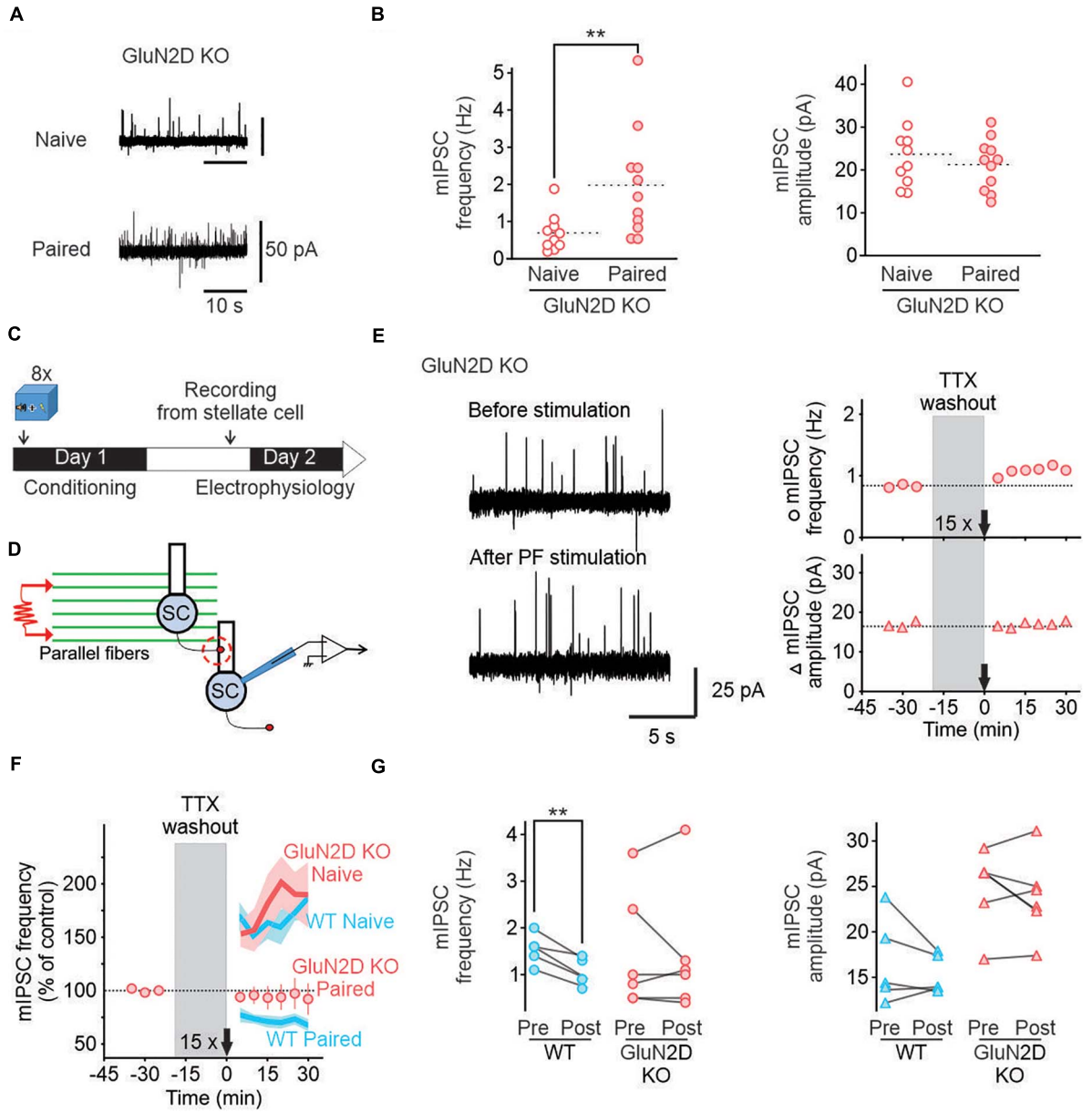

FIGURE 3 | Deletion of GluN2D subunits abolishes I-LTD$_{stim}$ in conditioned mice. **(A)** Representative traces of mIPSCs in stellate cells from naïve (*top*) and paired (*bottom*) GluN2D KO mice. **(B)** Individual frequencies and amplitudes of mIPSCs in naïve (open red circle, $n = 10$) and paired mutant animals (filled red circles, $n = 11$). **(C)** Fear conditioning protocol for electrophysiology experiments. **(D)** Schematic of the experimental procedure. **(E)** *Left*, Example traces of mIPSCs recorded in MLIs before (*top*) and after (*bottom*) parallel fiber stimulation (15 trains of four pulses at 100 Hz) in GluN2D KO mice after fear conditioning. *Right*, corresponding time course of mIPSC frequency (top) and amplitude (bottom). **(F)** Average time course of mIPSC frequency normalized to before parallel fiber stimulation in GluN2D KO mice (red circles, values are mean ± SEM) after fear learning. Wildtype naïve and paired group average values (blue lines) and SEM (light blue area) are data from **Figure 3** represented for reference. **(G)** Summary of the individual frequencies (*left*) and amplitudes (*right*) before (*Pre*) and 15–30 min after parallel fiber stimulation (*Post*). $^{**}P < 0.01$. Statistical analysis values can be found in the **Supplementary Table 1**.

similar level of total travel distance and time spent in the center, but reduced number of entries into the center square in the open field test (**Supplementary Figure 2**). During learning, tone-evoked freezing increased in GluN2D KO mice, which was comparable to the level observed in wildtype mice (**Figure 4B**). Thus, GluN2D deletion did not affect basal freezing nor fear learning acquisition. Next day, mice were tested for the retention of fear memory in context B. During the acclimation period both genotypes exhibited very little freezing (**Figure 4B**), indicating no fear generalization. When presented with a single tone, both wildtype and GluN2D KO mice exhibited tone-evoked freezing (**Figures 4B,C**). This

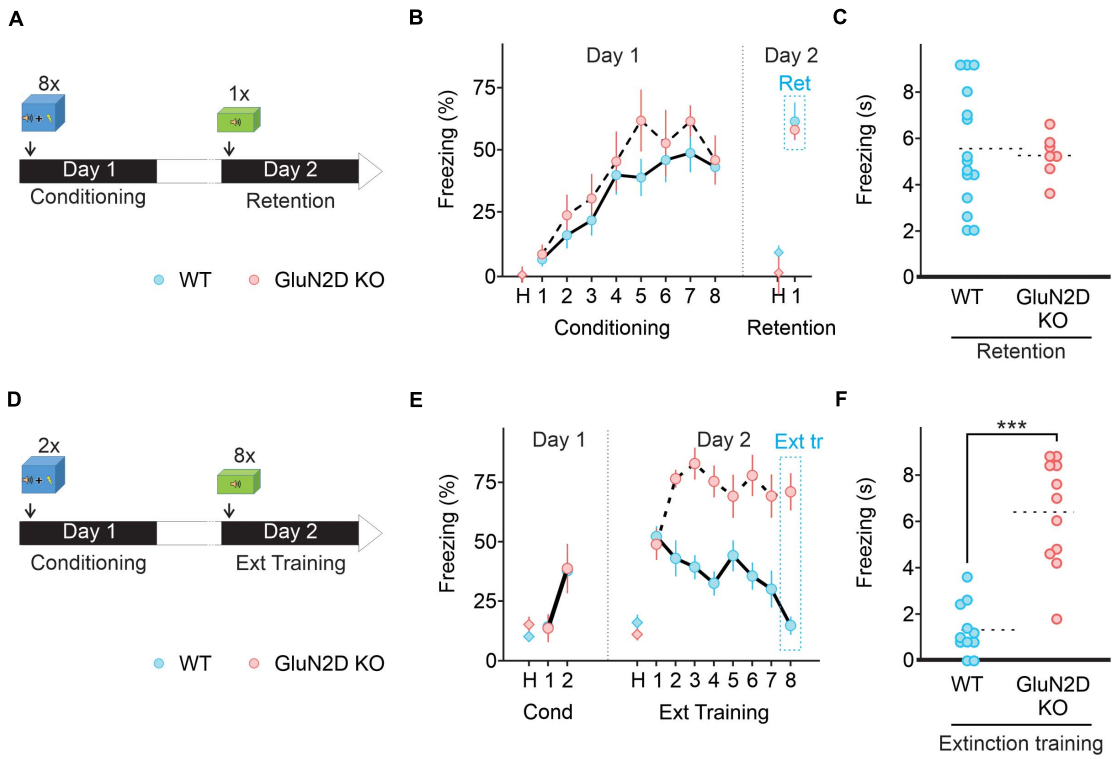

FIGURE 4 | Deletion of GluN2D does not alter fear conditioning learning or memory retention but abolishes extinction learning. **(A)** Protocol used for fear conditioning. Mice were habituated for 2 min in the conditioning chamber (context A) and exposed to eight pairings of a 10 s tone that co-terminated with a 1 s foot-shock. Mice were then left in the conditioning chamber for 2 min and returned to their home cage. Next day mice were exposed to a single 10 s tone in context B. **(B)** Percentage of freezing in wildtype (blue symbols, $n = 10$) and GluN2D KO mice (red symbols, $n = 8$) during the habituation period (H), the conditioning training (tones 1–8) and retention test tone. **(C)** Freezing time in individual animals during fear memory retention test. Mean values are represented as doted lines. **(D)** A two pairing conditioning paradigm was used. Next day retention and extinction learning (Ext tr) were tested in context B by exposing the animals to eight 10 s tones after 2 min of habituation. **(E)** GluN2D KO mice (red symbols, $n = 11$), but not wildtype (blue symbols, $n = 11$), showed impaired extinction learning assessed on the last tone. **(F)** Freezing time in individual animals at the end of extinction training. Mean values are represented as doted lines. $^{***}P < 0.001$. Values in the time courses are mean ± SEM. Statistical analysis values can be found in the **Supplementary Table 1**.

result indicates that genetic deletion of GluN2D did not affect memory retention.

Since GluN2D was not required for learning and memory retention, we determined its role in the extinction of fear memory. Mice were subject to two pairs of tone and footshocks on day one, a learning paradigm that has been widely used to evaluate subsequent extinction learning (**Figure 4D**). Next day wildtype mice exhibited an increase in freezing in response to the first tone of the extinction training, reflecting a successful fear memory retention (**Figure 4E**). The freezing time markedly decreased to the following tones and returned to the basal level on the last tone, indicating successful extinction learning. In contrast to wildtype mice, GluN2D KO mice exhibited a high level of freezing throughout the extinction protocol, and therefore did not show any extinction learning (**Figures 4E,F**). A subset of mice was re-exposed to tones on day 3 (**Supplementary Figure 3A**) to quantify extinction memory. On the first tone wildtype mice exhibited a low level of freezing response, as observed at the end of extinction training ($n = 4$). As expected GluN2D KO mice ($n = 5$) showed an elevated level of freezing during extinction memory test, indistinguishable from that detected in original memory retention test, (**Supplementary Figure 3**) suggesting the inability of these mice to extinguish fear memories. These results suggest that GluN2D-containing NMDA receptors are required for the extinction of fear memories.

D-Cycloserine and Retrieval-Extinction Paradigm Fail to Rescue Extinction Learning in GluN2D KO Mice

Extinction learning and retrieval behaviors are influenced by a number of pharmacological agents and behavior strategies (Pittig et al., 2016; Singewald and Holmes, 2019). One of the pharmacological agents is D-cycloserine (DCS) that binds to and potentiates NMDARs and can accelerate extinction learning and facilitates memory formation (Lee et al., 2006; Kuriyama et al., 2011; Peyrovian et al., 2019). Because deletion of GluN2D impaired extinction learning, we tested whether administration of D-cycloserine was able to reverse the deficit of extinction learning in GluN2D KO mice. Animals received an injection of saline or 10 mg/kg D-cycloserine 30 min before extinction learning (**Figure 5A**). We show that administration of

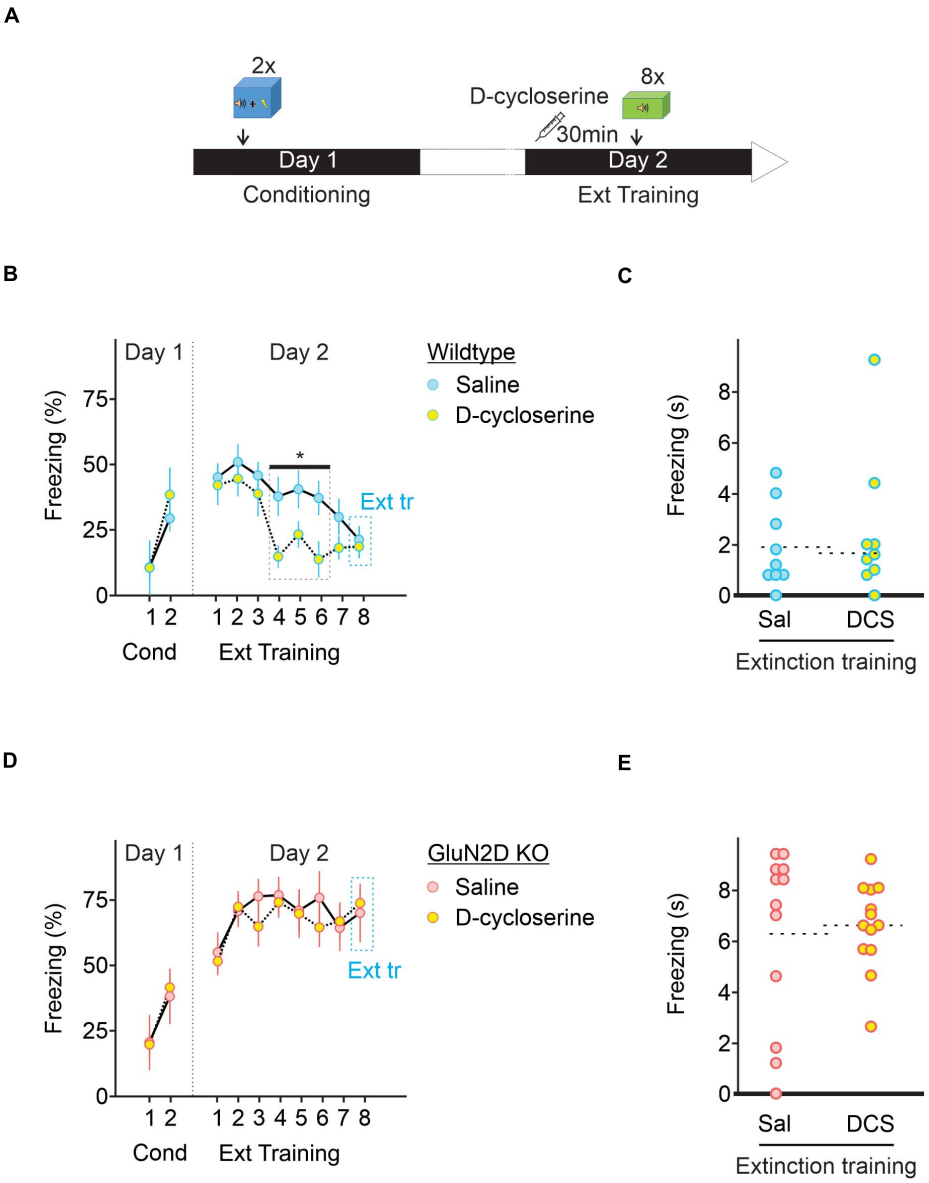

FIGURE 5 | D-cycloserine fails to rescue extinction learning in GluN2D KO mice. **(A)** Wildtype and GluN2D KO mice were injected with D-cycloserine (DCS, 10 mg/kg; i.p.) or saline (Sal), 30 min before fear extinction learning. **(B)** Freezing response in wildtype mice injected with either saline (blue symbols, $n = 9$) or D-cycloserine (yellow symbols, $n = 8$) showed that D-cycloserine administration significantly accelerated extinction learning on tones 4–6. **(C)** Individual values for freezing response during extinction training. **(D)** Freezing response in GluN2D KO mice injected with either saline (red symbols, $n = 12$) or D-cycloserine (yellow symbols, $n = 13$) showed that D-cycloserine administration failed to accelerate extinction learning. **(E)** Individual freezing values at the end of the extinction training. $^*P < 0.05$. Values are mean ± SEM. Statistical analysis values can be found in the **Supplementary Table 1**.

D-cycloserine did not affect fear memory retention in wildtype animals, but accelerated extinction learning, with a marked reduction in freezing response during tones 4–6 relative to saline injected animals ($n = 10$, **Figures 5B,C**). However, GluN2D KO mice exhibited a high level of freezing throughout extinction training and thus D-cycloserine failed to rescue extinction learning in these mice (**Figures 5D,E**). Therefore genetic deletion of GluN2D attenuates the ability of D-cycloserine to facilitate extinction learning. Considering that NMDA receptors containing this subunit have higher affinity for D-cycloserine (Dravid et al., 2010; Jessen et al., 2017), these receptors may represent the site of action of D-cycloserine.

One behavior strategy to enhance fear extinction is to include a retrieval trial, which is thought to initiate memory reconsolidation phase, a process that involves the cerebellum (Sacchetti et al., 2007). During the reconsolidation window extinction training can produce a persistent reduction in fear responses in mice (Monfils et al., 2009; Clem and Huganir,

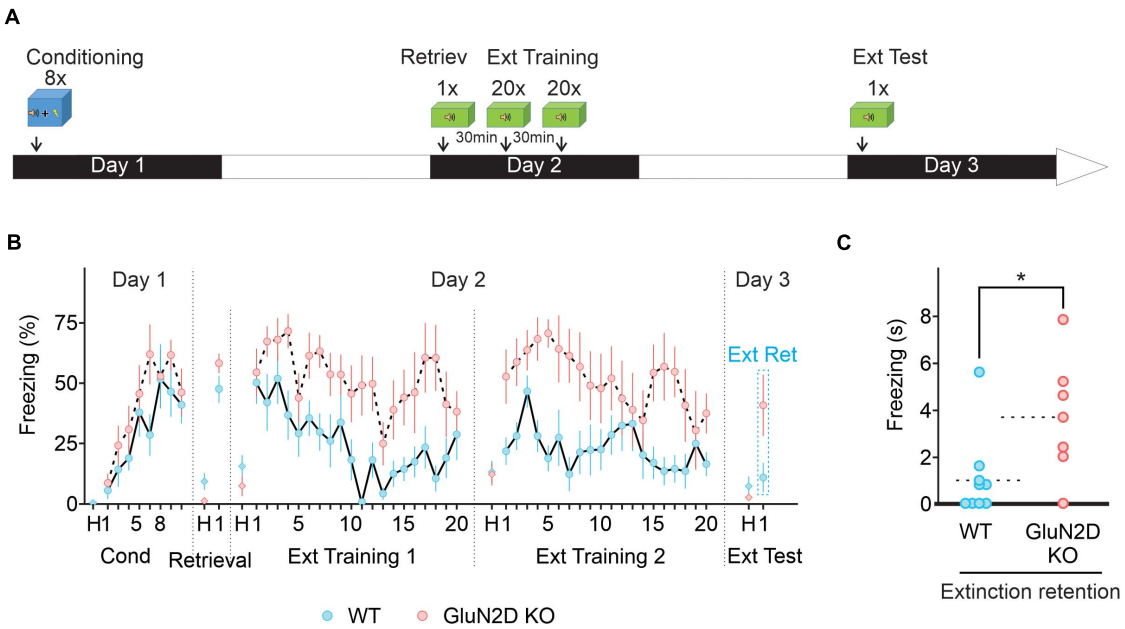

FIGURE 6 | Retrieval-extinction paradigm fails to rescue extinction learning in GluN2D KO mice. **(A)** Protocol used for retrieval-extinction paradigm. Following fear conditioning, mice were exposed to a retrieval tone in context B on day 2. Thirty min later mice underwent two extinction sessions of 20 tones 30 min apart. On day 3, mice were presented with four tones in context B to test for the retention of extinction memory. **(B)** Percentage of freezing in wildtype (blue symbols, $n = 10$) and GluN2D KO mice (red symbols, $n = 7$). Wild type mice exhibited a clear extinction learning. Extinction learning in GluN2D KO mice was attenuated compared with wild type animals. **(C)** Individual freezing values at the end of extinction training. Values in the time course are mean ± SEM. $^*P < 0.05$. Statistical analysis values can be found in the **Supplementary Table 1**.

2010) by destabilizing the original memory or facilitating the formation of extinction memory (Cahill and Milton, 2019). Retrieval-extinction protocol produces different effects on the expression levels of several molecular markers and patterns of Arc, compared with a standard extinction procedure (Tedesco et al., 2014; Lee et al., 2015), and may engage different neural mechanisms. We therefore determined whether extinction learning occurring during reconsolidation window when the memory becomes malleable also requires GluN2D. The extinction training consisted of one retrieval session (a single tone exposure) followed by two sessions of 20 tones (every 30 s) with a 30 min interval between the sessions (**Figure 6A**). In this paradigm, wildtype mice showed a marked reduction in freezing during extinction training ($n = 10$; **Figure 6B**). In contrast GluN2D KO mice displayed little extinction learning and there was no difference between the freezing on the first and the last tone during extinction learning ($n = 7$; **Figure 6B**). When extinction retention was tested on day 3 in context B, exposure to the first tone did not induce freezing in wildtype animals, indicative of a successful extinction of fear memory. However, GluN2D KO mice exhibited a high level of freezing, in response to the tone (**Figures 6B,C**). These results suggest that the GluN2D subunit of NMDARs is also critical for post-retrieval extinction of fear memories. Together our results that deletion of GluN2D subunits results in a strong inhibition of extinction learning reveal a new role for GluN2D-containing NMDARs in fear memory extinction.

DISCUSSION

NMDA receptors play a critical role in the extinction of associative fear memory by modulating synaptic plasticity (Dalton et al., 2012). Of the four NMDAR subunits, it has been shown that administration of a GluN2B inhibitor attenuates extinction (Sotres-Bayon et al., 2007) and GluN2C knockout impairs learning (Hillman et al., 2011). GluN2D subunits are expressed at a high level in GABAergic interneurons and are present at axon terminals where they modulate inhibitory transmission (Akazawa et al., 1994; Monyer et al., 1994; Thompson et al., 2000). GluN2D-containing NMDARs exhibit a very high affinity for glutamate and a brief activation of GluN2D receptors evokes a current with an exceedingly slow decay time. Such receptors are ideally suited for detecting the low levels of spillover glutamate that can modulate GABA release from inhibitory interneurons. We therefore determined the role of GluN2D in associative memory extinction and associated neural plasticity. Our results show that GluN2D-NMDARs are required for both extinction learning and an extinction-like stimulus-induced I-LTD$_{stim}$ in conditioned animals and are a key component of memory extinction and associated synaptic plasticity (**Figure 7**). Therefore selective activation of GluN2D is a novel strategy that could enhance the extinction of fear memory.

The cerebellum is not only critically involved in the consolidation and reconsolidation of associative fear memories (Sacchetti et al., 2002, 2007; Scelfo et al., 2008; Dubois et al., 2020), but also regulates extinction learning. A recent study

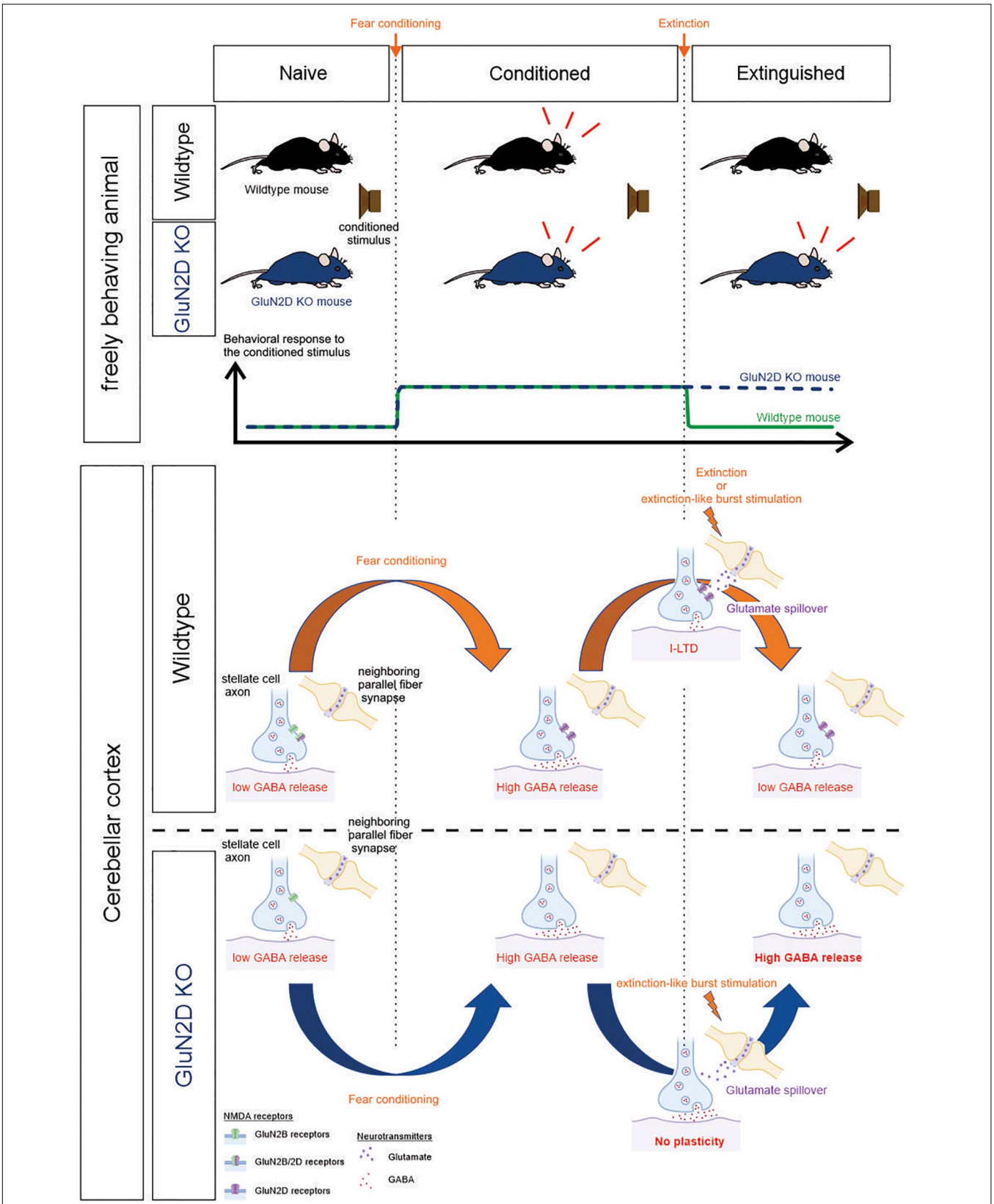

FIGURE 7 | Summary schematic. ***Top***, the behavioral response of wildtype and GluN2D KO mice during fear conditioning and extinction training. ***Bottom***, correlated cellular events at the stellate-to-stellate cell synapse in the cerebellar cortex. The bottom part of the schematic was created with biorender.com.

shows that optogenetic activation of cerebellar neurons in the fastigial nucleus that projects to vlPAG accelerates extinction learning, whereas chemogenetic inhibition of this pathway attenuates extinction (Frontera et al., 2020). Its involvement in memory extinction is further evidenced by human imaging studies (Kattoor et al., 2014; Utz et al., 2015), and impaired extinction learning of associative fear memory in mice with deletion of the L7 protein in Purkinje cells (Walton et al., 2012). Given that synaptic plasticity is the cellular substrate of learning and memory, one key question is whether extinction learning alters synaptic transmission and thereby the activity of cerebellar circuits. Here we show that while fear conditioning enhanced GABA release, extinction learning suppressed GABA release from cerebellar MLIs (I-LTD$_{ext}$). This long-term depression at inhibitory synapses in the cerebellar cortex may serve as one of the cellular mechanisms underlying extinction learning. Because an auditory tone activates the mossy fiber pathway (Aitkin and Boyd, 1978) that stimulates granule cells, burst stimulation of parallel fibers (the axons of granule cells) *in vitro* would mimic the repeated exposure to the extinction stimulus *in vivo*. We have previously shown that stimulation of parallel fibers induces a lasting increase in GABA release at MLI synapses in naïve mice (Lachamp et al., 2009; Dubois et al., 2016). In contrast to naïve mice, we show that after fear conditioning parallel fiber stimulation induces a sustained decrease in GABA release (I-LTD$_{stim}$). Thus learning enables subsequent extinction-like stimulus to induce a novel form of plasticity, and triggers synaptic metaplasticity. This form of I-LTD$_{stim}$ mimics the one observed after fear extinction learning.

Fear conditioning increases GABA release from MLIs onto Purkinje cells and other synaptically connected MLIs (Sacchetti et al., 2004; Scelfo et al., 2008; Dubois et al., 2020). We have recently shown that fear conditioning reduces tonic endocannabinoid levels in cerebellar lobules V/VI. This is driven by increased MLI activity, as optogenetic stimulation of MLIs in naïve animals is sufficient to induce the change. A decrease in endocannabinoid signaling elevates GABA release due to dis-inhibition and is responsible for a learning-induced increase in GABA release (Dubois et al., 2020). After fear conditioning, stimulation of parallel fibers, that mimics extinction learning, induces a decrease in GABA release. Importantly deletion of GluN2D did not prevent the learning-induced increase in GABA release but abolished I-LTD$_{stim}$ in conditioned mice. The GluN2D-dependent I-LTD$_{stim}$ may underlie the decrease in GABA release following extinction training (**Figure 7**).

MLIs are spontaneously active and innervate both Purkinje cells and neighboring MLIs. Purkinje cells form inhibitory synapses onto neurons in the cerebellar nuclei, which project to other brain regions. A learning-induced increase in spontaneous GABA release could reduce Purkinje cell activity and alter their firing pattern, and consequently increase the activity of neurons in the cerebellar nuclei. Fear conditioning induces LTP at both excitatory and inhibitory synapses onto Purkinje cell (Sacchetti et al., 2004). While the former facilitates temporal summation, the enhanced feedforward inhibition serves to maintain the temporal fidelity of the cerebellar circuit (Scelfo et al., 2008). Strengthening synaptic connections among MLIs may promote the synchronized activity of inhibitory network (Bartos et al., 2007). A decrease in GABA release following extinction would be expected to reduce the output of the cerebellar circuit and fear memory.

Our result show that genetic deletion of GluN2D subunits impaired extinction learning and abolished synaptic plasticity in cerebellar MLIs. Given that the cerebellar activity can regulate extinction learning (Walton et al., 2012; Frontera et al., 2020), the deficit in cerebellar neural plasticity is likely to translate to the impaired fear extinction in GluN2D KO mice. Consistent with this model we observed a strong correlation between behavioral phenotype and associated synaptic plasticity at the cerebellar inhibitory synapse, with no effects of GluN2D KO on fear learning and I-LTP, but complete disruption of both extinction learning and I-LTD$_{stim}$. However, other cells in the cerebellum also express GluN2D-containg NMDA receptors, including cells in the deep cerebellar nuclei and Golgi cells (Momiyama et al., 1996; Cull-Candy et al., 1997), the latter forming inhibitory synapses onto granule cells. Using a global GluN2D knockout mice, we cannot rule out possible roles of other GluN2D expressing neurons in extinction learning. Further work using a cerebellar MLI specific GluN2D KO would be required to test whether the lack of cerebellar I-LTD$_{stim}$ causes the extinction learning impairment in mutant mice. Current models of fear extinction circuitry encompass the medial prefrontal cortex, the amygdala, and the hippocampus (Maren and Quirk, 2004; Sotres-Bayon et al., 2004, 2007; Ogden et al., 2014). Since GluN2D subunits are also found in interneurons in the cortex, thalamus and hippocampus (Monyer et al., 1994; Standaert et al., 1996; Yamasaki et al., 2014; von Engelhardt et al., 2015; Alsaad et al., 2019), a GluN2D-dependent plasticity in inhibitory transmission in these brain regions may also contribute to extinction learning. Dopaminergic neurons in the substantia nigra are known to express GluN2D/2B triheteromeric receptors at synaptic and extra-synaptic sites and deletion of GluN2D subunits reduced agonist sensitivity (Jones and Gibb, 2005; Brothwell et al., 2008; Huang and Gibb, 2014; Wild et al., 2015; Morris et al., 2018). Activation of these neurons during fear extinction had no effect on acquisition of extinction, but enhanced fear extinction memory and blocked the renewal of fear in a novel context (Bouchet et al., 2018). It would be interesting to determine whether deletion of GluN2D receptors in these dopaminergic neurons influence fear extinction memory, although they are unlikely to contribute to extinction learning. Thus, the impaired fear extinction we observed may arise because of its effects on neural plasticity in multiple brain regions, including the cerebellum and similar metaplasticity may also occur in other brain regions.

Effects of genetic deletion of GluN2D subunits on emotional behaviors have been investigated in a number of studies (Ikeda et al., 1995; Miyamoto et al., 2002; Yamamoto et al., 2017; Shelkar et al., 2019; Salimando et al., 2020). They produce conflicting results, as global GluN2D KO mice show no difference in anxiety tests (Ikeda et al., 1995), but increased immobility in the forced swim test in another study (Shelkar et al., 2019). We did not detect any difference in basal freezing in the conditioning chamber (**Figures 4**, **5**, **6**) and time spent in the center square

of the open field test (**Supplementary Figure 1**), and this is consistent with no elevated generalized fear in mutant mice. These mutant mice exhibit lower susceptibility to stress induced by the elevated plus-maze, light–dark box, and forced swimming tests, and reduced locomotor activity in a novel environment, which is associated with altered monoamine neurotransmitter levels in several brain regions (Miyamoto et al., 2002). GluN2D receptors are also required for the antidepressant effects of ketamine (Sapkota et al., 2016; Ide et al., 2017), and mediate a stress-induced changes in cognitive function, as GluN2D KO mice show social stress-induced anhedonia and a deficit in social recognition/memory and spatial memory acquisition (Yamamoto et al., 2017). In this study we demonstrate that GluN2D-receptors mediate extinction learning of associative fear memory. This is unlikely to be attributable to a change in locomotor function as basal freezing before conditioning and total travel distance in the open field test were unaltered in mutant mice, consistent with the observation of normal rotarod motor performance (Yamamoto et al., 2013). A 10–30% decrease in total travel distance reported in GluN2D KO mice (Ikeda et al., 1995; Shelkar et al., 2019) cannot account for a fourfold higher freezing time in response to tones at the end of extinction training relative to wildtype mice (**Figures 4**–**6**), although what causes the conflicting results is unclear. A recent study show that GluN2D regulates emotional behavior in a region-specific manner as deletion of GluN2D from CRF neurons in the BNST mice increases depressive-like behaviors (Salimando et al., 2020). Our results provide further evidence for an important role of GluN2D NMDARs in emotional learning and behavior.

NMDAR subtypes that are expressed in diverse neuronal populations are involved in different aspects of learning and memory. D-cycloserine has been widely used for the treatment of fear-related pathologies (Otto et al., 2016), and was thought to act on GluN2C receptors (Ogden et al., 2014) due to its higher efficacy at GluN2C-containing NMDARs compared to GluN2A and 2B NMDARs (Sheinin et al., 2001; Dravid et al., 2010). However, we identified GluN2D-containing NMDARs as being responsible for extinction learning. Interneurons that express GluN2D subunits are likely to express GluN2B/D tri-heteromeric receptors in wildtype mice and GluN2B di-heteromeric receptors in the KO mice, as previously shown in cerebellar interneurons and dopaminergic neurons in the substantia nigra (Brickley et al., 2003; Huang and Gibb, 2014; Dubois et al., 2016). As a consequence this may reduce the ability of D-cycloserine to bind to NMDA receptors in these neurons, and thus decrease its efficacy in accelerating extinction learning. Alternatively, deletion of the GluN2D subunit may render extinction learning an NMDAR-independent process. Our finding that GluN2D receptors are critical for extinction learning highlights the need to develop pharmacological tools that selectively target this NMDAR subtype in the treatment of anxiety disorders.

DATA AVAILABILITY STATEMENT

The original contributions presented in the study are included in the article/**Supplementary Material**, further inquiries can be directed to the corresponding author.

ETHICS STATEMENT

The animal study was reviewed and approved by IACUC.

AUTHOR CONTRIBUTIONS

CJD performed experiments and analysis. CJD and SJL designed the study and wrote the manuscript. Both authors contributed to the article and approved the submitted version.

FUNDING

This work was supported by National Institutes of Health Grants NS58867, MH095948, and R01NS106915 and a Department of Veterans Affairs Grant I01 BX003893-01A1 (SL).

ACKNOWLEDGMENTS

We thank Drs. Matthew D. Whim, Joseph LeDoux, and Iaroslav Savtchouk for experimental advice, technical assistance, and helpful discussions, and Dr. Masayoshi Mishina (Ritsumeikan University) for providing the GluN2D KO mouse line.

SUPPLEMENTARY MATERIAL

The Supplementary Material for this article can be found online at: https://www.frontiersin.org/articles/10.3389/fnsyn.2021.681068/full#supplementary-material

REFERENCES

Aitkin, L. M., and Boyd, J. (1978). Acoustic input to the lateral pontine nuclei. *Hear. Res.* 1, 67–77.

Akazawa, C., Shigemoto, R., Bessho, Y., Nakanishi, S., and Mizuno, N. (1994). Differential expression of five N-methyl-D-aspartate receptor subunit mRNAs in the cerebellum of developing and adult rats. *J. Comp. Neurol.* 347, 150–160. doi: 10.1002/cne.903470112

Alsaad, H. A., DeKorver, N. W., Mao, Z., Dravid, S. M., Arikkath, J., and Monaghan, D. T. (2019). In the Telencephalon, GluN2C NMDA Receptor Subunit mRNA is Predominately Expressed in Glial Cells and GluN2D mRNA in Interneurons. *Neurochem. Res.* 44, 61–77. doi: 10.1007/s11064-018-2526-7

Apps, R., and Strata, P. (2015). Neuronal circuits for fear and anxiety - the missing link. *Nat. Rev. Neurosci.* 16:642. doi: 10.1038/nrn4028

Bartos, M., Vida, I., and Jonas, P. (2007). Synaptic mechanisms of synchronized gamma oscillations in inhibitory interneuron networks. *Nat. Rev. Neurosci.* 8, 45–56. doi: 10.1038/nrn2044

Bocchio, M., Nabavi, S., and Capogna, M. (2017).). Synaptic Plasticity, Engrams, and Network Oscillations in Amygdala Circuits for Storage and Retrieval of Emotional Memories. *Neuron* 94, 731–743. doi: 10.1016/j.neuron.2017.03.022

Bouchet, C. A., Miner, M. A., Loetz, E. C., Rosberg, A. J., Hake, H. S., Farmer, C. E., et al. (2018). Activation of Nigrostriatal Dopamine Neurons during Fear Extinction Prevents the Renewal of Fear. *Neuropsychopharmacology* 43, 665–672. doi: 10.1038/npp.2017.235

Bowers, M. E., and Ressler, K. J. (2015). An Overview of Translationally Informed Treatments for Posttraumatic Stress Disorder: animal Models of Pavlovian Fear Conditioning to Human Clinical Trials. *Biol. Psychiatry* 78, E15–E27. doi: 10.1016/j.biopsych.2015.06.008

Bresink, I., Benke, T. A., Collett, V. J., Seal, A. J., Parsons, C. G., Henley, J. M., et al. (1996). Effects of memantine on recombinant rat NMDA receptors expressed in HEK 293 cells. *Br. J. Pharmacol.* 119, 195–204. doi: 10.1111/j.1476-5381.1996.tb15971.x

Brickley, S. G., Misra, C., Mok, M., Mishina, M., and Cull-Candy, S. G. (2003). NR2B and NR2D subunits coassemble in cerebellar Golgi cells to form a distinct NMDA receptor subtype restricted to extrasynaptic sites. *J. Neurosci.* 23, 4958–4966.

Brothwell, S. L. C., Barber, J. L., Monaghan, D. T., Jane, D. E., Gibb, A. J., and Jones, S. (2008). NR2B- and NR2D-containing synaptic NMDA receptors in developing rat substantia nigra pars compacta dopaminergic neurones. *J. Physiol.* 586, 739–750. doi: 10.1113/jphysiol.2007.144618

Cahill, E. N., and Milton, A. L. (2019). Neurochemical and molecular mechanisms underlying the retrieval-extinction effect. *Psychopharmacology* 236, 111–132. doi: 10.1007/s00213-018-5121-3

Clem, R. L., and Huganir, R. L. (2010). Calcium-permeable AMPA receptor dynamics mediate fear memory erasure. *Science* 330, 1108–1112. doi: 10.1126/science.1195298

Cull-Candy, S. G., Brickley, S., Misra, C., Feldmeyer, D., Momiyama, A., and Farrant, M. (1997). NMDA receptor diversity in the cerebellum: identification of subunits contributing to functional receptors. *Neuropharmacology* 37, 1369–1380.

Cull-Candy, S. G., and Leszkiewicz, D. N. (2004). Role of distinct NMDA receptor subtypes at central synapses. *Sci. STKE* 2004:re16. doi: 10.1126/stke.2552004re16

Dalton, G. L., Wu, D. C., Wang, Y. T., Floresco, S. B., and Phillips, A. G. (2012). NMDA GluN2A and GluN2B receptors play separate roles in the induction of LTP and LTD in the amygdala and in the acquisition and extinction of conditioned fear. *Neuropharmacology* 62, 797–806. doi: 10.1016/j.neuropharm.2011.09.001

Davis, M. (2011). NMDA receptors and fear extinction: implications for cognitive behavioral therapy. *Dialogues Clin. Neurosci.* 13, 463–474.

Dravid, S. M., Burger, P. B., Prakash, A., Geballe, M. T., Yadav, R., Le, P., et al. (2010). Structural determinants of D-cycloserine efficacy at the NR1/NR2C NMDA receptors. *J. Neurosci.* 30, 2741–2754. doi: 10.1523/JNEUROSCI.5390-09.2010

Dubois, C. J., Fawcett-Patel, J., Katzman, P. A., and Liu, S. J. (2020). Inhibitory neurotransmission drives endocannabinoid degradation to promote memory consolidation. *Nat. Commun.* 11:6407. doi: 10.1038/s41467-020-20121-3

Dubois, C. J., Lachamp, P. M., Sun, L., Mishina, M., and Liu, S. J. (2016). Presynaptic GluN2D receptors detect glutamate spillover and regulate cerebellar GABA release. *J. Neurophysiol.* 115, 271–285. doi: 10.1152/jn.00687.2015

Dunsmoor, J. E., Niv, Y., Daw, N., and Phelps, E. A. (2015). Rethinking Extinction. *Neuron* 88, 47–63. doi: 10.1016/j.neuron.2015.09.028

Ernst, T. M., Brol, A. E., Gratz, M., Ritter, C., Bingel, U., Schlamann, M., et al. (2019). The cerebellum is involved in processing of predictions and prediction errors in a fear conditioning paradigm. *Elife* 8:e46831. doi: 10.7554/eLife.46831

Frontera, J. L., Baba Aissa, H., Sala, R. W., Mailhes-Hamon, C., Georgescu, I. A., Léna, C., et al. (2020). Bidirectional control of fear memories by cerebellar neurons projecting to the ventrolateral periaqueductal grey. *Nat. Commun.* 11:5207. doi: 10.1038/s41467-020-18953-0

Hillman, B. G., Gupta, S. C., Stairs, D. J., Buonanno, A., and Dravid, S. M. (2011). Behavioral analysis of NR2C knockout mouse reveals deficit in acquisition of conditioned fear and working memory. *Neurobiol. Learn. Mem.* 95, 404–414. doi: 10.1016/j.nlm.2011.01.008

Huang, Z., and Gibb, A. J. (2014). Mg2+ block properties of triheteromeric GluN1-GluN2B-GluN2D NMDA receptors on neonatal ratsubstantia nigra pars compacta dopaminergic neurones. *J. Physiol.* 592, 2059–2078. doi: 10.1113/jphysiol.2013.267864

Hulme, S. R., Jones, O. D., and Abraham, W. C. (2013). Emerging roles of metaplasticity in behaviour and disease. *Trends Neurosci.* 36, 353–362. doi: 10.1016/j.tins.2013.03.007

Hunt, D. L., and Castillo, P. E. (2012). Synaptic plasticity of NMDA receptors: mechanisms and functional implications. *Curr. Opin. Neurobiol.* 22, 496–508. doi: 10.1016/j.conb.2012.01.007

Ide, S., Ikekubo, Y., Mishina, M., Hashimoto, K., and Ikeda, K. (2017). Role of NMDA receptor GluN2D subunit in the antidepressant effects of enantiomers of ketamine. *J. Pharmacol. Sci.* 135, 138–140. doi: 10.1016/j.jphs.2017.11.001

Ikeda, K., Araki, K., Takayama, C., Inoue, Y., Yagi, T., Aizawa, S., et al. (1995). Reduced spontaneous activity of mice defective in the epsilon 4 subunit of the NMDA receptor channel. *Brain Res. Mol. Brain Res.* 33, 61–71.

Izquierdo, I., Furini, C. R. G., and Myskiw, J. C. (2016). Fear Memory. *Physiol. Rev.* 96, 695–750. doi: 10.1152/physrev.00018.2015

Jessen, M., Frederiksen, K., Yi, F., Clausen, R. P., Hansen, K. B., Bräuner-Osborne, H., et al. (2017). Identification of AICP as a GluN2C-Selective N-Methyl-d-Aspartate Receptor Superagonist at the GluN1 Glycine Site. *Mol. Pharmacol.* 92, 151–161. doi: 10.1124/mol.117.108944

Jones, S., and Gibb, A. J. (2005). Functional NR2B- and NR2D-containing NMDA receptor channels in rat substantia nigra dopaminergic neurones. *J. Physiol.* 569, 209–221. doi: 10.1113/jphysiol.2005.095554

Kattoor, J., Thürling, M., Gizewski, E. R., Forsting, M., Timmann, D., and Elsenbruch, S. (2014). Cerebellar contributions to different phases of visceral aversive extinction learning. *Cerebellum* 13, 1–8. doi: 10.1007/s12311-013-0512-9

Kuriyama, K., Honma, M., Soshi, T., Fujii, T., and Kim, Y. (2011). Effect of d-cycloserine and valproic acid on the extinction of reinstated fear-conditioned responses and habituation of fear conditioning in healthy humans: a randomized controlled trial. *Psychopharmacology* 218, 589–597. doi: 10.1007/s00213-011-2353-x

Lachamp, P. M., Liu, Y., and Liu, S. J. (2009). Glutamatergic modulation of cerebellar interneuron activity is mediated by an enhancement of GABA release and requires protein kinase A/RIM1alpha signaling. *J. Neurosci.* 29, 381–392. doi: 10.1523/JNEUROSCI.2354-08.2009

Lange, I., Kasanova, Z., Goossens, L., Leibold, N., De Zeeuw, C. I., van Amelsvoort, T., et al. (2015). The anatomy of fear learning in the cerebellum: a systematic meta-analysis. *Neurosci. Biobehav. Rev.* 59, 83–91. doi: 10.1016/j.neubiorev.2015.09.019

Ledgerwood, L., Richardson, R., and Cranney, J. (2005). d-cycloserine facilitates extinction of learned fear: effects on reacquisition and generalized extinction. *Biol. Psychiatry* 57, 841–847. doi: 10.1016/j.biopsych.2005.01.023

Lee, H. J., Haberman, R. P., Roquet, R. F., and Monfils, M.-H. (2015). Extinction and Retrieval + Extinction of Conditioned Fear Differentially Activate Medial Prefrontal Cortex and Amygdala in Rats. *Front. Behav. Neurosci.* 9:369. doi: 10.3389/fnbeh.2015.00369

Lee, J. L. C., Milton, A. L., and Everitt, B. J. (2006). Reconsolidation and Extinction of Conditioned Fear: inhibition and Potentiation. *J. Neurosci.* 26, 10051–10056. doi: 10.1523/JNEUROSCI.2466-06.2006

Linnman, C., Rougemont-Bücking, A., Beucke, J. C., Zeffiro, T. A., and Milad, M. R. (2011). Unconditioned responses and functional fear networks in human classical conditioning. *Behav. Brain Res.* 221, 237–245. doi: 10.1016/j.bbr.2011.02.045

Liu, S. Q., and Cull-Candy, S. G. (2000). Synaptic activity at calcium-permeable AMPA receptors induces a switch in receptor subtype. *Nature* 405, 454–458. doi: 10.1038/35013064

Liu, Y., Formisano, L, Savtchouk, I., Takayasu, Y., Szabó, G., Zukin, R. S., et al. (2010). A single fear-inducing stimulus induces a transcription-dependent switch in AMPA receptor phenotype. *Nat. Neurosci.* 13, 223–231. doi: 10.1038/nn.2474

Mao, S.-C., Hsiao, Y.-H., and Gean, P.-W. (2006). Extinction Training in Conjunction with a Partial Agonist of the Glycine Site on the NMDA Receptor Erases Memory Trace. *J. Neurosci.* 26, 8892–8899. doi: 10.1523/JNEUROSCI.0365-06.2006

Maren, S., and Quirk, G. J. (2004). Neuronal signalling of fear memory. *Nat. Rev. Neurosci.* 5, 844–852. doi: 10.1038/nrn1535

Miyamoto, Y., Yamada, K., Noda, Y., Mori, H., Mishina, M., and Nabeshima, T. (2002). Lower sensitivity to stress and altered monoaminergic neuronal function in mice lacking the NMDA receptor epsilon 4 subunit. *J. Neurosci.* 22, 2335–2342.

Momiyama, A., Feldmeyer, D., and Sg, C.-C. (1996). Identification of a native low-conductance NMDA channel with reduced sensitivity to Mg2+ in rat central neurones. *J. Physiol.* 494, 479–492.

Monfils, M.-H., Cowansage, K. K., Klann, E., and LeDoux, J. E. (2009). Extinction-Reconsolidation Boundaries: key to Persistent Attenuation of Fear Memories. *Science* 324, 951–955. doi: 10.1126/science.1167975

Monyer, H., Burnashev, N., Laurie, D. J., Sakmann, B., and Seeburg, P. H. (1994). Developmental and regional expression in the rat brain and functional properties of four NMDA receptors. *Neuron* 12, 529–540.

Morris, P. G., Mishina, M., and Jones, S. (2018). Altered Synaptic and Extrasynaptic NMDA Receptor Properties in Substantia Nigra Dopaminergic Neurons From Mice Lacking the GluN2D Subunit. *Front. Cell. Neurosci.* 12:354. doi: 10.3389/fncel.2018.00354

Ogden, K. K., Khatri, A., Traynelis, S. F., and Heldt, S. A. (2014). Potentiation of GluN2C/D NMDA receptor subtypes in the amygdala facilitates the retention of fear and extinction learning in mice. *Neuropsychopharmacology* 39, 625–637. doi: 10.1038/npp.2013.241

Otto, M. W., Kredlow, M. A., Smits, J. A. J., Hofmann, S. G., Tolin, D. F., de Kleine, R. A., et al. (2016). Enhancement of Psychosocial Treatment With D-Cycloserine: models, Moderators, and Future Directions. *Biol. Psychiatry* 80, 274–283. doi: 10.1016/j.biopsych.2015.09.007

Paoletti, P., Bellone, C., and Zhou, Q. (2013). NMDA receptor subunit diversity: impact on receptor properties, synaptic plasticity and disease. *Nat. Rev. Neurosci.* 14, 383–400. doi: 10.1038/nrn3504

Peyrovian, B., Rosenblat, J. D., Pan, Z., Iacobucci, M., Brietzke, E., and McIntyre, R. S. (2019). The glycine site of NMDA receptors: a target for cognitive enhancement in psychiatric disorders. *Prog. Neuropsychopharmacol. Biol. Psychiatry* 92, 387–404. doi: 10.1016/j.pnpbp.2019.02.001

Pittig, A., van den Berg, L., and Vervliet, B. (2016). The key role of extinction learning in anxiety disorders: behavioral strategies to enhance exposure-based treatments. *Curr. Opin. Psychiatry* 29, 39–47. doi: 10.1097/YCO.0000000000000220

Sacchetti, B., Baldi, E., Lorenzini, C. A., and Bucherelli, C. (2002). Cerebellar role in fear-conditioning consolidation. *Proc. Natl. Acad. Sci. U. S. A.* 99, 8406–8411. doi: 10.1073/pnas.112660399

Sacchetti, B., Sacco, T., and Strata, P. (2007). Reversible inactivation of amygdala and cerebellum but not perirhinal cortex impairs reactivated fear memories. *Eur. J. Neurosci.* 25, 2875–2884. doi: 10.1111/j.1460-9568.2007.05508.x

Sacchetti, B., Scelfo, B., Tempia, F., and Strata, P. (2004). Long-term synaptic changes induced in the cerebellar cortex by fear conditioning. *Neuron* 42, 973–982. doi: 10.1016/j.neuron.2004.05.012

Salimando, G. J., Hyun, M., Boyt, K. M., and Winder, D. G. (2020). BNST GluN2D-Containing NMDA Receptors Influence Anxiety- and Depressive-like Behaviors and ModulateCell-Specific Excitatory/Inhibitory Synaptic Balance. *J. Neurosci.* 40, 3949–3968. doi: 10.1523/JNEUROSCI.0270-20.2020

Sapkota, K., Mao, Z., Synowicki, P., Lieber, D., Liu, M., Ikezu, T., et al. (2016). GluN2D N-Methyl-d-Aspartate Receptor Subunit Contribution to the Stimulation of Brain Activity and Gamma Oscillations by Ketamine: implications for Schizophrenia. *J. Pharmacol. Exp. Ther.* 356, 702–711. doi: 10.1124/jpet.115.230391

Scelfo, B., Sacchetti, B., and Strata, P. (2008). Learning-related long-term potentiation of inhibitory synapses in the cerebellar cortex. *Proc. Natl. Acad. Sci. U. S. A.* 105, 769–774. doi: 10.1073/pnas.0706342105

Sheinin, A., Shavit, S., and Benveniste, M. (2001). Subunit specificity and mechanism of action of NMDA partial agonist D-cycloserine. *Neuropharmacology* 41, 151–158.

Shelkar, G. P., Pavuluri, R., Gandhi, P. J., Ravikrishnan, A., Gawande, D. Y., Liu, J., et al. (2019). Differential effect of NMDA receptor GluN2C and GluN2D subunit ablation on behavior and channel blocker-induced schizophrenia phenotypes. *Sci. Rep.* 9:7572. doi: 10.1038/s41598-019-43957-2

Singewald, N., and Holmes, A. (2019). Rodent models of impaired fear extinction. *Psychopharmacology* 236, 21–32. doi: 10.1007/s00213-018-5054-x

Sotres-Bayon, F., Bush, D. E. A., and LeDoux, J. E. (2004). Emotional perseveration: an update on prefrontal-amygdala interactions in fear extinction. *Learn. Mem.* 11, 525–535. doi: 10.1101/lm.79504

Sotres-Bayon, F., Bush, D. E. A., and LeDoux, J. E. (2007). Acquisition of fear extinction requires activation of NR2B-containing NMDA receptors in the lateral amygdala. *Neuropsychopharmacology* 32, 1929–1940. doi: 10.1038/sj.npp.1301316

Standaert, D. G., Landwehrmeyer, G. B., Kerner, J. A., Penney, J. B., and Young, A. B. (1996). Expression of NMDAR2D glutamate receptor subunit mRNA in neurochemically identified interneurons in the rat neostriatum, neocortex and hippocampus. *Brain Res. Mol. Brain Res.* 42, 89–102. doi: 10.1016/s0169-328x(96)00117-9

Tedesco, V., Roquet, R. F., DeMis, J., Chiamulera, C., and Monfils, M.-H. (2014). Extinction, applied after retrieval of auditory fear memory, selectively increases zinc-finger protein 268 and phosphorylated ribosomal protein S6 expression in prefrontal cortex and lateral amygdala. *Neurobiol. Learn. Mem.* 115, 78–85. doi: 10.1016/j.nlm.2014.08.015

Thompson, C. L., Drewery, D. L., Atkins, H. D., Stephenson, F. A., and Chazot, P. L. (2000). Immunohistochemical localization of N-methyl-D-aspartate receptor NR1, NR2A, NR2B and NR2C/D subunits in the adult mammalian cerebellum. *Neurosci. Lett.* 283, 85–88.

Timmann, D., Drepper, J., Frings, M., Maschke, M., Richter, S., Gerwig, M., et al. (2010). The human cerebellum contributes to motor, emotional and cognitive associative learning. A review. *Cortex* 46, 845–857. doi: 10.1016/j.cortex.2009.06.009

Tovote, P., Fadok, J. P., and Lüthi, A. (2015). Neuronal circuits for fear and anxiety. *Nat. Rev. Neurosci.* 16, 317–331. doi: 10.1038/nrn3945

Utz, A., Thürling, M., Ernst, T. M., Hermann, A., Stark, R., Wolf, O. T., et al. (2015). Cerebellar vermis contributes to the extinction of conditioned fear. *Neurosci. Lett.* 604, 173–177. doi: 10.1016/j.neulet.2015.07.026

von Engelhardt, J., Bocklisch, C., Tönges, L., Herb, A., Mishina, M., and Monyer, H. (2015). GluN2D-containing NMDA receptors-mediate synaptic currents in hippocampal interneurons and pyramidal cells in juvenile mice. *Front. Cell. Neurosci.* 9:95. doi: 10.3389/fncel.2015.00095

Walker, D. L., Ressler, K. J., Lu, K.-T., and Davis, M. (2002). Facilitation of conditioned fear extinction by systemic administration or intra-amygdala infusions of D-cycloserine as assessed with fear-potentiated startle in rats. *J. Neurosci.* 22, 2343–2351.

Walton, J. C., Schilling, K., Nelson, R. J., and Oberdick, J. (2012). Sex-Dependent Behavioral Functions of the Purkinje Cell-Specific Gαi/o Binding Protein, Pcp2(L7). *Cerebellum* 11, 982–1001. doi: 10.1007/s12311-012-0368-4

Wild, A. R., Bollands, M., Morris, P. G., and Jones, S. (2015). Mechanisms regulating spill-over of synaptic glutamate to extrasynaptic NMDA receptors in mouse substantia nigra dopaminergic neurons. *Eur. J. Neurosci.* 42, 2633–2643. doi: 10.1111/ejn.13075

Yamamoto, H., Kamegaya, E., Hagino, Y., Takamatsu, Y., Sawada, W., Matsuzawa, M., et al. (2017). Loss of GluN2D subunit results in social recognition deficit, social stress, 5-HT2C receptor dysfunction, and anhedonia in mice. *Neuropharmacology* 112, 188–197. doi: 10.1016/j.neuropharm.2016.07.036

Yamamoto, H., Kamegaya, E., Sawada, W., Hasegawa, R., Yamamoto, T., Hagino, Y., et al. (2013). Involvement of the N -methyl- d -aspartate receptor GluN2D subunit in phencyclidine-induced motor impairment, gene expression, and increased Fos immunoreactivity. *Mol. Brain* 6:56. doi: 10.1186/1756-6606-6-56

Yamasaki, M., Okada, R., Takasaki, C., Toki, S., Fukaya, M., Natsume, R., et al. (2014). Opposing role of NMDA receptor GluN2B and GluN2D in somatosensory development and maturation. *J. Neurosci.* 34, 11534–11548. doi: 10.1523/JNEUROSCI.1811-14.2014

Conflict of Interest: The authors declare that the research was conducted in the absence of any commercial or financial relationships that could be construed as a potential conflict of interest.

frontiers in Synaptic Neuroscience

ORIGINAL RESEARCH
published: 20 January 2022
doi: 10.3389/fnsyn.2021.811806

Transsynaptic Long-Term Potentiation in the Hippocampus of Behaving Mice

Maria Teresa Romero-Barragán, Agnes Gruart and José M. Delgado-García*

Division of Neurosciences, Pablo de Olavide University, Seville, Spain

Long-term potentiation (LTP) is an experimental procedure that shares certain mechanisms with neuronal learning and memory processes and represents a well-known example of synaptic plasticity. LTP consists of an increase of the synaptic response to a control stimulus following the presentation of a high-frequency stimulation (HFS) train to an afferent pathway. This technique is studied mostly in the hippocampus due to the latter's high susceptibility and its laminar nature which facilitates the location of defined synapses. Although most preceding studies have been performed *in vitro*, we have developed an experimental approach to carry out these experiments in alert behaving animals. The main goal of this study was to confirm the existence of synaptic changes in strength in synapses that are post-synaptic to the one presented with the HFS. We recorded field excitatory post-synaptic potentials (fEPSPs) evoked in five hippocampal synapses, from both hemispheres, of adult male mice. HFS was presented to the perforant pathway (PP). We characterized input/output curves, paired-pulse stimulation, and LTP of these synapses. We also performed depth-profile recordings to determine differences in fEPSP latencies. Collected data indicate that the five selected synapses have similar basic electrophysiological properties, a fact that enables an easier comparison of LTP characteristics. Importantly, we observed the presence of significant LTP in the contralateral CA1 (cCA1) area following the control stimulation of non-HFS-activated pathways. These results indicate that LTP appears as a physiological process present in synapses located far away from the HFS-stimulated afferent pathway.

Keywords: hippocampal synapses, long-term potentiation, high-frequency stimulation, mice, non-directly evoked long-term potentiation, input/output curves, paired-pulse facilitation

OPEN ACCESS

Edited by:
Fereshteh S. Nugent, Uniformed Services University, United States

Reviewed by:
Jung Hoon Shin, National Institute on Alcohol Abuse and Alcoholism (NIAAA), United States
Edward Mann, University of Oxford, United Kingdom

****Correspondence:***
Maria Teresa Romero-Barragán
mtrombar@upo.es

Received: *09 November 2021*
Accepted: *31 December 2021*
Published: *20 January 2022*

Citation:
Romero-Barragán MT, Gruart A and Delgado-García JM (2022) Transsynaptic Long-Term Potentiation in the Hippocampus of Behaving Mice. Front. Synaptic Neurosci. 13:811806. doi: 10.3389/fnsyn.2021.811806

INTRODUCTION

LTP of synaptic strength is an experimentally induced technique commonly used for studying the mechanisms involved in learning and memory processes, since changes in synaptic efficacy of both events share many properties with respect to the underlying physiological, cellular, and molecular phenomena (Bliss and Collingridge, 1993; Gruart et al., 2006). LTP is usually induced in excitatory synapses of the hippocampus and other cortical and subcortical sites by the HFS of an afferent pathway to a given set of postsynaptic neurons and consists of the increase in the amplitude or slope of excitatory post-synaptic potentials (EPSPs) recorded intracellularly or in the surroundings of the postsynaptic cell as fEPSPs. This electrophysiological potentiation of postsynaptic responses can last from several minutes or hours during *in vitro* experiments (Bortolotto et al., 2001; Lynch, 2004) to

days and weeks when synaptic electrophysiological events are recorded in alert behaving mammals (Abraham, 2003; Madroñal et al., 2007; Abraham and Williams, 2008).

Although there are many different ways of evoking and recording long-term changes in synaptic strength and functional efficacy, we are particularly interested here in the putative transsynaptic spread of LTP across relatively distant synapses (Helme-Guizon et al., 1998; Krug et al., 2001; Taylor et al., 2016). The question is whether LTP could be a general mechanism to activate distant but interconnected brain circuits involved in the different sensorimotor or cognitive aspects of newly acquired behavioral or mental abilities (Fernández-Ruiz et al., 2012).

The hippocampus seems to be a good place for the experimental approach to the above question. Indeed, the LTP of synaptic strength was described for the first time in the hippocampal formation (Bliss and Lømo, 1973) and it has been repeatedly studied since then with many different experimental procedures. The well-defined intrinsic circuit of the hippocampus and its specific ultrastructural organization in layers (Witter et al., 2000; Shepherd, 2004) have allowed an extensive and detailed study of LTP properties and putative functions (Collingridge et al., 1992; Bortolotto and Collingridge, 1993; Matsuzaki et al., 2004; Gruart et al., 2015; Volianskis et al., 2015; Korte and Schmitz, 2016; Fassin et al., 2020). However, most of these earlier studies describe only the effects of LTP in synaptic sites in direct contact (i.e., monosynaptic) with an activated afferent pathway, leaving further transsynaptic sites completely unexplored. *In vitro* studies present obvious technical limitations to the performance of transsynaptic recordings (Bortolotto et al., 2001; Volianskis and Jensen, 2003), but *in vivo* recordings carried out in alert behaving animals could certainly facilitate the proper study of LTP spread across cortical circuits following experimental (e.g., HFS-evoked) or functional (i.e., during actual learning) processes. For example, there are already studies carried out in behaving rats suggesting the presence of experimentally evoked transsynaptic LTP in hippocampal-to-contralateral medial prefrontal cortex (Taylor et al., 2016) and entorhinal cortex-to-contralateral dentate nucleus (Krug et al., 2001) circuits.

In this study, we aimed to explore any transsynaptic LTP in the hippocampal circuit in alert behaving mice. For this, we investigated the basic electrophysiological properties of five synapses of the hippocampal circuit (PP-CA3, PP-CA1, PP-cCA1, CA3-CA1, and CA3-cCA1) by performing input/output curves and testing paired-pulse facilitation. In a second step we studied changes in synaptic plasticity synapses directly (PP-CA3, PP-CA1) and non-directly (PP-cCA1, CA3-CA1, and CA3-cCA1) activated by HFS trains presented to the PP.

MATERIALS AND METHODS

Experimental Animals

C57Bl/6 male adult mice (3–4 months old) obtained from the University of Granada Animal House (Granada, Spain) were used in this study. Animals were housed in standard cages (n = 5 per cage) with a covering grid and enrichment materials inside (cardboard rolls and paper). After surgery, animals were kept in individual cages for a better preservation of the implanted electrodes. The mouse room remained on 12 h light/dark periods, at constant room temperature (21.5 ± 1°C) and humidity (55 ± 8%). Food and water were provided *ad libitum*. Experimental procedures were carried out in accordance with European Union guidelines (2003/65/CE) and Spanish regulations (BOE 252/34367–91, 2005) for the use of laboratory animals in acute and chronic studies. All protocols were also approved by the Pablo de Olavide Ethics Committee (JA 06/03/2018/025). Only animals with electrodes implanted in the proper site and presenting correct fEPSP waveforms across the whole experiment were further considered in this study.

Surgery

Animals were anesthetized with 1–2% isoflurane in a gas chamber provided with a calibrated Fluotec 5 (Fluotec-Ohmeda, Tewksbury, MA, United States) vaporizer, at a flow rate of 1–2 L/min oxygen (AstraZeneca, Madrid, Spain). Afterward, they were placed in a stereotaxic frame with a continuous supply of anesthesia (0.5% isoflurane) delivered by a special mouse mask (David Kopf Instruments, Tujunga, CA). Animals were covered with an electric blanket in order to maintain body temperature at 37°C.

First of all, depth profile recordings were carried out in anesthetized mice in order to characterize cCA1 responses to PP and CA3 stimulations (**Figure 1**) and to compare the collected fEPSPs with those evoked in the ipsilateral CA1 region (Gruart et al., 2015). For this purpose, a craniotomy was performed 2,2 mm posterior and 1,2 mm lateral to bregma. Following stereotaxic coordinates (Franklin and Paxinos, 2007) a stimulating electrode was implanted in the hippocampal CA3 region (A-P: –1.5 mm, L: –1.7 mm, and D: –1.5 mm) and in the perforant pathway (A-P: –3.8 mm and L: –2.0 mm relative to bregma, and 1.0 mm deep from the brain surface). A 10-μm glass micropipette filled with 2 M NaCl and held by a micromanipulator (Narishige, Tokyo, Japan) was used to record in 100 μm steps along the vertical axis of the cCA1 pyramidal layer.

For chronic recordings (**Figures 2–4**), animals were implanted with two bipolar stimulating and two recording electrodes. Stimulating electrodes were implanted in the perforant pathway and the hippocampal CA3 region using the stereotaxic coordinates already mentioned in the previous paragraph. The latter also worked as a recording electrode when needed. Recording electrodes were implanted in the CA1 area of both hemispheres (A-P: –2.2 mm, L: –1.2 mm, and 1.2 mm, and D: –1.3 mm; **Figure 5**). This experimental design enabled the study of five hippocampal synapses: PP-CA3, PP-CA1, PP-cCA1, CA3-CA1, and CA3-cCA1 (**Figures 2–4**). Animals used in the LTP experiment lacked the recording electrode in iCA1 to avoid any unnecessary brain damage. All electrodes were made from 50 μm, Teflon-coated tungsten wire (Advent Research, Eynsham, United Kingdom), with 0.5 mm of their tips bared. Two screws, affixed to the frontal and interparietal bones and soldered to bare silver wires, served as ground. Wires were soldered to two (6-pin and 4-pin) sockets (RS Amidata, Madrid, Spain) and covered

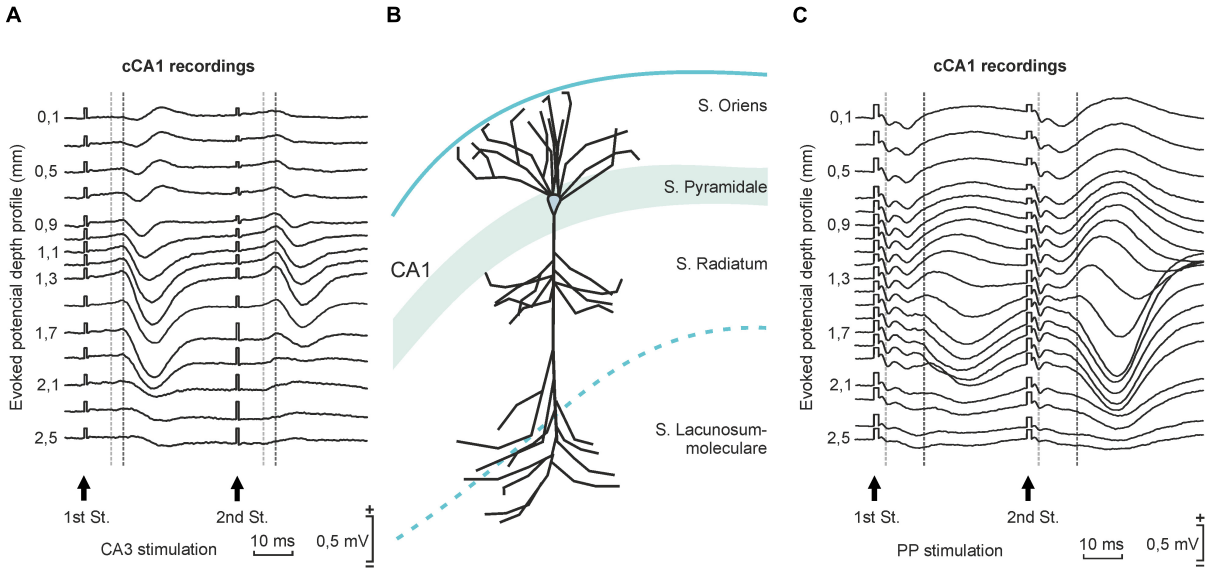

FIGURE 1 | Selective examples of preliminary depth-profile recordings that help to characterize the fEPSPs evoked at the contralateral CA1 synapses included in this study. **(A)** Depth-profile representation of fEPSPs evoked in the contralateral CA1 area by paired-pulse stimulation (40 ms of interpulse interval, red arrows) of Schaffer collaterals (CA3 stimulation). Stimulus intensity was set at 40% of the intensity (mA) necessary to evoke maximum fEPSP responses at 1.3 mm depth. Recordings were carried out in steps of 100 and 200 μm. Note that the latency of the fEPSP (dark gray) is longer than the one for the homolateral CA3-CA1 synapse, i.e., stimulating and recording in the same hemisphere (light gray; obtained from Gruart et al., 2015). **(B)** A diagrammatic representation of the location of somas and dendrites corresponding to CA1 pyramidal cells and to dentate granule neurons. The different strata are indicated. **(C)** Another field-potential depth profile corresponding to fEPSPs evoked in the contralateral CA1 area by the paired-pulse stimulation of the ipsilateral perforant pathway.

with dental cement in order to secure the implanted electrodes. Further details about these experimental procedures can be found elsewhere (Gruart et al., 2006).

For the head-fixed experiment (**Figures 6**, **7**), the skull was drilled at the previously mentioned coordinates for PP, CA3, and cCA1. Stimulating electrodes were implanted in PP and CA3 and soldered to a 4-pin socket (RS Amidata, Madrid, Spain). In addition, a recording chamber was built with dental cement around a craniotomy performed over the cCA1 area. The bone window was covered with gauze and bone wax until the recording session. In this case, mice were also implanted with a small metallic head-plate which would keep the animal's head attached to the recording setup in a stable position during experimental sessions. The holding plate and the implanted electrodes were affixed to the skull with the help of two small screws covered with cyanoacrylate and dental cement. A bare silver wire was soldered to the screws, serving as ground, and had a small loop at the other end that was left uncovered by the cement (López-Ramos et al., 2018).

After surgery, mice rested for a week for recovery until experiments began.

Stimulation and Recording Procedures

Chronic recordings were performed in 6 animals at a time, which were introduced into individual, small (5 cm × 5 cm × 10 cm) see-through plastic chambers located in a larger Faraday box (30 cm × 30 cm × 20 cm). fEPSPs were evoked by electrical pulses delivered by Cibertec CS20 stimulators across ISU-220 isolation units (Cibertec, Madrid, Spain) and recorded with Dagan Corporation EX4-400 Quad Differential amplifiers (Dagan Corporation, Minneapolis MN United States) at a bandwidth of 0.1 Hz–10 kHz, through a high-impedance probe (2 × 1,012 Ω , 10 pF).

Input/output curves (**Figure 2**) of each of the five selected synapses were tested by applying 100-μs, square, biphasic paired pulses (40 ms of interstimulus interval) of increasing intensities (0.02–0.4 mA, in steps of 0.02 mA). Ten pulses of each intensity were presented to the animals at intervals of > 10 s to avoid stimulus interactions (Gruart et al., 2006).

For the paired-pulse facilitation test (**Figure 3**) mice were stimulated in each synapse with paired pulses of increasing interstimulus interval (10, 20, 40, 100, 200, and 500 ms; ten pulses each) with intensities corresponding to 40% of the intensity necessary to evoke a saturating fEPSP response (Gureviciene et al., 2004).

In order to induce LTP in the chronic experiments (**Figure 4**), we applied a high-frequency stimulation (HFS) protocol always in the PP, consisting of five 200-Hz, 100-ms trains of pulses at a rate of 1/s. This protocol was presented 6 times (at 1/min). A 15-min baseline was established before LTP induction by evoking fEPSPs with paired (40-ms interstimulus interval) 100-μs square, biphasic pulses at a rate of 6/min. Pulse intensity was set at 40% of the amount necessary to evoke a maximum fEPSP response (0.05–0.4 mA; Gureviciene et al., 2004; Gruart et al., 2006). In order to prevent the appearance of large amplitude population spikes and/or hippocampal seizures, intensities used for evoking baseline recordings were maintained for the HFS protocol. None of the animals of this study suffered any of those unwanted

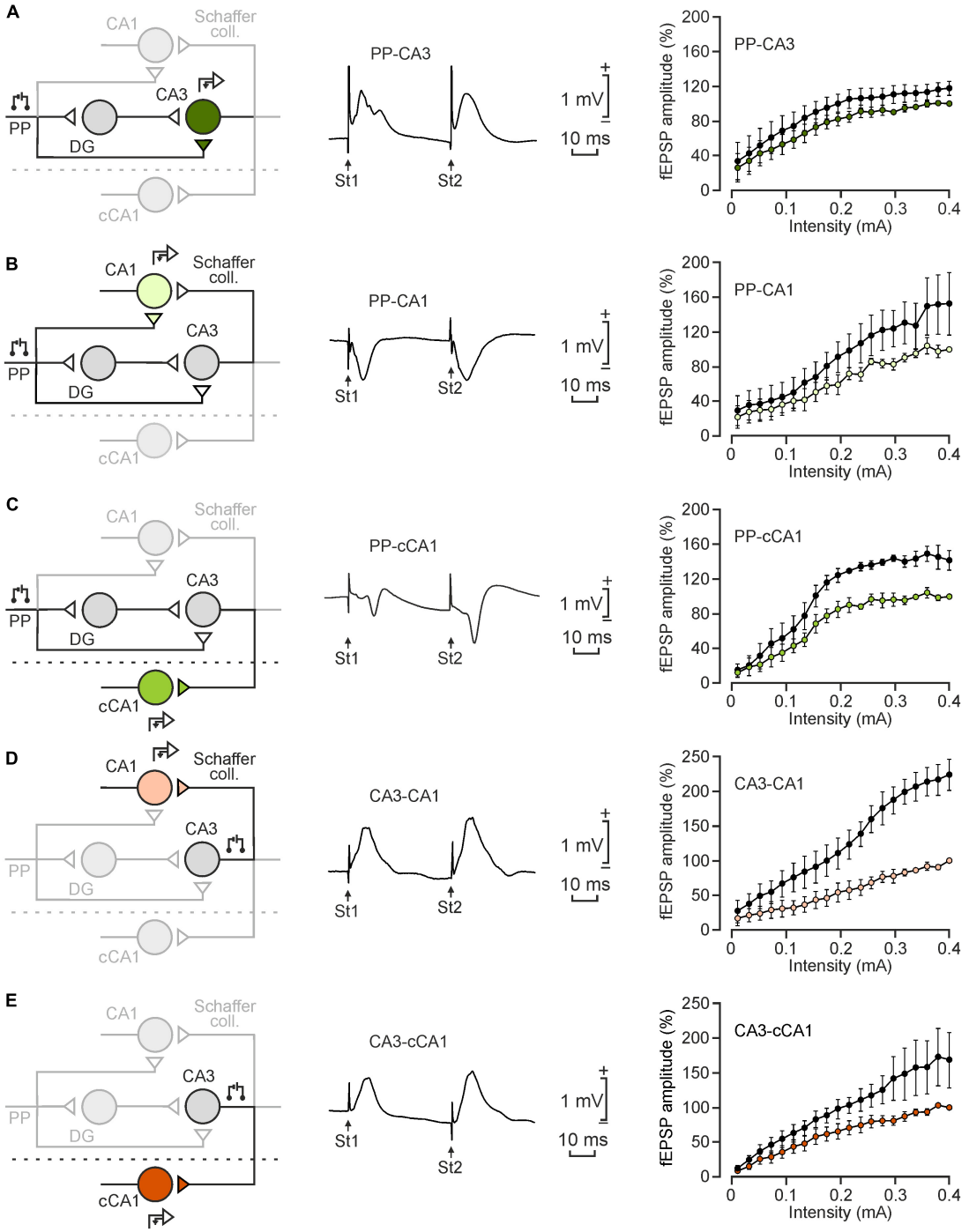

FIGURE 2 | Input/output curves of the five selected synapses. **(A–E)** From left to right are illustrated a schematic representation of the synapse under study, a representative example of the fEPSP recording at 2 × Threshold intensities (St1: first stimulus; St2: second stimulus) and input/output curves collected from the five illustrated synapses: **(A)**, PP-CA3; **(B)**, PP-CA1; **(C)**, PP-cCA1; **(D)**, CA3-CA1; and **(E)**, CA3-cCA1. Computed curves were normalized as the percentage of amplitude values reached under the maximum intensity. Black circles stand for the second stimulus. Data were collected from 5 animals/synapse.

events after receiving the HFS protocol, as checked in the on-line EEG recordings. Post-HFS recordings were acquired at the same intensity and frequency as in the baseline for 30 min the first day and for 15 min the 3 following days. fEPSPs were averaged every 15 pulses in order to measure the amplitude in both baseline and post-HFS recording and represented as a percentage of baseline (100%) values. With the purpose of recording the five hippocampal synapses, the following experimental design was

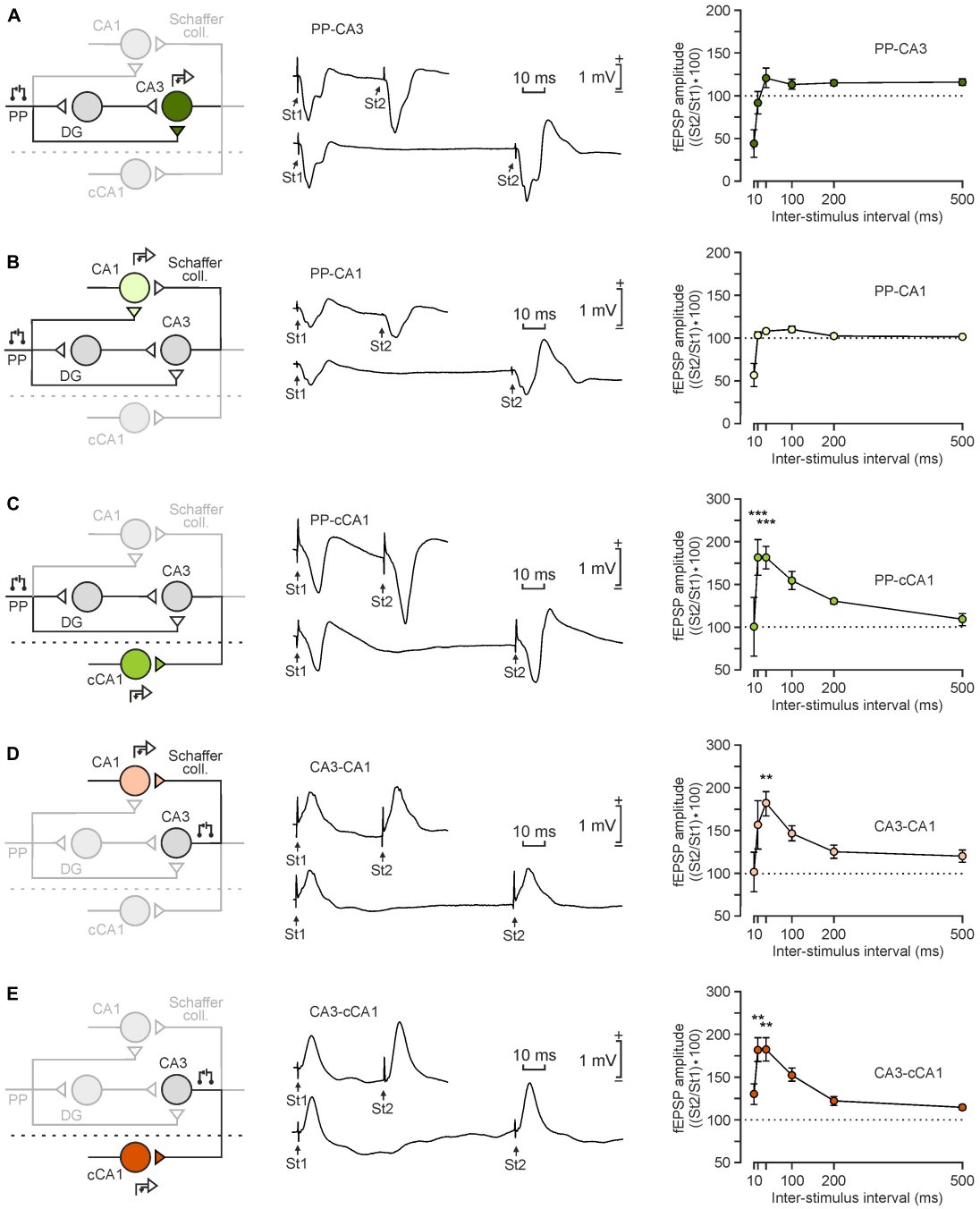

FIGURE 3 | Paired-pulse facilitation of the five selected synapses. **(A–E)** From left to right are illustrated a schematic representation of the synapse under study, a representative example of fEPSP evoked by the paired-pulse stimulation (St1: first stimulus; St2: second stimulus) at 40 and 100 ms interstimulus interval, and the paired-pulse facilitation induced in the five illustrated synapses: **(A)**, PP-CA3; **(B)**, PP-CA1; **(C)**, PP-cCA1; **(D)**, CA3-CA1; and **(E)**, CA3-cCA1. Each synapse is represented by a different color. Black circles stand for the second stimulus. Data were collected from 4 animals/synapse. Every point for each animal represents the mean value of 10 stimuli (with its corresponding SEM). The five synapses presented similar facilitation patterns in the same interstimulus intervals [$F_{(5,\ 15)} = 11.458$; $P < 0.001$]. $^{**}P < 0.01$, $^{***}P < 0.001$ in comparison with the values collected at 500 ms —i.e., the most similar to baseline values.

followed: first, fEPSP were evoked in CA3, CA1, and cCA1 by the stimulation of the PP. Second, fEPSP were evoked in CA1 and cCA1 by stimulating the CA3 area. These two configurations were alternated in a way that did not affect fEPSP recordings.

For the head-fixed recordings, mice were individually placed on a foam-covered running wheel supported by a system of aluminum bars. The animal had freedom of leg movements, but its head plate was screwed to the two tightened horizontal

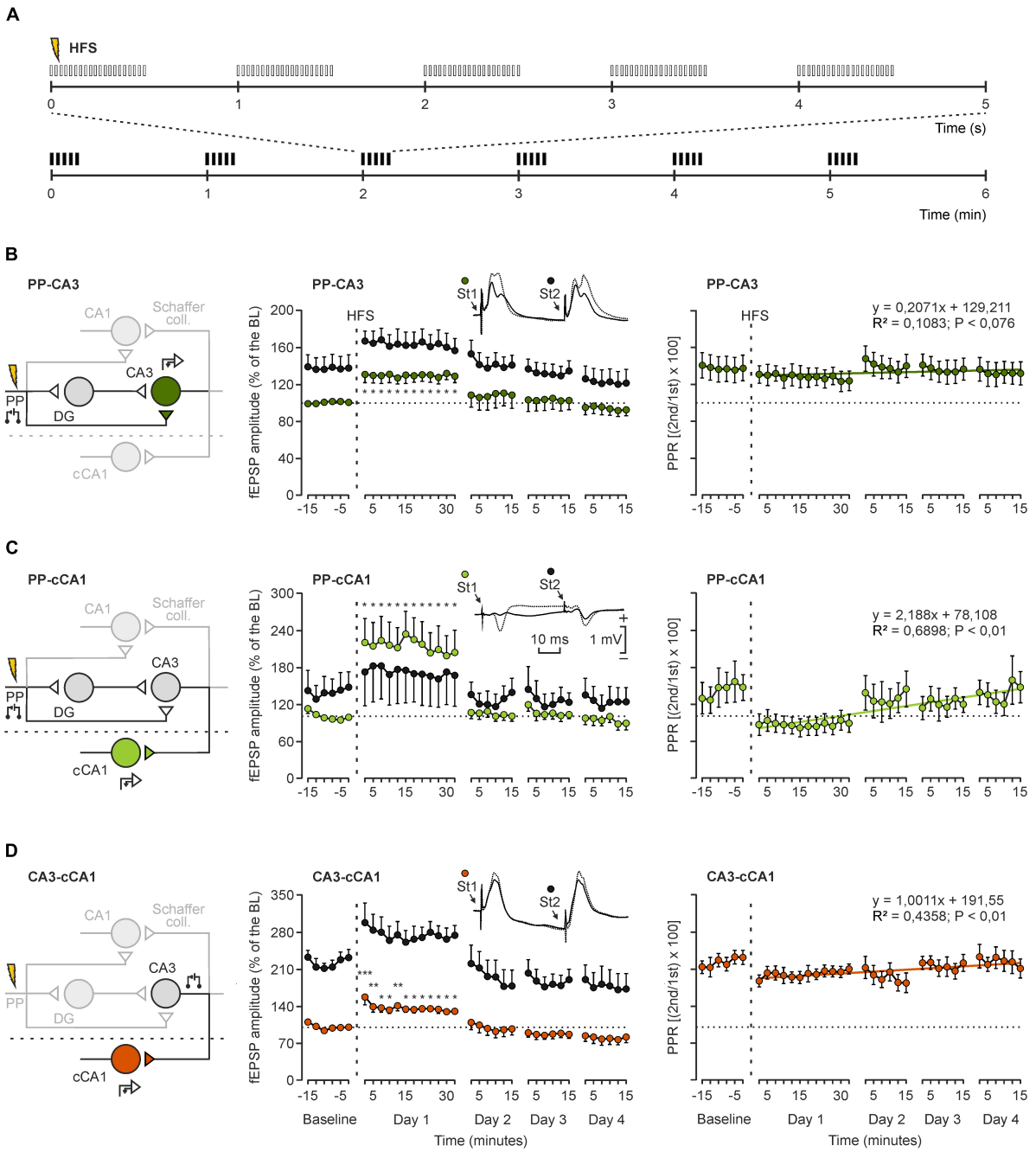

FIGURE 4 | High-frequency stimulation of the PP evoked LTP in CA3 and cCA1. **(A)** The high-frequency stimulation (HFS) protocol consisted of 5 trains (200 Hz, 100 ms) of pulses at a rate of 1/s. These trains were presented 6 times in total, at intervals of 1/min. **(B–D)** Schematic representation of the stimulating and recording sites during the experiment (left), LTP evolution of PP-CA3 **(B)**, PP-cCA1 **(C)** and CA3-cCA1 **(D)** synapses (middle) and their paired-pulse ratios and linear regression lines (right). Insets illustrate representative examples of recorded fEPSPs from the three indicated synapses –not necessarily from the same mouse. Each circle represents the average amplitude computed from 15 stimulus presentations ± SEM. LTP was evoked in the 3 synapses by HFS of the PP. In order to obtain a baseline, animals were stimulated every 10 s for 15 min in the afferent pathway. After HFS, the same stimulus was presented at the initial rate (6/min) for another 30 min. Recording sessions were repeated on 3 additional days (15 min each) (n = 10). *P < 0.05; **P < 0.01; ***P < 0.001 (one-way ANOVA, contrast analysis against baseline values).

holding bars (**Figure 6A**). Further information about this recording device can be found in a previous study by some of us (Heiney et al., 2014; López-Ramos et al., 2018). Mice had 3 days of habituation (5, 15, 25 min) in order to minimize stress during recording sessions. fEPSPs were evoked with the above-described stimulation equipment and recorded with

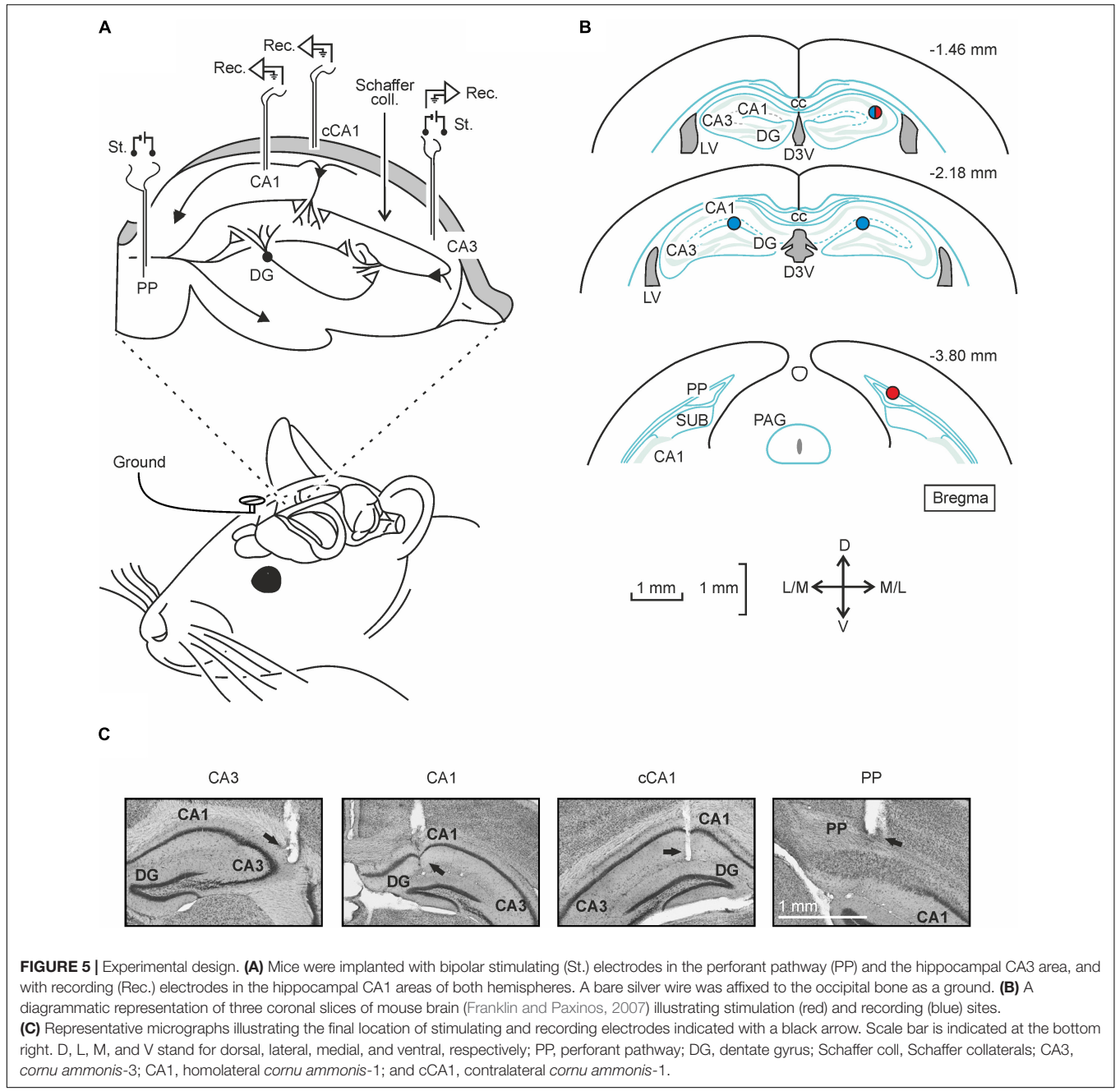

FIGURE 5 | Experimental design. **(A)** Mice were implanted with bipolar stimulating (St.) electrodes in the perforant pathway (PP) and the hippocampal CA3 area, and with recording (Rec.) electrodes in the hippocampal CA1 areas of both hemispheres. A bare silver wire was affixed to the occipital bone as a ground. **(B)** A diagrammatic representation of three coronal slices of mouse brain (Franklin and Paxinos, 2007) illustrating stimulation (red) and recording (blue) sites. **(C)** Representative micrographs illustrating the final location of stimulating and recording electrodes indicated with a black arrow. Scale bar is indicated at the bottom right. D, L, M, and V stand for dorsal, lateral, medial, and ventral, respectively; PP, perforant pathway; DG, dentate gyrus; Schaffer coll, Schaffer collaterals; CA3, *cornu ammonis*-3; CA1, homolateral *cornu ammonis*-1; and cCA1, contralateral *cornu ammonis*-1.

an AC/DC differential amplifier (Model 3000, A-M system, Carlsborg, WA) at a bandwidth of 0.1 Hz–3 kHz, through a high-impedance probe (2 × 1,012 Ω, 10 pF). Recordings in the contralateral CA1 area (cCA1) were carried out with a 10-μm glass micropipette filled with 2 M NaCl and mounted on a micromanipulator (M-2, Narishige, Tokyo, Japan). The electrode was introduced into the brain and the correct waveform searched for, using as a guide the depth-profile fEPSPs illustrated in **Figure 1**, obtained by stimulating with 40-ms ISI pulses in either PP or CA3. Firstly, a 5-min baseline was established in the PP-cCA1 synapse looking for a good fEPSP waveform to ensure that the position of the PP stimulating electrode was appropriate for a correct LTP induction. Next, a 15-min baseline for the CA3-cCA1 synapse was recorded. After that, LTP induction was elicited by presenting the above-described HFS protocol. Post-induction effects were recorded for 2 h. Electrical stimulation during baselines and post-HFS recordings consisted of 100-μs, square, biphasic, paired pulses (40 ms of interstimulus interval) at a rate of 1/20 s. Data were analyzed to measure fEPSP amplitudes, which were represented as a percentage of the baseline (100%) values. For that, fEPSPs were averaged (n = 15) every 5 min. The same stimulating and recording instruments were used for the depth-profile recordings. Stimulation intensity was set to obtain the 40% of the

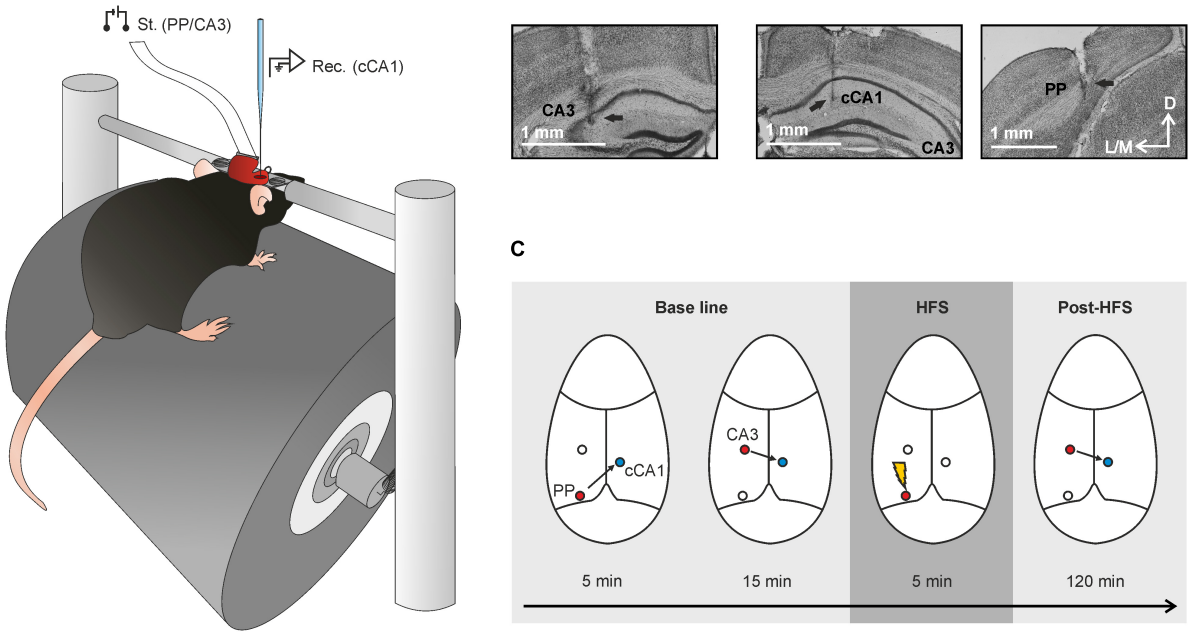

FIGURE 6 | Experimental procedures for recordings in alert head-fixed mice. **(A)** Mice were placed on a head-fixed set-up for the recording of cCA1 potentials evoked by stimulation of either the PP or the hippocampal CA3 area. **(B)** Photomicrographs of CA3, cCA1, and PP showing the electrode scar. **(C)** Schematic representation of the involved synapses during the experiment with indication of the stimulating (red) and recording (blue) locations. A 5-min baseline was recorded for the PP-CA3 synapse to ensure that the position of the electrode in the PP was good enough for the successive HFS, followed by a 15-min baseline for the CA3-cCA1 synapse. After the 5-min HFS, post-HFS recordings were carried out in the CA3-cCA1 synapse for 120 min.

maximum response at 1,3 mm depth and maintained for the rest of the experiment.

Histology

At the end of the experiments, mice were deeply anesthetized (sodium pentobarbital, 50 mg/kg) and perfused transcardially with 0.9% saline, followed by 4% paraformaldehyde phosphate buffer (PFA) as a fixative. Their brains were removed and maintained in the same solution overnight at 4°C. After a cryoprotectant treatment with an increasing gradient of sucrose in PBS (5, 15, and 30%), brains were cut into 50-μm slices in a cryotome (Leica, Wetzlar, Germany) and the slices of interest were mounted on gelatinized glass slides and stained with 0.1% toluidine blue (Nissl technique). Photomicrographs of electrode scars were taken using a 5 × objective of a Leica DMRE microscope equipped with a Leica DFC550 camera, and with the help of the LAS V4.2 software (Leica Microsystems GmbH, Wetzlar, Germany).

Data Collection and Analysis

fEPSPs and 1V square pulses corresponding to stimulus presentations were digitally stored on a computer through the analog/digital converter CED 1401 Plus (CED, Cambridge, England), at a sampling frequency of 5 kHz, and with an amplitude resolution of 16 bits. fEPSP amplitudes were quantified off-line using CED Spike 2 and Signal (Systat Software, San Jose, CA, United States) programs. For this, we averaged the amplitude of 15 fEPSPs collected every 2.5 min (chronic recordings) or 5 min (acute recordings). We used Microsoft Excel (Microsoft, Redmond, WA, United States) and CorelDraw (Corel Corporation, Ottawa, Canada) programs for data representation and the Sigma Stat for Windows package for statistical analysis. Unless otherwise indicated, data are represented as the mean ± SEM. Acquired data from PPF were analyzed using a two-way ANOVA, with synapse and interval as factors. LTP data were analyzed using a one-way ANOVA test, with sessions as repeated measure. When a normality test failed, the significance (p-value) was calculated with the Friedman Repeated Measures Analysis of Variance on Ranks test, a non-parametric method. Contrast analysis was added for a further study of significant differences after parametric (Student-Newman-Keuls Method) and non-parametric (Tukey) tests. In the PPF study, values of the 500 ms interstimulus interval were considered the baseline for contrast analysis.

RESULTS

The Five Selected Hippocampal Synapses Share Similar Basic Electrophysiological Properties

As explained in detail in "Materials and Methods" section, animals ($n \geq 5$ animals/synapse) were prepared for different electrophysiological studies in five hippocampal synapses:

PP-CA3, PP-CA1, PP-cCA1, CA3-CA1, and CA3-cCA1 (see **Figures 5A,B**). The proper electrode position was determined during surgery with the help of the field-potential depth profile recordings obtained in previous experiments involving ipsilateral (Gruart et al., 2015) and contralateral pathways (**Figure 1**). Once the experiments ended, we checked the final location of the implanted electrodes by means of histological techniques (**Figure 5C**).

In a first series of experiments on alert behaving mice, we studied the basic properties of the five synapses. For input/output curves, mice were presented with paired pulses (40 ms of interpulse interval) of increasing intensities (0.02–0.4 mA, in steps of 0.02 mA). All synapses presented similar input/output curves, with a sigmoid-like shape, to the presentation of the first pulse (**Figure 2**, right column).

We paid particular attention to the relationships between fEPSPs evoked by the second pulse and those evoked by the first one. Second pulse presentation evoked responses with a higher facilitation in the five selected synapses as the intensity became higher, especially in the CA3-CA1 synapse (**Figure 2D**). In contrast, the CA3-cCA1 synapse presented lower facilitation values at high stimulus intensities (**Figure 2E**). Interestingly, and as already indicated in a previous study (Gruart et al., 2015), the ratio 2nd/1st pulse in the PP-CA3 synapse stayed more stable across the increasing stimulus intensities with no signs of paired-pulse facilitation across the whole range of stimulus intensities (**Figure 2A**).

The additional purpose of the input/output curves test was to set the appropriate stimulation intensity for the rest of the experiments in each mouse—i.e., the intensity able to evoke an fEPSP with about 40% of the maximum amplitude obtained in the input/output test. Recorded fEPSP waveforms (**Figure 2**, middle panel) were indicative of the position of the electrode tip relative to the neuron's position in the hippocampal intrinsic circuit—namely, closer to the apical dendrites (negative) or to the somas (positive). All synapses presented evoked fEPSPs with latencies in the range of 1.5–3.5 ms, except for the PP-cCA1 synapse, which presented latencies ranging from 5.5 to 8 ms. This difference clearly indicates that this pathway is not monosynaptic, as illustrated in **Figure 2C** (left).

We also performed a paired-pulse facilitation test ($n \geq 4$ animals/synapse) at increasing (10, 20, 40, 100, 200, and 500 ms) interstimulus intervals. This experimental procedure offered an idea of the changes in short-term plasticity in the five synapses included in this study. Indeed, it is generally accepted that changes in paired-pulse facilitation (or depression) are related to the probability of release of the neurotransmitter at the presynaptic terminal (Volianskis and Jensen, 2003; Lauri et al., 2007).

The five selected synapses illustrated in **Figure 3** presented statistically significant differences after a 2-way ANOVA analysis on the effect of interstimulus interval [$F_{(5,\ 15)} = 11.458$; $P < 0.001$] and synapse [$F_{(4,\ 12)} = 10.520$; $P < 0.001$], as well as their interaction [$F_{(20,\ 60)} = 3{,}016$; $P < 0.001$]. Nevertheless, a deeper observation of the differences between synapses showed that there were two separated patterns. Firstly, synapses PP-CA3 (**Figure 3A**) and PP-CA1 (**Figure 3B**) presented similar responses since there were no significant differences ($P = 0{,}756$) between them. And, secondly, the other three hippocampal synapses (**Figures 3C,D**) did not present significant differences among them ($P \geq 0.878$), either.

Regarding the comparisons on the intervals effect, the 40-ms interstimulus interval presented the highest paired-pulse facilitation [$t_{(3,\ 0{\cdot}05)} = 4.158$; $P = 0.01$]. However, a further analysis with all Pairwise Multiple Comparison Procedures (Holm-Sidak method) determined that not all of the synapses present the same magnitude of facilitation. Thus, the paired-pulse facilitation in the 40-ms interval in the PP-CA3 and PP-CA1 synapses was significantly lower than in CA3-CA1, CA3-cCA1, and PP-cCA1 ($P < 0.01$). The two synapses involving the contralateral CA1 area (PP-cCA1 and CA3-cCA1) also presented a statistically significant facilitation at the 20-ms interpulse interval ($P < 0.01$; **Figures 3C,E**).

The High-Frequency Stimulation of the Perforant Pathway Evokes Long-Term Potentiation Not Only in the Different Ipsilateral Synapses but Also in the Contralateral CA1 Area

In order to study the functional changes evoked in the hippocampal synapses PP-CA3, PP-cCA1, and CA3-cCA1 following the experimental induction of LTP, 9–10 animals/synapse were presented with a well-known HFS protocol (Gruart et al., 2006), illustrated in **Figure 4A**. We focused on these main synapses involved in our hypothesis to avoid any unnecessary physical damage caused by electrodes implantation in the small mouse brain, thereby reducing alterations in synaptic transmission within the intrinsic hippocampal circuit. HFS trains were always presented at the same PP site (see left column of **Figures 4B–D**). Prior to the HFS protocol, a 15-min baseline recording was carried out in each synapse (at a rate of 6 stimuli/min). The stimulus intensity was always set at about 40% of the intensity necessary to evoke a maximum fEPSP response. Evoked fEPSPs were recorded for 1 h after the HFS induction at the indicated rate, and again during the next 3 days (30 min each), as previously explained in the "Materials and Methods" section.

We measured fEPSP amplitudes of the synapses PP-CA3, PP-cCA1, and CA3-cCA1 setting the cursor at the latencies of 2.6 ± 0.4, 6.1 ± 0.7, and 3.2 ± 0.5 ms after the artifact generated by the stimulus, respectively. LTP data are represented as a percentage of the baseline (100%) values and are shown in **Figures 4B–D** (right column). LTP effects recorded in the CA3 region after presenting the HFS protocol in the PP [$\chi^2_{(35,\ 315)} = 155.254$; $P < 0.001$] persisted for 2 days, reaching 130 ± 8.79% of baseline values, and gradually returned to basal values. When recording in the CA1 area of the contralateral hemisphere, there was also a significant increase of synaptic efficacy during the 1st day after the LTP induction, but this increase in synaptic strength returned to basal values the second day. The PP-cCA1 synapse presented a potentiation of 233.1 ± 37.9%

$[\chi^2_{(35,\ 315)} = 157.695;\ P < 0.001]$, and CA3-cCA1 values rose to 159.64 ± 14.00% of the baseline $[F_{(35,\ 280)} = 11{,}355;\ P < 0.001]$. Intriguingly, the latter synapse presented a slight depression in evoked fEPSP amplitudes the next 3 days of recordings. We also calculated the paired-pulse ratio (PPR) following LTP induction as an indicative of the relationship between the 1st and the 2nd pulse and, hence, the possibility of changes in presynaptic components of these hippocampal synapses. The PP-cCA1 synapse presented the steepest regression line (slope: 2,188), followed by the CA3-cCA1 synapse (slope: 1.0011). The PP-CA3 synapse presented PPRs across LTP sessions with minimum changes in slope (slope: 0.207). These results indicated that LTP can be evoked in hippocampal circuits not only in the presynaptically stimulated synapse, but also in synapses transsynaptically distant from the stimulated afferent pathway.

Long-Term Potentiation Evoked at the CA3-cCA1 Synapse After Presenting High-Frequency Stimulation Trains in the Perforant Pathway in Head-Fixed Mice

In order to confirm the transsynaptic effects of the LTP evoked in the hippocampal intrinsic circuit, we tried a different approach. In this case, animals were surgically prepared for being placed in a head-holding system that enabled recording fEPSPs using a 10-μm tip glass micropipette for cCA1 recordings (**Figure 6A**). This recording system allows a more accurate position of the electrodes while the animal's head is fixed to the set up and with no need of anesthesia, avoiding unwanted effects on NMDA receptors. LTP was evoked in 5 animals by presenting a HFS protocol in PP to study changes in synaptic strength of the CA3-cCA1 synapse. The final location of electrodes and glass pipette was also confirmed by histological procedures (**Figure 6B**). The experimental procedure illustrated in **Figure 6C** was as follows. An initial baseline was determined to establish the correct position of the stimulating electrode in the PP, as confirmed when recording fEPSP profiles in the cCA1 area (illustrated at the top of **Figure 6A**). After that, a second fEPSP baseline, this time in the CA3-cCA1 synapse, was recorded for 15 min at a rate of 3/min before presenting the HFS protocol in the PP. Changes in the synaptic efficacy were recorded for 2 h at the same initial rate after the LTP induction (**Figure 7A** bottom). Interestingly, again we noted an increase in the synaptic efficacy of the CA3-cCA1 synapse that lasted for at least 2 h $[F_{(8,\ 32)} = 5.920;\ P < 0.001$; **Figure 7B**]. In this case, unlike the regression line of the PPR presented a negative slope (–0.7025). It is not surprising that these results differ from those collected from the chronic experiments in the same synapse, given that in this case recordings are from only one recording session.

As far as we know, there is no report indicating the presence in mice of any noticeable direct axonal projection from the entorhinal cortex (via the PP) to the dorsal CA1 area of the contralateral hemisphere (van Groen et al., 2003; Sun et al., 2018; Tao et al., 2021). Thus, the present results strongly suggest that a significant increase in synaptic strength is transsynaptically evoked by LTP induction in the PP-cCA1 synapse.

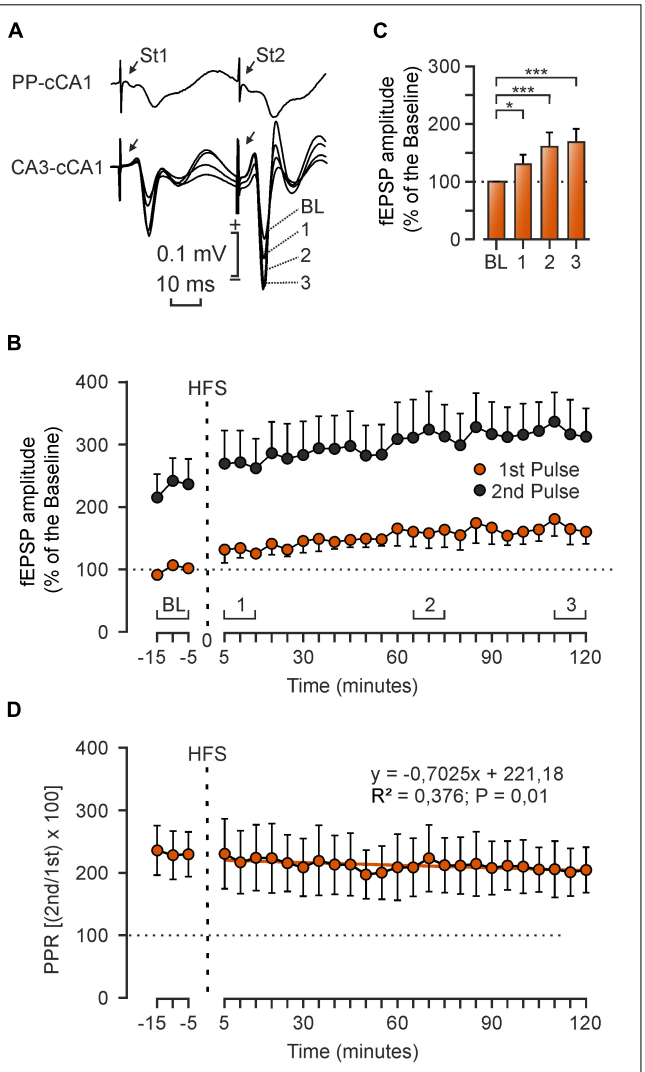

FIGURE 7 | Transsynaptic effects of LTP in alert head-fixed mouse. **(A)** Representative fEPSP collected from the PP-cCA1 and CA3-cCA1 synapses. **(B)** After presenting an HFS protocol to the ipsilateral PP, the LTP effects evoked in the CA3-cCA1 synapse persisted for at least 2 h. For the baseline, animals were stimulated every 20 s for 15 min in the CA3 area. The same stimuli were applied in the post-HFS recordings, which lasted 120 min. **(C)** Mean ± SEM. 1st pulse fEPSP values 1–15 min of baseline (BL), and 1–15 min (1), 65–75 min (2) and 110–120 min (3) after the HFS. Data were collected from 5 animals. $^*P < 0.05$, $^{***}P < 0.001$ (one-way ANOVA). **(D)** The relationship between 2nd and 1st pulses—the paired-pulse ratio (PPR) calculated with the formula (2nd/1st × 100)—presents a linear regression line with a negative slope. Equations corresponding to the linear regression analyses of PPRs are indicated in the plot.

DISCUSSION

Long-Term Potentiation Could Be a Physiological Process

The electrophysiological study presented here demonstrates that LTP experimentally induced by HFS in the PP transsynaptically propagates to the contralateral hippocampal CA1 area across

the CA3-cCA1 projection. It is evidenced the longer latency of fEPSPs evoked in the cCA1 area by PP stimulation, suggestive of a disynaptic projection, and by the presence of LTP in the CA3-cCA1 synapse not evoked by previous direct HFS of the CA3 area. Even in the case that some entorhinal fibers crossing to the contralateral side were activated in these experiments this fact will not explain the presence of LTP at CA3-cCA1 synapses. These interesting results further support two seminal studies reporting the induction of LTP in the dentate gyrus by HFS stimulation of the contralateral PP (Krug et al., 2001) and the presence of LTP in the contralateral medial prefrontal cortex transsynaptically evoked by stimulation of the ipsilateral ventral hippocampus in behaving rats (Taylor et al., 2016). In addition, these results suggest that this transmission from an experimentally potentiated synapse to the contiguous one could happen by means of physiologically evoked action potentials, and strongly support classical contentions (Bliss and Collingridge, 1993; Citri and Malenka, 2008; Neves et al., 2008; Dringenberg, 2020) indicating that LTP is an actual functional mechanism that can be studied in true physiological conditions.

Basic Electrophysiological Properties of the Five Selected Synapses

The latency of fEPSPs evoked at the studied synapses varied according to their physiological features. All of them but PP-cCA1 are monosynaptic projections in mice. The PP-cCA1 synapse presented the largest latency, since it is a disynaptic pathway consisting of the successive projection from entorhinal cortex axons to the CA3 region and its callosal projections to the cCA1 area (Finnerty and Jefferys, 1993). This is known to be a long-range projection (Yang and Sun, 2018), which is consistent with the larger latency observed in this study. Apparently, there is no significant direct axonal projection from the entorhinal cortex to the dorsal cCA1 area, as suggested in recently published works (van Groen et al., 2003; Sun et al., 2018; Tao et al., 2021). Consequently, for this study we focused on this disynaptic pathway to explore the transsynaptic effects of LTP. fEPSP waveforms recorded in these experiments presented positive as well as negative shapes. As illustrated in **Figure 1**, the final position of the recording electrode at the end of the implantation procedure explains the different profiles collected, depending on the location of the recording tip with respect to the sources or sinks of the selected synapses (Bliss and Lømo, 1973; Bliss and Collingridge, 1993; Gruart et al., 2006, 2015; Madroñal et al., 2009). Responses to PP stimulation (synapses PP-CA3, PP-CA1, and PP-cCA1) presented an earlier component corresponding to the direct connection we were interested in, and a later component evoked by the hippocampal trisynaptic circuit, which comprehends the DG. As known, the PP projects its axons to the granule cells of the DG and these send the information through the mossy fibers to the pyramidal cells of CA3.

The initial aim of this work was to study the basic properties of five different synapses belonging to the intrinsic hippocampal circuit in alert behaving mice by carrying out input/output curves and paired-pulse stimulation tests. The input/output curves of the five synapses presented sigmoid-like shapes, like the ones described in a previously published work (Gruart et al., 2015). For the selected synapses, peak fEPSP amplitudes evoked by the first pulse reached similar values, including those evoked at the CA3-cCA1 synapse, indicative of shared functional properties in this regard. With respect to the response of the selected synapses to paired-pulse stimulations at different time intervals, and in accord with previous reports in alert behaving mice (Gruart et al., 2006, 2015), the CA3-CA1 synapse presented the highest paired-pulse facilitation, indicating that this is a functionally weak projection that can be easily increased (Madroñal et al., 2009). Similar results were collected for CA3-cCA1 and PP-cCA1, indicating that this is a basic property of collateral Schaffer projections onto CA1 and cCA1 pyramidal cells. In contrast, PP-CA3 and PP-CA1 did not present signs of paired-pulse facilitation, indicating, according to the residual calcium hypothesis, the presence of a strong synaptic response to the first applied stimulus, leaving low amounts of residual calcium and hence reducing the probability of vesicle release for the presentation of the second pulse (Thomson, 2000; Zucker and Regehr, 2002). These minor differences in the magnitude of the facilitation/depression response could be of some relevance from a functional point of view within the intrinsic hippocampal circuit (Turrigiano and Nelson, 2004; Madroñal et al., 2009).

Main Characteristics of Mono- and Disynaptically Evoked Long-Term Potentiation Responses

In a second step, we studied changes in synaptic efficacy of the three selected synapses after inducing LTP by HFS of the PP in alert behaving mice. The significant effects of the LTP induced in the PP were recorded not only in the hippocampal CA3 area, but also in the contralateral CA1 region. Then, as PP-cCA1 is a disynaptic pathway, we also checked the monosynaptic projection from CA3 to cCA1, finding that the synaptic efficacy was also increased at this synapse, which did not receive the HFS train directly. As above indicated, the LTP evoked at the CA3-cCA1 synapse cannot be explained by the putative presence of activated entorhinal fibers projecting to the contralateral CA1 area. As shown in **Figures 4C,D**, LTP decreased to baseline values after the first day in the projections involving cCA1. Thus, we decided to determine how long these effects lasted within the first session after the HFS was applied to the PP. For this, we further confirmed the transsynaptic effects of LTP evoked in head-fixed mice, applying the HFS protocol in the PP and recording the fEPSPs of the CA3-cCA1 synapse for up to 2 h. The rather short duration of this transsynaptically evoked LTP could be due to the fact that it was not associated with any actual learning acquired by the stimulated animal (Madroñal et al., 2009, 2016). This technique enabled a more accurate control of the electrode position, since it was an acute procedure, meaning that the glass micropipette was implanted in the same recording session. At the same time, the head-fixed set-up granted access to the unanesthetized mouse brain, without missing small polysynaptic activities usually unrecorded with chronically implanted metal electrodes.

The results presented here agree with those of a previous study carried out by Krug et al. (2001), in which the authors were very able of evoking an LTP in the dentate gyrus following the HFS stimulation of the contralateral PP; they proposed that this transsynaptic LTP was evoked by disynaptic potentials induced via the commissural fibers connecting the two entorhinal cortices. In a subsequent report, Taylor et al. (2016) were able to evoke LTP in the contralateral medial prefrontal cortex after inducing HFS of the vHPC; they ascribed this result to the successive activation of a disynaptic crossed pathway. Based on the use of HFS protocols with different frequencies, Yeckel and Berger (1998) proposed that the mono- (by the PP) or disynaptic (by mossy fiber afferents) induction of LTP in the CA3 area by HFS of the ipsilateral entorhinal cortex depends upon the selected stimulation pattern. These changes in synaptic strength caused by HFS in a non-directly afferent pathway represent a very interesting event that could shed some light on the way our brain processes learning and memory phenomena. In fact, this finding is consistent with the currently accepted idea that long-term memories do not remain in restricted and/or isolated regions of the brain (Lashley, 1950; Wiltgen et al., 2004; Josselyn and Tonegawa, 2020), but that they are stored and consolidated in wide cortical neural networks (McClelland et al., 1995; Frankland and Bontempi, 2005). It has also been proposed that plastic phenomena induced by experimental procedures may intensify spontaneous information flow across specific transsynaptic pathways (Smirnova et al., 1993; Davis et al., 1996); this could represent a putative network mechanism underlying types of memory involving multiple sensory-motor components and, obviously, multiple brain structures (Fernández-Ruiz et al., 2012). Nonetheless, we have shown here that LTP was transsynaptically evoked in the CA3-cCA1 pathway as a persistent consequence of the LTP evoked in the CA3 area by HFS of the ipsilateral PP—a finding not reported until now. In this regard, further attention should be paid to the still unknown properties of physiologically evoked LTP of cortical circuits. An appropriate approach for this would be to study LTP effects in other well-known cortical and subcortical excitatory synapses organized in cascade circuits and also involved in learning and memory processes.

DATA AVAILABILITY STATEMENT

The original contributions presented in the study are included in the article/supplementary material, further inquiries can be directed to the corresponding author/s.

ETHICS STATEMENT

The animal study was reviewed and approved by the Pablo de Olavide Ethics Committee (JA 06/03/2018/025).

AUTHOR CONTRIBUTIONS

AG and JD-G conceived and designed the experiments and contributed to materials. MR-B performed the experiments. MR-B, AG, and JD-G designed the figures and analyzed the data. MR-B and JD-G wrote the manuscript. All authors revised the final version of the manuscript.

FUNDING

This work was supported by grants PY18-823 and BIO-122 from the Spanish Junta de Andalucía.

ACKNOWLEDGMENTS

We thank J. C. López-Ramos, and our technicians P. L. Giussani, J. M. González-Marín, and J. A. Santos-Naharro for their excellent technical assistance. We also thank Roger Churchill for his careful revision of the final version of the manuscript.

REFERENCES

Abraham, W. C. (2003). How long will long-term potentiation last? *Philos. Trans. R. Soc. B Biol. Sci.* 358, 735–744. doi: 10.1098/rstb.2002.1222

Abraham, W. C., and Williams, J. M. (2008). LTP maintenance and its protein synthesis-dependence. *Neurobiol. Learn. Mem.* 89, 260–268. doi: 10.1016/j.nlm.2007.10.001

Bliss, T. V. P., and Collingridge, G. L. (1993). A synaptic model of memory: long-term potentiation in the hippocampus. *Nature* 361, 31–39. doi: 10.1038/361031a0

Bliss, T. V. P., and Lømo, T. (1973). Long-lasting potentiation of synaptic transmission in the dentate area of the anaesthetized rabbit following stimulation of the perforant path. *J. Physiol.* 232, 331–356. doi: 10.1113/jphysiol.1973.sp010273

Bortolotto, Z. A., Anderson, W. W., Isaac, J. T. R., and Collingridge, G. L. (2001). Synaptic Plasticity in the Hippocampal Slice Preparation. *Curr. Protoc. Neurosci.* 2001:Unit 6.13. doi: 10.1002/0471142301.ns0613s16

Bortolotto, Z. A., and Collingridge, G. L. (1993). Characterisation of LTP induced by the activation of glutamate metabotropic receptors in area CA1 of the hippocampus. *Neuropharmacology* 32, 1–9. doi: 10.1016/0028-3908(93)90123-K

Citri, A., and Malenka, R. C. (2008). Synaptic plasticity: multiple forms, functions, and mechanisms. *Neuropsychopharmacology* 33, 18–41. doi: 10.1038/sj.npp.1301559

Collingridge, G. L., Randall, A. D., Davies, C. H., and Alford, S. (1992). The synaptic activation of NMDA receptors and Ca2+ signalling in neurons. *Ciba Found. Symp.* 164, 162–71. doi: 10.1002/9780470514207.ch11

Davis, S., Rodger, J., Hicks, A., Mallet, J., and Laroche, S. (1996). Brain structure and task-specific increase in expression of the gene encoding syntaxin 1B during learning in the rat: a potential molecular marker for learning-induced synaptic plasticity in neural networks. *Eur. J. Neurosci.* 8, 2068–2074. doi: 10.1111/j.1460-9568.1996.tb00727.x

Dringenberg, H. C. (2020). The history of long-term potentiation as a memory mechanism: controversies, confirmation, and some lessons to remember. *Hippocampus* 30, 987–1012. doi: 10.1002/hipo.23213

Fassin, M., Danhier, P., and Ris, L. (2020). Effect of oral administration of Magnesium N-Acetyltaurinate on synaptic plasticity in rodents. *Magnes Res.* 33, 106–113. doi: 10.1684/mrh.2021.0475

Fernández-Ruiz, A., Makarov, V. A., and Herreras, O. (2012). Sustained increase of spontaneous input and spike transfer in the CA3-CA1 pathway following long-term potentiation in vivo. *Front. Neural Circuits* 6:71. doi: 10.3389/fncir.2012.00071

Finnerty, G. T., and Jefferys, J. G. R. (1993). Functional connectivity from CA3 to the ipsilateral and contralateral CA1 in the rat dorsal hippocampus. *Neuroscience* 56, 101–108. doi: 10.1016/0306-4522(93)90566-X

Frankland, P. W., and Bontempi, B. (2005). The organization of recent and remote memories. *Nat. Rev. Neurosci.* 6, 119–130. doi: 10.1038/nrn1607

Franklin, K. B. J., and Paxinos, G. (2007). *The Mouse Brain in Stereotaxic Coordinates Third Edition*. New York: Elsevier.

Gruart, A., Muñoz, M. D., and Delgado-García, J. M. (2006). Involvement of the CA3-CA1 synapse in the acquisition of associative learning in behaving mice. *J. Neurosci.* 26, 1077–1087. doi: 10.1523/JNEUROSCI.2834-05.2006

Gruart, A., Sánchez-Campusano, R., Fernández-Guizán, A., and Delgado-García, J. M. (2015). A differential and timed contribution of identified hippocampal synapses to associative learning in mice. *Cereb. Cortex* 25, 2542–2555. doi: 10.1093/cercor/bhu054

Gureviciene, I., Ikonen, S., Gurevicius, K., Sarkaki, A., Van Groen, T., Pussinen, R., et al. (2004). Normal induction but accelerated decay of LTP in APP + PS1 transgenic mice. *Neurobiol. Dis.* 15, 188–195. doi: 10.1016/j.nbd.2003.11.011

Heiney, S. A., Wohl, M. P., Chettih, S. N., Ruffolo, L. I., and Medina, J. F. (2014). Cerebellar-dependent expression of motor learning during eyeblink conditioning in head-fixed mice. *J. Neurosci.* 34, 14845–14853. doi: 10.1523/JNEUROSCI.2820-14.2014

Helme-Guizon, A., Davis, S., Israel, M., Lesbats, B., Mallet, J., Laroche, S., et al. (1998). Increase in syntaxin 1B and glutamate release in mossy fibre terminals following induction of LTP in the dentate gyrus: a candidate molecular mechanism underlying transsynaptic plasticity. *Eur. J. Neurosci.* 10, 2231–2237. doi: 10.1046/j.1460-9568.1998.00232.x

Josselyn, S. A., and Tonegawa, S. (2020). Memory engrams: recalling the past and imagining the future. *Science* 367:eaaw4325. doi: 10.1126/science.aaw4325

Korte, M., and Schmitz, D. (2016). Cellular and System Biology of Memory: timing, Molecules, and Beyond. *Physiol. Rev.* 96, 647–693. doi: 10.1152/physrev.00010.2015

Krug, M., Brdemann, R., Matthies, R., Rthrich, H., and Wagner, M. (2001). Activation of the dentate gyrus by stimulation of the contralateral perforant pathway: evoked potentials and long-term potentiation after ipsi- and contralateral induction. *Hippocampus* 11, 157–167. doi: 10.1002/hipo.1033

Lashley, K. (1950). In search of the engram. *Symp. Soc. Exp. Biol.* 4, 454–482.

Lauri, S. E., Palmer, M., Segerstrale, M., Vesikansa, A., Taira, T., and Collingridge, G. L. (2007). Presynaptic mechanisms involved in the expression of STP and LTP at CA1 synapses in the hippocampus. *Neuropharmacology* 52, 1–11. doi: 10.1016/j.neuropharm.2006.06.017

López-Ramos, J. C., Houdek, Z., Cendelín, J., Vožeh, F., and Delgado-Garciá, J. M. (2018). Timing correlations between cerebellar interpositus neuronal firing and classically conditioned eyelid responses in wild-type and Lurcher mice. *Sci. Rep.* 8:10697. doi: 10.1038/s41598-018-29000-w

Lynch, M. A. (2004). Long-term potentiation and memory. *Physiol. Rev.* 84, 87–136. doi: 10.1152/physrev.00014.2003

Madroñal, N., Delgado-Garcia, J. M., Fernandez-Guizan, A., Chatterjee, J., Kohn, M., Mattucci, C., et al. (2016). Rapid erasure of hippocampal memory following inhibition of dentate gyrus granule cells. *Nat. Commun.* 7, 1–10. doi: 10.1038/ncomms10923

Madroñal, N., Delgado-García, J. M., and Gruart, A. (2007). Differential effects of long-term potentiation evoked at the CA3-CA1 synapse before, during, and after the acquisition of classical eyeblink conditioning in behaving mice. *J. Neurosci.* 27, 12139–12146. doi: 10.1523/JNEUROSCI.3397-07.2007

Madroñal, N., Gruart, A., and Delgado-García, J. M. (2009). Differing presynaptic contributions to LTP and associative learning in behaving mice. *Front. Behav. Neurosci.* 3:7. doi: 10.3389/neuro.08.007.2009

Matsuzaki, M., Honkura, N., Ellis-Davies, G. C. R., and Kasai, H. (2004). Structural basis of long-term potentiation in single dendritic spines. *Nature* 429, 761–766. doi: 10.1038/nature02617

McClelland, J. L., O'Reilly, R. C., and McNaughton, B. L. (1995). Why there are complementary learning systems in the hippocampus and neocortex: insights from the successes and failures of connectionist models of learning and memory. *Physiol. Rev.* 102, 419–457. doi: 10.1007/978-3-642-11202-7_20

Neves, G., Cooke, S. F., and Bliss, T. V. P. (2008). Synaptic plasticity, memory and the hippocampus: a neural network approach to causality. *Nat. Rev. Neurosci.* 9, 65–75. doi: 10.1038/nrn2303

Shepherd, G. M. (2004). *The Synaptic Organization of the Brain*. New York: Oxford University Press. doi: 10.1093/acprof:oso/9780195159561.001.1

Smirnova, T., Laroche, S., Errington, M. L., Hicks, A. A., Bliss, T. V. P., Mallet, J., et al. (1993). Transsynaptic expression of a presynaptic glutamate receptor during hippocampal long- term potentiation. *Science* 262, 433–436. doi: 10.1126/science.8105538

Sun, Y., Nitz, D. A., Holmes, T. C., and Xu, X. (2018). Opposing and complementary topographic connectivity gradients revealed by quantitative analysis of canonical and noncanonical hippocampal CA1 inputs. *Eneuro* 5, 322–317. doi: 10.1523/ENEURO.0322-17.2018

Tao, S., Wang, Y., Peng, J., Zhao, Y., He, X., Yu, X., et al. (2021). Whole-Brain Mapping the Direct Inputs of Dorsal and Ventral CA1 Projection Neurons. *Front. Neural Circuits* 15:643230. doi: 10.3389/fncir.2021.643230

Taylor, C. J., Ohline, S. M., Moss, T., Ulrich, K., and Abraham, W. C. (2016). The persistence of long-term potentiation in the projection from ventral hippocampus to medial prefrontal cortex in awake rats. *Eur. J. Neurosci.* 43, 811–822. doi: 10.1111/ejn.13167

Thomson, A. M. (2000). Facilitation, augmentation and potentiationat central synapses. *Trends Neurosci.* 23, 305–312. doi: 10.1016/s0166-2236(00)01580-0

Turrigiano, G. G., and Nelson, S. B. (2004). Homeostatic plasticity in the developing nervous system. *Nat. Rev. Neurosci.* 5, 97–107. doi: 10.1038/nrn1327

van Groen, T., Miettinen, P., and Kadish, I. (2003). The entorhinal cortex of the mouse: organization of the projection to the hippocampal formation. *Hippocampus* 13, 133–149. doi: 10.1002/hipo.10037

Volianskis, A., France, G., Jensen, M. S., Bortolotto, Z. A., Jane, D. E., and Collingridge, G. L. (2015). Long-term potentiation and the role of N-methyl-D-aspartate receptors. *Brain Res.* 1621, 5–16. doi: 10.1016/j.brainres.2015.01.016

Volianskis, A., and Jensen, M. S. (2003). Transient and sustained types of long-term potentiation in the CA1 area of the rat hippocampus. *J. Physiol.* 550, 459–492. doi: 10.1113/jphysiol.2003.044214

Wiltgen, B. J., Brown, R. A. M., Talton, L. E., and Silva, A. J. (2004). New circuits for old memories: the role of the neocortex in consolidation. *Neuron* 44, 101–108. doi: 10.1016/j.neuron.2004.09.015

Witter, M. P., Naber, P. A., Van Haeften, T., Machielsen, W. C. M., Rombouts, S. A. R. B., Barkhof, F., et al. (2000). Cortico-hippocampal communication by way of parallel parahippocampal-subicular pathways. *Hippocampus* 10, 398–410. doi: 10.1002/1098-1063200010:4<398::AID-HIPO6<3.0.CO;2-K

Yang, W., and Sun, Q. Q. (2018). Circuit-specific and neuronal subcellular-wide E-I balance in cortical pyramidal cells. *Sci. Rep.* 8:3971. doi: 10.1038/s41598-018-22314-9

Yeckel, M. F., and Berger, T. W. (1998). Spatial distribution of potentiated synapses in hippocampus: dependence on cellular mechanisms and network properties. *J. Neurosci.* 18, 438–450. doi: 10.1523/JNEUROSCI.18-01-00438.1998

Zucker, R. S., and Regehr, W. G. (2002). Short-term synaptic plasticity. *Annu. Rev. Physiol.* 64, 355–405. doi: 10.1146/annurev.physiol.64.092501.114547

Conflict of Interest: The authors declare that the research was conducted in the absence of any commercial or financial relationships that could be construed as a potential conflict of interest.

frontiers | Frontiers in Synaptic Neuroscience

TYPE Original Research
PUBLISHED 06 October 2022
DOI 10.3389/fnsyn.2022.1021832

OPEN ACCESS

EDITED BY
Lu Chen,
Stanford University, United States

REVIEWED BY
Yan Dong,
University of Pittsburgh, United States
Chu Chen,
The University of Texas Health Science Center at San Antonio, United States

*CORRESPONDENCE
Houhui Xia
Houhui_xia@urmc.rocheser.edu

RECEIVED 17 August 2022
ACCEPTED 09 September 2022
PUBLISHED 06 October 2022

CITATION
Foley K, Altimimi H, Hou H, Zhang Y, McKee C, Papasergi-Scott MM, Yang H, Mayer A, Ward N, MacLean DM, Nairn AC, Stellwagen D and Xia H (2022) Protein phosphatase-1 inhibitor-2 promotes PP1γ positive regulation of synaptic transmission. *Front. Synaptic Neurosci.* 14:1021832. doi: 10.3389/fnsyn.2022.1021832

Protein phosphatase-1 inhibitor-2 promotes PP1γ positive regulation of synaptic transmission

Karl Foley[1,2], Haider Altimimi[3], Hailong Hou[1], Yu Zhang[1], Cody McKee[1,2], Makaía M. Papasergi-Scott[1], Hongtian Yang[1], Abigail Mayer[2], Nancy Ward[1], David M. MacLean[1], Angus C. Nairn[4], David Stellwagen[3] and Houhui Xia[1,2]*

[1]Department of Pharmacology and Physiology, University of Rochester Medical Center, Rochester, NY, United States, [2]Neuroscience Graduate Program, Department of Neuroscience, School of Medicine and Dentistry, University of Rochester Medical Center, Rochester, NY, United States, [3]Department of Neurology and Neurosurgery, Center for Research in Neuroscience, McGill University, Montreal, QC, Canada, [4]Department of Psychiatry, Yale University, New Haven, CT, United States

Inhibitor-2 (I-2) is a prototypic inhibitor of protein phosphatase-1 (PP1), a major serine-threonine phosphatase that regulates synaptic plasticity and learning and memory. Although I-2 is a potent inhibitor of PP1 *in vitro*, our previous work has elucidated that, *in vivo*, I-2 may act as a positive regulator of PP1. Here we show that I-2 and PP1γ, but not PP1α, positively regulate synaptic transmission in hippocampal neurons. Moreover, we demonstrated that I-2 enhanced PP1γ interaction with its major synaptic scaffold, neurabin, by Förster resonance energy transfer (FRET)/Fluorescence lifetime imaging microscopy (FLIM) studies, while having a limited effect on PP1 auto-inhibitory phosphorylation. Furthermore, our study indicates that the effect of I-2 on PP1 activity *in vivo* is dictated by I-2 threonine-72 phosphorylation. Our work thus demonstrates a molecular mechanism by which I-2 positively regulates PP1 function in synaptic transmission.

KEYWORDS

protein phosphatase-1, scaffolding protein, regulatory subunit, synaptic transmission, FRET-Förster resonance energy transfer, hippocampus, inhibitor-2

Introduction

Inhibitor-2 (I-2) is a prototypic inhibitor of protein phosphatase-1 (PP1), a major serine-threonine phosphatase which plays a critical role in synaptic functions (Foley et al., 2021b). The mechanism of inhibition of PP1 by I-2 has been extensively studied *in vitro* for decades since its purification in 1976 (Cohen, 1989;

Lemaire and Bollen, 2020). Based on the crystal structure of the PP1–I-2 complex (Hurley et al., 2007) and other biochemical studies, PP1 binds to I-2 in a 1:1 stoichiometry, and an α-helix of I-2 (130–169) covers the active site of PP1, thereby inhibiting catalytic activity.

PP1 is inactive within the *in vitro* PP1–I-2 complex, but can be quickly (<1 min) activated when I-2 is phosphorylated at threonine 72 (pT72) by GSK3β (Cohen, 1989), MAPK or CDK5 (Li et al., 2006), presumably moving the I-2 α-helix away from the active site of PP1. However, I-2 pT72 acts as an intramolecular substrate for active PP1, and therefore must undergo dephosphorylation before PP1 is active toward other substrates. While PP1 is active, dephosphorylated I-2 T72 will lead to another slow (∼30 min) conformational change such that the α-helix of I-2 (residues 130–169) swings back into the active site, eventually leading to full inhibition of phosphatase activity (Cohen, 1989), completing the PP1 activation-inhibition cycle. Mutation of I-2 at T72 (T72A) blocks the activation step in the cycle and should be a constitutive PP1 inhibitor (Park et al., 1994; Huang et al., 1999).

While *in vitro* studies predominate, studies of I-2 function in intact cells and model organisms suggest more complex I-2 regulation and function (Wang et al., 2008a,b). Increasing evidence suggests that I-2 can function as a positive regulator of PP1 in addition to its role in PP1 inhibition (Tung et al., 1995; Lemaire and Bollen, 2020). For example, we found that I-2 knockdown, but not I-1 knockdown, in primary cortical neurons decreases PP1 activity based on increased PP1 inhibitory phosphorylation at T320 (Hou et al., 2013). Further, PP1 activity is required for long-term depression (LTD), but chemical LTD is defective in I-2 knockdown neurons (Hou et al., 2013). Similarly, PP1 constrains learning and memory and acts as a molecule of forgetfulness (Genoux et al., 2002), but global knockout (KO) of I-2 in mice, and knockdown of I-2 in rats, decreased memory formation as assayed by novel object recognition, contextual fear conditioning, and Morris water maze (Yang et al., 2015).

While we have found that I-2 plays an important role in LTD (Hou et al., 2013), synaptic downscaling (Siddoway et al., 2013a), and memory formation (Yang et al., 2015), whether I-2 plays a role in regulating synaptic transmission has not been examined. Additionally, the mechanism by which I-2 can promote PP1 function in the central nervous system is not clear, but, like other PP1 regulatory proteins, likely involves changing PP1 interaction with other proteins. Previous research has shown that I-2 can form a heterotrimeric complex with neurabin and PP1 (Terry-Lorenzo et al., 2002b; Dancheck et al., 2011), presenting an enticing model by which I-2 could regulate synaptic PP1.

Neurabin is a major PP1 regulatory protein that binds F-actin and targets PP1 to synaptic spines. Neurabin binds to PP1 *via* its $RvXF^{460}$ motif as well as adjacent disordered regions (Ragusa et al., 2010). Mutating F460 in the $RvXF^{460}$ motif leads to robust and significant decrease of neurabin-PP1 binding (Hu et al., 2006; Ragusa et al., 2010), as well as a decrease in synaptic transmission, suggesting that PP1 bound to neurabin promotes synaptic transmission (Hu et al., 2007). Neurabin binds PP1γ preferentially, PP1α to a lesser extent, and PP1β minimally (Terry-Lorenzo et al., 2002a; Carmody et al., 2008), suggesting PP1γ is most likely the PP1 isoform that promotes synaptic transmission. However, no direct test has validated this. Moreover, I-2, PP1, and neurabin all localize to excitatory synapses (Siddoway and Xia, 2011; Foley et al., 2021b), suggesting that they could act together in regulating synaptic transmission.

In this study, we employed over-expression of I-2 in combination with PP1α, PP1γ, and I-2 KO studies and found that I-2 and PP1γ both promote basal synaptic transmission. By introducing a phospho-null mutation at T72 in I-2, thereby disrupting the activation-inhibition cycle of PP1–I-2, we abolished the positive effect of I-2 on PP1 activity. Lastly, we found that I-2 promotes PP1γ targeting to neurabin, a critical synaptic PP1γ scaffolding protein for synaptic transmission. Our current work elucidates an important function of I-2 in promoting synaptic transmission and provides a mechanism of how I-2 positively regulates PP1 function.

Materials and methods

Conditional knockout mice

Nestin-cre and CaMKIIα-cre (T29-1) were purchased from Jackson Lab. PP1α and PP1γ conditional KO mouse were generated as described previously (Liu et al., 2015). I2 floxed mice, in which exon 1 and exon 2 were flanked by Cre recombinase-dependent loxP recognition sequences, were generated by the University of Rochester Medical Center Transgenic and Genome Editing Core.

Primary neuronal cell cultures, infections, immunoblotting and antibodies

Primary cortical neurons were prepared from mixed male/female E18 Sprague Dawley (SD) rat embryos as previously described (Siddoway et al., 2013b, 2014). ∼DIV21 neurons were used in our study. CFP, CFP-I-2(WT), and CFP-I-2(T72A) constructs and recombinant Sindbis virus generation and infection have been described previously (Hou et al., 2013). In brief, pSinRep5 (nsP2S) vector was used for CFP/I-2 subcloning, and targeted recombinant constructs were linearized, *in vitro* translated and electroplated into BHK21 cells, along with helper DHBB. Supernatant containing recombinant viruses were collected, concentrated *via* centrifugation before being

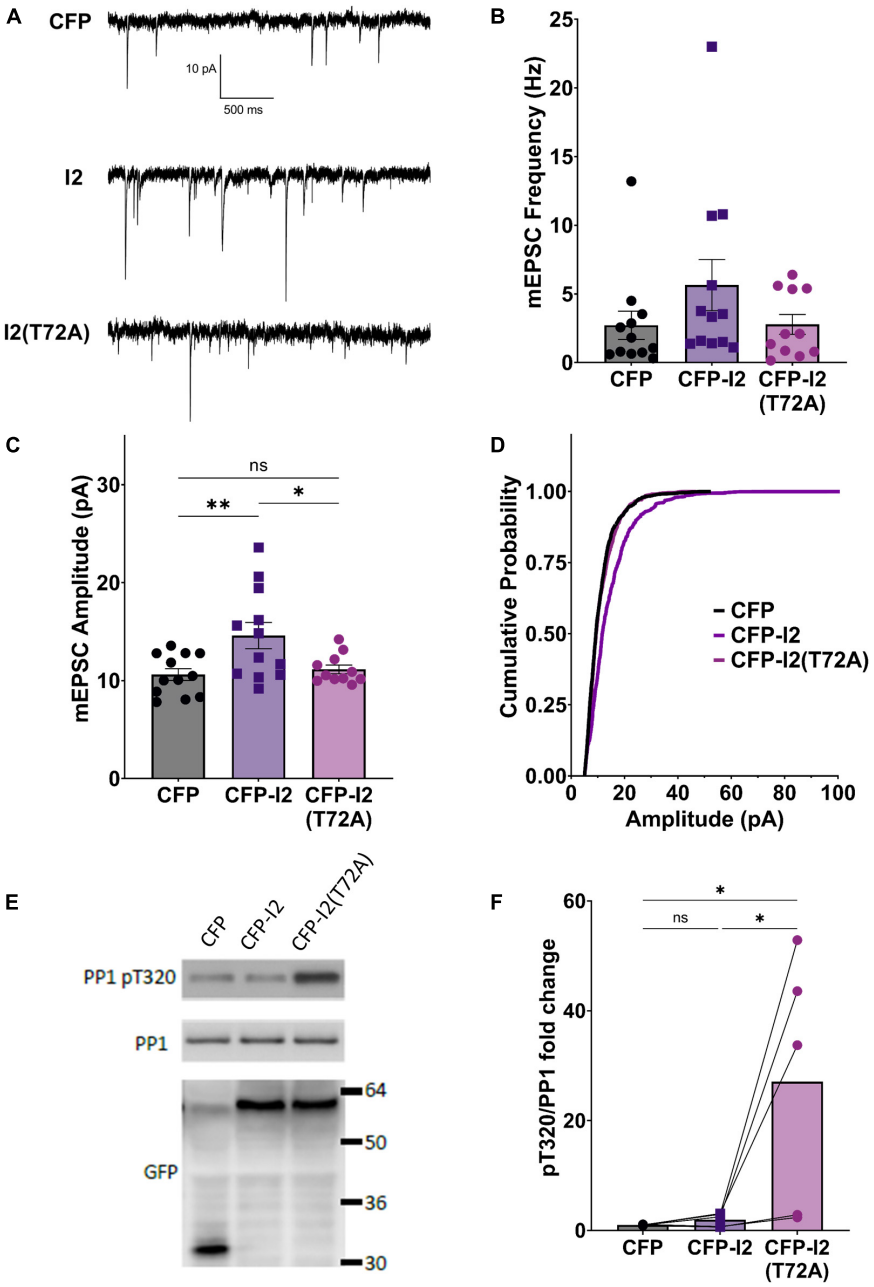

FIGURE 1
I-2 promotes synaptic transmission in primary cortical neurons. **(A)** Example traces of mEPSC recordings in primary cortical neurons (~DIV21) expressing CFP, CFP-I2, or CFP-I2(T72A). **(B,C)** Quantification of mEPSC amplitude **(B)** and frequency **(C)**. I-2 overexpression significantly increases mEPSC amplitude, but not frequency [one-way ANOVAs, $F_{(2,\ 32)} = 5.81$, $p < 0.01$; $F_{(2,\ 32)} = 1.62$, $p = 0.21$, respectively]. **(D)** Cumulative probability of mEPSC amplitude distribution [Kolmogorov-Smirnov test, $p < 0.0001$ between CFP and I-2(WT)-expressed neurons. $P = 0.48$ for between CFP and I2(T72A)]. Data in **(B–D)** are from the following number of cells, CFP: 12; I2: 12; I2(T72A): 11. **(E)** Western blot derived from ~DIV21 primary cortical neurons 24 h after infection with CFP-, CFP- I2-, or CFP-I2(T72A)-expressing Sindbis virus. **(F)** Quantification of western blot results from five sets of neuronal cultures. pT320 was first normalized to total PP1, then normalized to CFP control culture [one-way ANOVA, $F_{(2,\ 12)} = 6.01$, $p < 0.05$]. Tukey *post hoc* comparisons following one-way ANOVAs are displayed: $^{*}p < 0.05$, $^{*}p < 0.01$, ns, not significant.

applied to cultured neurons for 24 h. Medium from the 12-well neuronal plates were aspirated quickly, before 1X SDS gel loading buffer (contains protease and phosphatase inhibitor) was added to each well for about 10 min on ice before the cell lysates were harvested and heated for 10 min at 95°C followed by SDS-PAGE and immunoblotting. Anti-PP1 pT320 (1:1,000;

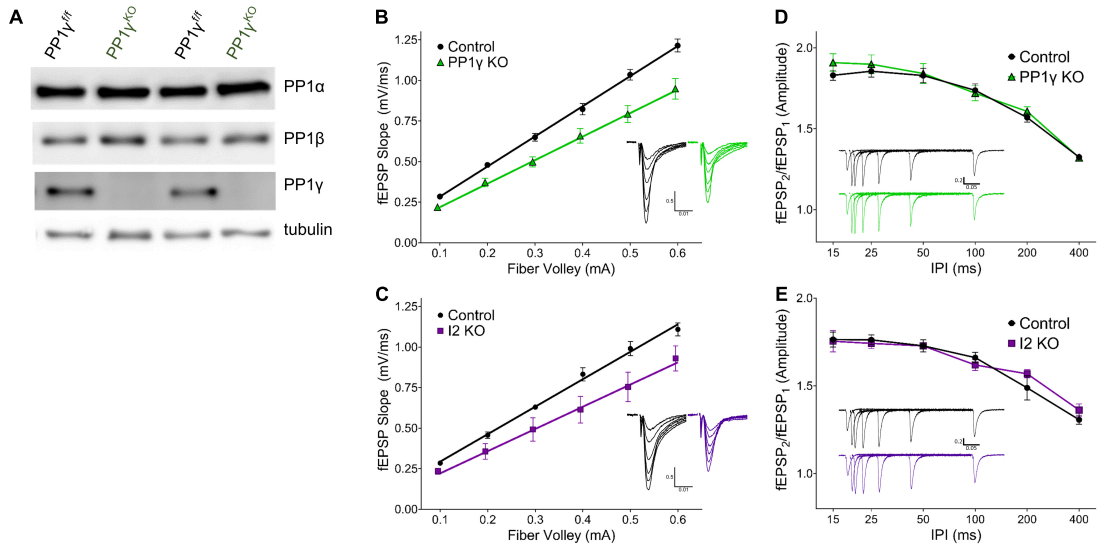

FIGURE 2
I-2 and PP1γ promote synaptic transmission in acute hippocampal slices. **(A)** Successful knockout of PP1γ protein in nestin-cre;PP1$\gamma^{f/f}$ mice. There is a slight upregulation of PP1β protein. **(B–E)** Results from field recordings in acute hippocampal slices at Sch-CA1 synapses. **(B,C)** There is a decrease in basal synaptic transmission in PP1γ^{KO} and I-2^{KO} mice [two-way RM-ANOVAs, genotype: $F_{(1,\ 16)} = 14.39$, $p < 0.01$; $F_{(1,\ 8)} = 6.987$, $p < 0.05$, respectively]. **(D,E)** There is no change in paired pulse facilitation (PPF) in PP1γ^{KO} or I-2^{KO} mice [two-way RM-ANOVAs, genotype: $F_{(1,\ 12)} = 0.280$, $p = 0.606$; $F_{(1,\ 8)} = 0.068$, $p = 0.801$, respectively]. Data are from the following number of mice/slices: **(B)**, control 3/9, knockout 3/9; **(C)**, control 3/6, knockout 2/4; **(D)**, control 3/7, knockout 3/7; **(E)**, control 3/6, knockout 2/4.

Cell Signaling Technology), anti-PP1 (1:1,000; E-9, Santa Cruz Biotechnology, Inc.), and anti-GFP (1:1,000, 0.4 μg/ml; Roche).

Electrophysiology

Whole-cell patch-clamp recordings on cultured cortical neurons were recorded at ∼DIV21, as described (Siddoway et al., 2013a). Neurons were transfected with CFP, CFP-I-2^{WT} or CFP-I-2^{T72A} by calcium phosphate precipitation method 3 days prior. Pipettes were filled with (in mM): 117 Cs-methylsulfonate, 20 HEPES, 1 EGTA, 0.1 CaCl2, 5 CsCl, 2.5 MgATP, 0.25 Na3GTP, pH 7.4. External solution consisted of (in mM): 135 NaCl, 3.5 KCl, 2 CaCl2, 1.3 MgCl2, 10 HEPES, 20 glucose, supplemented with 200 nM TTX, 25 μM D-AP5, and 50 μM picrotoxin. mEPSCs were detected using template fitting in Clampfit 10.3 with a 5 pA threshold. Cumulative distributions were generated by histogram cumulative distribution of all mEPSC events for CFP (981 events) and $I2^{T72A}$ (932 events) groups. An equivalent number of events was randomly sampled from each I-2^{WT} cell, yielding 946 events. mEPSC amplitude distributions were separately compared for the CFP vs. I2 (WT) groups, and the CFP vs. I2 (T72A) groups using non-parametric Kolmogorov-Smirnov test in GraphPad Prism 9.4.1.

Acute hippocampal slices were prepared from 1 to 2-month old mice bred as previously described (Foley et al., 2021a). Four hundred micrometer thick slices were prepared after decapitation and rapid extraction of the brains into ice-cold artificial cerebrospinal fluid (ACSF). Slices were then recovered in room temperature (RT) ACSF for at least 1 h prior to field recordings. Recordings were conducted at Schaffer collateral-CA1 synapses in RT ACSF at a flow rate of 2–3 mL/min. A borosilicate recording electrode (1–3 MΩ) filled with 1 M NaCl was placed in CA1 stratum radiatum and a monopolar borosilicate filled with ACSF (**Figure 2**) or tungsten concentric bipolar stimulating electrode (FHC) (**Supplementary Figure 1**) placed on Schaffer collaterals between CA3 and CA1. Responses were elicited every 15 s, with stimulation delivered by an ISO-Flex stimulus isolator (AMPI). The ACSF solution consisted of (in mM): 126.0 NaCl; 2.5 KCl; 2.5 $CaCl_2$; 1.3 $MgSO_4$; 1.25 NaH_2PO_4; 26.0 $NaHCO_3$; and 10.0 D-glucose. ACSF was continuously aerated with carbogen (95% O_2, 5% CO_2) during incubation and recordings. Basal synaptic transmission was assessed by input-output (IO) curves. Short-term pre-synaptic plasticity was assayed using paired-pulse facilitation (PPF) of varying inter-pulse intervals. Recordings were collected with a MultiClamp 700A amplifier (Axon Instruments), PCI-6221 data acquisition device (National Instruments), and Igor Pro 7 (Wavemetrics) with a customized software package (Recording Artist)[1]. All experimental protocols for live animals were approved by the University Committee on Animal Resources of the University of Rochester Medical Center.

1 http://github.com/rgerkin/recording-artist

10.3389/fnsyn.2022.1021832

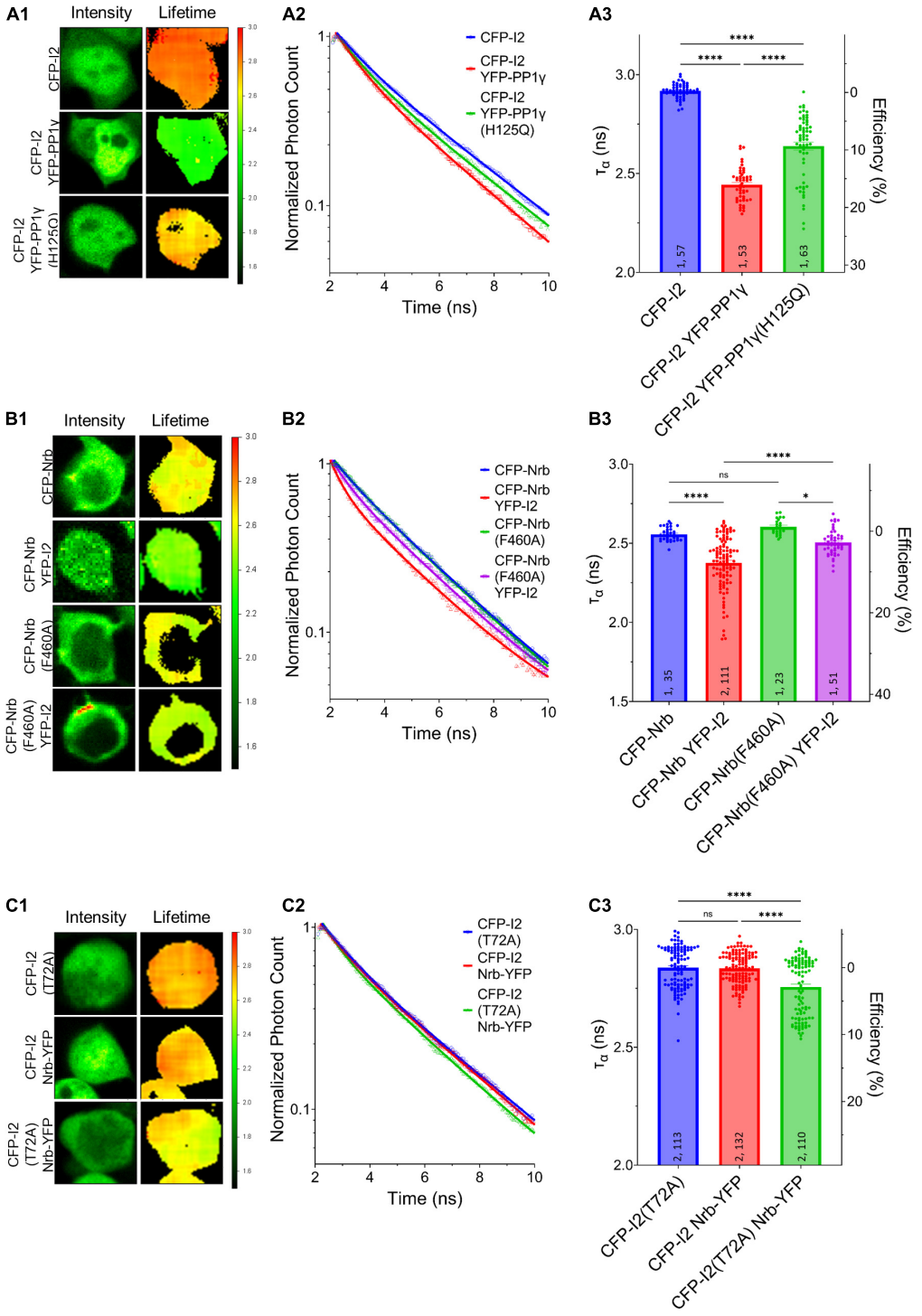

FIGURE 3
Regulation of I-2 interactions with PP1γ and neurabin *in vivo* as assessed by FLIM. **(A1–C1)** Intensity (left) and lifetime (right) of example cells. Lifetime expressed in nanoseconds (ns), with a color scale shown on the right. **(A2–C2)** Time-correlated single photon counting (TCSPC) histograms from example fields of view. **(A3–C3)** Mean lifetimes and SEM from the indicated constructs. **(A3)** YFP-PP1γ, but not YFP-PP1γ^{H125Q}, co-expression decreases CFP-I2 lifetime [one-way ANOVA, $F_{(4,\ 289)} = 417.9$, $p < 0.0001$]. **(B3)** YFP-I2 co-expression decreases CFP-Nrb lifetime. The interaction between CFP-$Nrb^{1-490}$and YFP-I2 is attenuated by PP1-binding-deficient Nrb, CFP-$Nrb^{1-490,\ F60A}$ [one-way ANOVA, $F_{(3,\ 216)} = 35.60$, $p < 0.0001$]. **(C3)** Nrb^{1-490}-YFP does not affect CFP-I2 lifetime, but decreases CFP-$I2^{T72A}$ lifetime [one-way ANOVA, $F_{(2,\ 352)} = 27.86$, $p < 0.0001$]. Tukey *post hoc* comparisons following one-way ANOVAs are displayed: $^{*}p < 0.05$, $^{**}p < 0.01$, $^{***}p < 0.001$, $^{****}p < 0.0001$, ns, not significant. Number of cultures and number of cells are shown within bars. All data represent independent experiments; lifetime data was not reused between subfigures.

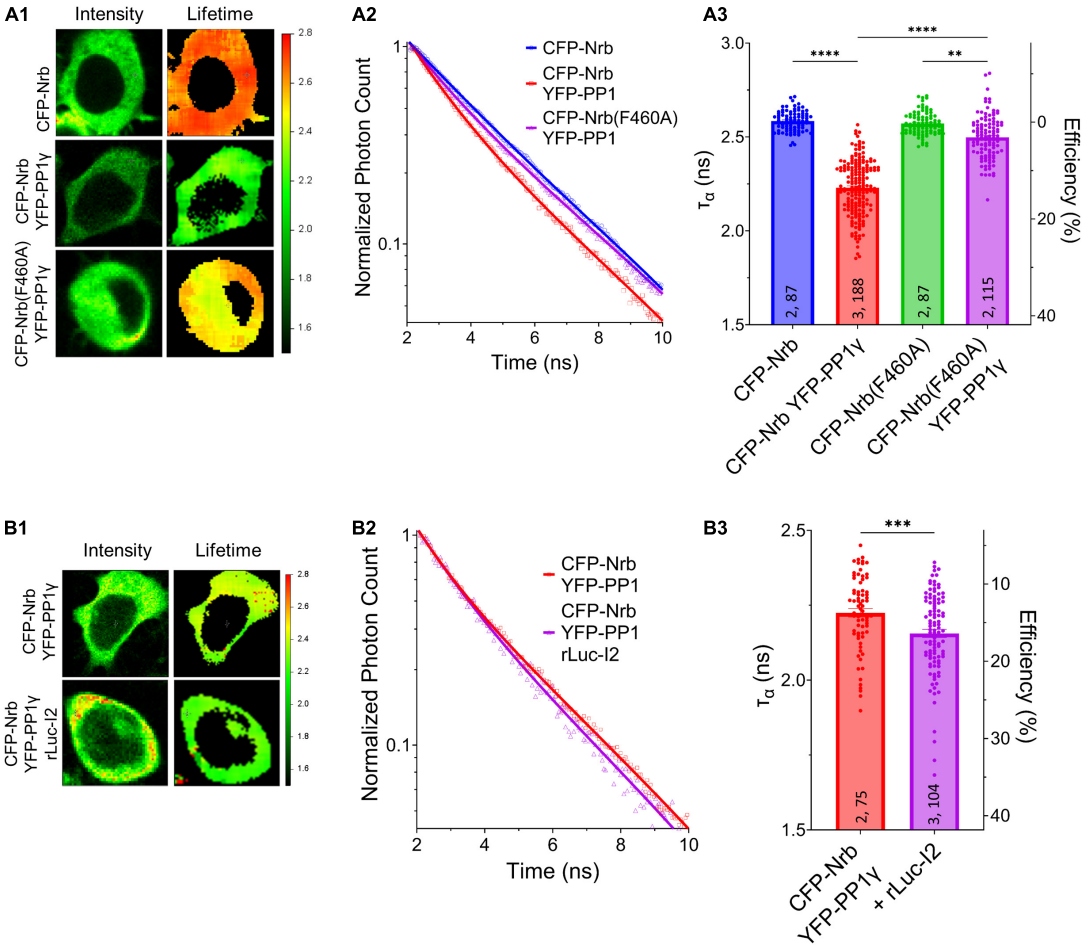

FIGURE 4
I-2 promotes neurabin-PP1 interaction. **(A1,B1)** Intensity (left) and lifetime (right) of example cells. Lifetime expressed in ns. **(A2,B2)** Time-correlated single photon counting (TCSPC) histograms from example fields of view. **(A3,B3)** Mean lifetimes and SEM from the indicated constructs. **(A3)** YFP-PP1γ co-expression decreases CFP-Nrb$^{1-490}$ lifetime. CFP-Nrb$^{1-490\ F460A}$ significantly attenuates the YFP-PP1γ-mediated decrease in lifetime [one-way ANOVA, $F_{(7,\ 694)} = 190.4$, $p < 0.0001$]. **(B3)** rLuc-I2 co-expression promotes CFP-Nrb$^{1-490}$ interaction with YFP-PP1γ, further decreasing lifetime [two-tailed *t*-test, $t_{(177)} = 3.443$, $p < 0.001$]. *t*-test results **(B3)** or Tukey *post hoc* comparisons following one-way ANOVAs (A3) are displayed: $^{*}p < 0.05$, $^{**}p < 0.01$, $^{***}p < 0.001$, $^{****}p < 0.0001$, ns, not significant. Number of cultures and number of cells are shown within bars. All data represent independent experiments; lifetime data was not reused between subfigures.

Fluorescence lifetime imaging microscopy

HEK293 cells were transfected in 35 mm culture dishes and imaging was performed 2 days later. Images were captured on an Olympus BX51WI upright microscope using a water-immersion 25x objective (Olympus XLPlan N). Two-photon 850 nm excitation was achieved with a Mai Tai Ti:Sapphire multi-photon laser (Spectra Physics), using a repetition rate of 80 MHz and a pulse width of approximately 100 fs, and emission was filtered with a 480-20 filter. Emission was measured by a H72422P Hamamatsu hybrid avalanche photodiode. Time-correlated single photon counting was performed using a Becker and Hickl module with a 25 ps resolution. VistaVision software (ISS) was used for lifetime analysis. Donor fluorescence from individual cells was binned and fit with a double exponential function, consistent with the lifetime properties of CFP.

Analysis

GraphPad Prism (9.3.0) (in mEPSC it was 9.4.1) was used for statistical analyses and data visualization. Statistical significance between means was calculated using unpaired, two-tailed *t*-tests or ANOVAs. Repeated-measure (RM)-ANOVAs were used for IO and PPF comparisons. Tukey and Bonferroni *post hoc* comparisons were performed for one- and two-way ANOVAs, respectively. The arithmetic mean and standard error of the mean are displayed in all figures unless otherwise specified.

Results and discussion

In order to study the potential role of I-2 in regulating basal synaptic transmission, we expressed CFP (control), CFP-tagged wild type (WT) I-2, or CFP-tagged I-2^{T72A} in primary cortical neurons and performed whole-cell recordings 3 days after transfection (**Figure 1A**). We found that mEPSC amplitude, but not frequency, was robustly increased in CFP-I-2-expressing neurons compared to control neurons (**Figures 1B–D**). Interestingly, neither mEPSC amplitude nor mEPSC frequency showed significant change in CFP-I-2^{T72A}-expressing neurons (**Figures 1B–D**). Our data thus suggest that I-2 promotes synaptic transmission, but this effect depends on the T72-mediated activation-inhibition cycle. While the mean mEPSC frequency was not significantly different overall, a subset of CFP-I-2^{WT}-expressing neurons showed a robust increase in mEPSC frequency, though this potential effect was not further pursued in this study.

In order to determine the effect of overexpressed I-2^{WT} and I-2^{T72A} on PP1 activity, we examined the status of endogenous PP1's inhibitory phosphorylation at threonine 320 (pT320) (Hou et al., 2013). Consistent with I-2^{T72A} as a constitutive PP1 inhibitor, we found that overexpressed CFP-I-2^{T72A} robustly (~30 fold) and significantly increased pT320 (**Figures 1E,F**), an inverse marker of PP1 activity (Dohadwala et al., 1994). Surprisingly, there was no significant difference in pT320 between CFP-I-2^{WT} and CFP (one-way ANOVA, Tukey *post hoc*, $n = 5$ per group, adjusted $p = 0.9927$) (**Figures 1E,F**), a drastic difference from the effect of CFP-I-2^{T72A} on pT320. This result is contrary to the simple interpretation of I-2 as a PP1 inhibitor from *in vitro* studies, but consistent with our previous report of robust PP1 activity in I-2 immunoprecipitate (Yang et al., 2015). This is also consistent with the model of PP1 inhibition-activation by I-2: the rate-limiting step in the PP1 activation-inhibition cycle is the inhibition step (Cohen, 1989) and the robust I-2 T72 kinase activity seen in neurons (Hou et al., 2013) should favor the activation state. On the other hand, I-2^{T72A} blocks the activation step and potently inhibits PP1 (**Figures 1E,F**).

Since I-2^{WT} (**Figure 1**) and the neurabin-PP1 holoenzyme (Hu et al., 2007) both promote basal synaptic transmission in neuronal cultures, we next sought to directly compare the function of I-2 and PP1 on synaptic transmission in acute hippocampal slices *via* genetic ablation. As neurabin has minimal binding to PP1β, and PP1β is not as enriched in dendritic spines (Bordelon et al., 2005), we focused our study on PP1α and PP1γ. While mice with PP1α or PP1γ KO in neural progenitor cells (NPCs; Nestin-Cre, JAX) were viable, I-2 NPC KO was embryonic lethal. We therefore generated I-2 conditional KO mice with a hippocampus-specific Cre (CaMKII-cre^{T-29}, JAX). We then measured basal synaptic transmission *via* input-output (I/O) curves at hippocampal CA3-CA1 Schaffer-collateral synapses in each transgenic mouse line. We found that synaptic transmission was significantly decreased in both I-2 and PP1γ KO mice compared to control littermates (**Figures 2B,C** and **Supplementary Figure 1**). On the other hand, the I/O curve from PP1α KO mice was not significantly different compared to control littermates (**Supplementary Figure 1**), consistent with its lower binding affinity to neurabin. We did not observe a difference in paired-pulse facilitation (PPF) in any mouse model (**Figures 2D,E** and **Supplementary Figure 1**), indicating no change in glutamate release by CA3 neurons. These results thus suggest that I-2 and PP1γ, but not PP1α, promote AMPAR-mediated basal synaptic transmission in CA1 pyramidal neurons.

Our data so far suggest that PP1γ and I-2^{WT}, but not I-2^{T72A}, promote excitatory synaptic transmission. Since we did not observe a change in PP1 activity by overexpressed I-2^{WT} (**Figure 1E**), we next sought to determine the effect of I-2 on PP1 interaction with its regulatory proteins. We first established direct I-2–PP1 interaction *via* fluorescence lifetime imaging microscopy (FLIM). The fluorescence lifetime of CFP ($\mathcal{T}_{CFP}$) on CFP-I-2 was robustly decreased when YFP-PP1γ was co-expressed in HEK 293 cells (**Figures 3A1–A3**). Moreover, we found that the decrease of $\mathcal{T}_{CFP-I-2}$ was attenuated if YFP-PP1γ^{H125Q} was co-expressed, a PP1 mutant made to disrupt the binding interface between I-2 and PP1 (Hurley et al., 2007; **Figure 3A**). This suggests that the FRET observed between CFP-I-2 and YFP-PP1γ is derived from I-2–PP1 interaction. We next examined the interaction between neurabin and I-2. We observed a robust decrease of $\mathcal{T}_{CFP}$ of CFP-neurabin$^{1-490}$ when YFP-I-2 was co-expressed (**Figures 3B1–B3**). This decrease was not observed with a PP1-binding-deficient neurabin, CFP-neurabin$^{1-490,F460A}$ (**Figures 3B1–B3**). Because the RvXF motif on neurabin does not participate in interaction with I-2 (Dancheck et al., 2011), this result suggests that the FRET between CFP- neurabin$^{1-490}$ and YFP-I-2 involves a trimeric complex with endogenous PP1. We did not observe FRET between CFP-I-2 and neurabin$^{1-490}$-YFP (**Figures 3C1–C3**), demonstrating that FRET between fluorescently tagged I-2 and neurabin is sensitive to N- vs. C-terminal positioning of the fluorophores. However, we observed significant FRET between CFP-I-2^{T72A} and neurabin$^{1-490}$-YFP (**Figures 3C1–C3**), supporting the idea that T72A mutation leads to a conformational change in I-2, large enough to position the fluorophores close enough and/or in optimal orientation for FRET to occur.

We next determined whether I-2 could promote neurabin-PP1γ holoenzyme formation. We observed a robust decrease of $\mathcal{T}_{CFP}$ on CFP-neurabin$^{1-490}$ when it was co-expressed with YFP-PP1γ (**Figure 4A**). Moreover, the decrease of $\mathcal{T}_{CFP}$ was significantly reduced when YFP-PP1γ was co-expressed with PP1-binding deficient CFP-neurabin$^{1-490,F460A}$ (**Figure 4A**). This suggests that the FRET observed between CFP-neurabin$^{1-490}$ and YFP-PP1γ is derived from their interaction. Notably, we found that co-expressing rLuc-I-2^{WT}

with CFP-neurabin (1-490) and YFP-PP1γ significantly further decreased the $\mathcal{T}_{CFP}$ on CFP-neurabin$^{1-490}$, relative to CFP-neurabin$^{1-490}$ and YFP-PP1γ double transfection (**Figure 4B**). This suggests that I-2 promotes neurabin-PP1γ holoenzyme formation, thus regulating PP1γ function in a positive manner. This finding is consistent with previous *in vitro* binding data showing I-2 promotes neurabin-PP1 binding (Terry-Lorenzo et al., 2002b). A similar study of I-2 function in tobacco leaves showed that I-2 promotes PP1 binding to its scaffolding protein SNF1-related protein kinase 2 (SnRK2) (Hou et al., 2016). Overall, our study suggests that overexpressed I-2^{WT} increases synaptic transmission, not *via* promoting the enzymatic activity of individual PP1 molecules (**Figures 1D,E**), rather *via* increasing the number of PP1 molecules targeted by neurabin.

Conclusion

In summary, we found that I-2, PP1γ, but not PP1α, promotes basal synaptic transmission, and that I-2 positively regulates PP1γ function *via* enhancing neurabin-PP1γ holoenzyme formation, without affecting PP1γ enzymatic activity. Our study provides a fundamental mechanism by which I-2 can positively regulate PP1 function. This mechanism may regulate PP1 *in vivo* function beyond synaptic transmission.

Data availability statement

The datasets generated and/or analyzed during the current study are available from the corresponding author on reasonable request.

Ethics statement

The animal study was reviewed and approved by UCAR committee of the University of Rochester Medical Center.

Author contributions

HX: conceptualization, supervision, writing – original draft, and project administration. KF: investigation, formal analysis, and writing – original draft. HA: investigation, formal analysis, and writing – review and editing. HH and HY: investigation. YZ and DM: investigation and formal analysis. CM: formal analysis and writing – review and editing. MP-S: investigation and writing – review and editing. AM: formal analysis. AN: resources and writing – review and editing. DS: supervision and writing–review and editing. All authors contributed to the article and approved the submitted version.

Funding

This work was supported by the National Institutes of Health (NIH) R01 MH109719 and National Science Foundation (NSF) IOS-1457336 to HX; NIH DA10044 to AN, NIH F30 MH122046 to KF, NIH R35GM137951 to DM, the Heart and Stroke Foundation, Canada, to HA, and the Natural Sciences and Engineering Research Council of Canada to DS. We have institution start-up for covering the publication fee; however, HX was an associate editor for the Frontier in Molecular Neuroscience and thus enjoy one free publication per year.

Conflict of interest

The authors declare that the research was conducted in the absence of any commercial or financial relationships that could be construed as a potential conflict of interest.

Publisher's note

Supplementary material

The Supplementary Material for this article can be found online at: https://www.frontiersin.org/articles/10.3389/fnsyn.2022.1021832/full#supplementary-material

SUPPLEMENTARY FIGURE 1
PP1α does not play a role in synaptic transmission. **(A)** Successful knockout of PP1α protein in nestin-cre;PP1α$^{f/f}$ mice. **(B–E)** Results from field recordings in acute hippocampal slices at Sch-CA1 synapses. **(B,C)** There is no difference in basal synaptic transmission in PP1α^{KO} mice, but a significant decrease in PP1γ^{KO} mice [two-way RM-ANOVAs, genotype: $F_{(1,\ 10)} = 0.02$, $p = 0.899$; $F_{(1,14)} = 4.79$, $p < 0.05$, respectively). **(D,E)** There is no change in paired pulse facilitation (PPF) at the Sch-CA1 pyramidal synapses in PP1α^{KO} or PP1γ^{KO} mice [two-way RM-ANOVAs, genotype: $F_{(1,\ 10)} = 0.172$, $p = 0.687$; $F_{(1,\ 14)} = 0.006$, $p = 0.938$, respectively). Data are from the following number of mice/slices: **(B)**, control 2/7, knockout 2/5; **(C)**, control 3/7, knockout 3/9; **(D)**, control 2/6, knockout 2/6; **(E)**, control 3/6, knockout 3/10.

References

Bordelon, J. R., Smith, Y., Nairn, A. C., Colbran, R. J., Greengard, P., and Muly, E. C. (2005). Differential localization of protein phosphatase-1alpha, beta and gamma1 isoforms in primate prefrontal cortex. *Cereb. Cortex* 15, 1928–1937. doi: 10.1093/cercor/bhi070

Carmody, L. C., Baucum, A. J. II., Bass, M. A., and Colbran, R. J. (2008). Selective targeting of the gamma1 isoform of protein phosphatase 1 to F-actin in intact cells requires multiple domains in spinophilin and neurabin. *Faseb J.* 22, 1660–1671. doi: 10.1096/fj.07-092841

Cohen, P. (1989). The structure and regulation of protein phosphatases. *Annu. Rev. Biochem.* 58, 453–508.

Dancheck, B., Ragusa, M. J., Allaire, M., Nairn, A. C., Page, R., and Peti, W. (2011). Molecular investigations of the structure and function of the protein phosphatase 1-spinophilin-inhibitor 2 heterotrimeric complex. *Biochemistry* 50, 1238–1246. doi: 10.1021/bi101774g

Dohadwala, M., da Cruz e Silva, E. F., Hall, F. L., Williams, R. T., Carbonaro-Hall, D. A., Nairn, A. C., et al. (1994). Phosphorylation and inactivation of protein phosphatase 1 by cyclin-dependent kinases. *Proc. Natl. Acad. Sci. U. S. A.* 91, 6408–6412.

Foley, K. F. W., Barnett, D., Cory-Slechta, D. A., and Xia, H. (2021a). Early low-level arsenic exposure impacts post-synaptic hippocampal function in juvenile mice. *Toxics* 9:206. doi: 10.3390/toxics9090206

Foley, K., McKee, C., Nairn, A. C., and Xia, H. (2021b). Regulation of synaptic transmission and plasticity by protein phosphatase 1. *J. Neurosci.* 41, 3040–3050.

Genoux, D., Haditsch, U., Knobloch, M., Michalon, A., Storm, D., and Mansuy, I. M. (2002). Protein phosphatase 1 is a molecular constraint on learning and memory. *Nature* 418, 970–975. doi: 10.1038/nature00928

Hou, H., Sun, L., Siddoway, B. A., Petralia, R. S., Yang, H., Gu, H., et al. (2013). Synaptic NMDA receptor stimulation activates PP1 by inhibiting its phosphorylation by Cdk5. *J. Cell Biol.* 203, 521–535. doi: 10.1083/jcb.201303035

Hou, Y. J., Zhu, Y., Wang, P., Zhao, Y., Xie, S., Batelli, G., et al. (2016). Type one protein phosphatase 1 and its regulatory protein inhibitor 2 negatively regulate ABA signaling. *PLoS Genet.* 12:e1005835. doi: 10.1371/journal.pgen.1005835

Hu, X. D., Huang, Q., Roadcap, D. W., Shenolikar, S. S., and Xia, H. (2006). Actin-associated neurabin-protein phosphatase-1 complex regulates hippocampal plasticity. *J. Neurochem.* 98, 1841–1851. doi: 10.1111/j.1471-4159.2006.04070.x

Hu, X. D., Huang, Q., Yang, X., and Xia, H. (2007). Differential regulation of AMPA receptor trafficking by neurabin-targeted synaptic protein phosphatase-1 in synaptic transmission and long-term depression in hippocampus. *J. Neurosci.* 27, 4674–4686. doi: 10.1523/JNEUROSCI.5365-06.2007

Huang, H. B., Horiuchi, A., Watanabe, T., Shih, S. R., Tsay, H. J., Li, H. C., et al. (1999). Characterization of the inhibition of protein phosphatase-1 by DARPP-32 and inhibitor-2. *J. Biol. Chem.* 274, 7870–7878.

Hurley, T. D., Yang, J., Zhang, L., Goodwin, K. D., Zou, Q., Cortese, M., et al. (2007). Structural basis for regulation of protein phosphatase 1 by inhibitor-2. *J. Biol. Chem.* 282, 28874–28883. doi: 10.1074/jbc.M703472200

Lemaire, S., and Bollen, M. (2020). Protein phosphatase-1: Dual activity regulation by inhibitor-2. *Biochem. Soc. Trans.* 48, 2229–2240.

Li, M., Stefansson, B., Wang, W., Schaefer, E. M., and Brautigan, D. L. (2006). Phosphorylation of the Pro-X-Thr-Pro site in phosphatase inhibitor-2 by cyclin-dependent protein kinase during M-phase of the cell cycle. *Cell Signal* 18, 1318–1326. doi: 10.1016/j.cellsig.2005.10.020

Liu, R., Correll, R. N., Davis, J., Vagnozzi, R. J., York, A. J., Sargent, M. A., et al. (2015). Cardiac-specific deletion of protein phosphatase 1beta promotes increased myofilament protein phosphorylation and contractile alterations. *J. Mol. Cell Cardiol.* 87, 204–213. doi: 10.1016/j.yjmcc.2015.08.018

Park, I. K., Roach, P., Bondor, J., Fox, S. P., and DePaoli-Roach, A. A. (1994). Molecular mechanism of the synergistic phosphorylation of phosphatase inhibitor-2. Cloning, expression, and site-directed mutagenesis of inhibitor-2. *J. Biol. Chem.* 269, 944–954.

Ragusa, M. J., Dancheck, B., Critton, D. A., Nairn, A. C., Page, R., and Peti, W. (2010). Spinophilin directs protein phosphatase 1 specificity by blocking substrate binding sites. *Nat. Struct. Mol. Biol.* 17, 459–464. doi: 10.1038/nsmb.1786

Siddoway, B. A., Altimimi, H. F., Hou, H., Petralia, R. S., Xu, B., Stellwagen, D., et al. (2013a). An essential role for inhibitor-2 regulation of protein phosphatase-1 in synaptic scaling. *J. Neurosci.* 33, 11206–11211. doi: 10.1523/JNEUROSCI.5241-12.2013

Siddoway, B. H. H., and Xia, H. (2011). Glutamatergic synapses: Molecular organisation. *eLS* doi: 10.1002/9780470015902.a0000235.pub2 [Epub ahead of print].

Siddoway, B., Hou, H., Yang, H., Petralia, R., and Xia, H. (2014). Synaptic activity bidirectionally regulates a novel sequence-specific S-Q phosphoproteome in neurons. *J. Neurochem.* 128, 841–851. doi: 10.1111/jnc.12487

Siddoway, B., Hou, H., Yang, J., Sun, L., Yang, H., Wang, G. Y., et al. (2013b). Potassium channel Kv2.1 is regulated through protein phosphatase-1 in response to increases in synaptic activity. *Neurosci. Lett.* 583, 142–147. doi: 10.1016/j.neulet.2014.08.051

Terry-Lorenzo, R. T., Carmody, L. C., Voltz, J. W., Connor, J. H., Li, S., Smith, F. D., et al. (2002a). The neuronal actin-binding proteins, neurabin I and neurabin II, recruit specific isoforms of protein phosphatase-1 catalytic subunits. *J. Biol. Chem.* 277, 27716–27724. doi: 10.1074/jbc.M203365200

Terry-Lorenzo, R. T., Elliot, E., Weiser, D. C., Prickett, T. D., Brautigan, D. L., and Shenolikar, S. (2002b). Neurabins recruit protein phosphatase-1 and inhibitor-2 to the actin cytoskeleton. *J. Biol. Chem.* 277, 46535–46543. doi: 10.1074/jbc.M206960200

Tung, H. Y., Wang, W., and Chan, C. S. (1995). Regulation of chromosome segregation by Glc8p, a structural homolog of mammalian inhibitor 2 that functions as both an activator and an inhibitor of yeast protein phosphatase 1. *Mol. Cell Biol.* 15, 6064–6074. doi: 10.1128/MCB.15.11.6064

Wang, W., Cronmiller, C., and Brautigan, D. L. (2008a). Maternal phosphatase inhibitor-2 is required for proper chromosome segregation and mitotic synchrony during *Drosophila* embryogenesis. *Genetics* 179, 1823–1833. doi: 10.1534/genetics.108.091959

Wang, W., Stukenberg, P. T., and Brautigan, D. L. (2008b). Phosphatase inhibitor-2 balances protein phosphatase 1 and aurora B kinase for chromosome segregation and cytokinesis in human retinal epithelial cells. *Mol. Biol. Cell* 19, 4852–4862. doi: 10.1091/mbc.e08-05-0460

Yang, H., Hou, H., Pahng, A., Gu, H., Nairn, A. C., Tang, Y. P., et al. (2015). Protein phosphatase-1 inhibitor-2 is a novel memory suppressor. *J. Neurosci.* 35, 15082–15087. doi: 10.1523/JNEUROSCI.1865-15.2015

frontiers | Frontiers in Synaptic Neuroscience

TYPE Mini Review
PUBLISHED 06 January 2023
DOI 10.3389/fnsyn.2022.1087042

OPEN ACCESS

EDITED BY
Fereshteh S. Nugent,
Uniformed Services University,
United States

REVIEWED BY
Arianna Maffei,
Stony Brook University, United States

*CORRESPONDENCE
Hey-Kyoung Lee
✉ heykyounglee@jhu.edu

RECEIVED 01 November 2022
ACCEPTED 19 December 2022
PUBLISHED 06 January 2023

CITATION
Lee H-K (2023) Metaplasticity framework for cross-modal synaptic plasticity in adults.
Front. Synaptic Neurosci. 14:1087042.
doi: 10.3389/fnsyn.2022.1087042

Metaplasticity framework for cross-modal synaptic plasticity in adults

Hey-Kyoung Lee*

The Solomon H. Snyder Department of Neuroscience, Zanvyl Krieger Mind/Brain Institute, Kavli Neuroscience Discovery Institute, Johns Hopkins University, Baltimore, MD, United States

Sensory loss leads to widespread adaptation of neural circuits to mediate cross-modal plasticity, which allows the organism to better utilize the remaining senses to guide behavior. While cross-modal interactions are often thought to engage multisensory areas, cross-modal plasticity is often prominently observed at the level of the primary sensory cortices. One dramatic example is from functional imaging studies in humans where cross-modal recruitment of the deprived primary sensory cortex has been observed during the processing of the spared senses. In addition, loss of a sensory modality can lead to enhancement and refinement of the spared senses, some of which have been attributed to compensatory plasticity of the spared sensory cortices. Cross-modal plasticity is not restricted to early sensory loss but is also observed in adults, which suggests that it engages or enables plasticity mechanisms available in the adult cortical circuit. Because adult cross-modal plasticity is observed without gross anatomical connectivity changes, it is thought to occur mainly through functional plasticity of pre-existing circuits. The underlying cellular and molecular mechanisms involve activity-dependent homeostatic and Hebbian mechanisms. A particularly attractive mechanism is the sliding threshold metaplasticity model because it innately allows neurons to dynamically optimize their feature selectivity. In this mini review, I will summarize the cellular and molecular mechanisms that mediate cross-modal plasticity in the adult primary sensory cortices and evaluate the metaplasticity model as an effective framework to understand the underlying mechanisms.

KEYWORDS

cross-modal plasticity, cortical plasticity, sensory experience, homeostatic synaptic plasticity, sliding threshold, LTP, LTD, adult plasticity

1. Introduction

Cross-modal plasticity refers to changes in brain function following a sensory loss that allows the spared senses to be used more effectively to guide behavior. There are two main changes: cross-modal recruitment of the brain areas that serve the lost sensory modality and compensatory plasticity of the brain areas that process the spared senses

(**Figure 1**). Cross-modal recruitment has been observed in blind subjects where braille reading activates the deprived visual cortex (Sadato et al., 1996; Buchel et al., 1998; Burton et al., 2002b) and in deaf subjects where visual stimuli activate the deprived auditory cortex (Sandmann et al., 2012). This functional cross-modal recruitment of the deprived cortices is thought to enhance the processing of the remaining senses by increasing the cortical territory. This idea stems from the notion that cortical circuits are functionally equivalent and can process any sensory information presented to them. One of the supporting evidence for the functional equivalence of cortical circuits comes from a study, which rewired visual inputs to the primary auditory cortex (A1) of ferrets during early development causing visually guided behavior to become dependent on A1 (von Melchner et al., 2000). However, primary sensory cortices can be quite specialized in their anatomical organization, for example, barrel cortex in rodents and ocular dominance columns present in primary visual cortex (V1) of some carnivores and primates. Whether such anatomical specializations may affect the functional equivalence of cortical processing is unclear. In addition to the cross-modal recruitment, compensatory plasticity of the spared sensory areas is thought to allow refinement and increase the sensitivity of the spared sensory systems (Pascual-Leone and Torres, 1993; Sterr et al., 1998a,b; Roder et al., 1999; Elbert et al., 2002).

In animal models, early sensory loss results in cross-modal anatomical changes to the primary sensory cortices, especially of thalamocortical inputs (Henschke et al., 2018; Dooley and Krubitzer, 2019), but in adults, most of the cross-modal plasticity likely occurs through functional plasticity of pre-existing circuits (Lee and Whitt, 2015; Ewall et al., 2021). Cross-modal functional plasticity is observed in both the deprived and the spared primary sensory cortices (**Figure 1**). Evidence from animal studies suggests that these involve experience-dependent plasticity mechanisms based on Hebbian, both long-term potentiation (LTP) and long-term depression (LTD), and homeostatic mechanisms (Lee and Whitt, 2015; Ewall et al., 2021). In this mini-review, I will summarize the synaptic plasticity mechanisms of adult cross-modal plasticity and explain how utilizing the framework of the metaplasticity model can easily account for the global cortical adaptation in adults. To do this, I will first provide a brief introduction to the sliding threshold metaplasticity model.

2. Metaplasticity

Metaplasticity refers to the regulation of synaptic plasticity (Abraham and Bear, 1996) and often refers to the sliding threshold model proposed by Bienenstock, Cooper, and Monroe (BCM theory); a theoretical model that can provide stability to Hebbian plasticity (Bienenstock et al., 1982; Bear et al., 1987; Cooper and Bear, 2012). It was recognized that synaptic plasticity solely based on Hebbian mechanisms is limited and is unable to provide network stability that is necessary for neural function on its own. This is due to the fact that correlation based synaptic plasticity mechanisms, such as LTP and LTD, have in-built positive feedback. Strengthening synapse by LTP causes postsynaptic neurons to respond to inputs more strongly, which increases the coincidence of pre- and post-synaptic activity. This in turn promotes further LTP leading to over-excitability when left unchecked. Similar positive feedback occurs upon weakening synapses *via* LTD, but in the opposite direction that ultimately leads to inactivity. Such bistable property of Hebbian plasticity on neural network activity suggests a need for homeostatic control to provide stability. The sliding threshold model allows such homeostatic control by postulating that the induction threshold for LTP and LTD, referred to as the synaptic modification threshold (θm), slides as a function of the integrated past activity of a neuron (**Figure 2**). This key property of the sliding threshold allows neurons to dynamically tune their feature selectivity to the dominant input at the moment as a function of the history of overall activity (Bienenstock et al., 1982; Bear et al., 1987; Cooper and Bear, 2012). Here I will discuss the two main properties of the BCM model: the generation of feature selectivity and its dynamic regulation by past activity that endows homeostasis.

One of the main features of the sliding threshold model is the development of feature selectivity by LTP and LTD. Stronger inputs that exceed the θm undergo LTP, while weaker inputs that fail to produce sufficient postsynaptic activity are depressed *via* LTD. Thus neurons "select" the dominant input, at the expense of other weaker inputs. The ability of sensory cortical neurons to express feature selectivity is critical for sensory processing by enabling discrimination of distinct inputs to generate a percept of a certain feature in the sensory environment. While the initial setup of feature selectivity arises from the developmental organization of axonal projections based on guidance cues (Crowley and Katz, 1999, 2000), the refinement of feature selectivity is known to depend on the activity and in particular sensory experience (Sengpiel and Kind, 2002; Hooks and Chen, 2020). An essential feature of the sliding threshold is its ability to provide network stability, which is endowed by the regulation of θm as a function of the integrated past activity. If the neuron has been under high activity regime for a duration of time, θm increases (i.e., slides up) to make LTP more difficult to induce and promote LTD across the majority of synapses. Weakening the majority of the inputs *via* LTD causes the overall postsynaptic activity to decrease, hence providing homeostatic control of neural activity. In contrast, if the postsynaptic neuronal activity is low, θm is reduced to promote LTP and decreases the range of activity that produces LTD. While stabilizing the neural activity, the sliding threshold model preserves feature selectivity because stronger inputs will surpass θm to strengthen their connections at the expense of weaker inputs whether

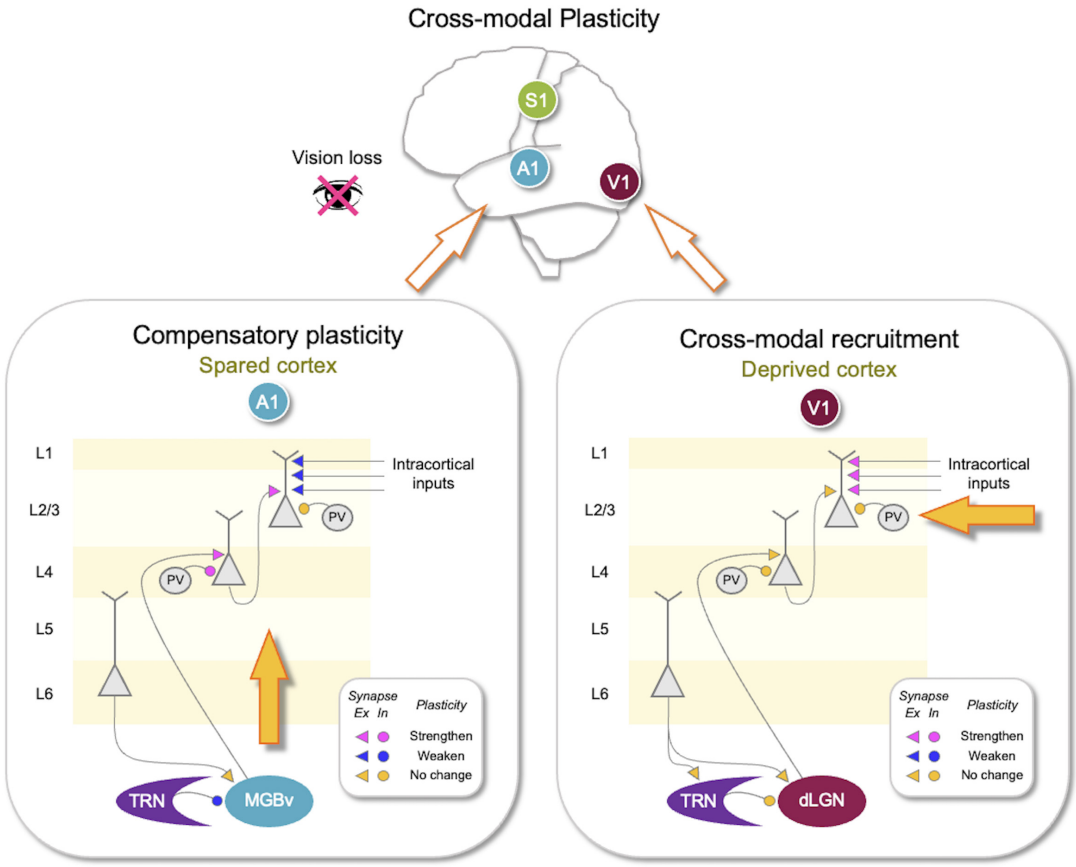

FIGURE 1
Synaptic changes associated with adult cross-modal plasticity. Sensory loss produces compensatory plasticity in the spared sensory cortices and cross-modal recruitment plasticity in the deprive sensory cortex. Lower panels show compilation of synaptic plasticity data from adult mice after vision loss (Petrus et al., 2014, 2015; Whitt et al., 2022). **(Lower right panel)** In the deprived primary visual cortex (V1), there is no plasticity of the feedforward (thalamocortical inputs to L4 and L4–L2/3) or the thalamic circuit, but lateral inputs to L2/3 potentiate. There is no change in parvalbumin (PV) inhibition onto L4 or L2/3 neurons. Corticothalamic synapses from V1 to thalamic reticular nucleus (TRN) or the primary visual thalamus [dorsal lateral geniculate nucleus (dLGN)] did not change. Adaptation of V1 circuit could allow cross-modal recruitment of V1 for processing other sensory inputs arriving through the potentiated lateral inputs to L2/3. **(Lower left panel)** In the spared primary auditory cortex (A1), there is potentiation of the feedforward synapses, including thalamocortical synapses and L4–L2/3 synapses. The strength of lateral inputs to L2/3 is weakened. Cortical inhibition mediated by PV neurons becomes stronger in L4 but does not change in L2/3. In addition, there is plasticity in the thalamic circuit, where TRN inhibition to the primary auditory thalamic nucleus [ventral portion of medial geniculate body (MGBv)] is reduced. Corticothalamic synapses to MGBv were not altered. Such adaptation of A1 is expected to amplify auditory signals and allow sharpening of tuning properties to mediate compensatory plasticity. Plasticity of synaptic strength following vision loss is color coded as shown in the insets. Pink, potentiated synapses; Blue, depressed synapses; Yellow: no change in synaptic strength. Triangles, excitatory (*Ex*) synapses; Circles, inhibitory (*In*) synapses.

the θm is high or low. Implementing the sliding threshold to computational neural networks successfully explains the development of feature selectivity based on LTP/LTD while maintaining network stability (Bienenstock et al., 1982). As will be discussed later sliding threshold also enables dynamic regulation of the neuronal feature selectivity when there are changes to the type of inputs available to the neurons (**Figure 2**). The sliding threshold model was first experimentally demonstrated in V1, where reducing overall neural activity by dark rearing from birth promotes LTP and reduces LTD (Kirkwood et al., 1996). Since then, it has been confirmed across many brain regions (Lebel et al., 2001; Krucker et al., 2002; Solger et al., 2004; Muller et al., 2007; Narayanan and Johnston, 2010; Hulme et al., 2012) and malfunctioning of the sliding threshold has been reported in various neurological disease models (Hulme et al., 2013; Megill et al., 2015; Jang and Chung, 2016) suggesting its critical role in normal brain function.

At a molecular level, the sliding threshold is implemented by alterations in either the induction or the expression mechanisms of LTP/LTD. The initial postulate of the sliding threshold model stated a horizontal shift of the synaptic modification function (**Figure 2**), but now there is evidence that the synaptic modification function could shift vertically (Seol et al., 2007;

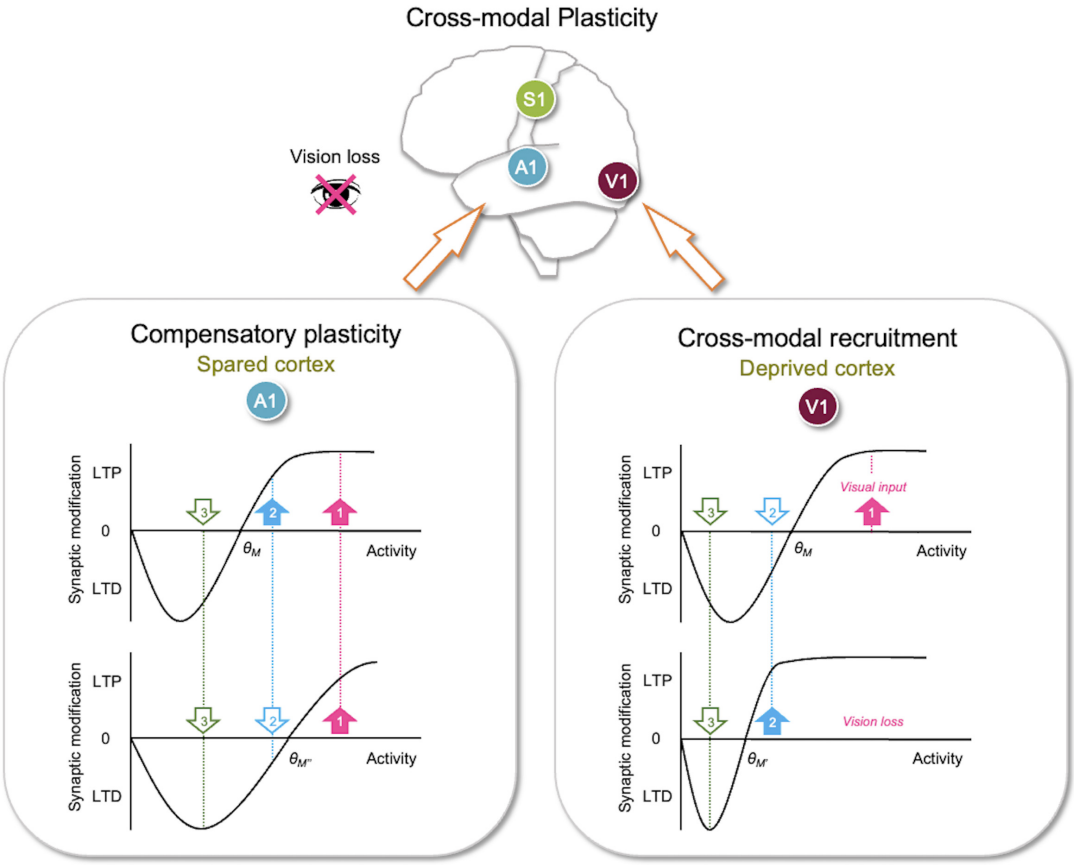

FIGURE 2
Metaplasticity sliding threshold model to explain adult cross-modal plasticity. Sliding threshold model can account for synaptic plasticity observed in the deprived sensory cortex (cross-modal recruitment) and the spared sensory cortices (compensatory plasticity). **(Lower right panel)** The sliding threshold model states that when past activity is low, the synaptic modification threshold (θm) slides down (from $\theta_M - \theta_{M'}$). This is expected to be the case in primary visual cortex (V1) with vision loss. Lower θm ($\theta_{M'}$) now allows the second strongest input (cyan, 2), which carries non-visual input, to potentiate. This may recruit V1 to process other sensory inputs in the absence of vision. The weakest input (green, 3) is still below the lowered θm ($\theta_{M'}$), hence stay in the LTD zone. This allows the neurons to maintain selectivity for the newly adopted feature (cyan, 2). **(Lower left panel)** According to the sliding threshold model, an increase in past activity slides up θm (from $\theta_M - \theta_{M''}$) to limit LTP induction and increase the range in which LTD can be induced. Vision loss in adults potentiates feedforward synapses in primary auditory cortex (A1) and reduces inhibition in the auditory thalamus (**Figure 1**), which is predicted to increase input activity to A1 L2/3 leading to a higher θm ($\theta_{M''}$). This causes activity from only the strongest input (pink, 1) to exceed the new θm ($\theta_{M''}$) to produce LTP, while the second strongest input (cyan, 2) now falls below the new θm ($\theta_{M''}$) and undergoes LTD. This in essence makes A1 neurons more selective, which would aid in the discrimination of auditory signals. Because the sliding threshold maintains a range for LTP and LTD, it is ideally suited to dynamically allow neurons to adopt new features in the absence of their main input to mediate cross-modal recruitment or become more feature selective when there is an increase in overall activity as would occur during compensatory plasticity. Filled upward pointing arrows, inputs with activity that surpasses θm, which will undergo LTP. Open downward pointing arrows, inputs with activity that falls below θm, which will undergo LTD.

Huang et al., 2012; Hong et al., 2020). Both the horizontal and vertical shift in the synaptic modification function slides the θm in the same manner, but the molecular mechanisms underlying the two are distinct. The horizontal shift in synaptic modification occurs by changes in the induction mechanisms of LTP/D, which in molecular terms has been demonstrated as changes in N-methyl-D-aspartate (NMDA) receptor (NMDAR) subunit composition. Low neuronal activity upregulates the expression of NMDAR GluN2B (or NR2B) subunit (Quinlan et al., 1999; Philpot et al., 2001, 2003), which confers longer current duration compared to GluN2A (or NR2A) containing NMDARs (Chen et al., 1999; Rumbaugh and Vicini, 1999). This in essence allows larger intracellular Ca^{2+} increase through NMDARs to promote LTP. With heightened neuronal activity, GluN2A becomes the dominant subunit for NMDARs, which increases the θm to make LTP induction more stringent. In contrast, the vertical shift in synaptic modification (also referred to as the Pull-Push model) has been shown to occur with neuromodulators acting on LTP/LTD expression mechanisms (Seol et al., 2007; Huang et al., 2012; Hong et al., 2020; Mihalas et al., 2021). Neuromodulators linked to cyclic adenosine 3′,5′-monophosphate (cAMP) signaling promote LTP by

increasing phosphorylation of α-amino-3-hydroxy-5-methyl-4-isoxazolepropionic acid receptors (AMPARs), especially on the protein kinase A target serine-845 (S845) residue of the GluA1 subunit to promote LTP (Seol et al., 2007; Qian et al., 2012). GluA1-S845 phosphorylation has been shown to increase the content of cell surface AMPARs (Oh et al., 2006; He et al., 2011) and prime AMPARs for synaptic recruitment by LTP (Lee and Kirkwood, 2011; Diering and Huganir, 2018). In contrast, neuromodulators linked to phospholipase C (PLC) slide up the θm by promoting LTD and preventing LTP expression (Huang et al., 2012). The main difference between the horizontal and vertical shift in synaptic modification function is that the latter puts synapses into an LTP-only or an LTD-only mode while the former preserves the full range of LTP and LTD (**Figure 2**).

Next, I will review the synaptic mechanisms of cross-modal plasticity in the adult primary sensory cortices and discuss how the horizontal shift in synaptic modification function could account for the observed findings.

3. Cross-modal synaptic plasticity in adult primary sensory cortices

In the adult primary sensory cortices, the superficial layers (L2/3) are likely a major substrate for adult cross-modal plasticity. L2/3 synapses retain their ability to undergo LTP and LTD as well as homeostatic synaptic plasticity into adulthood (Goel and Lee, 2007; Jiang et al., 2007). This contrasts plasticity in L4, where thalamocortical LTP/LTD and homeostatic synaptic plasticity display a short early critical period for plasticity (Crair and Malenka, 1995; Feldman et al., 1998; Desai et al., 2002; Jiang et al., 2007; Barkat et al., 2011; Rodriguez et al., 2018). Moreover, the functional connectivity of the L2/3 neurons is well poised to integrate top-down contextual information with the bottom-up sensory responses from thalamorecipient neurons in L4. Besides feedforward inputs from L4, L2/3 principal neurons receive long-range inputs from multisensory association cortices and higher order sensory cortices, direct connections from other primary sensory cortices, as well as inputs from higher order thalamic nuclei that carry multisensory information (Ewall et al., 2021).

3.1. Synaptic plasticity of the deprived sensory cortex

Even a short duration of sensory loss impacts normal development (Sengpiel and Kind, 2002; Hooks and Chen, 2020), but there is some degree of plasticity in adult sensory cortices (Lee and Whitt, 2015; Ribic, 2020), especially in the superficial layers. For example, a couple of days of complete visual deprivation leads to homeostatic strengthening of excitatory synapses measured as miniature excitatory postsynaptic currents (mEPSCs) in adult V1 L2/3 neurons (Goel and Lee, 2007). These changes can be interpreted in the framework of synaptic scaling (Turrigiano and Nelson, 2004; Turrigiano, 2008) or sliding threshold (Ewall et al., 2021). Synaptic scaling model would allow network activity (i.e., firing rate) homeostasis that can prevent overall silencing of the cortical network caused by lost inputs, while sliding threshold would enable dynamic remapping of neuronal features in addition to activity homeostasis. Synaptic scaling and sliding threshold likely operate across different activity regimes to maintain network homeostasis (Lee and Kirkwood, 2019).

Key distinguishing features of synaptic scaling and sliding threshold model are dependence on activity, especially of NMDARs, and input-specific nature of plasticity. Inactivity-driven synaptic scaling was first demonstrated in neuronal cultures upon pharmacological blockade of activity using tetrodotoxin (TTX) or AMPAR blockers (O'Brien et al., 1998; Turrigiano et al., 1998). Subsequent studies demonstrated that NMDAR blockade can accelerate the rate of scaling up synapses with TTX (Sutton et al., 2006). In contrast, according to the sliding threshold model, while the sliding of the θm can happen in the absence of activity, the manifestation of changes in AMPAR-mediated synaptic transmission requires LTP or LTD that is dependent on NMDAR activity (Cooper and Bear, 2012). It is demonstrated that the potentiation of mEPSCs in V1 L2/3 following visual deprivation is blocked by NMDAR antagonist application (Rodriguez et al., 2019) and in particular by blockers of GluN2B (Bridi et al., 2018). These data support the sliding threshold model and are at odds with the synaptic scaling model. Furthermore, the potentiation of mEPSCs in V1 L2/3 neurons following visual deprivation is not multiplicative across all synapses in adults (Goel and Lee, 2007) and is specific to lateral inputs but not observed at feedforward inputs from L4 (Petrus et al., 2015; Chokshi et al., 2019; **Figure 1**). These results corroborate that in intact cortical circuits with distinct inputs that carry different patterns of activity, homeostatic adaptation is not uniform across all the synapses. Such input-specific and NMDAR-dependent plasticity supports the sliding threshold model, but we cannot exclude the role of synaptic scaling especially with extreme changes in activity (Lee and Kirkwood, 2019).

According to the sliding threshold model, loss of a major input, such as visual input to V1 neurons, is expected to decrease the overall neuronal activity (**Figure 2**). If this persists, the theory states that θm will slide down, which allows a subset of previously weak inputs to cross the lowered θm and strengthen *via* LTP. This allows V1 neurons, devoid of visual inputs, to adopt these newly potentiated inputs as their main driver. Inputs with activity below the new θm will still undergo LTD, which permits V1 neurons to maintain selectivity to the newly adopted inputs. Therefore, the sliding threshold model enables neurons to dynamically adopt new features based on

the changes in the landscape of sensory experience. Particularly for cross-modal plasticity, the metaplasticity model allows V1 neurons to respond to non-visual activity carried by the newly potentiated inputs. This could serve as a substrate for cross-modal recruitment observed in blind subjects (Sadato et al., 1996; Buchel et al., 1998; Burton et al., 2002a; Sandmann et al., 2012). While the main function of the primary sensory cortices is to process their respective sensory information, multisensory information is readily available at this early stage of sensory processing. Indeed, *in vivo* whole-cell recordings demonstrate subthreshold functional connections between primary sensory cortices (Iurilli et al., 2012). Furthermore, these subthreshold cortico-cortical connections provide multisensory modulation of the primary inputs. For example, loud sound sharpens the orientation tuning of L2/3 V1 neurons *via* direct input from A1 L5 neurons (Ibrahim et al., 2016; Deneux et al., 2019). Conceivable then, visual deprivation-induced sliding down of θm in V1 L2/3 neurons could allow these subthreshold A1 inputs to potentiate, thus enabling recruitment of V1 for auditory processing.

3.2. Synaptic plasticity of the spared sensory cortices

Plasticity of the spared primary sensory cortices is thought to refine the processing of the spared sensory inputs, improving discrimination, and detection. At a cellular level, cross-modal sensory loss strengthens feedforward connections of spared primary sensory cortices (**Figure 1**). For example, depriving vision of adult mice potentiates the thalamocortical synapses in L4 and L4–L2/3 synapses in A1 (Petrus et al., 2014, 2015) and potentiates L4–L2/3 synapses in the rat barrel cortex (Jitsuki et al., 2011). Similarly, deafening adult mice strengthens thalamocortical synapses in V1 L4 (Petrus et al., 2014; Rodriguez et al., 2018). The potentiation of thalamocortical synapses in adults is of interest because both thalamocortical LTP and LTD were shown to be restricted to an early postnatal critical period (Crair and Malenka, 1995; Feldman et al., 1998; Desai et al., 2002; Jiang et al., 2007; Barkat et al., 2011). Cross-modal potentiation of thalamocortical synapses is likely to occur *via* recovery of NMDAR-dependent thalamocortical LTP in adults (Rodriguez et al., 2018), but the mechanism is currently unknown.

L4–L2/3 synapses, unlike thalamocortical synapses, retain plasticity in adults (Goel and Lee, 2007; Jiang et al., 2007). The potentiation of the feedforward inputs in the spared sensory cortices suggests that feedforward activity increases to a level above θm to produce LTP. For cross-modal plasticity in A1, the evidence suggests a central mechanism that may amplify auditory activity. This may be achieved by a targeted reduction in thalamic inhibition (Whitt et al., 2022). Specifically, depriving vision of adult mice caused a selective reduction of thalamic reticular nucleus (TRN) inhibition to the auditory thalamus [ventral portion of medial geniculate body (MGBv)] but not to the visual thalamus [dorsal lateral geniculate nucleus (dLGN)] (**Figure 1**). Such reduction in inhibition is expected to increase feedforward activity to A1, which would exceed the θm to induce LTP of feedforward synapses (**Figure 2**).

Concomitantly, cross-modal sensory deprivation reduces the strength of lateral intracortical synapses to L2/3 neurons (Petrus et al., 2015; **Figure 1**). The cross-modal synaptic depression of the lateral inputs in L2/3 of the spared sensory cortices can be explained by an increase in θm that results from enhanced feedforward activity (**Figure 2**). Cross-modal sensory deprivation-induced increase in θm would induce LTD in the majority of inputs as their activity will now fall within the LTD range below the new θm. This theoretically can explain the observed depression of the lateral excitatory inputs (Petrus et al., 2015), which by definition will produce weaker activity compared to the feedforward inputs. At a functional level, the decrease in the θm results in enhanced feature selectivity of the neurons in the spared sensory cortices, because only the few highly active inputs will cross the θm to remain strengthened to drive postsynaptic firing (**Figure 2**). The spared cortical circuit also exhibits increased inhibition from parvalbumin (PV) interneurons (Petrus et al., 2015), which will aid in the sharpening of the feature selectivity.

4. Conclusions

The sliding threshold model is compatible with experimental observations of synaptic plasticity related to both cross-modal recruitment and compensatory plasticity. Viewing cross-modal plasticity in the framework of sliding threshold presents testable predictions. Because the synaptic plasticity is ultimately driven by NMDAR-dependent Hebbian modification in accordance with the newly defined synaptic modification threshold, it suggests that cross-modal plasticity will be dependent on sensory experience in the spared modalities. Such requirement of experience may explain the varied observations of the outcome of cross-modal plasticity in human subjects, especially when a sensory modality is lost later in life (Frasnelli et al., 2011; Lazzouni and Lepore, 2014). Furthermore, observations that pre-existing functional connections across the sensory cortices remain plasticity even in adults suggest that cross-modal plasticity mechanisms could be used for enhancing adult brain function.

5. Nomenclature

A1, primary auditory cortex; AMPAR, α-amino-3-hydroxy-5-methyl-4-isoxazolepropionic acid receptor; cAMP, cyclic adenosine 3′,5′-monophosphate; dLGN, dorsal lateral

geniculate nucleus; GluN2A, glutamate ionotropic receptor NMDA type 2A; GluN2B, glutamate ionotropic receptor NMDA type subunit 2B; L2/3, layer 2/3; L4, layer 4; L5, layer 5; LTD, long-term depression; LTP, long-term potentiation; mEPSCs, miniature excitatory postsynaptic currents; MGBv, ventral portion of medial geniculate body; NMDAR, N-methyl-D-aspartate (NMDA) receptor; NR2A, NMDAR 2A subunit; NR2B, NMDAR 2B subunit; PLC, phospholipase C; TRN, thalamic reticular nucleus; TTX, tetrodotoxin; V1, primary visual cortex; θm, synaptic modification threshold.

Author contributions

H-KL synthesized and conceptualized the ideas and wrote the manuscript.

Funding

This work was supported by the NIH grant R01-EY014882 to H-KL.

Acknowledgments

We thank Dr. Alfredo Kirkwood for helpful discussions.

Conflict of interest

The author declares that the research was conducted in the absence of any commercial or financial relationships that could be construed as a potential conflict of interest.

Publisher's note

References

Abraham, W. C., and Bear, M. F. (1996). Metaplasticity: The plasticity of synaptic plasticity. *Trends Neurosci.* 19, 126–130. doi: 10.1016/S0166-2236(96)80018-X

Barkat, T. R., Polley, D. B., and Hensch, T. K. (2011). A critical period for auditory thalamocortical connectivity. *Nat. Neurosci.* 14, 1189–1194. doi: 10.1038/nn.2882

Bear, M. F., Cooper, L. N., and Ebner, F. F. (1987). A physiological basis for a theory of synapse modification. *Science* 237, 42–48. doi: 10.1126/science.3037696

Bienenstock, E. L., Cooper, L. N., and Munro, P. W. (1982). Theory for the development of neuron selectivity: Orientation specificity and binocular interaction in visual cortex. *J. Neurosci.* 2, 32–48. doi: 10.1523/JNEUROSCI.02-01-00032.1982

Bridi, M. C. D., De Pasquale, R., Lantz, C. L., Gu, Y., Borrell, A., Choi, S. Y., et al. (2018). Two distinct mechanisms for experience-dependent homeostasis. *Nat. Neurosci.* 21, 843–850. doi: 10.1038/s41593-018-0150-0

Buchel, C., Price, C., Frackowiak, R. S., and Friston, K. (1998). Different activation patterns in the visual cortex of late and congenitally blind subjects. *Brain* 121(Pt 3), 409–419. doi: 10.1093/brain/121.3.409

Burton, H., Snyder, A. Z., Diamond, J. B., and Raichle, M. E. (2002b). Adaptive changes in early and late blind: A FMRI study of verb generation to heard nouns. *J. Neurophysiol.* 88, 3359–3371. doi: 10.1152/jn.00129.2002

Burton, H., Snyder, A. Z., Conturo, T. E., Akbudak, E., Ollinger, J. M., and Raichle, M. E. (2002a). Adaptive changes in early and late blind: A fMRI study of Braille reading. *J. Neurophysiol.* 87, 589–607. doi: 10.1152/jn.00285.\break2001 doi: 10.1152/jn.00285.2001

Chen, N., Luo, T., and Raymond, L. A. (1999). Subtype-dependence of NMDA receptor channel open probability. *J. Neurosci.* 19, 6844–6854. doi: 10.1523/JNEUROSCI.19-16-06844.1999

Chokshi, V., Gao, M., Grier, B. D., Owens, A., Wang, H., Worley, P. F., et al. (2019). Input-specific metaplasticity in the visual cortex requires Homer1a-mediated mGluR5 signaling. *Neuron* 104, 736–748.e6. doi: 10.1016/j.neuron.2019.08.017

Cooper, L. N., and Bear, M. F. (2012). The BCM theory of synapse modification at 30: Interaction of theory with experiment. *Nat. Rev. Neurosci.* 13, 798–810. doi: 10.1038/nrn3353

Crair, M. C., and Malenka, R. C. (1995). A critical period for long-term potentiation at thalamocortical synapses. *Nature* 375, 325–328. doi: 10.1038/375325a0

Crowley, J. C., and Katz, L. C. (1999). Development of ocular dominance columns in the absence of retinal input. *Nat. Neurosci.* 2, 1125–1130. doi: 10.1038/16051

Crowley, J. C., and Katz, L. C. (2000). Early development of ocular dominance columns. *Science* 290, 1321–1324. doi: 10.1126/science.290.5495.1321

Deneux, T., Harrell, E. R., Kempf, A., Ceballo, S., Filipchuk, A., and Bathellier, B. (2019). Context-dependent signaling of coincident auditory and visual events in primary visual cortex. *Elife* 8:e44006. doi: 10.7554/eLife.44006

Desai, N. S., Cudmore, R. H., Nelson, S. B., and Turrigiano, G. G. (2002). Critical periods for experience-dependent synaptic scaling in visual cortex. *Nat. Neurosci.* 5, 783–789. doi: 10.1038/nn878

Diering, G. H., and Huganir, R. L. (2018). The AMPA receptor code of synaptic plasticity. *Neuron* 100, 314–329. doi: 10.1016/j.neuron.2018.10.018

Dooley, J. C., and Krubitzer, L. A. (2019). Alterations in cortical and thalamic connections of somatosensory cortex following early loss of vision. *J. Comp. Neurol.* 527, 1675–1688. doi: 10.1002/cne.24582

Elbert, T., Sterr, A., Rockstroh, B., Pantev, C., Muller, M. M., and Taub, E. (2002). Expansion of the tonotopic area in the auditory cortex of the blind. *J. Neurosci.* 22, 9941–9944. doi: 10.1523/JNEUROSCI.22-22-09941.2002

Ewall, G., Parkins, S., Lin, A., Jaoui, Y., and Lee, H.-K. (2021). Cortical and subcortical circuits for cross-modal plasticity induced by loss of vision. *Front. Neural Circuits* 15:665009. doi: 10.3389/fncir.2021.665009

Feldman, D. E., Nicoll, R. A., Malenka, R. C., and Isaac, J. T. (1998). Long-term depression at thalamocortical synapses in developing rat somatosensory cortex. *Neuron* 21, 347–357. doi: 10.1016/S0896-6273(00)80544-9

Frasnelli, J., Collignon, O., Voss, P., and Lepore, F. (2011). Crossmodal plasticity in sensory loss. *Prog. Brain Res.* 191, 233–249. doi: 10.1016/B978-0-444-53752-2.00002-3

Goel, A., and Lee, H. K. (2007). Persistence of experience-induced homeostatic synaptic plasticity through adulthood in superficial layers of mouse visual cortex. *J. Neurosci.* 27, 6692–6700. doi: 10.1523/JNEUROSCI.5038-06.2007

He, K., Goel, A., Ciarkowski, C. E., Song, L., and Lee, H. K. (2011). Brain area specific regulation of synaptic AMPA receptors by phosphorylation. *Commun. Integr. Biol.* 4, 569–572. doi: 10.4161/cib.15890

Henschke, J. U., Oelschlegel, A. M., Angenstein, F., Ohl, F. W., Goldschmidt, J., Kanold, P. O., et al. (2018). Early sensory experience influences the development of multisensory thalamocortical and intracortical connections of primary sensory cortices. *Brain Struct. Funct.* 223, 1165–1190. doi: 10.1007/s00429-017-1549-1

Hong, S. Z., Huang, S., Severin, D., and Kirkwood, A. (2020). Pull-push neuromodulation of cortical plasticity enables rapid bi-directional shifts in ocular dominance. *Elife* 9:e54455. doi: 10.7554/eLife.54455

Hooks, B. M., and Chen, C. (2020). Circuitry underlying experience-dependent plasticity in the mouse visual system. *Neuron* 106, 21–36. doi: 10.1016/j.neuron.2020.01.031

Huang, S., Trevino, M., He, K., Ardiles, A., Pasquale, R., Guo, Y., et al. (2012). Pull-push neuromodulation of LTP and LTD enables bidirectional experience-induced synaptic scaling in visual cortex. *Neuron* 73, 497–510. doi: 10.1016/j.neuron.2011.11.023

Hulme, S. R., Jones, O. D., and Abraham, W. C. (2013). Emerging roles of metaplasticity in behaviour and disease. *Trends Neurosci.* 36, 353–362. doi: 10.1016/j.tins.2013.03.007

Hulme, S. R., Jones, O. D., Ireland, D. R., and Abraham, W. C. (2012). Calcium-dependent but action potential-independent BCM-like metaplasticity in the hippocampus. *J. Neurosci.* 32, 6785–6794. doi: 10.1523/JNEUROSCI.0634-12.2012

Ibrahim, L. A., Mesik, L., Ji, X. Y., Fang, Q., Li, H. F., Li, Y. T., et al. (2016). Cross-modality sharpening of visual cortical processing through layer-1-mediated inhibition and disinhibition. *Neuron* 89, 1031–1045. doi: 10.1016/j.neuron.2016.01.027

Iurilli, G., Ghezzi, D., Olcese, U., Lassi, G., Nazzaro, C., Tonini, R., et al. (2012). Sound-driven synaptic inhibition in primary visual cortex. *Neuron* 73, 814–828. doi: 10.1016/j.neuron.2011.12.026

Jang, S. S., and Chung, H. J. (2016). Emerging link between Alzheimer's disease and homeostatic synaptic plasticity. *Neural Plast.* 2016:7969272. doi: 10.1155/2016/7969272

Jiang, B., Trevino, M., and Kirkwood, A. (2007). Sequential development of long-term potentiation and depression in different layers of the mouse visual cortex. *J. Neurosci.* 27, 9648–9652. doi: 10.1523/JNEUROSCI.2655-07.2007

Jitsuki, S., Takemoto, K., Kawasaki, T., Tada, H., Takahashi, A., Becamel, C., et al. (2011). Serotonin mediates cross-modal reorganization of cortical circuits. *Neuron* 69, 780–792. doi: 10.1016/j.neuron.2011.01.016

Kirkwood, A., Rioult, M. C., and Bear, M. F. (1996). Experience-dependent modification of synaptic plasticity in visual cortex. *Nature* 381, 526–528. doi: 10.1038/381526a0

Krucker, T., Siggins, G. R., Mcnamara, R. K., Lindsley, K. A., Dao, A., Allison, D. W., et al. (2002). Targeted disruption of RC3 reveals a calmodulin-based mechanism for regulating metaplasticity in the hippocampus. *J. Neurosci.* 22, 5525–5535. doi: 10.1523/JNEUROSCI.22-13-05525.2002

Lazzouni, L., and Lepore, F. (2014). Compensatory plasticity: Time matters. *Front. Hum. Neurosci.* 8:340. doi: 10.3389/fnhum.2014.00340

Lebel, D., Grossman, Y., and Barkai, E. (2001). Olfactory learning modifies predisposition for long-term potentiation and long-term depression induction in the rat piriform (olfactory) cortex. *Cereb. Cortex* 11, 485–489. doi: 10.1093/cercor/11.6.485

Lee, H. K., and Kirkwood, A. (2011). AMPA receptor regulation during synaptic plasticity in hippocampus and neocortex. *Semin Cell Dev. Biol.* 22, 514–520. doi: 10.1016/j.semcdb.2011.06.007

Lee, H. K., and Kirkwood, A. (2019). Mechanisms of homeostatic synaptic plasticity in vivo. *Front. Cell. Neurosci.* 13:520. doi: 10.3389/fncel.2019.00520

Lee, H. K., and Whitt, J. L. (2015). Cross-modal synaptic plasticity in adult primary sensory cortices. *Curr. Opin. Neurobiol.* 35, 119–126. doi: 10.1016/j.conb.2015.08.002

Megill, A., Tran, T., Eldred, K., Lee, N. J., Wong, P. C., Hoe, H. S., et al. (2015). Defective age-dependent metaplasticity in a mouse model of Alzheimer's disease. *J. Neurosci.* 35, 11346–11357. doi: 10.1523/JNEUROSCI.5289-14.2015

Mihalas, S., Ardiles, A., He, K., Palacios, A., and Kirkwood, A. (2021). A multisubcellular compartment model of AMPA receptor trafficking for neuromodulation of Hebbian synaptic plasticity. *Front. Synaptic Neurosci.* 13:703621. doi: 10.3389/fnsyn.2021.703621

Muller, J. F., Orekhov, Y., Liu, Y., and Ziemann, U. (2007). Homeostatic plasticity in human motor cortex demonstrated by two consecutive sessions of paired associative stimulation. *Eur. J. Neurosci.* 25, 3461–3468. doi: 10.1111/j.1460-9568.2007.05603.x

Narayanan, R., and Johnston, D. (2010). The h current is a candidate mechanism for regulating the sliding modification threshold in a BCM-like synaptic learning rule. *J. Neurophysiol.* 104, 1020–1033. doi: 10.1152/jn.01129.2009

O'Brien, R. J., Kamboj, S., Ehlers, M. D., Rosen, K. R., Fischbach, G. D., and Huganir, R. L. (1998). Activity-dependent modulation of synaptic AMPA receptor accumulation. *Neuron* 21, 1067–1078. doi: 10.1016/S0896-6273(00)80624-8

Oh, M. C., Derkach, V. A., Guire, E. S., and Soderling, T. R. (2006). Extrasynaptic membrane trafficking regulated by GluR1 serine 845 phosphorylation primes AMPA receptors for long-term potentiation. *J. Biol. Chem.* 281, 752–758. doi: 10.1074/jbc.M509677200

Pascual-Leone, A., and Torres, F. (1993). Plasticity of the sensorimotor cortex representation of the reading finger in Braille readers. *Brain* 116(Pt 1), 39–52. doi: 10.1093/brain/116.1.39

Petrus, E., Isaiah, A., Jones, A. P., Li, D., Wang, H., Lee, H. K., et al. (2014). Crossmodal induction of thalamocortical potentiation leads to enhanced information processing in the auditory cortex. *Neuron* 81, 664–673. doi: 10.1016/j.neuron.2013.11.023

Petrus, E., Rodriguez, G., Patterson, R., Connor, B., Kanold, P. O., and Lee, H. K. (2015). Vision loss shifts the balance of feedforward and intracortical circuits in opposite directions in mouse primary auditory and visual cortices. *J. Neurosci.* 35, 8790–8801. doi: 10.1523/JNEUROSCI.4975-14.2015

Philpot, B. D., Espinosa, J. S., and Bear, M. F. (2003). Evidence for altered NMDA receptor function as a basis for metaplasticity in visual cortex. *J. Neurosci.* 23, 5583–5588. doi: 10.1523/JNEUROSCI.23-13-05583.2003

Philpot, B. D., Sekhar, A. K., Shouval, H. Z., and Bear, M. F. (2001). Visual experience and deprivation bidirectionally modify the composition and function of NMDA receptors in visual cortex. *Neuron* 29, 157–169. doi: 10.1016/S0896-6273(01)00187-8

Qian, H., Matt, L., Zhang, M., Nguyen, M., Patriarchi, T., Koval, O. M., et al. (2012). beta2-Adrenergic receptor supports prolonged theta tetanus-induced LTP. *J. Neurophysiol.* 107, 2703–2712. doi: 10.1152/jn.00374.2011

Quinlan, E. M., Olstein, D. H., and Bear, M. F. (1999). Bidirectional, experience-dependent regulation of N-methyl-D-aspartate receptor subunit composition in the rat visual cortex during postnatal development. *Proc. Natl. Acad. Sci. U.S.A.* 96, 12876–12880. doi: 10.1073/pnas.96.22.12876

Ribic, A. (2020). Stability in the face of change: Lifelong experience-dependent plasticity in the sensory cortex. *Front. Cell. Neurosci.* 14:76. doi: 10.3389/fncel.2020.00076

Roder, B., Teder-Salejarvi, W., Sterr, A., Rosler, F., Hillyard, S. A., and Neville, H. J. (1999). Improved auditory spatial tuning in blind humans. *Nature* 400, 162–166. doi: 10.1038/22106

Rodriguez, G., Chakraborty, D., Schrode, K. M., Saha, R., Uribe, I., Lauer, A. M., et al. (2018). Cross-modal reinstatement of thalamocortical plasticity accelerates ocular dominance plasticity in adult mice. *Cell Rep.* 24, 3433–3440.e4. doi: 10.1016/j.celrep.2018.08.072

Rodriguez, G., Mesik, L., Gao, M., Parkins, S., Saha, R., and Lee, H. K. (2019). Disruption of NMDA receptor function prevents normal experience-dependent homeostatic synaptic plasticity in mouse primary visual cortex. *J. Neurosci.* 39, 7664–7673. doi: 10.1523/JNEUROSCI.2117-18.2019

Rumbaugh, G., and Vicini, S. (1999). Distinct synaptic and extrasynaptic NMDA receptors in developing cerebellar granule neurons. *J. Neurosci.* 19, 10603–10610. doi: 10.1523/JNEUROSCI.19-24-10603.1999

Sadato, N., Pascual-Leone, A., Grafman, J., Ibanez, V., Deiber, M. P., Dold, G., et al. (1996). Activation of the primary visual cortex by Braille reading in blind subjects. *Nature* 380, 526–528. doi: 10.1038/380526a0

Sandmann, P., Dillier, N., Eichele, T., Meyer, M., Kegel, A., Pascual-Marqui, R. D., et al. (2012). Visual activation of auditory cortex reflects maladaptive plasticity in cochlear implant users. *Brain* 135, 555–568. doi: 10.1093/brain/awr329

Sengpiel, F., and Kind, P. C. (2002). The role of activity in development of the visual system. *Curr. Biol.* 12, R818–R826. doi: 10.1016/S0960-9822(02)01318-0

Seol, G. H., Ziburkus, J., Huang, S., Song, L., Kim, I. T., Takamiya, K., et al. (2007). Neuromodulators control the polarity of spike-timing-dependent synaptic plasticity. *Neuron* 55, 919–929. doi: 10.1016/j.neuron.2007.08.013

Solger, J., Wozny, C., Manahan-Vaughan, D., and Behr, J. (2004). Distinct mechanisms of bidirectional activity-dependent synaptic plasticity in superficial and deep layers of rat entorhinal cortex. *Eur. J. Neurosci.* 19, 2003–2007. doi: 10.1111/j.1460-9568.2004.03292.x

Sterr, A., Muller, M. M., Elbert, T., Rockstroh, B., Pantev, C., and Taub, E. (1998a). Changed perceptions in Braille readers. *Nature* 391, 134–135. doi: 10.1038/34322

Sterr, A., Muller, M. M., Elbert, T., Rockstroh, B., Pantev, C., and Taub, E. (1998b). Perceptual correlates of changes in cortical representation of fingers in blind multifinger Braille readers. *J. Neurosci.* 18, 4417–4423. doi: 10.1523/JNEUROSCI.18-11-04417.1998

Sutton, M. A., Ito, H. T., Cressy, P., Kempf, C., Woo, J. C., and Schuman, E. M. (2006). Miniature neurotransmission stabilizes synaptic function via tonic suppression of local dendritic protein synthesis. *Cell* 125, 785–799. doi: 10.1016/j.cell.2006.03.040

Turrigiano, G. G. (2008). The self-tuning neuron: Synaptic scaling of excitatory synapses. *Cell* 135, 422–435. doi: 10.1016/j.cell.2008.10.008

Turrigiano, G. G., and Nelson, S. B. (2004). Homeostatic plasticity in the developing nervous system. *Nat. Rev. Neurosci.* 5, 97–107. doi: 10.1038/nrn1327

Turrigiano, G. G., Leslie, K. R., Desai, N. S., Rutherford, L. C., and Nelson, S. B. (1998). Activity-dependent scaling of quantal amplitude in neocortical neurons. *Nature* 391, 892–896. doi: 10.1038/36103

von Melchner, L., Pallas, S. L., and Sur, M. (2000). Visual behaviour mediated by retinal projections directed to the auditory pathway. *Nature* 404, 871–876. doi: 10.1038/35009102

Whitt, J. L., Ewall, G., Chakraborty, D., Adegbesan, A., Lee, R., Kanold, P. O., et al. (2022). Visual deprivation selectively reduces thalamic reticular nucleus-mediated inhibition of the auditory thalamus in adults. *J. Neurosci.* 42, 7921–7930. doi: 10.1523/JNEUROSCI.2032-21.2022

frontiers | Frontiers in Synaptic Neuroscience

TYPE Original Research
PUBLISHED 02 March 2023
DOI 10.3389/fnsyn.2023.1123294

OPEN ACCESS

EDITED BY
Fereshteh S. Nugent,
Uniformed Services University, United States

REVIEWED BY
Nicholas Graziane,
College of Medicine, The Pennsylvania State University, United States
Ricardo C. Araneda,
University of Maryland, College Park, United States

*CORRESPONDENCE
Alfredo Kirkwood
✉ elkirkwood@gmail.com

RECEIVED 13 December 2022
ACCEPTED 13 February 2023
PUBLISHED 02 March 2023

CITATION
Valdivia G, Ardiles AO, Idowu A, Salazar C, Lee H-K, Gallagher M, Palacios AG and Kirkwood A (2023) mGluR-dependent plasticity in rodent models of Alzheimer's disease.
Front. Synaptic Neurosci. 15:1123294.
doi: 10.3389/fnsyn.2023.1123294

mGluR-dependent plasticity in rodent models of Alzheimer's disease

Gonzalo Valdivia[1,2], Alvaro O. Ardiles[2], Abimbola Idowu[1], Claudia Salazar[2], Hey-Kyoung Lee[1], Michela Gallagher[3], Adrian G. Palacios[2] and Alfredo Kirkwood[1]*

[1]Mind/Brain Institute and Department of Neurosciences, Johns Hopkins University, Baltimore, MD, United States, [2]Centro Interdisciplinario de Neurociencia de Valparaíso, Facultad de Ciencias, Universidad de Valparaíso, Valparaíso, Chile, [3]Department of Psychological and Brain Sciences, Johns Hopkins University, Baltimore, MD, United States

Long-term potentiation (LTP) and depression (LTD) are currently the most comprehensive models of synaptic plasticity models to subserve learning and memory. In the CA1 region of the hippocampus LTP and LTD can be induced by the activation of either NMDA receptors or mGluR5 metabotropic glutamate receptors. Alterations in either form of synaptic plasticity, NMDAR-dependent or mGluR-dependent, are attractive candidates to contribute to learning deficits in conditions like Alzheimer's disease (AD) and aging. Research, however, has focused predominantly on NMDAR-dependent forms of LTP and LTD. Here we studied age-associated changes in mGluR-dependent LTP and LTD in the APP/PS1 mouse model of AD and in *Octodon degu*, a rodent model of aging that exhibits features of AD. At 2 months of age, APP/PS1 mouse exhibited robust mGluR-dependent LTP and LTD that was completely lost by the 8th month of age. The expression of mGluR protein in the hippocampus of APP/PS1 mice was not affected, consistent with previous findings indicating the uncoupling of the plasticity cascade from mGluR5 activation. In *O. degu*, the average mGluR-LTD magnitude is reduced by half by the 3rd year of age. In aged *O. degu* individuals, the reduced mGluR-LTD correlated with reduced performance in a radial arm maze task. Altogether these findings support the idea that the preservation of mGluR-dependent synaptic plasticity is essential for the preservation of learning capacity during aging.

KEYWORDS

LTP (long term potentiation), LTD (long term pepression), mGluR5, Alzheimer's disease, aging

Introduction

Alzheimer's disease (AD) is a progressive neurodegenerative disorder that initially manifests as a severe impairment in memory formation. Consequently, much research interest focuses on alterations in synaptic mechanisms subserving the remodeling of brain circuitry during learning and memory formation. A wealth of studies on animal models, particularly mouse lines carrying genes of familial AD (FAD) have revealed

clear impairments in the induction of Hebbian synaptic plasticity, specifically NMDAR-dependent forms of long-term potentiation (LTP) and long-term depression (LTD) (Selkoe, 2008; Ondrejcak et al., 2010; Mango et al., 2019; Zhang et al., 2022). Indeed, it has long been a widespread idea that disrupted synaptic plasticity contributes to initiating the AD pathological cascade (Selkoe, 2002). It must be noted, however, that reduced NMDAR-dependent synaptic plasticity is not unique to the AD condition, but a common consequence of aging. For example, both NMDAR-LTP and NMDAR-LTD are both reduced in aged Long-Evans rats (Lee et al., 2005; Boric et al., 2008), a non-pathological model of aging that does not exhibit AD signatures (Gallagher et al., 2003).

Besides NMDAR-dependent plasticity, LTD and LTP can also be induced by mechanisms requiring the activation of the metabotropic glutamate receptor 5 (Palmer et al., 1997; Huber et al., 2000; Wang et al., 2016). These two distinct systems of bidirectional plasticity are independent, complementary of each other, and can co-exist in the same synapse. Importantly, in models of non-pathological aging model what distinguishes learning-impaired individuals from non-impaired ones is their capacity to upregulate mGluR-dependent plasticity to compensate for the age-related reduction in NMDAR-dependent plasticity (Lee et al., 2005; Boric et al., 2008; Lu et al., 2019).

In contrast to NMDAR-dependent plasticity, the status of mGluR-dependent plasticity in models of AD remains largely unexplored. This is despite the fact that Aβ amyloid peptide oligomers, a leading candidate player in the pathological cascade (Li and Selkoe, 2020), stimulate internalization of AMPARs in a fashion comparable to mGluR-LTD (Kamenetz et al., 2003; Hsieh et al., 2006; Menard and Quirion, 2012a,b). Motivated by this paucity of information we examined the induction of mGluR-dependent synaptic plasticity in rodent models: the well-characterized APP/PS1 mouse (APPswe;PS1ΔE9) carrying two FAD mutations and *Octodon Degu*. *O degu* is a Chilean rodent model in which by the 3rd year of age some individuals spontaneously began expressing several signatures of AD including elevated levels of Aβ amyloid peptide oligomers associated with reduced memory performance and reduced NMDAR-LTP (Ardiles et al., 2012). We found that mGluR-dependent plasticity was absent in 8-month-old APP/PS1 mice, while it was reduced and associated with memory impairment in *O. degu* older than 30 months of age.

Materials and methods

Animals

Young (2-month-old) and adult (8-month-old) APPswe;PS1ΔE9 Tg and their wild-type (WT) littermate mice (129/C57BL/6 mixed background) of both sexes were used. APPswe;PS1ΔE9 Tg mice have accelerated amyloid pathologies and have a substantial number of plaque deposits by 6 months of age (Jankowsky et al., 2004; Savonenko et al., 2005). Therefore, these mice were used at both pre-amyloidogenic and post-amyloidogenic ages. All procedures performed with these animals were approved by the Institutional Animal Care and Use Committees of Johns Hopkins University.

Degus came from an inbreeding colony in the animal facility of the University de Valparaíso. Animals were kept at a controlled temperature (22 ± 1°C), in light/dark cycles (12:12) with water and food *ad libitum*. Animals of both sexes were used in age groups of 7–36 months (young), and 49–96 months (old). All procedures performed with these animals were approved according to the institutional program of animal care and use of the University de Valparaíso, Chile.

Synaptic responses

Hippocampal slices (400 μm) were prepared as described previously (Boric et al., 2008; Ardiles et al., 2012; Megill et al., 2015). Before isolating the brain, the subjects were transcardially perfused, under isoflurane anesthesia with ice-cold dissection buffer containing: 212.7 mM sucrose, 2.6 mM KCl, 1.23 mM NaH_2PO_4, 26 mM $NaHCO_3$, 10 mM dextrose, 3 mM $MgCl_2$, and 1 mM $CaCl_2$ bubbled with a mixture of 5%CO_2 and 95%O_2 and recovered at room temperature in Artificial Spinal Cerebral Fluid (ACSF) that replaced the sucrose by 124 mM NaCl. Synaptic responses were evoked with 0.2 ms pulses (10–80 μA) delivered through concentric bipolar theta glass micropipettes filled with ACSF, recorded extracellularly in CA1, and quantified as the initial slope of the field potential. Baseline responses were recorded at 0.033 Hz using a stimulation intensity that evoked a half-maximal response, defined as the maximal response without a population spike (pop-spike). Slices were discarded when the pop-spike appeared in the initial rising phase (an indication of hyperexcitability), when paired-pulse facilitation at a 50 ms interval was less than ∼10% (i.e., response 2/response 1 < 1.1), or when the baseline was not stable (∼5% drift). High-frequency tetanus consisted of four 200 Hz epochs (0.5 s) delivered at 0.2 Hz (in the presence of an NMDA receptor antagonist (100 μM D, L-APV). Under our experimental conditions, this protocol induces robust LTP in Long–Evans rats in both CA1 (Boric et al., 2008) and CA3 synapses (Yang et al., 2013; Wang et al., 2016). mGluR-LTD was induced using a paired-pulse 1 Hz (50 ms ISI) 900 pulse stimulation train in the presence of 100 μM APV. LTP and LTD magnitudes were calculated as the average (normalized to baseline) of the responses recorded 50–60 min after conditioning stimulation, corresponding to the early phase of LTP (to distinguish it from late LTP). Drugs included 2-Methyl-6-(phenylethynyl) pyridine (MPEP), LY-367385, (2R)-amino-5-phosphonovaleric acid (APV) from Tocris Bioscience; all other chemicals were from Sigma or Fisher Scientific.

Western blot analysis

About 6–9 month-old of both genotypes were used (APPswe/PS1ΔE9 and Wild Type). Following decapitation under isoflurane anesthesia, the brains were quickly removed and placed in dissection buffer at 4°C to remove the hippocampus. Each hemisphere was placed in an Eppendorf tube on dry ice. Five hundred microliter of 1X lysis buffer was added immediately after (lysis buffer: 20 mM Phosphate buffer pH 7.4, 150 mM NaCl, 10 mM EDTA, 10 mM EGTA, 10 mM NaPPi, 50 mM NaF, 1 mM

$NaCO_3$) with 1% Triton X-100, protease inhibitor (Aprotinin 10 U/mL) and phosphatase inhibitor (1 μM okadaic acid). The samples were sonicated (Sonifier 450, Branson Ultrasonics) with 10 pulses in a cold room (4°C). SDS was then added to a concentration of 0.2%, and the samples were rotated (Rotisserie, Labquake) for 30 min to ensure complete lysis. The homogenate was centrifuged at 100 *g* (model 5415R centrifuge, Eppendorf) for 10 min. The supernatant was collected, and the protein concentration was calculated through the BCA assay (BCA Kit 23250, Pierce) using a spectrophotometer (Biophotometer model, Eppendorf). To 400 ml of sample, 200 ml of 3X GSB was added, and the protein concentration was normalized to 1.33 μg using 1X GSB (2% SDS (w/v), 10% glycerol (v/v), 5% β-Meracaptoethanol (v/v) in 0.125 M Tris, pH 6.8).

For gel electrophoresis, 16 μg of protein per sample was loaded in 6% polyacrylamide gel using 1X Tris-Glycine running buffer (25 mM Tris, 192 mM glycine, 0.1% SDS, pH 8.8). Protein separation was performed at 100 V for 1 h and 30 min.

Gels were transferred to PVDF membranes (ImmunBlot, Bio-Rad) at 26 V overnight using 1× Tris-Glycine blotting buffer with 20% methanol. The membranes were then fixed in destain (25% methanol, 10% acetic acid) for 15 min and blocked with blocking buffer (1% BSA, 0.1% Tween-20 in PBS, pH 7.4) for 1 hfff at room temperature.

Then, membranes were incubated with the primary antibodies anti-β-tubulin and anti-mGluR5 for 1 h at room temperature. After five washes with PBS-T, membranes were incubated with secondary antibodies conjugated to the fluorescent probe Cy3 and Cy5, which allowed the detection of anti-β-tubulin and anti-mGluR5, respectively, for 1 h at room temperature. Finally, membranes were washed with PBS-T and stored in the dark until detection. Blots were detected and scanned by a fluorescent scanner (Model 9419, Typhoon) and analyzed using the Image-J program (NIH).

Behavioral analysis

For evaluating hippocampal-dependent spatial working memory in degus a Radial Arm Maze task was performed. The maze consists of an octagon with access to 8 arms (60 cm long), made of transparent methacrylate, and located 1 m above the ground. The experimental room had several external 3D visual keys that help the spatial orientation of the animal.

The behavioral protocol was based on a previous study (Chappell et al., 1998); this consisted of 4 stages: (i) *habituation:* the animal visited the maze for 10 min a day for 4 days. (ii) *Training phase*: animals seek a reward at the end of the arms once a day for 18 days. Each trial is finished when an animal visits the 8 arms or after 10 min of testing. (iii) *Test*: three trials were performed per day, for 9 days. The test consists of 2 phases, information phase (IP), where 4 arms are closed, and the animal visits open arms. This phase ends when the animal visits the 4 open arms or after 10 min. After 60 s the animal performs a memory phase (MP), where the 8 arms are open and the reward is present in the 4 arms that were kept closed during IP. In this last phase, retroactive memory (RAM) errors were evaluated, which are considered each time the animal enters an arm that had already visited during IP. The trial was finished when the animal visits the 4 arms that had the reward or after 10 min. The animals were positioned in the maze center for each trial in all the phases. The percentage of retroactive memory (RAM) error is determined for each trial, where an error of 0% corresponds to visiting the 4 arms not visited during IP and an error of 100% corresponds to visiting the 4 arms already visited in IP. Finally, for each animal, the RAM error was calculated as the mean of the 27 trials performed for MP.

Statistics

Normality was determined by the Shapiro–Wilk test using Prism (GraphPad Software, San Diego, CA, USA). Mann–Whitney, *t*-Test, Kruskal–Wallis test, or ANOVA test were performed according to normality and the number of comparisons using Prism. Multiple comparisons were followed by the *post-hoc* Holm–Sidak test. Data are presented as averages ± SEM.

Results

We examined the status of mGluR-dependent synaptic plasticity in two rodent models of aging, the APP/PS1 transgenic mouse model of AD (Jankowsky et al., 2004) and the Chilean rodent *Octodon degus*, which exhibits some traits associated with AD (Ardiles et al., 2012). To that end, we employed extracellular field potential recording methods (see methods for details) to test the induction of mGluR-LTD and mGluR-LTP in the Schaffer collateral to CA1 pathway in acute 400 μm slices.

In the first set of experiments, we evaluated the induction mGluR-LTD (with ppLFS in the presence of 100 μM APV in the ACSF) in the APP/PS1 transgenic mouse (Tg). As shown in **Figure 1A**, in young (2-month-old) mice ppLFS induced robust mGluR-LTD in Tg individuals (81.64 ± 4.07% of initial baseline at 50–60 min after conditioning; n = 3 mice, 7 slices), which was comparable to the magnitude of mGluR-LTD induced in age-matched control wild type (WT) littermates (81.94 ± 2.94%; n = 5 mice, 11 slices; p = 0.9523, Mann–Whitney test). In contrast, as shown in **Figure 1B**, in slices from 8-month mice, when cognitive deficits and alterations in NMDAR-dependent plasticity are well developed in the Tg line (Megill et al., 2015), the induction of mGluR-LTD was virtually absent in Tg mice (104.2 ± 2.31%; n = 9, 31) and still robust in age-matched control WT mice (85.94 ± 2.48, n = 12, 31). A Kruskal–Wallis test (KW = 37.02; $p < 0.0001$) followed by a Dunn's multiple comparison test confirmed the difference in the magnitude of mGluR-LTD between 8-month Tg mice and all the other groups (**Figure 1D**). Moreover, the effect size of the differences was very large (Cohen's d value = 1.37). These results indicate a virtual complete age-dependent loss of mGluR-LTD in CA1 synapses of the APP/PS1 transgenic mouse model of AD.

In a subsequent set of studies, we evaluated the induction of mGluR-LTP (with repeated 200 Hz tetanus in the presence of 100 μM APV in the ACSF) in the APP/PS1 model at 8 months of age. Consistent with previous observations done in slices of younger individuals (Wang et al., 2016), the conditioning tetanus induced robust LTP in the slices from WT individuals (122.8 ± 4.67%, n = 11 slices from 3 mice). In contrast, **Figure 1C**

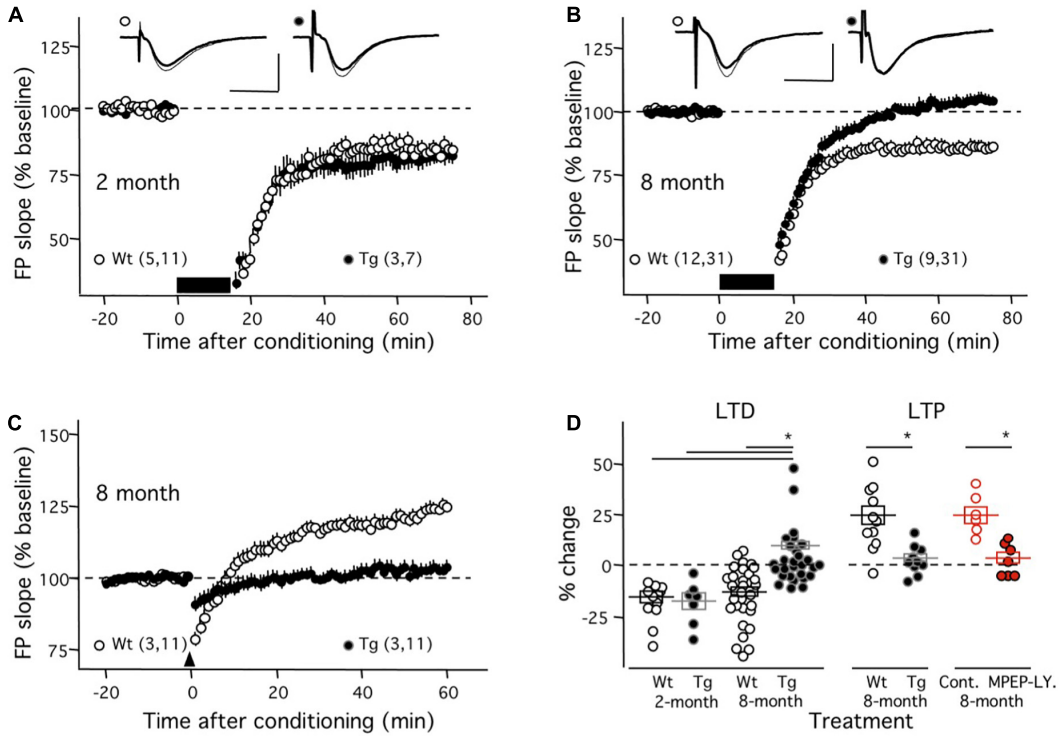

FIGURE 1
Absence on mGluR-dependent synaptic plasticity in middle-aged APP/PS1 transgenic mice. The graphs in panels **(A–C)** compare the time course of mGluR-LTD and mGluR-LTP induced in APP/PS1 transgenic mice (Tg: black circles) and age-matched control wild-type littermates (Wt: white circles). **(A)** In slices from young mice (2 months old) there is no difference in mGluR-LTD induced with ppLFS (black horizontal bar) between Wt and Tg mice. Example experiments are depicted on the top (Wt: left; Tg: right). The superimposed traces are averages of 4 consecutive responses recorded right before (thin line) and 60 min after conditioning (thick line). **(B)** At 8 months of age, ppLFS induces robust mGluR-LTD in slices from WT mice, but not from Tg mice. Example experiments are shown at the top with conventions as in panel **(A)**. **(C)** At 8 months of age the 200 Hz tetanus elicits robust mGluR-LTP in Wt but not Tg mice. **(D)** Summary results showing the magnitudes of mGluR-LTD and mGluR-LTP (50–60 min after conditioning) for all individual experiments in panels **(A–C)** (black symbols; Wt: open symbols; Tg: filled symbols) and also the blockade of mGluR-LTP by mGluR5 antagonists (red symbols) in slices from 8-month old WT mice (control: open circles; 10 mM MPEP and 100 mM LY367385: filled circles). Boxes in panel **(D)** and data points in panels **(A–C)** depict average ± SEM. Asterisks denote significance ($p < 0.005$). The number of mice and slices is indicated in parentheses). Calibration bars in panels **(A,B)**: 10 ms, 1 mV.

shows that little changes were elicited in the slices of age-matched Tg mice (102.8 ± 1.98%, n = 11 slices from 3 mice). A t-test firmed the significance of these differences (p = 0.012). Finally, we confirmed that, like in slices from younger individuals (Wang et al., 2016), in slices from 8-month WT mice, this form of LTP requires mGluR5 function, as it was fully blocked by a combination of mGluR5 antagonists (**Figure 1D**; Control: 125.2 ± 4% change, n = 6 slices; in 110 μM MPEP and 100 μM LY341495 02.9 ± 3.0%, n = 7 slices; Mann–Whitney test: p = 0.0023). The effect size of these differences was large (Cohen's d value = 1.19). Altogether the results indicate that at 8 months of age, the induction either of mGluR-LTP or mGluR-LTD is virtually absent in CA1 synapses from APP/PS1 transgenic mice.

The virtual complete loss of mGluR-LTP and mGluR-LTD at 8-month in the APP/PS1 Tg mice suggests alterations early in the plasticity pathway, at stages that are common to LTP and LTD. In that context, it was of interest to evaluate possible changes in the expression mGluR5 protein in the APP/PS1 Tg mice. To that end, we determined with Western blots the mGluR5 protein content in the hippocampus of six 8-month WT and six Tg mice. The results, shown in **Figure 2**, revealed no differences between WT and Tg mice in the content of either the monomeric (WT: 1.00 ± 0.04, Tg: 1.00 ± 0.04; $p > 0.999$, Mann–Whitney test) or the D1 (WT: 1.00 ± 0.08, Tg: 0.99 ± 0.05; p = 0.937, Mann–Whitney test) and D2 (WT: 1.01 ± 0.05, Tg: 1.06 ± 0.06; p = 0.818, Mann–Whitney test) dimeric forms of the mGluR5. This similar content of mGluR5 in WT and Tg mice suggests an impairment downstream in the pathway.

As mentioned, aging *O. degu* exhibit clear cellular and molecular features common to the early stages of AD. Therefore, we examined how aging affects mGluR-LTD in O. degu and used the same induction approach described above for the APP/PS1 Tg mice. We quantified mGluR-LTD of the CA3➔CA1 synapse in slices from individuals ranging from 7 to 94 months of age, which covers the full life expectancy of adult O. degu. As shown in **Figure 3A**, in slices from young individuals, aged 7–18 months, mGluR-LTD induction was robust (74.1 ± 3.8, n = 8 degu, 28 slices), whereas in slices from older individuals, aged 49–85 months, GluR-LTD induction was negligible (100.0 ± 3.4, n = 11 degu, 37 slices). These differences were significant ($p < 0.001$ Mann–Whitney test). Importantly, a more detailed analysis indicated that the average magnitude of mGluR-LTD correlated with the age of the animals (**Figure 3B**). In slices from young individuals, we confirmed that this form of LTD is blocked by the combination

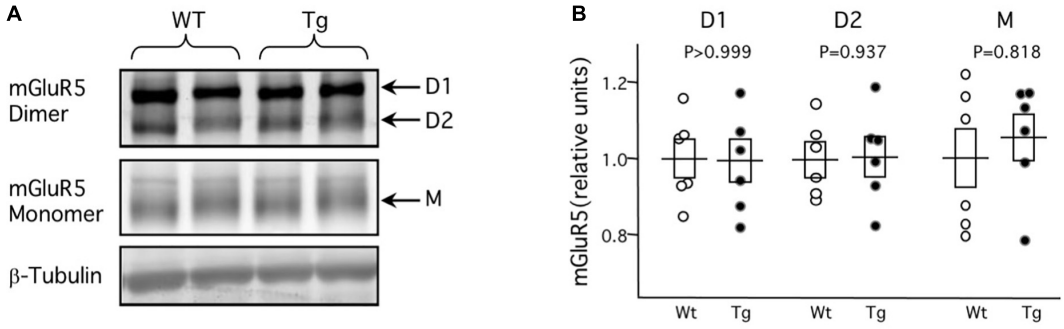

FIGURE 2
Normal expression of mGluR protein in middle-aged APP/PS1 transgenic mice. Western blot analysis of mGluR5 content in hippocampal tissue obtained from 8-month APP/PS1 transgenic mice (Tg) and age-matched control wild-type littermates. **(A)** Example blot showing lanes loaded with tissue from Wt (left two lanes) and Tg (right lanes) mice. D1 and D2 correspond to dimers with molecular weights of 290 and 260 KDa, respectively; M corresponds to the 130 KDa monomers. **(B)** Summary of the quantification of D1, D2, and M in 6 Wt mice (white circles) and 6 Tg mice (black circles). For each group (D1, D2, M) individual data points are normalized to the average value of the corresponding Wt. Boxes depict average ± SEM.

of antagonists of mGluR5 used in **Figure 1D** (**Figure 3C**; Control: 27.2 ± 5.9 change, n = 10 slices; MPEP-LY: 5.8 ± 3.5, n = 6 slices; p = 0.011; Mann–Whitney test). On the other hand, concerning the status of mGluR-LTP, the protocols developed for rat and mouse did induce NMDAR-independent LTP in *O. degu*, but with a very low success yield, inadequate to address developmental changes and to correlate them with behavior.

Finally, we determined whether the diminished capacity for mGluR-LTD in aged *O. degu* has a behavioral correlate. To that end, we tested *O. degu* individuals in a radial maze task, developed for rats (Chappell et al., 1998), where subjects get rewarded by avoiding exploring previously visited arms (see methods). Performance in this task was quantified as the percentage of retroactive memory (RAM) error, basically, the percentage of revisited arms. First, we confirmed that the% of RAM error is lower in young (7.7 ± 0.4 month) than in old (64.2 ± 4.2 month) individuals (Young: 37.4 ± 3.1%, n = 9; old: 57.2 ± 7.6, n = 11; t-test: p = 0.039; **Figure 3D**). Subsequently, we determined the average mGluR-LTD *ex vivo* in the aged individuals behaviorally characterized. As shown in **Figure 3E**, the behavioral score (% RAM error) and the average mGluR-LTD magnitude per individual exhibited a significant linear correlation.

Discussion

Previously we and others showed that preserving learning in aged rats and mice requires the enhancement of mGluR-dependent plasticity in CA3➔CA1 synapses (Lee et al., 2005; Boric et al., 2008; Lu et al., 2019). Here we found that in APP/PS1 mice the induction of mGluR-LTD and mGluR-LTP, both robust in young 3-month-old individuals, virtually disappears by the 8-month of age. We also found a profound loss of mGluR-LTD in aging *O. degu* that correlates with diminished performance in a radial maze. These findings further support the notions that mGluR-dependent forms of plasticity are necessary for learning during aging and their early impairment in the path to AD. The results also underscored different age-related trajectories toward cognitive decline among rodent species: in aged Long-Evans rats impaired learning associates with failure to enhance mGluR-dependent plasticity (Lee et al., 2005; Boric et al., 2008), whereas in aged *O. degu* impaired learning correlates with loss of mGluR-LTD.

As mentioned, few studies have explored the status of mGluR-LTD in AD models. Intriguingly, these few studies document discrepant findings. The first reports indicated a diminished induction of mGluR-LTD in the CA3➔CA1 path in 12-15 month-old APP/PS1 mice when attempted with bath application of the type I agonist DHPG (Yang et al., 2016, 2021). This substantially agrees with the virtual absence of LFS-induced mGluR-LTD that we report in **Figure 1**. The difference in the magnitude of impairment, partial versus complete, might relate to the protocol used, as bath applied agonist would likely activate maximally the full complement of mGluR5 receptors, whereas ppLFS would activate only those accessible to endogenously released glutamate. Notably, however, a recent study reported that ppLFS-induced mGluR-LTD in CA3➔CA1 is enhanced, not reduced, in 7month APP/PS1 mice (Privitera et al., 2022). The enhancement of mGluR-LTD was found to be transient as it declined back to wild-type levels by the 13th month of age (Privitera et al., 2022). In sum, opposite outcomes were obtained in the same model of AD (APP/PS1), with the same induction paradigm (ppLFS) applied at comparable ages (7 and 8 months).

These seemingly discrepant outcomes are each concordant with distinct segments of the literature. In the case of the reduction in mGluR-LTD, which also associates with diminished learning performance in aged Degu (**Figure 3**), the finding dovetails well with the notion that an enhancement of mGluR-dependent plasticity is necessary to compensate for the loss of NMDAR-dependent plasticity during non-pathological aging (Menard and Quirion, 2012a,b). In addition, the normal expression of mGluR5 protein in the face of null mGluR-LTD/P at 8 months APP/PS1 (**Figure 2**), and the previous finding that wild-type levels of mGluR-LTD can be restored by targeting the kinase PERK (Yang et al., 2016), are both consistent with the notion that the uncoupling of type 1 mGluRs is a main contributing factor to age-related cognitive decline (Nicolle et al., 1999). However, in the 5XFAD mouse, a more extreme model of AD, studies report a progressive loss of functional mGluR5Rs (Lee et al., 2019). Nevertheless, whether via uncoupling or loss of the receptors, the deleterious consequences of

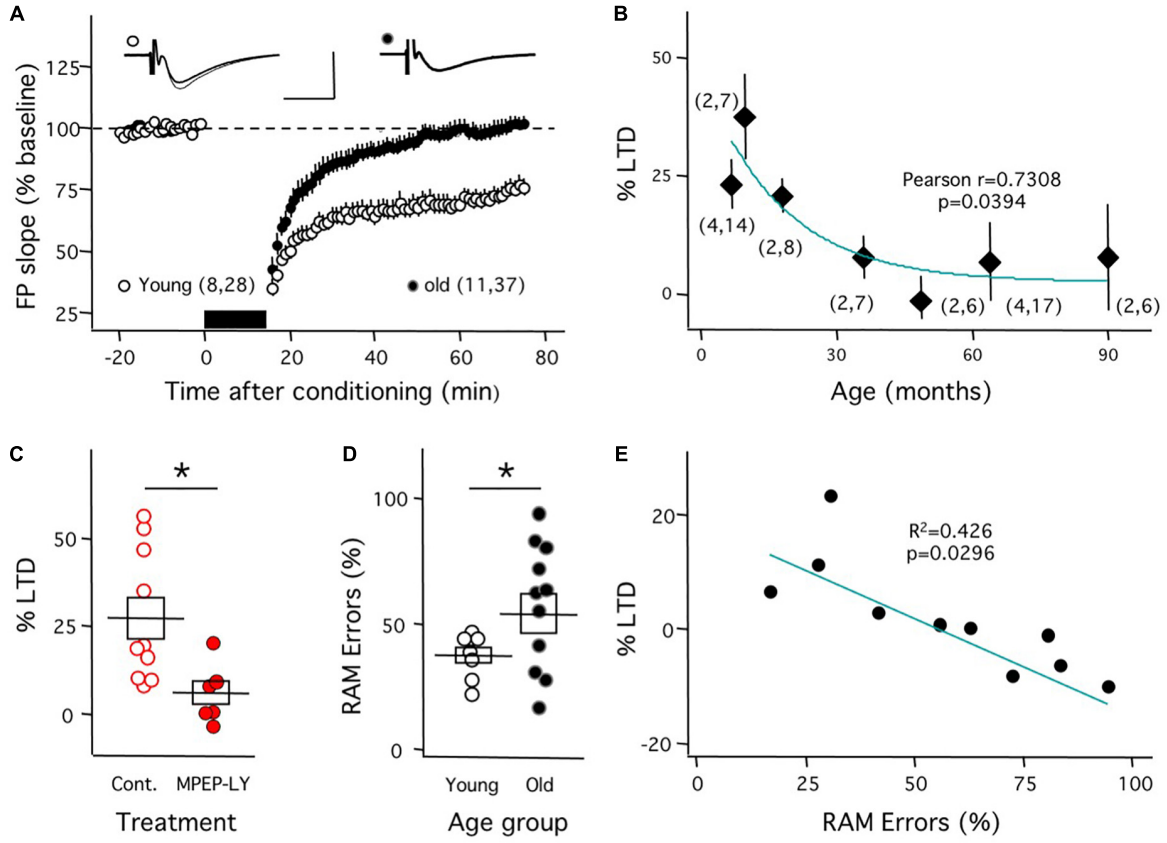

FIGURE 3
Reduced mGluR-LTD correlates with diminished performance in the radial arm maze in aged *O. degu*. Decline in mGluR-LTD in *O. degus*. **(A)** ppLFS induces robust mGluR-LTD in slices mGluR-LTD in slices from young (7–18 months-old: white circles) individuals, but from aged (49–94 months-old: black circles) individuals. Example experiments are depicted on the top (Young: left; Old: right). The superimposed traces are averages of 4 consecutive responses recorded right before (thin line) and 60 minutes after conditioning (thick line). **(B)** The average magnitude of mGluR-LTD (measured 60 min after conditioning) declines with age. The curve was drawn for illustrative purposes. **(C)** Blockade of mGluR-LTD by mGluR5 antagonists in slices from young *O. degus* (control: open circles; 10mM MPEP&100mM LY367385: filled circles). **(D)** Aged (49-94 months-old) *O. degus* display a larger individual variability in the fraction of wrong choices (%errors) in the radial arm maze (RAM) than young individuals (7–10 month-old). **(E)** In aged *O. degus* the mGluR-LTD does correlate with the behavioral score. The graph plots the mGluR-LTD averaged by individual against the individual's behavioral score. Data points in **(A,B)** and boxes in **(C,D)** depict average ± SEM. Asterisks denote significance ($p < 0.005$). The number of mice and slices is indicated in parentheses). The blue lines in panels **(B,E)** are drawn for visual purposes; the *p* values in panels **(B,E)** correspond to the Pearson correlation. Calibration bars in panel **(A)**: 10 ms, 1 mV.

a reduced mGluR5 functionality complement the observation that increasing mGluR5 function with allosteric modulators ameliorates some pathological signatures in other mouse models of AD (Bellozi et al., 2019). Finally, the loss of mGluR-LTD is consistent with the early observation that *in vitro* overexpression of APP occludes the induction of DHPG-LTD (Hsieh et al., 2006), although the occlusion scenario seems unlikely in the APP/PS1 mice because basal synaptic strength is normal in these mice (Megill et al., 2015). On the other hand, the case of an increased mGluR-LTD in the APP/PS1 mice (Privitera et al., 2022) agrees well with the observation of elevated mGluR-LTD in rats that model AD via intraventricular injection of synthetic Aβ peptide (Hu et al., 2022). Moreover, the idea that enhanced mGluR-LTD contributes to AD is in line with studies reporting that blocking mGluRs improve cognitive deficits in AD models (Um et al., 2013; Hamilton et al., 2016; Sanderson et al., 2016; Haas et al., 2017; Kazim et al., 2017). See (Brody and Strittmatter, 2018) for a review), and with the observation that Aβ oligomers enhance clustering and functionality of mGluR5's (Renner et al., 2010). Conceptually, the idea of enhanced mGluR-LTD impairing cognition in AD resonates with the well-recognized negative effects of enhanced mGluR-LTD, and mGluR5 functionality, on cognition in a mouse model of Fragile X syndrome (Luscher and Huber, 2010; Ribeiro et al., 2017; Wilkerson et al., 2018). Indeed, the potential negative consequences of excessive mGluR-LTD were first noted in its initial characterization (Huber et al., 2000, 2002; Bear et al., 2004), when defining features became its dependence on protein synthesis and its excess in Fragile X mice.

A widely held tenet is that plasticity mechanisms need to be at a strict permissive range for optimal neural function. Hence excessive and diminished mGluR-LTD can both be deleterious for cognition. The conundrum is how these two opposite conditions might show up in the same mouse line, the APP/PS1. Differences in mice age at the time of testing seem unplausible. Like the magnitude of NMDAR-dependent plasticity (Lee et al., 2005; Boric et al., 2008; Megill et al., 2015) the magnitude of mGluR-LTD declines with age (in mice and degu), but in a monotonous trend. To account for the reported discrepancies between us and the Privitera et al. (2022)

report the changes in the APP/PS1 need to fluctuate in a roller-coaster manner, from normal at 3 months of age, to excessive at 7 months, disappearing by 8 months, and finally recovering to wild type levels by the 13th month. Two methodological differences were noted between the two labs where the sucrose dissection buffer was used in our lab and the pharmacological blockade of synaptic inhibition was used by Privitera et al. (2022). It is unclear, however, how these treatments could affect preferentially, and transiently, mGluR-LTD only in the APP/PS1 mice but not in the wild types, which expressed comparable levels in both labs.

It is important to note in the APP/PS1 mice the discrepancies in synaptic plasticity are not restricted to mGluR-LTD and multiple studies also report disparate results on NMDAR-dependent LTP (Marchetti and Marie, 2011). These discrepancies in LTP have been attributed in part to abnormal developmental metaplasticity of LTP in APP/PPS1 (Megill et al., 2015). Metaplasticity refers to feedback mechanisms that dynamically maintain the induction and gain of synaptic plasticity within ranges that ensure stability and optimal processing of the neural network (Abraham and Bear, 1996). Importantly, altered metaplasticity is well-documented for NMDAR-dependent forms (Singh et al., 2019; Sanderson et al., 2021). It is conceivable that mGluR-dependent plasticity, like NMDAR-LTP, is also normally governed by that type of feedback mechanism. Disruption of metaplasticity might destabilize mGluR-LTD induction such that, which can drift to extremely high or low values. The particular endpoint of the drift could depend on external contingencies like colony conditions or husbandry protocols. We surmise that is worth considering that altered metaplasticity contributes to discrepancies in plasticity reported by different labs. In that vein, perhaps in AD, the fundamental alteration might be the control of plasticity, not plasticity itself.

Data availability statement

The raw data supporting the conclusions of this article will be made available by the authors, without undue reservation.

Ethics statement

Animal protocols reviewed and approved by Universidad de Valparaiso and Johns Hopkins University.

Author contributions

GV, AA, AI, and CS performed the experiments. H-KL, MG, AP, and AK provided the funding. All authors contributed to design and writing.

Funding

This work was supported by NIH grants P01 AG009973 and R01-EY014882, and Chilean grants MILENIO ICM-ANID P09-022-F, FONDECYT 1200880, and FONDECYT 1201342.

Conflict of interest

The authors declare that the research was conducted in the absence of any commercial or financial relationships that could be construed as a potential conflict of interest.

Publisher's note

All claims expressed in this article are solely those of the authors and do not necessarily represent those of their affiliated organizations, or those of the publisher, the editors and the reviewers. Any product that may be evaluated in this article, or claim that may be made by its manufacturer, is not guaranteed or endorsed by the publisher.

References

Abraham, W., and Bear, M. (1996). Metaplasticity: The plasticity of synaptic plasticity. *Trends Neurosci.* 19, 126–130.

Ardiles, A. O., Tapia-Rojas, C. C., Mandal, M., Alexandre, F., Kirkwood, A., Inestrosa, N. C., et al. (2012). Postsynaptic dysfunction is associated with spatial and object recognition memory loss in a natural model of Alzheimer's disease. *Proc. Natl. Acad. Sci. U.S.A.* 109, 13835–13840. doi: 10.1073/pnas.1201209109

Bear, M. F., Huber, K. M., and Warren, S. T. (2004). The mGluR theory of fragile X mental retardation. *Trends Neurosci.* 27, 370–377.

Bellozi, P. M. Q., Gomes, G. F., da Silva, M. C. M., Lima, I. V. A., Batista, C. R. A., Carneiro Junior, W. O., et al. (2019). A positive allosteric modulator of mGluR5 promotes neuroprotective effects in mouse models of Alzheimer's disease. *Neuropharmacology* 160:107785. doi: 10.1016/j.neuropharm.2019.107785

Boric, K., Munoz, P., Gallagher, M., and Kirkwood, A. (2008). Potential adaptive function for altered long-term potentiation mechanisms in aging hippocampus. *J. Neurosci.* 28, 8034–8039.

Brody, A. H., and Strittmatter, S. M. (2018). Synaptotoxic signaling by amyloid beta oligomers in Alzheimer's disease through prion protein and mGluR5. *Adv. Pharmacol.* 82, 293–323. doi: 10.1016/bs.apha.2017.09.007

Chappell, J., McMahan, R., Chiba, A., and Gallagher, M. (1998). A re-examination of the role of basal forebrain cholinergic neurons in spatial working memory. *Neuropharmacology* 37, 481–487. doi: 10.1016/s0028-3908(98)00032-x

Gallagher, M., Bizon, J. L., Hoyt, E. C., Helm, K. A., and Lund, P. K. (2003). Effects of aging on the hippocampal formation in a naturally occurring animal model of mild cognitive impairment. *Exp. Gerontol.* 38, 71–77. doi: 10.1016/s0531-5565(02)00159-6

Haas, L. T., Salazar, S. V., Smith, L. M., Zhao, H. R., Cox, T. O., Herber, C. S., et al. (2017). Silent allosteric modulation of mGluR5 maintains glutamate signaling while rescuing Alzheimer's mouse phenotypes. *Cell Rep.* 20, 76–88. doi: 10.1016/j.celrep.2017.06.023

Hamilton, A., Vasefi, M., Vander Tuin, C., McQuaid, R. J., Anisman, H., and Ferguson, S. S. (2016). Chronic pharmacological mGluR5 inhibition prevents cognitive impairment and reduces pathogenesis in an Alzheimer disease mouse model. *Cell Rep.* 15, 1859–1865. doi: 10.1016/j.celrep.2016.04.077

Hsieh, H., Boehm, J., Sato, C., Iwatsubo, T., Tomita, T., Sisodia, S., et al. (2006). AMPAR removal underlies Abeta-induced synaptic depression and dendritic spine loss. *Neuron* 52, 831–843. doi: 10.1016/j.neuron.2006.10.035

Hu, Z., Yu, P., Zhang, Y., Yang, Y., Zhu, M., Qin, S., et al. (2022). Inhibition of the ISR abrogates mGluR5-dependent long-term depression and spatial memory deficits in a rat model of Alzheimer's disease. *Transl. Psychiatry* 12:96. doi: 10.1038/s41398-022-01862-9

Huber, K. M., Gallagher, S. M., Warren, S. T., and Bear, M. F. (2002). Altered synaptic plasticity in a mouse model of fragile X mental retardation. *Proc. Natl. Acad. Sci. U.S.A.* 99, 7746–7750. doi: 10.1073/pnas.122205699

Huber, K., Kayser, M., and Bear, M. (2000). Role for rapid dendritic protein synthesis in hippocampal mGluR-dependent long-term depression. *Science* 288, 1254–1257.

Jankowsky, J. L., Slunt, H. H., Gonzales, V., Jenkins, N. A., Copeland, N. G., and Borchelt, D. R. (2004). APP processing and amyloid deposition in mice haplo-insufficient for presenilin 1. *Neurobiol. Aging* 25, 885–892. doi: 10.1016/j.neurobiolaging.2003.09.008

Kamenetz, F., Tomita, T., Hsieh, H., Seabrook, G., Borchelt, D., Iwatsubo, T., et al. (2003). APP processing and synaptic function. *Neuron* 37, 925–937.

Kazim, S. F., Chuang, S. C., Zhao, W., Wong, R. K., Bianchi, R., and Iqbal, K. (2017). Early-onset network hyperexcitability in presymptomatic Alzheimer's disease transgenic mice is suppressed by passive immunization with anti-human APP/Abeta antibody and by mGluR5 blockade. *Front. Aging Neurosci.* 9:71. doi: 10.3389/fnagi.2017.00071

Lee, H. K., Min, S. S., Gallagher, M., and Kirkwood, A. (2005). NMDA receptor-independent long-term depression correlates with successful aging in rats. *Nat. Neurosci.* 8, 1657–1659. doi: 10.1038/nn1586

Lee, M., Lee, H. J., Jeong, Y. J., Oh, S. J., Kang, K. J., Han, S. J., et al. (2019). Age dependency of mGluR5 availability in 5xFAD mice measured by PET. *Neurobiol. Aging* 84, 208–216. doi: 10.1016/j.neurobiolaging.2019.08.006

Li, S., and Selkoe, D. J. (2020). A mechanistic hypothesis for the impairment of synaptic plasticity by soluble Abeta oligomers from Alzheimer's brain. *J. Neurochem.* 154, 583–597. doi: 10.1111/jnc.15007

Lu, Z., Zhao, T., Tao, L., Yu, Q., Yang, Y., Cheng, J., et al. (2019). Cystathionine beta-synthase-derived hydrogen sulfide correlates with successful aging in mice. *Rejuvenation Res.* 22, 513–520. doi: 10.1089/rej.2018.2166

Luscher, C., and Huber, K. M. (2010). Group 1 mGluR-dependent synaptic long-term depression: Mechanisms and implications for circuitry and disease. *Neuron* 65, 445–459. doi: 10.1016/j.neuron.2010.01.016

Mango, D., Saidi, A., Cisale, G. Y., Feligioni, M., Corbo, M., and Nistico, R. (2019). Targeting synaptic plasticity in experimental models of Alzheimer's disease. *Front. Pharmacol.* 10:778. doi: 10.3389/fphar.2019.00778

Marchetti, C., and Marie, H. (2011). Hippocampal synaptic plasticity in Alzheimer's disease: What have we learned so far from transgenic models? *Rev. Neurosci.* 22, 373–402.

Megill, A., Tran, T., Eldred, K., Lee, N. J., Wong, P. C., Hoe, H. S., et al. (2015). Defective age-dependent metaplasticity in a mouse model of Alzheimer's disease. *J. Neurosci.* 35, 11346–11357. doi: 10.1523/JNEUROSCI.5289-14.2015

Menard, C., and Quirion, R. (2012a). Group 1 metabotropic glutamate receptor function and its regulation of learning and memory in the aging brain. *Front. Pharmacol.* 3:182. doi: 10.3389/fphar.2012.00182

Menard, C., and Quirion, R. (2012b). Successful cognitive aging in rats: A role for mGluR5 glutamate receptors, homer 1 proteins and downstream signaling pathways. *PLoS One* 7:e28666. doi: 10.1371/journal.pone.0028666

Nicolle, M. M., Colombo, P. J., Gallagher, M., and McKinney, M. (1999). Metabotropic glutamate receptor-mediated hippocampal phosphoinositide turnover is blunted in spatial learning-impaired aged rats. *J. Neurosci.* 19, 9604–9610. doi: 10.1523/JNEUROSCI.19-21-09604.1999

Ondrejcak, T., Klyubin, I., Hu, N. W., Barry, A. E., Cullen, W. K., and Rowan, M. J. (2010). Alzheimer's disease amyloid beta-protein and synaptic function. *Neuromol. Med.* 12, 13–26.

Palmer, M., Irving, A., Seabrook, G., Jane, D., and Collingridge, G. (1997). The group I mGlu receptor agonist DHPG induces a novel form of LTD in the CA1 region of the hippocampus. *Neuropharmacology* 36, 1517–1532. doi: 10.1016/s0028-3908(97)00181-0

Privitera, L., Hogg, E. L., Lopes, M., Domingos, L. B., Gaestel, M., Muller, J., et al. (2022). The MK2 cascade mediates transient alteration in mGluR-LTD and spatial learning in a murine model of Alzheimer's disease. *Aging Cell* 21:e13717. doi: 10.1111/acel.13717

Renner, M., Lacor, P. N., Velasco, P. T., Xu, J., Contractor, A., Klein, W. L., et al. (2010). Deleterious effects of amyloid beta oligomers acting as an extracellular scaffold for mGluR5. *Neuron* 66, 739–754. doi: 10.1016/j.neuron.2010.04.029

Ribeiro, F. M., Vieira, L. B., Pires, R. G., Olmo, R. P., and Ferguson, S. S. (2017). Metabotropic glutamate receptors and neurodegenerative diseases. *Pharmacol. Res.* 115, 179–191.

Sanderson, J. L., Freund, R. K., Gorski, J. A., and Dell'Acqua, M. L. (2021). beta-amyloid disruption of LTP/LTD balance is mediated by AKAP150-anchored PKA and calcineurin regulation of Ca(2+)-permeable AMPA receptors. *Cell Rep.* 37:109786. doi: 10.1016/j.celrep.2021.109786

Sanderson, T. M., Hogg, E. L., Collingridge, G. L., and Correa, S. A. (2016). Hippocampal metabotropic glutamate receptor long-term depression in health and disease: Focus on mitogen-activated protein kinase pathways. *J. Neurochem.* 139(Suppl. 2), 200–214. doi: 10.1111/jnc.13592

Savonenko, A., Xu, G. M., Melnikova, T., Morton, J. L., Gonzales, V., Wong, M. P., et al. (2005). Episodic-like memory deficits in the APPswe/PS1dE9 mouse model of Alzheimer's disease: Relationships to beta-amyloid deposition and neurotransmitter abnormalities. *Neurobiol. Dis.* 18, 602–617. doi: 10.1016/j.nbd.2004.10.022

Selkoe, D. J. (2002). Alzheimer's disease is a synaptic failure. *Science* 298, 789–791.

Selkoe, D. J. (2008). Soluble oligomers of the amyloid beta-protein impair synaptic plasticity and behavior. *Behav. Brain Res.* 192, 106–113.

Singh, A., Jones, O. D., Mockett, B. G., Ohline, S. M., and Abraham, W. C. (2019). Tumor necrosis factor-alpha-mediated metaplastic inhibition of LTP is constitutively engaged in an Alzheimer's disease model. *J. Neurosci.* 39, 9083–9097. doi: 10.1523/JNEUROSCI.1492-19.2019

Um, J. W., Kaufman, A. C., Kostylev, M., Heiss, J. K., Stagi, M., Takahashi, H., et al. (2013). Metabotropic glutamate receptor 5 is a coreceptor for Alzheimer abeta oligomer bound to cellular prion protein. *Neuron* 79, 887–902. doi: 10.1016/j.neuron.2013.06.036

Wang, H., Ardiles, A. O., Yang, S., Tran, T., Posada-Duque, R., Valdivia, G., et al. (2016). Metabotropic glutamate receptors induce a form of LTP controlled by translation and arc signaling in the hippocampus. *J. Neurosci.* 36, 1723–1729. doi: 10.1523/JNEUROSCI.0878-15.2016

Wilkerson, J. R., Albanesi, J. P., and Huber, K. M. (2018). Roles for arc in metabotropic glutamate receptor-dependent LTD and synapse elimination: Implications in health and disease. *Semin. Cell Dev. Biol.* 77, 51–62. doi: 10.1016/j.semcdb.2017.09.035

Yang, S., Megill, A., Ardiles, A. O., Ransom, S., Tran, T., Koh, M. T., et al. (2013). Integrity of mGluR-LTD in the associative/commissural inputs to CA3 correlates with successful aging in rats. *J. Neurosci.* 33, 12670–12678. doi: 10.1523/JNEUROSCI.1086-13.2013

Yang, W., Zhou, X., Ryazanov, A. G., and Ma, T. (2021). Suppression of the kinase for elongation factor 2 alleviates mGluR-LTD impairments in a mouse model of Alzheimer's disease. *Neurobiol. Aging* 98, 225–230. doi: 10.1016/j.neurobiolaging.2020.11.016

Yang, W., Zhou, X., Zimmermann, H. R., Cavener, D. R., Klann, E., and Ma, T. (2016). Repression of the eIF2alpha kinase PERK alleviates mGluR-LTD impairments in a mouse model of Alzheimer's disease. *Neurobiol Aging* 41, 19–24. doi: 10.1016/j.neurobiolaging.2016.02.005

Zhang, H., Jiang, X., Ma, L., Wei, W., Li, Z., Chang, S., et al. (2022). Role of Abeta in Alzheimer's-related synaptic dysfunction. *Front. Cell Dev. Biol.* 10:964075. doi: 10.3389/fcell.2022.964075

frontiers | Frontiers in Synaptic Neuroscience

TYPE Original Research
PUBLISHED 23 March 2023
DOI 10.3389/fnsyn.2023.1135479

OPEN ACCESS

EDITED BY
Fereshteh S. Nugent,
Uniformed Services University, United States

REVIEWED BY
Xinxing Wang,
Stony Brook University, United States
Maija Liisa Castrén,
University of Helsinki, Finland

*CORRESPONDENCE
Yi Zuo
yizuo@ucsc.edu

RECEIVED 31 December 2022
ACCEPTED 07 March 2023
PUBLISHED 23 March 2023

CITATION
Gredell M, Lu J and Zuo Y (2023) The effect of single-cell knockout of Fragile X Messenger Ribonucleoprotein on synaptic structural plasticity.
Front. Synaptic Neurosci. 15:1135479.
doi: 10.3389/fnsyn.2023.1135479

The effect of single-cell knockout of Fragile X Messenger Ribonucleoprotein on synaptic structural plasticity

Marie Gredell, Ju Lu and Yi Zuo*

Department of Molecular, Cell and Developmental Biology, University of California, Santa Cruz, Santa Cruz, CA, United States

Fragile X Syndrome (FXS) is the best-known form of inherited intellectual disability caused by the loss-of-function mutation in a single gene. The *FMR1* gene mutation abolishes the expression of Fragile X Messenger Ribonucleoprotein (FMRP), which regulates the expression of many synaptic proteins. Cortical pyramidal neurons in postmortem FXS patient brains show abnormally high density and immature morphology of dendritic spines; this phenotype is replicated in the *Fmr1* knockout (KO) mouse. While FMRP is well-positioned in the dendrite to regulate synaptic plasticity, intriguing *in vitro* and *in vivo* data show that wild type neurons embedded in a network of *Fmr1* KO neurons or glia exhibit spine abnormalities just as neurons in *Fmr1* global KO mice. This raises the question: does FMRP regulate synaptic morphology and dynamics in a cell-autonomous manner, or do the synaptic phenotypes arise from abnormal pre-synaptic inputs? To address this question, we combined viral and mouse genetic approaches to delete FMRP from a very sparse subset of cortical layer 5 pyramidal neurons (L5 PyrNs) either during early postnatal development or in adulthood. We then followed the structural dynamics of dendritic spines on these *Fmr1* KO neurons by *in vivo* two-photon microscopy. We found that, while L5 PyrNs in adult *Fmr1* global KO mice have abnormally high density of thin spines, single-cell *Fmr1* KO in adulthood does not affect spine density, morphology, or dynamics. On the contrary, neurons with neonatal FMRP deletion have normal spine density but elevated spine formation at 1 month of age, replicating the phenotype in *Fmr1* global KO mice. Interestingly, these neurons exhibit elevated thin spine density, but normal total spine density, by adulthood. Together, our data reveal cell-autonomous FMRP regulation of cortical synaptic dynamics during adolescence, but spine defects in adulthood also implicate non-cell-autonomous factors.

KEYWORDS

Fragile X syndrome (FXS), FMRP, *Fmr1*, dendritic spine, synaptic plasticity, cell-autonomous

1. Introduction

Fragile X syndrome (FXS) is the most common inherited intellectual disorder (Warren and Nelson, 1994), characterized by a variety of physical, behavioral, and cognitive symptoms (Berry-Kravis, 2002; Turk, 2011). It is caused by the expansion of a CGG trinucleotide repeat in the *FMR1* gene on the X chromosome (Verkerk et al., 1991), which silences *FMR1* transcription (Pieretti et al., 1991). The *Fmr1* global knockout (KO) mouse generated over three decades ago (The Dutch-Belgian Fragile X Consortium, 1994) exhibits a variety of neurological and behavioral phenotypes, including audiogenic seizures, hypersensitivity to auditory stimuli, hyperactivity, repetitive behaviors, and memory deficits (Pietropaolo et al., 2011; Kramvis et al., 2013; Li et al., 2020), mimicking symptoms in FXS patients (Wisniewski et al., 1991; Musumeci et al., 1999; Rais et al., 2018).

The Fragile X Messenger Ribonucleoprotein (FMRP), which is encoded by the *Fmr1* gene, is present in dendrites and dendritic spines (Weiler et al., 1997; Antar et al., 2004; Ferrari et al., 2007), postsynaptic sites important for the induction and maintenance of synaptic plasticity. FMRP is involved in regulating almost all aspects of gene expression (Richter and Zhao, 2021), and is particularly critical for the transportation and local translation of mRNAs that regulate dendritic growth, synaptic development, and plasticity (Bassell and Warren, 2008). Indeed, postmortem examination shows a higher density of long and thin dendritic spines on cortical neurons in FXS patients than in healthy people (Rudelli et al., 1985; Hinton et al., 1991; Irwin et al., 2001; Beckel-Mitchener and Greenough, 2004). *Fmr1* global KO mice also display an increased density of dendritic spines, as well as a higher percentage of immature-appearing spines, than wild type controls (Comery et al., 1997; Irwin et al., 2002; Galvez and Greenough, 2005; McKinney et al., 2005; Grossman et al., 2006). In addition to altered morphology and density, *Fmr1* global KO mice have altered structural dynamics (formation and elimination) of cortical spines in an age-, region-, and cell type-specific manner (Cruz-Martín et al., 2010; Pan et al., 2010; Padmashri et al., 2013; Hodges et al., 2017).

Previous studies have shown that *Fmr1* global KO mice have abnormal neuronal activity pattern and synchronization in the neocortex and the hippocampus (Gibson et al., 2008; Hays et al., 2011; Paluszkiewicz et al., 2011; Arbab et al., 2018; Scharkowski et al., 2018; Cheyne et al., 2019). Such functional abnormalities may have profound impacts on the synaptic circuit. It is well-recognized that many intracellular signaling pathways that regulate spine formation and maturation are activity-dependent (Saneyoshi et al., 2010). As spine elimination has been associated with activity-dependent processes such as long-term depression and competition between active and inactive neighboring synapses (Stein and Zito, 2019), these plasticity mechanisms may translate the anomalous neuronal activities into defective structural plasticity of synapses. Such complex interplay between cellular and network-level mechanisms raises an interesting question: is the alteration in FXS spine structure and dynamics the result of cell-autonomous dysregulation, or of abnormal activities in the neuronal network?

To address this question, we combined viral and mouse genetic approaches to eliminate FMRP from a small, sparse subset of cortical neurons in an *Fmr1* conditional knockout (CKO) mouse line (Mientjes et al., 2006), and performed *in vivo* two-photon imaging of dendritic spines over time to compare the spine dynamics between FMRP-null neurons and controls. We found that FMRP deletion during postnatal development, but not in adulthood, leads to altered spine dynamics in cortical pyramidal neurons (PyrNs), which reveals a crucial cell-autonomous function of FMRP in development. In addition, the density and morphology of spines on neurons with neonatal FMRP deletion only partially replicate the phenotypes in *Fmr1* global KO mice in adulthood, suggesting the contribution of factors extrinsic to individual cells.

2. Materials and methods

2.1. Experimental animals

The *Fmr1* global KO mouse line (JAX #003025) was obtained from Dr. Stephen T. Warren's lab at Emory University; the *Fmr1* CKO mouse line (Mientjes et al., 2006) was obtained from Dr. David L. Nelson's lab at Baylor College of Medicine; the *Thy1*-GFP-M (JAX #007788) mouse line was obtained from The Jackson Laboratory (Bar Harbor, ME, USA). All mice have been maintained in the C57BL6/J (JAX #000664) background for many generations. Mice were group-housed with littermates and maintained on a 12 h light/dark cycle. All animal experiments were carried out in accordance with protocols approved by The Institutional Animal Care and Use Committee of University of California, Santa Cruz. Only male mice were used for experiments.

2.2. Virus injection and cranial window implantation in adult mice

Virus injection and cranial window implantation in adult mice (6–8 weeks old) were performed as described previously (Lu et al., 2021). Briefly, the mouse was anesthetized with isoflurane in oxygen (4% for induction and 1.5% for maintenance), then placed on the stereotaxic frame. Ophthalmic ointment was applied to the eyes to prevent desiccation and irritation. Carprofen (5 mg/kg bodyweight, intraperitoneal), buprenorphine (0.1 mg/kg, subcutaneous), enrofloxacin (5 mg/kg, subcutaneous), and dexamethasone (2 mg/kg, intramuscular) were administered. The fur on the top of the head was removed with a blade; the exposed scalp was sterilized with betadine followed by 70% alcohol. A midline scalp incision was made, and the periosteum was gently scraped off from the skull. A circular piece of the skull (centered at AP = −1 mm, ML = 1.5 mm) was removed with a trephine (diameter = 2.3 mm, Fine Science Tools, Foster City, CA, USA) driven by a high-speed micro-drill (Foredom K1070, Blackstone Industries, LLC, Bethal, CT, USA). AAV2/1-hSyn-Cre virus (Addgene 105553-AAV1, 2.6×10^{13} gc/ml) or AAV2/1-CaMKII0.4-Cre-SV40 virus (2.94×10^{13} gc/ml; The Penn Vector Core, University of Pennsylvania, Philadelphia, PA, USA) was diluted 1:5,000 in sterile saline and then mixed in a 1:1 ratio with AAV2/1-CAG-Flex-EGFP (Addgene 51502-AAV1, 2.96×10^{13} gc/ml). A total of 100 nl of the virus mixture was injected into the center of the window at a depth of 0.6 mm from the cortical surface at a rate of 20 nl/min using a custom-made injection

system based on a single-axis oil hydraulic micromanipulator (MO-10, Narishige, Tokyo, Japan). The imaging port was made by gluing a circular cover glass (#2, diameter = 2.2 mm) underneath a donut-shaped glass (#1, inner diameter = 2 mm, outer diameter = 3 mm; Potomac Photonics, Inc., Baltimore, MD, USA). The imaging port was mounted so that the bottom cover glass fit snugly into the cranial window and the top glass donut rested above the skull. The imaging port was secured with a UV-cured adhesive (Fusion Flo, Prevest DenPro, Jammu, India) onto the skull. After the solidification of the adhesive, the scalp flaps were closed with suture. Following 2 weeks of recovery and virus incubation, the central piece of the scalp was excised, and a custom-made stainless-steel head-bar was secured over the skull with dental cement (Jet Denture Repair, Lang Dental, Wheeling, IL, USA). The mouse received enrofloxacin, buprenorphine, and dexamethasone once per day for two extra days post-surgery and was allowed to recover for an additional week prior to imaging.

2.3. *In vivo* imaging of dendritic spines through the cranial window

In vivo imaging of dendritic spines through the cranial window was performed on a two-photon microscope (Ultima Investigator, Bruker Co., Middleton, WI, USA) using a 16x/0.8 NA water-immersion objective (Nikon Instruments, Inc., Melville, NY, USA) and an ultrafast two-photon laser (Mai Tai, Spectra-Physics, Santa Clara, CA, USA) operating at 940 nm wavelength. The mouse was anesthetized with a mixture of ketamine (20 mg/ml) and xylazine (2.0 mg/ml) in 0.9% sterile saline administered intraperitoneally (5 ml/kg bodyweight). It was then placed onto a custom-made holding stage, secured by the head-bar. Prior to the first imaging session, images of blood vessels were taken under a dissection microscope as a reference for subsequent relocations. Stacks of two-photon images were taken at 12x zoom with a z-step size of 1 μm. After the first imaging session, low-magnification image stacks (1x and 4x zoom, z-step size = 3 μm) were taken to facilitate relocation.

2.4. Virus injection in neonatal mice

Virus injection in neonatal mice was performed as previously described (Chen et al., 2018). Briefly, the postnatal (P) day 1–3 mouse was cryo-anesthetized by placement on ice. AAV2/1-CaMKII0.4-Cre-SV40 (2.94×10^{13} gc/ml; The Penn Vector Core, University of Pennsylvania, Philadelphia, PA, USA) was diluted 1:5,000 in sterile saline and then mixed in a 1:1 ratio with AAV2/1-CAG-Flex-EGFP (Addgene 51502-AAV1, 2.96×10^{13} gc/ml). A total of 100 nl of the virus mixture was injected at a rate of 40 nl/min into the primary somatosensory cortex (AP = 1.75 mm from lambda, ML = 1.25 mm; depth = 0.35 mm) through the scalp and the skull. A total of 4 weeks of incubation were allowed before imaging and immunohistochemical experiments.

2.5. Thin skull preparation for *in vivo* imaging of dendritic spines

The thin skull procedure was performed on young (1 month old) mice as previously described (Xu et al., 2009). Briefly, the mouse was anesthetized with a mixture of ketamine (20 mg/ml) and xylazine (2.0 mg/ml) in 0.9% sterile saline administered intraperitoneally (5 ml/kg body weight). Ophthalmic ointment was applied to the eyes to prevent desiccation and irritation, and the fur over the scalp was removed with a blade. A midline incision was made through the scalp and the periosteum was gently scraped off from the skull. A high-speed micro-drill (Foredom K1070, Blackstone Industries, LLC, Bethal, CT, USA) and a microblade were used to thin a small region of the skull to ∼20 μm thickness. A custom-made head-plate with a central opening was attached to the skull by cyanoacrylate glue (Krazy Glue, Elmer's Products, Westerville, OH, USA), centered over the thinned region. The head-plate was secured onto a custom-made metal baseplate to stabilize the mouse's head during imaging. Two-photon imaging was performed as described above. After imaging, the head-plate was detached from the skull, the skull was cleaned with sterile saline, and the scalp was sutured.

2.6. Dendritic spine data analysis

Images were analyzed using ImageJ as described previously (Xu et al., 2009). A spine was considered eliminated if it was present in the initial image but not in the subsequent image. A spine was considered to have newly formed if it was not present in the initial image but present in the subsequent image. The percentage of spines eliminated/formed was calculated as the number of spines eliminated/formed over the total spines counted from the first imaging session. Spine density was measured by dividing the number of spines on a dendritic segment by the length of the segment. Spines were classified into four morphological categories (mushroom, stubby, thin, and other) as previously described (Hodges et al., 2017).

2.7. Immunohistochemistry

The mouse was transcardially perfused with 4% paraformaldehyde (PFA) in 0.01 M phosphate buffered saline (PBS). The brain was removed and post-fixed in 4% PFA overnight at 4°C. For all experiments, the brain was cut into 40 μm sections using a vibratome (VT1000S, Leica Biosystems, Deer Park, IL, USA). Sections were permeabilized and blocked with 0.5% Triton X-100 and 10% normal goat serum in PBS, then incubated with rabbit anti-FMRP (1:1,000; F4055, Sigma-Aldrich, St. Louis, MO, USA) and mouse anti-NeuN (1:1,000; MAB377, MilliporeSigma, Burlington, MA, USA) in 0.5% Triton X-100 in PBS at 4°C overnight. Sections were then incubated with goat anti-rabbit secondary antibody conjugated to Alexa Fluor 594 (1:1,000; A11037, Life Technologies, Carlsbad, CA, USA) and goat anti-mouse secondary antibody conjugated to Alexa Fluor 647 (1:1,000; A21235, Life Technologies, Carlsbad, CA, USA) in 10% normal goat serum in PBS for 2 h at room temperature. After rinsing in PBS, sections were incubated in 4',6-diamidino-2-phenylindole (DAPI, 1:36,000) for 15 min. Sections were then mounted with Fluoromount-G mounting medium (Cat# 0100-01, SouthernBiotech, Birmingham, AL, USA). Images were captured with a Zeiss Axiolmager Z2 widefield fluorescence microscope using a 2.5x/0.12 NA or 10x/0.45 NA, or with a Zeiss 880 confocal

10.3389/fnsyn.2023.1135479

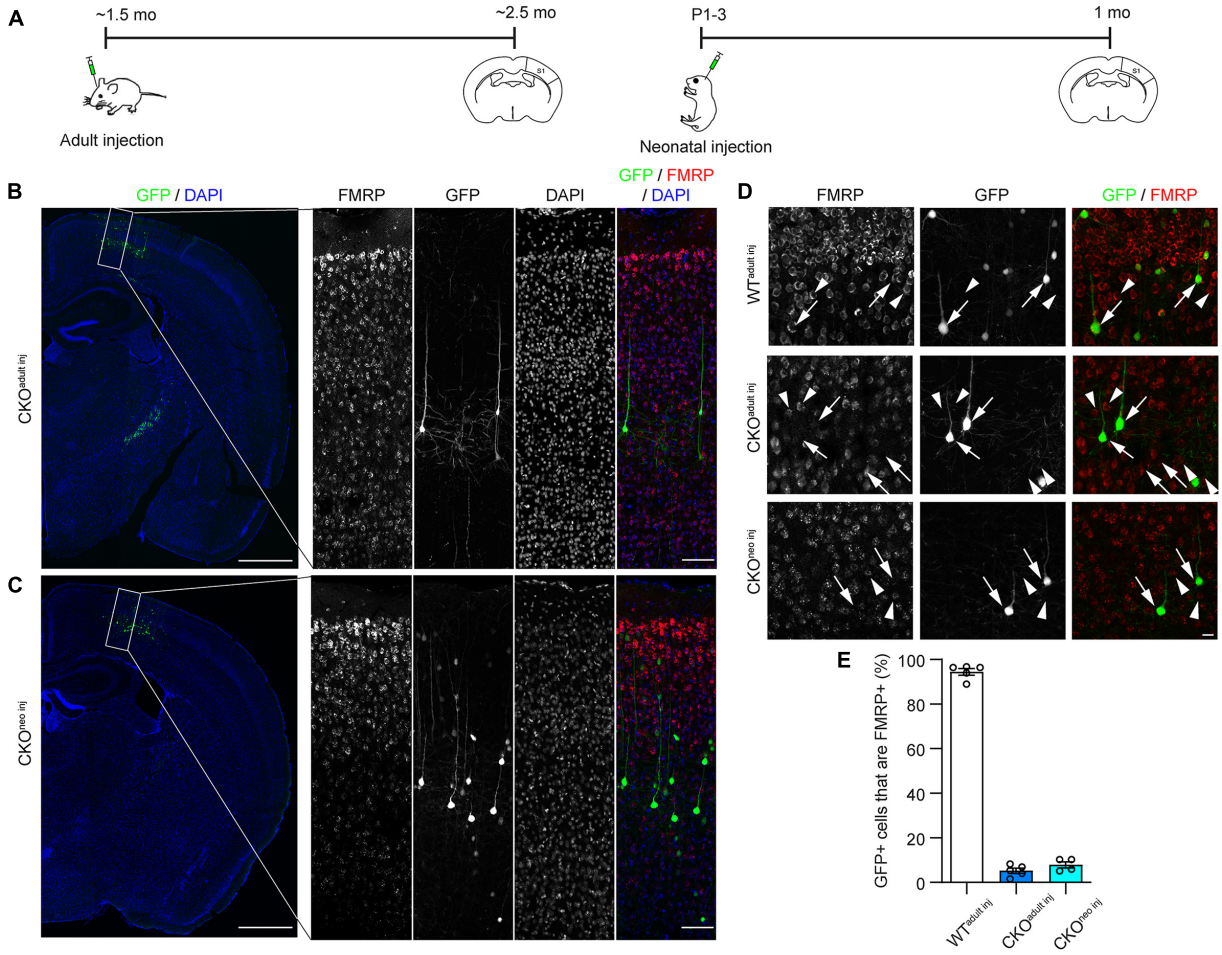

FIGURE 1
Cre-lox recombination strategy successfully eliminates Fragile X Messenger Ribonucleoprotein (FMRP) from individual infected cells. **(A)** Timeline of virus injection and histology. **(B)** Left: Example of Cre-dependent green fluorescent protein (GFP) expression and *Fmr1* knockout (KO) in a sparse subset of S1 L5 PyrNs of a *Fmr1* conditional knockout (CKO)$^{adult\ inj}$ mouse. Scale bar: 500 μm. Right: Enlarged view of the rectangular region in the left panel showing FMRP and GFP expression. Scale bar: 100 μm. **(C)** Examples of *Fmr1* KO in a CKO$^{neo\ inj}$ mouse, with the same magnification and arrangement as in **(B)**. **(D)** FMRP and GFP expression in WT$^{adult\ inj}$ (top), CKO$^{adult\ inj}$ (middle), and CKO$^{neo\ inj}$ (bottom) mice imaged with confocal microscopy. Arrows: GFP+ cells; arrowheads: GFP-/FMRP+ cells. Scale bar: 20 μm. **(E)** Percentages of cells co-expressing GFP and FMRP in WT$^{adult\ inj}$, CKO$^{adult\ inj}$, and CKO$^{neo\ inj}$ mice. WT$^{adult\ inj}$ n = 5 mice (335 cells); CKO$^{adult\ inj}$ n = 5 mice (397 cells); CKO$^{neo\ inj}$ n = 4 mice (404 cells).

microscope using a 20x/0.8 NA air objective. The density of neurons with GFP, FMRP, or NeuN labeling was quantified using Neurolucida Explorer 11 (MBF Bioscience, Williston, VT, USA). Individual cells were analyzed for the presence of GFP, FMRP, and NeuN.

2.8. Statistical analysis

Statistical analyses were performed using GraphPad Prism 9.3.1 (GraphPad Software, Boston, MA, USA). The Shapiro–Wilk test was used to test for normality. If samples passed the normality test, Student's *t*-test was used for two-sample comparison; otherwise Mann-Whitney test was used. For multi-sample comparison, one-way or two-way ANOVA was used, followed by post-hoc Dunnett's or Šidák test (compared with the control group). The sample difference was considered significant if $p < 0.05$. Data are presented as mean ± s.e.m.

3. Results

3.1. Virus-induced FMRP knockout in single neurons in adolescent and adult mice

To investigate whether FMRP regulates the structural plasticity of synapses cell-autonomously, we knocked out FMRP from a sparse subset of layer 5 (L5) PyrNs in the primary somatosensory cortex (S1) of *Fmr1* CKO mice. We chose to target S1 because previous studies have revealed altered tactile information processing (Juczewski et al., 2016; He et al., 2017) and abnormal dendritic spine development (Galvez and Greenough, 2005; Till et al., 2012) in this area of adult *Fmr1* global KO ("GKO") mice. We accomplished this by injecting a mixture of highly diluted adeno-associated virus (AAV) encoding the Cre recombinase and another AAV encoding floxed green fluorescent protein

(GFP) into S1 of CKO mice either in adulthood (~6 weeks old) or at postnatal day 1-3 (P1-3; **Figure 1A**). Hereafter we will refer to these mice as "CKO$^{adult\ inj}$" and "CKO$^{neo\ inj}$," respectively. This strategy removes the promoter region and the first exon of the *Fmr1* gene via Cre-dependent recombination, thus preventing *Fmr1* transcription. At the same time, the Cre-dependent GFP expression allows us to visualize the cells in which *Fmr1* has been knocked out. We verified the specificity and effectiveness of this strategy with immunohistochemistry (**Figures 1B–D**). After 3 weeks of virus incubation, we found in CKO$^{adult\ inj}$ mice, a sparse subset of L5 PyrNs were GFP+ (**Figures 1B, D**). Among these cells, only 5.3 ± 1.2% were FMRP+ (**Figure 1E**). Similarly, CKO$^{neo\ inj}$ mice exhibited sparse GFP labeling of L5 PyrNs (**Figures 1C, D**), and only 7.3 ± 1.1% of such cells were FMRP+ (**Figure 1E**). In contrast, wild type (WT) mice that received the same virus injection in adulthood ("WT$^{adult\ inj}$") continued to express FMRP in infected cells, with 94.5 ± 1.5% of GFP+ cells being FMRP+ (**Figure 1E**). These data confirm the effectiveness and specificity of our knockout strategy.

3.2. Single-cell FMRP knockout does not alter spine density

To assess the effects of single-cell *Fmr1* KO on the structural dynamics of dendritic spines, we performed longitudinal *in vivo* two-photon imaging either through a cranial window (Holtmaat et al., 2009) or with the thin-skull preparation (Xu et al., 2009). We first compared the density of spines on apical dendritic tufts of L5 PyrNs in WT$^{adult\ inj}$, CKO$^{adult\ inj}$, and GKO mice receiving virus injection in adulthood ("GKO$^{adult\ inj}$") when the mice reached 10 weeks of age (**Figure 2A**). We found that in GKO$^{adult\ inj}$ mice, the spine density was 0.43 ± 0.02 per μm, significantly higher than that in WT$^{adult\ inj}$ mice [0.35 ± 0.02 per μm; one-way ANOVA, $F(2,12) = 6.111$, $p < 0.05$; post-hoc Dunnett's multiple comparisons test $p < 0.05$; **Figure 2B**], which is consistent with reports in the literature (Galvez and Greenough, 2005). We further analyzed the density of spines in different morphological categories (**Figure 2C**). Only thin spines exhibited significant density difference between GKO$^{adult\ inj}$ and WT$^{adult\ inj}$ mice [two-way repeated measures ANOVA, $F(6, 36) = 10.02$, $p < 0.0001$; post-hoc Dunnett's multiple comparisons test $p < 0.01$]; the rest showed no difference (post-hoc Dunnett's multiple comparisons test $p = 0.4707$, 0.6510, and 0.9983 for stubby, mushroom, and others, respectively). Interestingly, spine density in CKO$^{adult\ inj}$ mice (0.37 ± 0.01 per μm) was not significantly different from that in WT$^{adult\ inj}$ mice (post-hoc Dunnett's multiple comparisons test $p = 0.8378$; **Figure 2B**). Nor was there significant density difference in spines belonging to any morphological category between CKO$^{adult\ inj}$ and WT$^{adult\ inj}$ mice (post-hoc Dunnett's multiple comparisons test $p = 0.9518$, 0.0955, 0.9908, and 0.1754 for stubby, mushroom, thin, and others, respectively). To control for the possibility that virus infection *per se* affects spine density, we also measured spine density in *Thy1*-GFP-M mice (which are *Fmr1*+, hence denoted "WT^{M}") as well as in GKO × *Thy1*-GFP-M ("GKO^{M}") mice. These animals express cytoplasmic GFP in a sparse subset of cortical L5 PyrNs, thus obviating the need for viral labeling. We found no difference in spine density between WT$^{adult\ inj}$ mice and WT^{M} mice, or between GKO$^{adult\ inj}$ and GKO^{M} mice (**Supplementary Figure 1**). These results demonstrate that the viral knockout strategy *per se* does not affect spine density.

We next compared the spine density of adolescent (~P30) WT^{M}, GKO^{M}, and CKO$^{neo\ inj}$ mice (**Figure 2D**). We found no significant difference among these three groups: the spine density was 0.43 ± 0.02 per μm in WT^{M}, 0.44 ± 0.01 per μm in GKO^{M}, and 0.46 ± 0.01 per μm in CKO$^{neo\ inj}$ mice [one-way ANOVA, $F(2,13) = 1.421$, $p = 0.2766$; **Figure 2E**]. This agrees with previous findings (Nimchinsky et al., 2001; Galvez and Greenough, 2005; Pan et al., 2010; Hodges et al., 2017; Bland et al., 2021). Furthermore, CKO$^{neo\ inj}$ mice showed no significant difference in the density of any spine type in comparison with WT^{M} mice (two-way repeated measures ANOVA, $F(3,27) = 0.4985$, $p = 0.6864$; **Figure 2F**), similar to the previous report on adolescent GKO mice (Hodges et al., 2017).

3.3. Neither global nor single-cell knockout of FMRP affects the structural dynamics of dendritic spines in adult mice

We then examined the structural dynamics of spines in WT$^{adult\ inj}$, GKO$^{adult\ inj}$, and CKO$^{adult\ inj}$ mice starting at about 2 months of age, over 4 and 16 days intervals (**Figures 3A–D**). We found no significant difference in the rate of spine formation and elimination over 4 days: the spine formation rate was 4.4 ± 0.3% in WT$^{adult\ inj}$, 4.1 ± 0.3% in GKO$^{adult\ inj}$, and 3.8 ± 0.3% in CKO$^{adult\ inj}$ [one-way ANOVA, $F(2,12) = 1.017$, $p = 0.3907$; **Figure 3E**], and the spine elimination rate was 5.8 ± 0.4% in WT$^{adult\ inj}$, 5.9 ± 0.2% in GKO$^{adult\ inj}$, and 5.2 ± 0.3% in CKO$^{adult\ inj}$ [one-way ANOVA, $F(2,12) = 1.122$, $p = 0.3574$; **Figure 3F**]. Likewise, there was no significant difference in spine dynamics over 16 days. The spine formation rate was 5.9 ± 0.4%, 6.0 ± 0.8%, and 5.5 ± 0.9% in WT$^{adult\ inj}$, GKO$^{adult\ inj}$, and CKO$^{adult\ inj}$, respectively [one-way ANOVA, $F(2,12) = 0.1352$, $p = 0.8748$; **Figure 3G**], and the corresponding spine elimination rate was 8.6 ± 0.5% in WT$^{adult\ inj}$, 9.6 ± 0.3% in GKO$^{adult\ inj}$, and 8.7 ± 0.9% in CKO$^{adult\ inj}$ [one-way ANOVA, $F(2,12) = 0.7999$, $p = 0.4719$; **Figure 3H**]. Following new spines formed by day 4 till day 16, we found no significant difference in their survival rate [WT$^{adult\ inj}$ 34.0 ± 10.7%, GKO$^{adult\ inj}$ 22.5 ± 6.7%, CKO$^{adult\ inj}$ 26.7 ± 8.5%; one-way ANOVA, $F(2,12) = 0.4419$, $p = 0.6529$; **Figure 3I**]. These results suggest that deleting FMRP from single neurons in adulthood does not affect its spine dynamics. Again, to control for potential confounding effects of virus infection, we measured spine dynamics in WT^{M} and GKO^{M} mice at comparable ages. Spine dynamics did not differ significantly between WT$^{adult\ inj}$ and WT^{M} mice, or between GKO$^{adult\ inj}$ and GKO^{M} mice (**Supplementary Figure 2**). This confirms that the viral labeling strategy does not affect spine dynamics either.

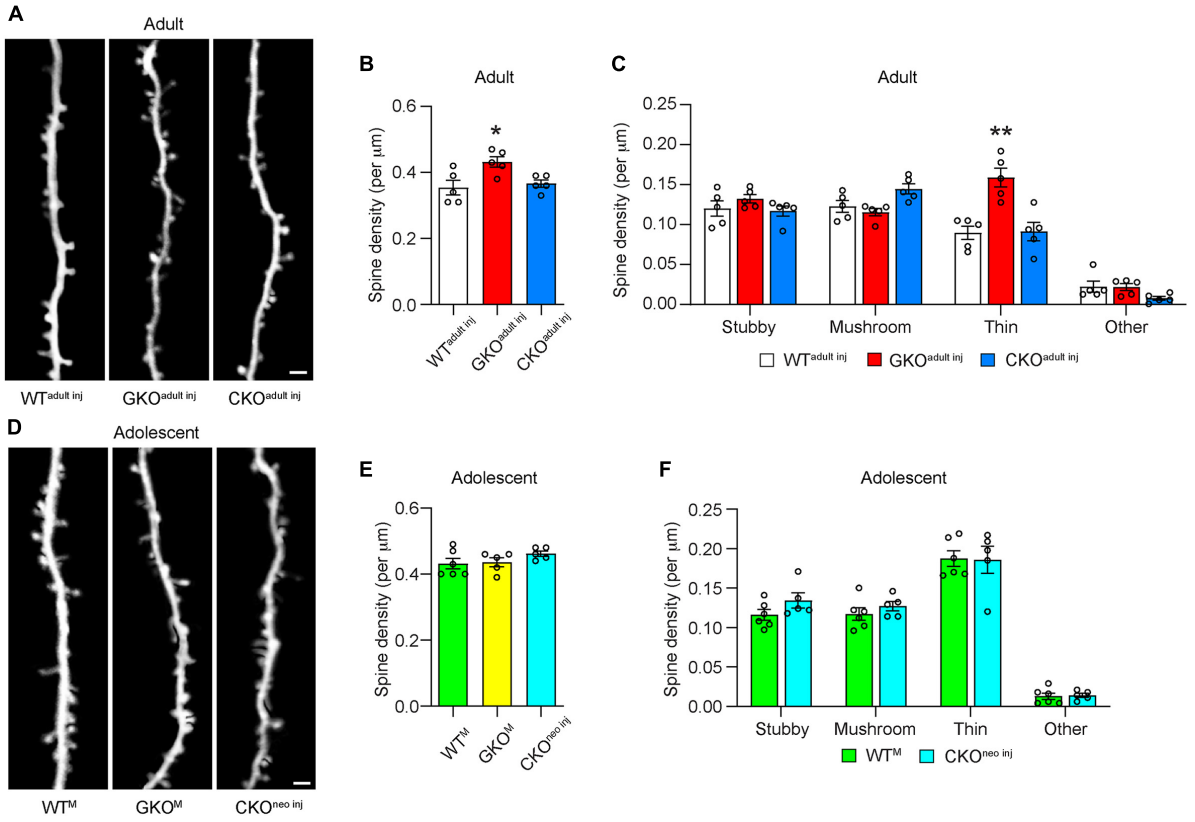

FIGURE 2
Cell-autonomous *Fmr1* knockout (KO) in adolescence or adulthood does not alter spine density. **(A)** Examples of dendritic spines imaged *in vivo* in adult mice. **(B)** Total spine density in $WT^{adult\ inj}$, global knockout ($GKO^{adult\ inj}$), and conditional knockout ($CKO^{adult\ inj}$) mice. $n = 5$ per group. **(C)** Density of different types of spines in $WT^{adult\ inj}$, $GKO^{adult\ inj}$, and $CKO^{adult\ inj}$ mice. $n = 5$ per group. **(D)** Examples of dendritic spines imaged *in vivo* in adolescent mice. **(E)** Total spine density in adolescent mice. $n = 6$ for WT^{M}, 5 for GKO^{M}, and $CKO^{neo\ inj}$ mice. **(F)** Density of different types of spines in adolescent mice. $n = 6$ for WT^{M} and 5 for $CKO^{neo\ inj}$ mice. Scale bar = 2 µm. Hereinafter $^{*}p < 0.05$, $^{**}p < 0.01$; post-hoc comparisons with the control group.

3.4. Single-cell FMRP knockout results in elevated dendritic spine formation in adolescent mice

As previous studies suggest that *Fmr1* KO affects spine dynamics most prominently in adolescence (Hodges et al., 2017), we examined 4 and 16 days spine dynamics in $CKO^{neo\ inj}$, WT^{M}, and GKO^{M} mice starting at 1 month of age (**Figures 4A–D**). We found that spine formation over 4 days was significantly elevated in $CKO^{neo\ inj}$ mice (7.4 ± 0.3%) and GKO^{M} mice (8.1 ± 0.5%) compared to WT^{M} mice [4.6 ± 0.3%; one-way ANOVA, $F(2,13) = 23.71$, $p < 0.001$; post-hoc Dunnett's multiple comparisons test: $p < 0.001$ for $CKO^{neo\ inj}$ vs. WT^{M} and for GKO^{M} vs WT^{M}; **Figure 4E**]. However, spine elimination over 4 days was unaffected [WT^{M} 7.2 ± 0.4%, GKO^{M}: 6.5 ± 0.4%, $CKO^{neo\ inj}$: 6.7 ± 0.3%; one-way ANOVA, $F(2,13) = 1.225$, $p = 0.3255$; **Figure 4F**]. A similar phenomenon emerged over the 16 days interval: $CKO^{neo\ inj}$ mice had a spine formation rate of 13.5 ± 1.1%, which was comparable to that in GKO^{M} mice (13.7 ± 0.3%) but differed significantly from that in WT^{M} mice [9.2 ± 0.5%; one-way ANOVA, $F(2,12) = 12.05$, $p < 0.01$; post-hoc Dunnett's multiple comparisons test: $p < 0.01$ for both $CKO^{neo\ inj}$ vs WT^{M} and GKO^{M} vs. WT^{M}; **Figure 4G**]. The 16 days spine elimination did not significantly differ among the three groups, with rates of 13.3 ± 0.4% (WT^{M}), 13.8 ± 0.4% (GKO^{M}), and 13.9 ± 0.9% ($CKO^{neo\ inj}$), respectively [one-way ANOVA, $F(2,12) = 0.3124$, $p = 0.7374$; **Figure 4H**].

We further followed $CKO^{neo\ inj}$ mice into adulthood and re-examined their spine density and morphology. To our surprise, spine density on the FMRP-null neurons was comparable to that in $WT^{adult\ inj}$ mice [unpaired *t*-test, $t(8) = 1.116$, $p = 0.2966$; **Figure 4I**]. Morphological analysis, however, revealed an elevated density of thin spines on FMRP-null neurons [two-way repeated measures ANOVA, $F(3,24) = 22.56$, $p < 0.0001$; post-hoc Šidák multiple comparisons test, $p < 0.01$; **Figure 4J**]. The normalization of total spine density was due to decreased density of all other types of spines. Together with findings in adult animals, these results suggest that FMRP regulates the structural dynamics of spines cell-autonomously in adolescence, but the development of spine defects into adulthood also involves non-cell-autonomous factors.

4. Discussion

The abundance of dendritic spines with an immature morphology in the adult brain is an anatomical hallmark of

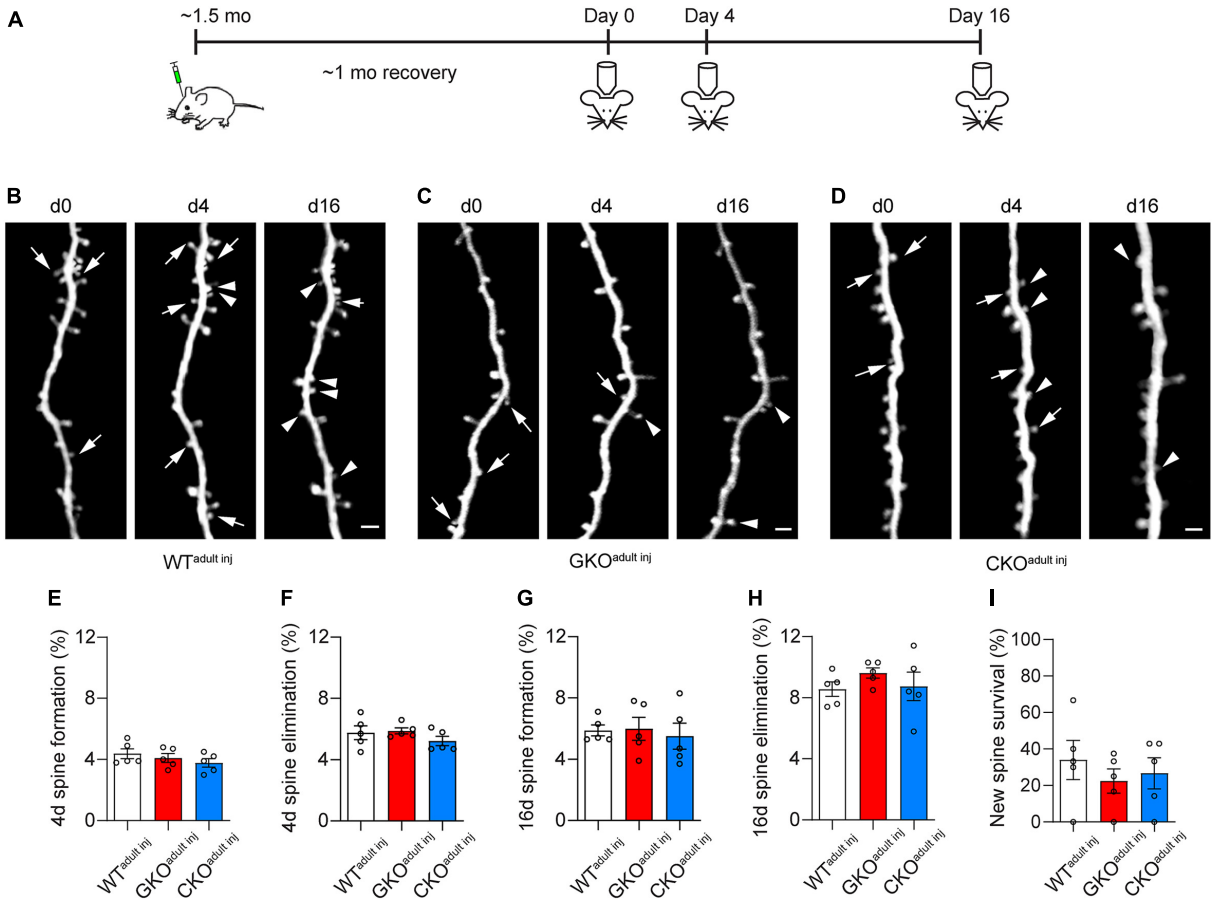

FIGURE 3
Cell-autonomous *Fmr1* knockout (KO) in adulthood does not affect spine formation or elimination. **(A)** Timeline of virus injection and *in vivo* two-photon imaging. **(B–D)** Examples of spine formation and elimination in WT$^{adult\ inj}$ **(B)**, global knockout (GKO$^{adult\ inj}$) **(C)**, and conditional knockout (CKO$^{adult\ inj}$) **(D)** mice. Arrows: eliminated spines; arrowheads: formed spines. Scale bar = 2 μm. **(E,F)** Spine formation **(E)** and elimination **(F)** rates over 4 days in WT$^{adult\ inj}$, GKO$^{adult\ inj}$, and CKO$^{adult\ inj}$ mice. **(G,H)** Spine formation **(G)** and elimination **(H)** rates over 16 days in WT$^{adult\ inj}$, GKO$^{adult\ inj}$, and CKO$^{adult\ inj}$ mice. **(I)** Percentage of new spines formed by day 4 that survived till day 16. *n* = 5 mice per group.

FXS in humans and in mouse models. Traditionally, it is conjectured that this phenotype results from defective spine pruning during development (Greenough et al., 2001; Churchill et al., 2002; Bagni and Greenough, 2005; Bardoni et al., 2006). More recent *in vivo* imaging studies, however, reveal elevated spine formation in adolescence (Pan et al., 2010; Padmashri et al., 2013; Nagaoka et al., 2016; Hodges et al., 2017), and some of them in addition suggest that spine elimination during this developmental stage is elevated as well. The cellular underpinning of such altered structural dynamics is likely complex. It may involve abnormal neural activity patterns operating through activity-dependent mechanisms to prevent the maturation of new spines and the competitive removal of weak and immature spines. It may also implicate altered intrinsic excitability of neurons due to ion channel dysregulation, excitation/inhibition imbalance induced by dysfunctional local inhibitory circuits, and altered homeostatic plasticity (Gibson et al., 2008; Soden and Chen, 2010; Goel et al., 2018; Liu et al., 2021). Moreover, astrocytes may contribute to the spine pathology, as astrocyte-specific KO of *Fmr1* suffices to elevate spine formation (Hodges et al., 2017). Other studies in addition suggests altered inflammatory response of microglia (Parrott et al., 2021) and reduced microglia-mediated synaptic pruning (Jawaid et al., 2018) in *Fmr1* global KO mice. Such a plethora of participants makes it difficult to isolate the contribution of cell-autonomous dysregulation from that of external factors, if *Fmr1* is knocked out globally. In fact, even studies that leverage the random X-linked inactivation of *Fmr1* in heterozygous females to generate mosaicism (approximately half of the neurons are FMRP-null and the other half FMRP+) still suffer from the caveat that network effects cannot be ruled out (Bland et al., 2021).

In this study, we circumvented this problem by a virus-based strategy to induce *Fmr1* KO only in a very small subset of cortical PyrNs. Thus, the perturbation to the activity pattern in the neuronal network is negligible. Furthermore, as each PyrN receives thousands of inputs (Iascone et al., 2020), the vast majority of them are from neurons that express FMRP normally. We observed that in adolescent CKO$^{neo\ inj}$ mice, FMRP-null neurons exhibited the same spine dynamics as in *Fmr1* global KO mice, indicating that FMRP regulates spine dynamics cell-autonomously at this developmental stage. This result is consistent with a recent electrophysiological study (Zhang et al., 2021) showing that

10.3389/fnsyn.2023.1135479

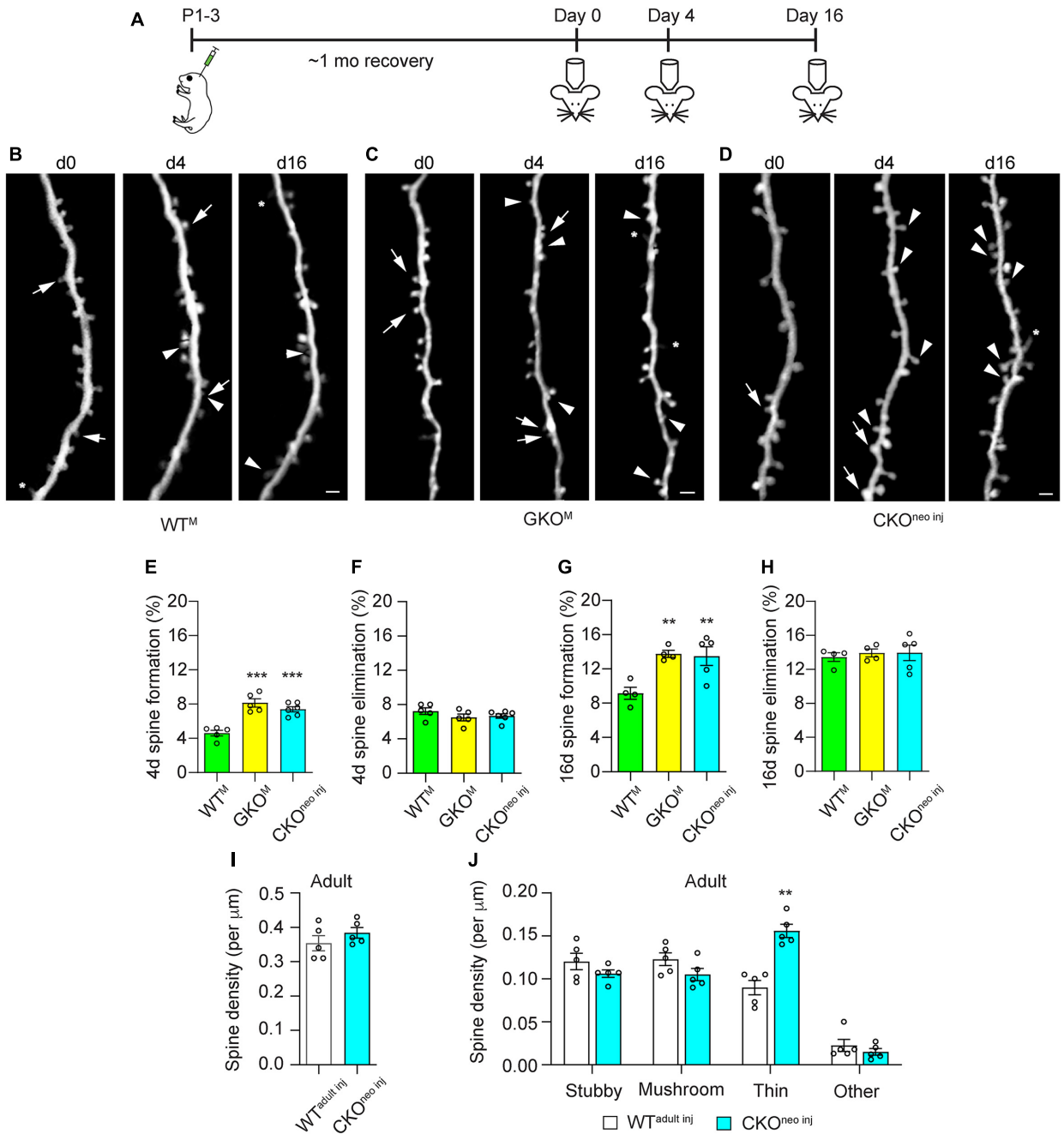

FIGURE 4

Cell-autonomous *Fmr1* knockout (KO) in adolescence selectively affects spine formation but not elimination. **(A)** Timeline of virus injection and *in vivo* two-photon imaging. **(B–D)** Examples of spine formation and elimination in adolescent WT^{M} **(B)**, global knockout (GKO^{M}) **(C)**, and conditional knockout ($CKO^{neo\ inj}$) **(D)** mice. Arrows: eliminated spines; arrowheads: formed spines; asterisks: filopodia. Scale bar = 2 µm. **(E,F)** Spine formation **(E)** and elimination **(F)** rates over 4 days in WT^{M}, GKO^{M}, and $CKO^{neo\ inj}$ mice. n = 5 mice for WT^{M} and GKO^{M}, and six mice for $CKO^{neo\ inj}$. **(G,H)** Spine formation **(G)** and elimination **(H)** rates over 16 days in WT^{M}, GKO^{M}, and $CKO^{neo\ inj}$ mice. n = 5 mice per group. **(I)** Total spine density in $WT^{adult\ inj}$ and $CKO^{neo\ inj}$ mice at adulthood. n = 5 mice per group. **(J)** Density of different types of spines in $WT^{adult\ inj}$ and $CKO^{neo\ inj}$ mice at adulthood. n = 5 mice per group. $^{**}p < 0.01$, $^{***}p < 0.001$.

virus-based cell-autonomous deletion of FMRP from L2/3 or L5 neurons weakens callosal excitatory synapses. It is also consistent with the earlier study (Pfeiffer and Huber, 2007) showing that acute, postsynaptic expression of FMRP in *Fmr1* KO neurons *in vitro* reduces their synapse number. This suggests that in *Fmr1* global KO mice, which more realistically reflect the condition in FXS patients, the lack of FMRP in the neurons to which the spines belong is the determining factor of the pathology in spine density and dynamics. Interestingly, although neurons with neonatal FMRP deletion exhibit abnormally high density of thin spines when the animal reaches adulthood, the total spine density remains at the WT level. In contrast, the elevated

density of thin spines on neurons in adult GKO mice increases total spine density as well. This intriguing phenomenon calls for further investigations into the contribution of the neuronal network and other extrinsic factors. It is worth noting that the regulation of spine dynamics by FMRP does not imply that the effect is mediated completely intracellularly. It has been reported that genetic deletion of matrix metalloproteinase-9 (MMP-9), an FMRP target enzyme involved in the degradation of the extracellular matrix, can rescue spine morphological and behavioral deficits in *Fmr1* global KO mice (Sidhu et al., 2014). Another work shows that injecting an MMP-9 inhibitor likewise rescues the baseline spine dynamics in such animals (Nagaoka et al., 2016).

Most *in vivo* imaging studies of spine dynamics in FXS focus on the apical dendrites of L5 PyrNs, leveraging the sparse but very bright neuronal labeling conveniently offered by the *Thy1*-YFP-H or *Thy1*-GFP-M line (Pan et al., 2010; Padmashri et al., 2013; Nagaoka et al., 2016; Hodges et al., 2017). However, there is evidence that FMRP regulates spine morphology differentially in different compartments of the dendritic arbor. For example, a histological study (Bland et al., 2021) shows that *Fmr1* KO or inactivation affects the density of spines on basal dendrites of L5 PyrNs minimally. It will be interesting to examine whether the dynamics of such spines are altered by the loss of FMRP; such experiments have become possible with recent advances in imaging techniques such as three-photon microscopy and adaptive optics (Rodriguez and Ji, 2018; Sinefeld et al., 2022).

The regulatory role of postsynaptic FMRP may also be input-specific. A recent immunofluorescent array tomography study of cortical tissues from adult *Fmr1* global KO mice (Simhal et al., 2019) revealed an increase of small synapses that expressed vesicular glutamate transporter 1 (VGluT1+) in L4 and a decrease of large VGluT1+ synapses in L1 and L4; moreover, VGluT2+ synapse density consistently decreased in L1 and L2/3. As VGluT1+ and VGluT2+ excitatory synapses are generally considered to be corticocortical and thalamocortical, respectively, this work suggests an input-specific defect associated with *Fmr1* KO. More interestingly, it was recently found (Zhang et al., 2021) that, while barrel cortex L2/3 neurons with cell-autonomous *Fmr1* KO had weaker long-range callosal synaptic connections, their excitatory postsynaptic currents (EPSCs) evoked by local inputs (L4 of home or adjacent barrels, L5A or L2/3 neurons) were unaffected. Similarly, L5 PyrNs with postsynaptic *Fmr1* KO had weakened callosal inputs around their somata and apical dendrites. These findings are intriguing, as only a very small percentage of the neurons were FMRP-null, and hence their presynaptic partners should be predominantly normal no matter where they resided. The mechanisms through which postsynaptic FMRP differentially regulate the maturation and strength of synapses from different input sources remain to be elucidated.

Data availability statement

The raw data supporting the conclusions of this article will be made available by the authors, without undue reservation.

Ethics statement

This animal study was reviewed and approved by Institutional Animal Care and Use Committee (IACUC), University of California, Santa Cruz.

Author contributions

YZ, JL, and MG designed the study and wrote the manuscript. MG and JL performed the experiments and analyzed the data. All authors approved the submitted version of the manuscript.

Funding

This work was supported by grants from the Eunice Kennedy Shriver National Institute of Child Health and Human Development (R21HD101266), National Institute of Mental Health (R01MH109475 and R01MH127737), National Institute on Aging (R01AG071787), and a Max Planck Fellowship from Max Planck Florida Institute for Neuroscience to YZ. The Zeiss 880 confocal microscope used in this study was funded by an NIH S10 Grant (1S10OD23528).

Acknowledgments

We thank Stephen T. Warren and David L. Nelson for sharing the transgenic mouse lines, Dan Turner-Evans for help with two-photon imaging, Chia-Chien Eric Chen for advice on neonatal viral injection, and Benjamin Abrams (UCSC Life Sciences Microscopy Center) for technical support.

Conflict of interest

The authors declare that the research was conducted in the absence of any commercial or financial relationships that could be construed as a potential conflict of interest.

Publisher's note

Supplementary material

The Supplementary Material for this article can be found online at: https://www.frontiersin.org/articles/10.3389/fnsyn.2023.1135479/full#supplementary-material

References

Antar, L. N., Afroz, R., Dictenberg, J. B., Carroll, R. C., and Bassell, G. J. (2004). Metabotropic glutamate receptor activation regulates fragile X mental retardation protein and FMR1 mRNA localization differentially in dendrites and at synapses. *J. Neurosci.* 24, 2648–2655. doi: 10.1523/JNEUROSCI.0099-04.2004

Arbab, T., Battaglia, F. P., Pennartz, C. M. A., and Bosman, C. A. (2018). Abnormal hippocampal theta and gamma hypersynchrony produces network and spike timing disturbances in the Fmr1-KO mouse model of fragile X syndrome. *Neurobiol. Dis.* 114, 65–73. doi: 10.1016/j.nbd.2018.02.011

Bagni, C., and Greenough, W. T. (2005). From mRNP trafficking to spine dysmorphogenesis: The roots of fragile X syndrome. *Nat. Rev. Neurosci.* 6, 376–387. doi: 10.1038/nrn1667

Bardoni, B., Davidovic, L., Bensaid, M., and Khandjian, E. W. (2006). The fragile X syndrome: Exploring its molecular basis and seeking a treatment. *Expert Rev. Mol. Med.* 8, 1–16. doi: 10.1017/S1462399406010751

Bassell, G. J., and Warren, S. T. (2008). Fragile X syndrome: Loss of local mRNA regulation alters synaptic development and function. *Neuron* 60, 201–214.

Beckel-Mitchener, A., and Greenough, W. T. (2004). Correlates across the structural, functional, and molecular phenotypes of fragile X syndrome. *Ment. Retard. Dev. Disabil. Res. Rev.* 10, 53–59.

Berry-Kravis, E. (2002). Epilepsy in fragile X syndrome. *Dev. Med. Child Neurol.* 44, 724–728.

Bland, K. M., Aharon, A., Widener, E. L., Song, M. I., Casey, Z. O., Zuo, Y., et al. (2021). FMRP regulates the subcellular distribution of cortical dendritic spine density in a non-cell-autonomous manner. *Neurobiol. Dis.* 150:105253. doi: 10.1016/j.nbd.2021.105253

Chen, C. C., Lu, J., Yang, R., Ding, J. B., and Zuo, Y. (2018). Selective activation of parvalbumin interneurons prevents stress-induced synapse loss and perceptual defects. *Mol. Psychiatry* 23, 1614–1625. doi: 10.1038/mp.2017.159

Cheyne, J. E., Zabouri, N., Baddeley, D., and Lohmann, C. (2019). Spontaneous activity patterns are altered in the developing visual cortex of the Fmr1 knockout mouse. *Front. Neural Circuits* 13:57. doi: 10.3389/fncir.2019.00057

Churchill, J. D., Grossman, A. W., Irwin, S. A., Galvez, R., Klintsova, A. Y., Weiler, I. J., et al. (2002). A converging-methods approach to fragile X syndrome. *Dev. Psychobiol.* 40, 323–338. doi: 10.1002/dev.10036

Comery, T. A., Harris, J. B., Willems, P. J., Oostra, B. A., Irwin, S. A., Weiler, I. J., et al. (1997). Abnormal dendritic spines in fragile X knockout mice: Maturation and pruning deficits. *Proc. Natl. Acad. Sci. U.S.A.* 94, 5401–5404.

Cruz-Martín, A., Crespo, M., and Portera-Cailliau, C. (2010). Delayed stabilization of dendritic spines in fragile X mice. *J. Neurosci.* 30, 7793–7803. doi: 10.1523/JNEUROSCI.0577-10.2010

Ferrari, F., Mercaldo, V., Piccoli, G., Sala, C., Cannata, S., Achsel, T., et al. (2007). The fragile X mental retardation protein-RNP granules show an mGluR-dependent localization in the post-synaptic spines. *Mol. Cell Neurosci.* 34, 343–354. doi: 10.1016/j.mcn.2006.11.015

Galvez, R., and Greenough, W. T. (2005). Sequence of abnormal dendritic spine development in primary somatosensory cortex of a mouse model of the fragile X mental retardation syndrome. *Am. J. Med. Genet. A* 135, 155–160. doi: 10.1002/ajmg.a.30709

Gibson, J. R., Bartley, A. F., Hays, S. A., and Huber, K. M. (2008). Imbalance of neocortical excitation and inhibition and altered UP states reflect network hyperexcitability in the mouse model of fragile X syndrome. *J. Neurophysiol.* 100, 2615–2626. doi: 10.1152/jn.90752.2008

Goel, A., Cantu, D. A., Guilfoyle, J., Chaudhari, G. R., Newadkar, A., Todisco, B., et al. (2018). Impaired perceptual learning in a mouse model of fragile X syndrome is mediated by parvalbumin neuron dysfunction and is reversible. *Nat. Neurosci.* 21, 1404–1411.

Greenough, W. T., Klintsova, A. Y., Irwin, S. A., Galvez, R., Bates, K. E., and Weiler, I. J. (2001). Synaptic regulation of protein synthesis and the fragile X protein. *Proc. Natl. Acad. Sci. U.S.A.* 98, 7101–7106.

Grossman, A. W., Elisseou, N. M., Mckinney, B. C., and Greenough, W. T. (2006). Hippocampal pyramidal cells in adult Fmr1 knockout mice exhibit an immature-appearing profile of dendritic spines. *Brain Res.* 1084, 158–164. doi: 10.1016/j.brainres.2006.02.044

Hays, S. A., Huber, K. M., and Gibson, J. R. (2011). Altered neocortical rhythmic activity states in Fmr1 KO mice are due to enhanced mGluR5 signaling and involve changes in excitatory circuitry. *J. Neurosci.* 31, 14223–14234. doi: 10.1523/JNEUROSCI.3157-11.2011

He, C. X., Cantu, D. A., Mantri, S. S., Zeiger, W. A., Goel, A., and Portera-Cailliau, C. (2017). Tactile defensiveness and impaired adaptation of neuronal activity in the Fmr1 knock-out mouse model of autism. *J. Neurosci.* 37, 6475–6487. doi: 10.1523/JNEUROSCI.0651-17.2017

Hinton, V. J., Brown, W. T., Wisniewski, K., and Rudelli, R. D. (1991). Analysis of neocortex in three males with the fragile X syndrome. *Am. J. Med. Genet.* 41, 289–294.

Hodges, J. L., Yu, X., Gilmore, A., Bennett, H., Tjia, M., Perna, J. F., et al. (2017). Astrocytic contributions to synaptic and learning abnormalities in a mouse model of fragile X syndrome. *Biol. Psychiatry* 82, 139–149. doi: 10.1016/j.biopsych.2016.08.036

Holtmaat, A., Bonhoeffer, T., Chow, D. K., Chuckowree, J., De Paola, V., Hofer, S. B., et al. (2009). Long-term, high-resolution imaging in the mouse neocortex through a chronic cranial window. *Nat. Protoc.* 4, 1128–1144.

Iascone, D. M., Li, Y., Sumbul, U., Doron, M., Chen, H., Andreu, V., et al. (2020). Whole-neuron synaptic mapping reveals spatially precise excitatory/inhibitory balance limiting dendritic and somatic spiking. *Neuron* 106, 566–578.e8. doi: 10.1016/j.neuron.2020.02.015

Irwin, S. A., Idupulapati, M., Gilbert, M. E., Harris, J. B., Chakravarti, A. B., Rogers, E. J., et al. (2002). Dendritic spine and dendritic field characteristics of layer V pyramidal neurons in the visual cortex of fragile-X knockout mice. *Am. J. Med. Genet.* 111, 140–146. doi: 10.1002/ajmg.10500

Irwin, S. A., Patel, B., Idupulapati, M., Harris, J. B., Crisostomo, R. A., Larsen, B. P., et al. (2001). Abnormal dendritic spine characteristics in the temporal and visual cortices of patients with fragile-X syndrome: A quantitative examination. *Am. J. Med. Genet.* 98, 161–167. doi: 10.1002/1096-8628(20010115)98:2<161::aid-ajmg1025>3.0.co;2-b

Jawaid, S., Kidd, G. J., Wang, J., Swetlik, C., Dutta, R., and Trapp, B. D. (2018). Alterations in CA1 hippocampal synapses in a mouse model of fragile X syndrome. *Glia* 66, 789–800. doi: 10.1002/glia.23284

Juczewski, K., Von Richthofen, H., Bagni, C., Celikel, T., Fisone, G., and Krieger, P. (2016). Somatosensory map expansion and altered processing of tactile inputs in a mouse model of fragile X syndrome. *Neurobiol. Dis.* 96, 201–215. doi: 10.1016/j.nbd.2016.09.007

Kramvis, I., Mansvelder, H. D., Loos, M., and Meredith, R. (2013). Hyperactivity, perseveration and increased responding during attentional rule acquisition in the fragile X mouse model. *Front. Behav. Neurosci.* 7:172. doi: 10.3389/fnbeh.2013.00172

Li, J., Jiang, R. Y., Arendt, K. L., Hsu, Y. T., Zhai, S. R., and Chen, L. (2020). Defective memory engram reactivation underlies impaired fear memory recall in fragile X syndrome. *Elife* 9:e61882. doi: 10.7554/eLife.61882

Liu, X., Kumar, V., Tsai, N. P., and Auerbach, B. D. (2021). Hyperexcitability and homeostasis in fragile X syndrome. *Front. Mol. Neurosci.* 14:805929. doi: 10.3389/fnmol.2021.805929

Lu, J., Tjia, M., Mullen, B., Cao, B., Lukasiewicz, K., Shah-Morales, S., et al. (2021). An analog of psychedelics restores functional neural circuits disrupted by unpredictable stress. *Mol. Psychiatry* 26, 6237–6252. doi: 10.1038/s41380-021-01159-1

McKinney, B. C., Grossman, A. W., Elisseou, N. M., and Greenough, W. T. (2005). Dendritic spine abnormalities in the occipital cortex of C57BL/6 Fmr1 knockout mice. *Am. J. Med. Genet. B Neuropsychiatr. Genet.* 136B, 98–102. doi: 10.1002/ajmg.b.30183

Mientjes, E. J., Nieuwenhuizen, I., Kirkpatrick, L., Zu, T., Hoogeveen-Westerveld, M., Severijnen, L., et al. (2006). The generation of a conditional Fmr1 knock out mouse model to study Fmrp function in vivo. *Neurobiol. Dis.* 21, 549–555.

Musumeci, S. A., Hagerman, R. J., Ferri, R., Bosco, P., Dalla Bernardina, B., Tassinari, C. A., et al. (1999). Epilepsy and EEG findings in males with fragile X syndrome. *Epilepsia* 40, 1092–1099.

Nagaoka, A., Takehara, H., Hayashi-Takagi, A., Noguchi, J., Ishii, K., Shirai, F., et al. (2016). Abnormal intrinsic dynamics of dendritic spines in a fragile X syndrome mouse model in vivo. *Sci. Rep.* 6:26651. doi: 10.1038/srep26651

Nimchinsky, E. A., Oberlander, A. M., and Svoboda, K. (2001). Abnormal development of dendritic spines in FMR1 knock-out mice. *J. Neurosci.* 21, 5139–5146.

Padmashri, R., Reiner, B. C., Suresh, A., Spartz, E., and Dunaevsky, A. (2013). Altered structural and functional synaptic plasticity with motor skill learning in a mouse model of fragile X syndrome. *J. Neurosci.* 33, 19715–19723. doi: 10.1523/JNEUROSCI.2514-13.2013

Paluszkiewicz, S. M., Olmos-Serrano, J. L., Corbin, J. G., and Huntsman, M. M. (2011). Impaired inhibitory control of cortical synchronization in fragile X syndrome. *J. Neurophysiol.* 106, 2264–2272. doi: 10.1152/jn.00421.2011

Pan, F., Aldridge, G. M., Greenough, W. T., and Gan, W. B. (2010). Dendritic spine instability and insensitivity to modulation by sensory experience in a mouse model of fragile X syndrome. *Proc. Natl. Acad. Sci. U.S.A.* 107, 17768–17773. doi: 10.1073/pnas.1012496107

Parrott, J. M., Oster, T., and Lee, H. Y. (2021). Altered inflammatory response in FMRP-deficient microglia. *iScience* 24:103293. doi: 10.1016/j.isci.2021.103293

Pfeiffer, B. E., and Huber, K. M. (2007). Fragile X mental retardation protein induces synapse loss through acute postsynaptic translational regulation. *J. Neurosci.* 27, 3120–3130.

Pieretti, M., Zhang, F. P., Fu, Y. H., Warren, S. T., Oostra, B. A., Caskey, C. T., et al. (1991). Absence of expression of the FMR-1 gene in fragile X syndrome. *Cell* 66, 817–822.

Pietropaolo, S., Guilleminot, A., Martin, B., D'amato, F. R., and Crusio, W. E. (2011). Genetic-background modulation of core and variable autistic-like symptoms in Fmr1 knock-out mice. *PLoS One* 6:e17073. doi: 10.1371/journal.pone.0017073

Rais, M., Binder, D. K., Razak, K. A., and Ethell, I. M. (2018). Sensory Processing Phenotypes in Fragile X Syndrome. *ASN Neuro* 10:1759091418801092.

Richter, J. D., and Zhao, X. (2021). The molecular biology of FMRP: New insights into fragile X syndrome. *Nat. Rev. Neurosci.* 22, 209–222.

Rodriguez, C., and Ji, N. (2018). Adaptive optical microscopy for neurobiology. *Curr. Opin. Neurobiol.* 50, 83–91.

Rudelli, R. D., Brown, W. T., Wisniewski, K., Jenkins, E. C., Laure-Kamionowska, M., Connell, F., et al. (1985). Adult fragile X syndrome. Clinico-neuropathologic findings. *Acta Neuropathol.* 67, 289–295. doi: 10.1007/BF00687814

Saneyoshi, T., Fortin, D. A., and Soderling, T. R. (2010). Regulation of spine and synapse formation by activity-dependent intracellular signaling pathways. *Curr. Opin. Neurobiol.* 20, 108–115.

Scharkowski, F., Frotscher, M., Lutz, D., Korte, M., and Michaelsen-Preusse, K. (2018). Altered connectivity and synapse maturation of the hippocampal mossy fiber pathway in a mouse model of the fragile X syndrome. *Cereb. Cortex* 28, 852–867. doi: 10.1093/cercor/bhw408

Sidhu, H., Dansie, L. E., Hickmott, P. W., Ethell, D. W., and Ethell, I. M. (2014). Genetic removal of matrix metalloproteinase 9 rescues the symptoms of fragile X syndrome in a mouse model. *J. Neurosci.* 34, 9867–9879. doi: 10.1523/JNEUROSCI.1162-14.2014

Simhal, A. K., Zuo, Y., Perez, M. M., Madison, D. V., Sapiro, G., and Micheva, K. D. (2019). Multifaceted changes in synaptic composition and astrocytic involvement in a mouse model of fragile X syndrome. *Sci. Rep.* 9:13855. doi: 10.1038/s41598-019-50240-x

Sinefeld, D., Xia, F., Wang, M., Wang, T., Wu, C., Yang, X., et al. (2022). Three-photon adaptive optics for mouse brain imaging. *Front. Neurosci.* 16:880859. doi: 10.3389/fnins.2022.880859

Soden, M. E., and Chen, L. (2010). Fragile X protein FMRP is required for homeostatic plasticity and regulation of synaptic strength by retinoic acid. *J. Neurosci.* 30, 16910–16921. doi: 10.1523/JNEUROSCI.3660-10.2010

Stein, I. S., and Zito, K. (2019). Dendritic spine elimination: Molecular mechanisms and implications. *Neuroscientist* 25, 27–47.

The Dutch-Belgian Fragile X Consortium (1994). Fmr1 knockout mice: A model to study fragile X mental retardation. *Cell* 78, 23–33.

Till, S. M., Wijetunge, L. S., Seidel, V. G., Harlow, E., Wright, A. K., Bagni, C., et al. (2012). Altered maturation of the primary somatosensory cortex in a mouse model of fragile X syndrome. *Hum. Mol. Genet.* 21, 2143–2156. doi: 10.1093/hmg/dds030

Turk, J. (2011). Fragile X syndrome: Lifespan developmental implications for those without as well as with intellectual disability. *Curr. Opin. Psychiatry* 24, 387–397. doi: 10.1097/YCO.0b013e328349bb77

Verkerk, A. J., Pieretti, M., Sutcliffe, J. S., Fu, Y. H., Kuhl, D. P., Pizzuti, A., et al. (1991). Identification of a gene (FMR-1) containing a CGG repeat coincident with a breakpoint cluster region exhibiting length variation in fragile X syndrome. *Cell* 65, 905–914. doi: 10.1016/0092-8674(91)90397-h

Warren, S. T., and Nelson, D. L. (1994). Advances in molecular analysis of fragile X syndrome. *JAMA* 271, 536–542.

Weiler, I. J., Irwin, S. A., Klintsova, A. Y., Spencer, C. M., Brazelton, A. D., Miyashiro, K., et al. (1997). Fragile X mental retardation protein is translated near synapses in response to neurotransmitter activation. *Proc. Natl. Acad. Sci. U.S.A.* 94, 5395–5400.

Wisniewski, K. E., Segan, S. M., Miezejeski, C. M., Sersen, E. A., and Rudelli, R. D. (1991). The Fra(X) syndrome: Neurological, electrophysiological, and neuropathological abnormalities. *Am. J. Med. Genet.* 38, 476–480. doi: 10.1002/ajmg.1320380267

Xu, T., Yu, X., Perlik, A. J., Tobin, W. F., Zweig, J. A., Tennant, K., et al. (2009). Rapid formation and selective stabilization of synapses for enduring motor memories. *Nature* 462, 915–919. doi: 10.1038/nature08389

Zhang, Z., Gibson, J. R., and Huber, K. M. (2021). Experience-dependent weakening of callosal synaptic connections in the absence of postsynaptic FMRP. *Elife* 10:e71555. doi: 10.7554/eLife.71555

frontiers | Frontiers in Synaptic Neuroscience

TYPE Original Research
PUBLISHED 05 April 2023
DOI 10.3389/fnsyn.2023.1128640

OPEN ACCESS

EDITED BY
Fereshteh S. Nugent,
Uniformed Services University, United States

REVIEWED BY
Jason Aoto,
University of Colorado Denver, United States
Ryan David Shepard,
ICF, United States

*CORRESPONDENCE
Lulu Y. Chen
✉ chenly@uci.edu

†These authors have contributed equally to this work and share first authorship

RECEIVED 21 December 2022
ACCEPTED 10 February 2023
PUBLISHED 05 April 2023

CITATION
de Carvalho G, Khoja S, Haile MT and Chen LY (2023) Early life adversity impaired dorsal striatal synaptic transmission and behavioral adaptability to appropriate action selection in a sex-dependent manner.
Front. Synaptic Neurosci. 15:1128640.
doi: 10.3389/fnsyn.2023.1128640

Early life adversity impaired dorsal striatal synaptic transmission and behavioral adaptability to appropriate action selection in a sex-dependent manner

Gregory de Carvalho[1†], Sheraz Khoja[1†], Mulatwa T. Haile[1] and Lulu Y. Chen[1,2*]

[1]Department of Anatomy & Neurobiology, School of Medicine, University of California, Irvine, Irvine, CA, United States, [2]UCI-Conte Center, UCI-NIMH, University of California, Irvine, Irvine, CA, United States

Early life adversity (ELA) is a major health burden in the United States, with 62% of adults reporting at least one adverse childhood experience. These experiences during critical stages of brain development can perturb the development of neural circuits that mediate sensory cue processing and behavioral regulation. Recent studies have reported that ELA impaired the maturation of dendritic spines on neurons in the dorsolateral striatum (DLS) but not in the dorsomedial striatum (DMS). The DMS and DLS are part of two distinct corticostriatal circuits that have been extensively implicated in behavioral flexibility by regulating and integrating action selection with the reward value of those actions. To date, no studies have investigated the multifaceted effects of ELA on aspects of behavioral flexibility that require alternating between different action selection strategies or higher-order cognitive processes, and the underlying synaptic transmission in corticostriatal circuitries. To address this, we employed whole-cell patch-clamp electrophysiology to assess the effects of ELA on synaptic transmission in the DMS and DLS. We also investigated the effects of ELA on the ability to update action control in response to outcome devaluation in an instrumental learning paradigm and reversal of action-outcome contingency in a water T-maze paradigm. At the circuit level, ELA decreased corticostriatal glutamate transmission in male but not in female mice. Interestingly, in DMS, glutamate transmission is decreased in male ELA mice, but increased in female ELA mice. ELA impaired the ability to update action control in response to reward devaluation in a context that promotes goal-directedness in male mice and induced deficits in reversal learning. Overall, our findings demonstrate the sex- and region-dependent effects of ELA on behavioral flexibility and underlying corticostriatal glutamate transmission. By establishing a link between ELA and circuit mechanisms underlying behavioral flexibility, our findings will begin to identify novel molecular mechanisms that can represent strategies for treating behavioral inflexibility in individuals who experienced early life traumatic incidents.

KEYWORDS

early life adversity, corticostriatal circuits, synaptic transmission, action-outcome contingency, outcome devaluation, reversal learning, behavioral flexibility

1. Introduction

Early life adversity (ELA) is commonly reported in the United States, with 62% of adults reporting at least one adverse childhood experience (Merrick et al., 2019). Adversity during a critical developmental period can negatively impact neural circuits and has long been associated with neuropsychiatric disorders later in life, with many studies reporting behavioral, cognitive, and emotional impairments (Kessler et al., 1994; Dias-Ferreira et al., 2009; Wang et al., 2011; Baram et al., 2012; Gershon et al., 2013; Molet et al., 2016; Davis et al., 2017; Bolton et al., 2018a; Glynn and Baram, 2019; Gasser et al., 2020; He et al., 2021; Levis et al., 2022; Xu et al., 2022). Investigating the molecular mechanisms underlying ELA-induced cognitive and emotional deficits is critical to laying the foundation for novel strategies in therapeutic intervention.

ELA-induced neurodevelopmental and behavioral deficits were initially documented by using the maternal separation (MS) model in rodents, in which the mother was separated from her pups intermittently over a specific period of time (Russell, 1973; Hall, 1998; Ladd et al., 2000). However, these models lacked translational validity since mothers who are diagnosed with psychiatric disorders (depression, schizophrenia, or drug addiction) can be negligent in their children's care or abusive towards them, even though they are still present in the household.

The limited bedding and nesting (LBN) paradigm induces an impoverished environment that negatively impacts the quality of maternal care, leading to fragmented and unpredictable nurturing behaviors (Gilles et al., 1996; Brunson et al., 2005; Ivy et al., 2008). Multiple investigations have reported the effects of ELA on cognitive (spatial, working, and contextual memory) and emotional behaviors using the LBN paradigm (Ivy et al., 2008, 2010; Naninck et al., 2015; Arp et al., 2016; Bath et al., 2017; Davis et al., 2017; Xu et al., 2022). These behavioral deficits were linked to alterations in developmental neurogenesis and structural abnormalities, especially in the hippocampus, hypothalamus, and paraventricular nucleus (Ivy et al., 2010; Korosi et al., 2010; Naninck et al., 2015; Lapp et al., 2020; Levis et al., 2022).

While novel and exciting insights have been achieved in determining the effects of ELA in the hippocampus, very little attention has been given to other anatomically and functionally interacting brain regions such as the dorsal striatum. The dorsal striatum is densely innervated by cortical regions such as the sensorimotor, motor, and cingulate cortex (Hunnicutt et al., 2016; Hadjas et al., 2020) and regulates the balance between goal-directed and habitual actions (Yin and Knowlton, 2004; Yin et al., 2004, 2005a,b, 2006; Gremel and Costa, 2013; Gremel et al., 2016). To date, only two studies using the LBN paradigm have reported neurodevelopmental deficits in the dorsal striatum and perturbations in associated behavioral functions, including decision-making (He et al., 2021; Xu et al., 2022). ELA delayed dendritic differentiation in the dorsolateral (DLS), but not in the dorsomedial (DMS) striatum, in mice at P16 (He et al., 2021); which was later accompanied by a significant increase in thin and mushroom-type spines in DLS at P120 (Xu et al., 2022). At the behavioral level, ELA-induced mice shifted from goal-directed to habitual control upon extensive instrumental training in a context that promotes goal-directedness (Xu et al., 2022). However, this study did not address the adaptability of ELA-induced mice to alternate between goal-directed and habitual actions under differing contingencies of reward delivery that can bias differential action control. Additionally, previous studies have not investigated the ability of ELA mice to disengage from preferred behavioral patterns and learn new ones in behavioral paradigms that assess intradimensional shifts in behavior, such as reversal learning tasks. Moreover, the functional impact of ELA on synaptic activity in brain regions linked to the balance between goal-directed and habitual actions, such as the dorsal striatum, has not been thoroughly investigated.

To this end, our study begins to explore three questions that remain unanswered: (i) whether ELA impacts corticostriatal glutamate transmission in a manner that explains behavioral impairments; (ii) whether ELA affects the flexibility of mice to adopt different action selection strategies; and (iii) whether ELA impairs reversal learning. We also aim to address these questions in a sex-dependent manner on the basis of a plethora of studies showing differences in cognitive and emotional behaviors between male and female mice subjected to ELA (Colich et al., 2017; Ellis and Honeycutt, 2021; Bondar et al., 2018; Ruigrok et al., 2021a,b). The sex-dependent differences in behaviors can be attributed to discrepancies in maternal care, where male mice receive more care than their female siblings (Oomen et al., 2009; van Hasselt et al., 2012). Additionally, ELA has also been reported to induce behavioral and structural brain abnormalities in a sex-dependent manner in the clinical population (Frodl et al., 2010; Alastalo et al., 2013; Zoladz et al., 2022).

We performed whole-cell patch-clamp recordings in medium spiny neurons (MSNs) of DLS and DMS. We assessed the ability of LBN mice to alternate between different action-selection strategies under different contingencies of reinforcement delivery, in a context-dependent operant conditioning paradigm. Finally, we employed a water T-maze paradigm to test the impact of ELA on reversal learning capacity. Electrophysiology recordings revealed that ELA broadly decreased excitatory transmission of cortical inputs to the dorsal striatum of males, whereas only the DMS in females was affected. Failed execution of goal-directed action strategies was observed in male LBN mice, without any impairments in action selection strategies in female LBN mice. LBN mice exhibited reversal learning deficits. Together, our results suggest that LBN can disrupt the ability to integrate the value of rewards with action-selection strategies in a sex-dependent manner and to learn new actions upon contingency reversal in a sex-independent manner. Region-specific and sex-dependent impairments observed in excitatory synaptic transmission constitute a plausible synaptic mechanism underlying behavioral inflexibility in LBN mice. These findings can lay the groundwork for therapeutic strategies for behavioral inflexibility in individuals who experienced adverse childhood experiences.

2. Methods

2.1. Animals

Male and female C57BL/6J mice for breeding and generation of litters for control (CTL) and LBN group were purchased

from Jackson laboratories (Bar Harbor, ME). Breeding pairs were maintained on a 12/12 h light/dark cycle with *ad libitum* access to water and a high-fat chow. All procedures were conducted in accordance with the National Institute of Health Guide for the Care and Use of Laboratory Animals and protocols approved by the Institutional Animal Care and Use Committee of the University of California Irvine, including efforts to minimize suffering and the number of animals used.

2.2. LBN paradigm

LBN was carried out as previously described (Rice et al., 2008). On postnatal day 2 (P2), the dams and pups were transferred to cages fitted with an iron mesh (in cm: 15.24 wide × 33.02 long, 2.54 tall) which was placed at approximately 2.5 cm above the cage floor to allow for the collection of droppings. The cage floor was sparsely covered with bedding materials and half of a nestlet was provided. For the CTL group, the dams and pups were transferred to cages with a normal amount of bedding material and one full nestlet. The cages were left undisturbed from P2 till P9. At P10, the pups and the dams from CTL and LBN group were transferred to cages with a normal amount of bedding material and one nestlet. Mice were weaned at P21 and were used for behavioral tests at 2–4 months of age and electrophysiology experiments at 2–5 months of age. Separate cohorts of mice were used for electrophysiological and behavioral experiments. For the behavioral experiments, separate cohorts of mice were used for instrumental learning paradigm and water T-maze.

2.3. Instrumental learning paradigm

2.3.1. Behavioral apparatus

The balance between goal-directed and habitual behaviors was investigated by using two identical operant chambers (Med-Associates, St. Albans, VT), enclosed in sound attenuating boxes that were differentiated by contextual cues (15 mm wide multi-colored washi tape that was vertically and horizontally aligned on chamber walls to give a checkerboard-like pattern or clear plexiglass chamber walls). Each chamber was equipped with a pellet dispenser that delivered 20 mg food pellets (Bio-Serv, Flemington, NJ) into a recessed food magazine, two retractable levers on either side of the food magazine, a house light, a stainless-steel grid floor and an 8 input/16 output connection panel that serves as an interface between the chambers, and a computer that runs the MED-PC V software (Med-Associates, St. Albans, VT) to operate the experimental paradigms and record lever pressing behavior. Prior to training, mice were handled, and food restricted to 85%–90% of their baseline body weight. Their body weights were maintained within this range during the entirety of the instrumental learning paradigm.

2.3.2. Context-dependent training paradigm

Behavioral training and testing were conducted as previously described (Gremel et al., 2016). Briefly, following 3 days of handling and food restriction, mice underwent a training session on days 4–11. Each training session commenced with switching on of the house light and extension of a single lever and ended following completion of the instrumental learning task or after 60 min with the lever withdrawn and switching off of the house light. The lever position, order of context exposure, and schedule order were constant for each mouse throughout the entire training period and outcome devaluation test and counterbalanced between mice. On the first day, mice were trained to associate the food magazine with reinforcement presentation in two separate contexts, using a random time (RT) schedule in which a food pellet was delivered on an average of 60 s in the absence of levers. This session would continue for a total period of 15 min or when 15 reinforcers had been delivered. Following the RT schedule, on the same day, mice were trained to press a single lever under a continuous ratio of reinforcement (CRF1) in each context, wherein every lever press was reinforced with one pellet. Mice underwent CRF1 on days 4–5, with the number of earned reinforcers increasing on each day (i.e., 5 reinforcers on day 4, 15 and then 30 reinforcers on day 5). All the CRF sessions continued for a total period of 60 min or when the maximum number of earned reinforcers was dispensed. Following the acquisition of lever pressing behavior, mice underwent random interval (RI) and random ratio (RR) schedules of reinforcement that were differentiated by contexts from days 6–11. On days 6 and 7, mice were trained to press the lever under RI30, wherein the passing of an interval period of 30 s had a 15% probability of delivering a food pellet and RR10, in which every lever press had a 10% chance of delivering a food pellet. This was followed by RI60 and RR20 on days 8–11. All the RI and RR sessions ended once 60 min had elapsed or 15 reinforcers were dispensed. Following the RI and RR sessions, mice were provided with 1 h access to a 20% sucrose solution in their home cage as a satiety control for the outcome devaluation test.

2.3.3. Outcome devaluation test

This procedure was undertaken on days 12 and 13 of the post training phase. On the valued day, mice had 1 h *ad libitum* access to a 20% sucrose solution in their home cage, followed by brief, non-reinforced test sessions for 5 min in both RI and RR contexts. On the devalued day, mice had 1 h *ad libitum* access to 20 mg food pellets that they previously acquired by lever pressing, followed by brief, non-reinforced test sessions for 5 min in both the RI and RR contexts. The order of devaluation was counterbalanced between mice.

2.3.4. Water T-maze

Spatial learning and reversal learning was assessed by the water T-maze paradigm (Guariglia and Chadman, 2013). The T-maze was filled with 20°C (±1°C) water to a depth of 13 cm which is 1 cm above the surface of the platform. Water was made opaque by using non-fat dry milk. On the first day (pre-training phase), mice were allowed to swim freely in the T-maze without the platform for 60 s and the first arm that the mice entered was recorded. On all the training days, the platform was placed in the arm opposite to the one chosen during pre-training. The training session began 24 h after the pre-training phase in which the mice were given 10 trials per day with 7–10 min of rest in between each trial. Mice were placed in the start arm and given 60 s to find the platform. Once the

platform was found, the mice were forced to stay on the platform for 5 s. If they were not able to find the platform within 60 s, they were gently guided to the platform and forced to stay on it for 10 s. Mice were charged with errors if: (1) they left the start arm and entered the arm that does not contain the platform or (2) they entered the arm with the platform but left that arm without staying on the platform. A trial is considered successful when the mouse leaves the start arm and enters the arm with the platform and stays on it. The training session ended and the reversal learning phase began when the mice reached the criteria of eight successful trials or greater for two consecutive days. For the reversal learning phase, the platform was placed in the arm opposite to the one chosen during the training session, and the same procedure for charging errors and determining a successful trial was followed as described above. The number of incorrect arm entries and the success rate (percent of trials without an error) were calculated for the training and reversal learning phase.

2.4. Electrophysiology

2.4.1. Slice preparation

Mice were deeply anesthetized with isoflurane and quickly decapitated. Acute coronal slices (300 μm) were obtained using a vibratome (Leica V1200S) in an ice-cold N-Methyl D-Glucamine (NMDG) cutting solution containing (in mM): 110 NMDG, 20 HEPES, 25 glucose, 30 $NaHCO_3$, 1.2 NaH_2PO_4, 2.5 KCl, 5 Na-ascorbate, 3 Na- pyruvate, 2 Thiourea, 10 $MgSO_4$-7 H_2O, and 0.5 $CaCl_2$ (305–310 mOsm, pH 7.4). Slices equilibrated in a homemade chamber for 25–30 min (31°C) and an additional 45 min in room temperature aCSF containing (in mM): 119 NaCl, 26 $NaHCO_3$, 1 NaH_2PO_4, 2.5 KCl, 11 Glucose, 10 Sucrose, 1.3 $MgSO_4$-7 H_2O, and 2.5 $CaCl_2$ (290–300 mOsm, pH 7.4), before being transferred to a recording chamber. All solutions were continuously bubbled with 95% O_2/5%CO_2.

2.4.2. Whole-cell patch-clamp

Whole-cell patch-clamp recordings were obtained from MSNs in the DLS or DMS. Data were collected with a Multiclamp 700B, Digidata 1550B, and Clampex 11 (pClamp; Molecular Devices, San Jose, CA). All recordings were acquired in voltage clamp at 31°C and were low pass filtered at 2 kHz and digitized at 10 kHz. Membrane voltage was held at −70 mV for all measures unless otherwise specified. Recording pipette was filled with internal solution containing (in mM): 135 $CsMeSO_4$, 8 CsCl, 10 HEPES, 0.25 EGTA, 5 Phosphocreatine, 4 MgATP, 0.3 NaGTP, and 1 mg/ml NeuroBiotin (295–305 mOsm, pH 7.4 with CsOH). Picrotoxin (50 μM) was added to aCSF, and only excitatory postsynaptic currents (EPSCs) were recorded. All pipettes (3–4 MΩ) were pulled from borosilicate glass (Narishige PC-100). Access resistance (Ra) was monitored throughout the recording and cells that increased Ra by > 20% were discarded. Cells were visualized under infrared direct interference contrast (Olympus BX51WI; Olympus, Philadelphia). The current study did not distinguish between D1 and D2 MSNs. Recordings in either DMS (DMS-MSN) or DLS (DLS-MSN) were stimulated using a tungsten bipolar stereotrode (MicroProbes, Maryland), placed dorsal to the recorded cell and at the border of the corpus callosum and striatum. Distance of the stimulating electrode from the recorded cell did not exceed 200 μm and was no less than 150 μm. Electrical pulse durations were limited to a 50–100 μs range. For all recordings, electrical stimulation was delivered every 10 s (0.1 Hz). **Input/Output (I/O)** relationship between stimulation intensity and EPSC amplitude was measured by stimulating the cortical inputs in increments of 10 μA, starting at 0 μA and terminating at 200 μA. Slices were not stimulated past 200 μA to ensure slice health and allow for recordings of multiple cells on the same slice. **Paired-Pulse Ratio (PPR)** was measured by electrically evoking EPSCs with two pulses at an inter-pulse interval of 25 ms (40 Hz). Ratio was determined by dividing the amplitude of the second EPSC by the amplitude of the first EPSC. **α-amino-3-hydroxy-5-methyl-4-isoxazole propionic acid/ N-Methyl-D-aspartate (AMPA/NMDA) ratio** was measured by evoking EPSCs while holding the cell at −70 mV then at +40 mV. Peak amplitudes at −70 mV were used as the measure for the AMPA component. 150 ms after the onset of the response at +40 mV was used as the measure for the NMDA component. Ratio was calculated by dividing the AMPA component by the NMDA component. Total recording time for each cell was 15 min minimum to allow for adequate dialyzing of NeuroBiotin in the cytosolic space. After recording, slices were post-fixed in 4% paraformaldehyde overnight at 4°C. Post-fixed slices were then transferred to a 0.1 M phosphate buffer until histology processing.

2.4.3. Immunohistochemistry

Visualization of NeuroBiotin-filled cells was performed as previously described (Gunn et al., 2019). Briefly, slices used for whole-cell patch-clamp (300 μm) were sectioned to 40 μm thickness using a Microm HM440E sliding microtome (Fisher Scientific, Pittsburgh), and stained with Streptavidin Alexa Fluor 568 conjugate (1:200: Molecular Probes, Oregon) for visualization of NeuroBiotin-filled cell, using an epifluorescent microscope (BZ-X800, Keyence Corporation, Illinois). Images were taken using a 60× oil immersion objective, and a z-stack (0.5 μm step) spanning the entire cell was applied; range of images taken per cell was 25–30 images. Imaged cells were visually inspected to confirm cell identity based on morphological characteristics. Round soma (around 10–20 μm in diameter) and well-defined dendritic spines were used as the criteria for cell inclusion as these have been shown to be characteristics of MSNs (Tepper et al., 1998). Cells that did not fit these criteria were excluded from analysis.

2.5. Statistical analyses

The behavioral experiments were analyzed by repeated measures (RM) ANOVA using day (for instrumental performance and water T-maze) or devaluation state (for outcome devaluation test) as the repeated variable and LBN condition as the independent variable, followed by Sidak's *post-hoc* test for multiple comparisons. To investigate the within-subject distribution of lever presses between valued and devalued states, the number of lever presses for valued and devalued states was normalized to the total number of lever presses for both states (valued + devalued) in each context. This was followed by conducting a one sample t-test

10.3389/fnsyn.2023.1128640

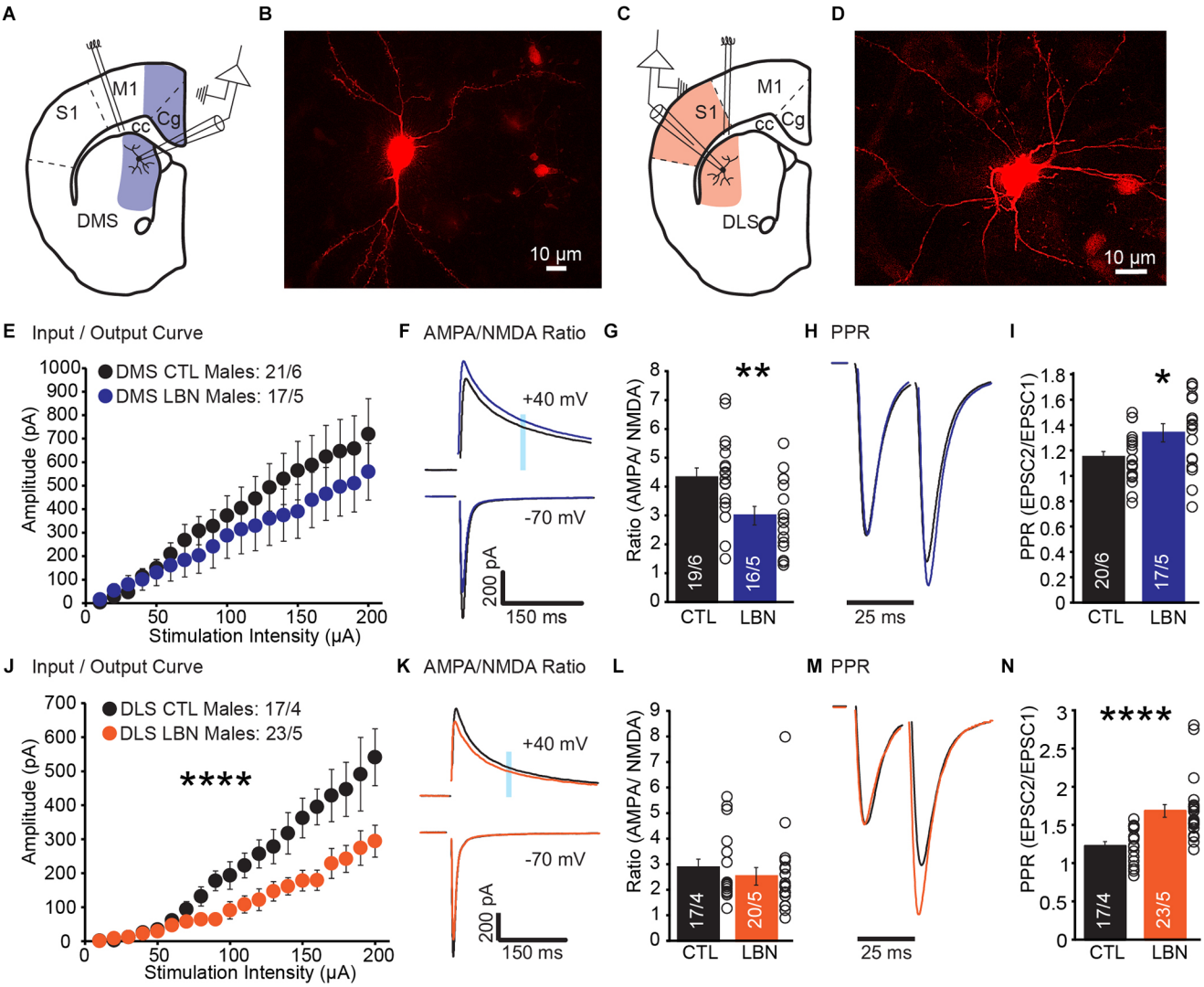

FIGURE 1
Male LBN mice exhibited decreased cortical glutamate release probability in the DLS and DMS. **(A)** Recording schematic for whole-cell patch-clamp experiments in the DMS. **(B)** Representative image of a recorded MSN in DMS; NeuroBiotin-filled cells were processed with an Alexa Fluor 568 conjugated streptavidin for morphological identification of MSN. **(C)** Recording schematic for whole-cell patch-clamp experiments in the DLS. **(D)** Representative image of a recorded MSN in DLS; NeuroBiotin-filled cells were processed with an Alexa Fluor 568 conjugated streptavidin for morphological identification of MSN. **(E)** Summary graph of input/output curve showing no changes of amplitudes in response to increasing stimulation intensities in the DMS-MSN of male LBN mice. **(F,G)** LBN altered relative contribution of AMPA and NMDA receptors to overall EPSCs in the DMS-MSN. **(F)** Representative traces of AMPA currents (−70 mV) and NMDA currents (+40 mV); shaded area denotes the region used to measure the NMDA component of EPSCs. **(G)** Summary graph of AMPA and NMDA ratio showing a decrease in ratio for male LBN mice. **(H,I)** Male LBN mice exhibited decreased probability of glutamate release in the DMS-MSN. **(H)** Representative traces of paired-pulse recordings; inter-stimulus interval was fixed at 25 ms (40 Hz) and traces were normalized to the first EPSC. **(I)** Summary graph of PPR showing a increase in ratio for male LBN mice. **(J)** Summary graph of input/output curve showing a significant decrease of amplitudes in response to increasing stimulation intensities in the DLS-MSN of male LBN mice. **(K,L)** LBN changed relative contribution of AMPA and NMDA receptors to overall EPSCs in the DLS-MSN. **(K)** Representative traces of AMPA currents (−70 mV) and NMDA currents (+40 mV); shaded area denotes the region used to measure the NMDA component of EPSCs. **(L)** Summary graph of AMPA and NMDA ratio showing no changes in ratio for male LBN mice. **(M,N)** Male LBN mice exhibited decreased probability of glutamate release in DLS-MSN. **(M)** Representative traces of paired-pulse recordings; inter-stimulus interval was fixed at 25 ms (40 Hz) and traces were normalized to the first EPSC. **(N)** Summary graph of PPR showing an increase in ratio for male LBN mice. Data is represented as means ± SEM. Number of neurons/mice are listed inside the bar graphs. Each open circle in the summary graphs represents the average of each recorded cell. Statistical assessments were performed by unpaired two-tailed Student's t-test **(G,I,L,N)** and RM two-way ANOVA **(E,J)** by comparing male LBN to CTL mice with $*p < 0.05$, $**p < 0.01$, $****p < 0.0001$.

to determine whether the normalized value of lever presses in each state significantly differed from a hypothetical mean of 0.5, which normally reflects equal distribution of lever presses between valued and devalued states. A devaluation index was calculated by using the formula: [(valued presses − devalued presses)/total number of lever presses] in each context. I/O curve measures were analyzed by repeated measures ANOVA with stimulation intensity as the repeated variable and LBN condition as the independent variable. AMPA/NMDA and PPR measures were analyzed using a Student's *t*-test to compare averages between groups. Sexes were separated for instrumental learning, outcome devaluation, and electrophysiology experiments but were combined

for water T-maze. Two-way ANOVA analysis was conducted to assess effects of sex on PPR, AMPA/NMDA ratio, spatial navigation and reversal learning using day as repeated variable and sex or LBN condition as two independent variables. All data were expressed as mean ± standard error of the mean (SEM). Number of neurons/mouse or number of mice were indicated inside bars or by their respective plots. Significance was set at $P < 0.05$. All data were analyzed by GraphPad Prism software (San Diego, CA).

3. Results

3.1. Fragmented maternal care early in life decreased cortical glutamate release in DLS and DMS of male mice

A previous study showed that densities of dendritic spine and postsynaptic density protein-95 (PSD-95) were increased in DLS-MSN, but not DMS-MSN, of LBN male mice (Xu et al., 2022), suggesting that LBN mice had more synapses in DLS-MSN than CTL mice. However, direct measurements of synaptic transmission in MSNs post-ELA have not been investigated. To address this, we performed whole-cell patch-clamp recordings from DLS-MSN and DMS-MSN (**Figures 1A–D**). We recorded EPSCs and measured overall glutamate transmission from cortical synapses (I/O Curve), contribution of AMPA and NMDA receptors to overall EPSCs (AMPA/NMDA Ratio), and presynaptic probability of neurotransmitter release (PPR).

In DMS, male LBN mice showed no changes in I/O curve (RM 2-way ANOVA: $F_{(19,665)} = 1.01$, $p = 0.45$), indicating that overall cortical excitatory transmission to DMS-MSNs remained unchanged following ELA (**Figure 1E**). The ratio between AMPA and NMDA currents was significantly decreased in LBN mice (**Figures 1F,G**), suggesting that ELA caused changes in the relative contribution of AMPA and NMDA receptors to overall EPSCs (CTL = 4.32 ± 0.32, LBN = 2.99 ± 0.32; $p < 0.01$; two-tailed Student's *t*-test). Closer examination of AMPA and NMDA currents suggest that the difference in ratio could be due to smaller amplitudes of AMPA currents (CTL: -918.1 pA; LBN: -766.1 pA) and larger NMDA currents (CTL: 212.3 pA; LBN: 251.1 pA), albeit comparisons of raw amplitudes for each current between CTL and LBN mice were not significantly different. Finally, PPR was significantly increased (**Figures 1H,I**), indicating a decrease in the probability of glutamate release (CTL = 1.14 ± 0.04, LBN = 1.34 ± 0.07; $p < 0.05$; two-tailed Student's *t*-test).

In DLS, male LBN mice showed a significant impairment in I/O curve (RM 2-way ANOVA: $F_{(19,722)} = 9.465$, $p < 0.001$), indicating that overall cortical excitatory transmission to DLS-MSNs was impaired following LBN (**Figure 1J**). However, a decrease in I/O curve does not inform us if the impairment is pre- or post-synaptic. AMPA/NMDA ratio was measured to investigate if ELA induced any postsynaptic alterations in DLS-MSNs. The AMPA/NMDA ratio did not differ between LBN and CTL mice in DLS (**Figures 1K,L**), suggesting that the relative contribution of AMPA and NMDA receptors to EPSCs was not affected by LBN (CTL = 2.87 ± 0.33, LBN = 2.52 ± 0.34; $p = 0.47$; two-tailed Student's *t*-test). Next, we asked if the results observed in DLS were due to impairments in the presynaptic probability of glutamate release. PPR recordings revealed a significant increase (**Figures 1M,N**) in ratio for LBN mice in the DLS (CTL = 1.23 ± 0.06, LBN = 1.69 ± 0.08; $p < 0.0001$; two-tailed Student's *t*-test).

Together, these results show a region-specific impairment caused by ELA in sub-regions within the dorsal striatum. While the probability of glutamate release decreased in both regions, only DMS showed changes in AMPA/NMDA ratio. In DLS, it is likely that the synaptic impairment is localized predominately in presynaptic compartments, while in DMS it is likely that pre- and post-synaptic alterations occurred post-ELA.

3.2. Fragmented maternal care early in life increased cortical glutamate release in DMS of female mice

There is a growing body of work showing that ELA induced differential effects in males and females (Naninck et al., 2015; Arp et al., 2016; Bath et al., 2017; Colich et al., 2017; Bondar et al., 2018; Ellis and Honeycutt, 2021; Ruigrok et al., 2021a,b). Thus, we hypothesized that the impact of ELA on corticostriatal synapses would show sex-specific impairments. We recorded EPSCs and measured I/O curve, AMPA/NMDA ratio, and PPR (**Figures 2A–D**).

In DMS of female mice, I/O curve (RM 2-way ANOVA: $F_{(19,494)} = 0.97$, $p = 0.50$) and AMPA/NMDA ratio (CTL = 5.05 ± 0.43, LBN = 5.16 ± 0.42; $p = 0.85$; two-tailed Student's *t*-test) showed no significant changes between CTL and LBN mice (**Figures 2E–G**). PPR was significantly decreased in female LBN mice (CTL = 1.29 ± 0.07, LBN = 1.11 ± 0.03; $p < 0.05$; two-tailed Student's *t*-test), indicating an increase in the probability of glutamate release after LBN (**Figures 2H,I**).

In DLS, female LBN mice showed no significant impairments in I/O curve (RM 2-way ANOVA: $F_{(19,513)} = 0.871$, $p = 0.62$), AMPA/NMDA ratio (CTL = 5.85 ± 0.52, LBN = 5.95 ± 0.85; $p = 0.91$; two-tailed Student's *t*-test), or PPR (CTL = 1.37 ± 0.05, LBN = 1.33 ± 0.07; $p = 0.64$; two-tailed Student's *t*-test; **Figures 2J–N**). Overall, female LBN mice only showed increased glutamate release probability in the DMS with no other synaptic impairments observed.

3.3. Fragmented maternal care early in life differentially affected synaptic transmission in a sex-dependent manner

In the DMS, AMPA/NMDA ratio showed a trend towards significant LBN condition × sex interaction (2-way ANOVA: $F_{(1,57)} = 3.776$, $p = 0.057$) and a significant main effect of sex (2-way ANOVA: $F_{(1,57)} = 15.003$, $p < 0.001$; **Supplementary Figure 1A**). Sex comparisons for PPR measures in the DMS revealed a significant LBN condition × sex interaction (2-way ANOVA: $F_{(1, 62)} = 11.05$, $p < 0.01$). Sidak's multiple comparison test revealed that PPR for male LBN mice was significantly increased compared

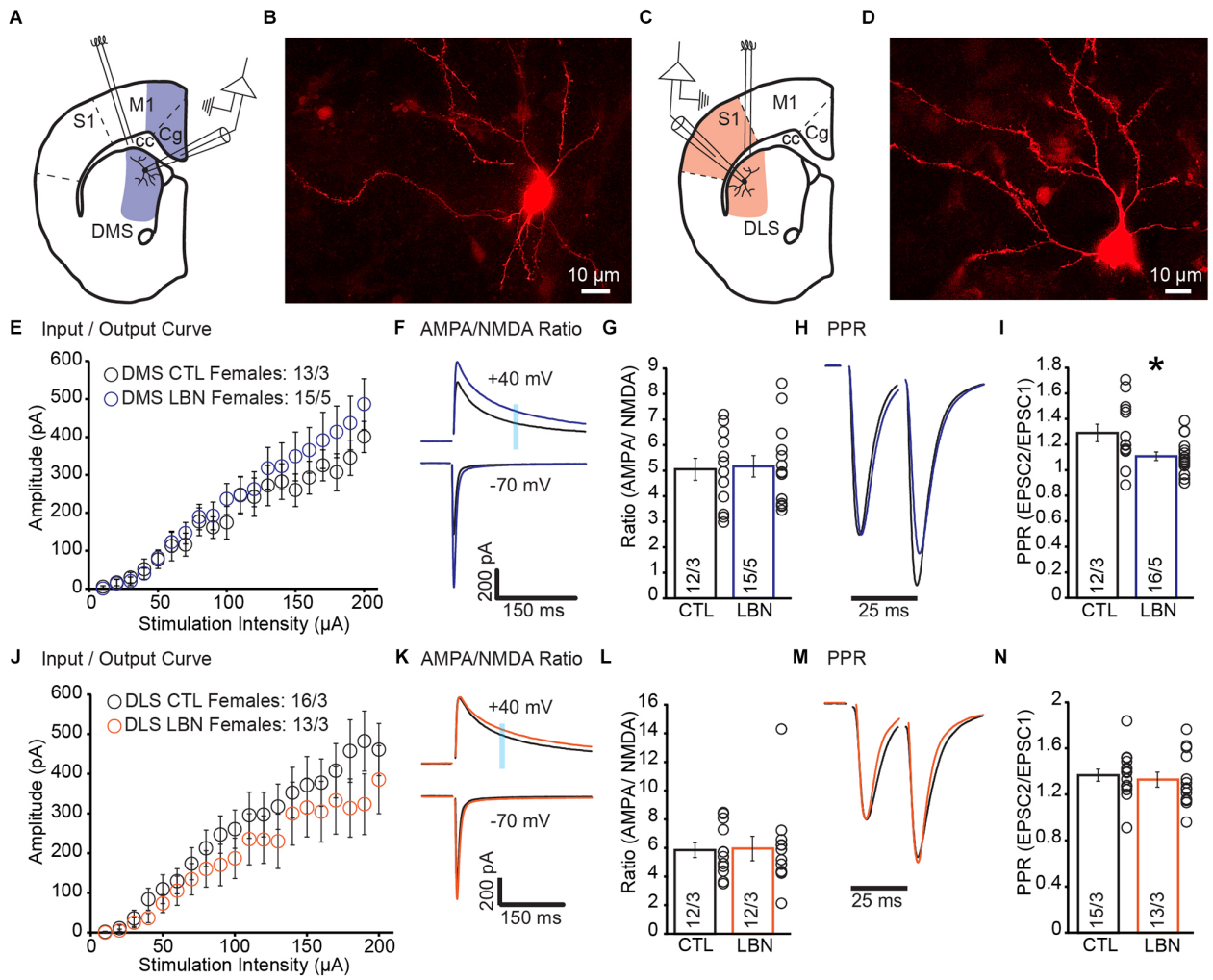

FIGURE 2
Female LBN mice exhibited increased cortical glutamate release probability in the DMS. **(A)** Recording schematic for whole-cell patch-clamp experiments in the DMS. **(B)** Representative image of a recorded MSN in DMS; NeuroBiotin-filled cells were processed with an Alexa Fluor 568 conjugated streptavidin for morphological identification of MSN. **(C)** Recording schematic for whole-cell patch-clamp experiments in the DLS. **(D)** Representative image of a recorded MSN in DLS; NeuroBiotin-filled cells were processed with an Alexa Fluor 568 conjugated streptavidin for morphological identification of MSN. **(E)** Summary graph of input/output curve showing no changes of amplitudes in response to increasing stimulation intensities in the DMS-MSN of female LBN mice. **(F,G)** LBN has no effect on the relative contribution of AMPA and NMDA receptors to overall EPSC in the DMS-MSN. **(F)** Representative traces of AMPA currents (−70 mV) and NMDA currents (+40 mV); shaded area denotes the region used to measure the NMDA component of EPSCs. **(G)** Summary graph of AMPA and NMDA ratio showing no changes in ratio for female LBN mice. **(H,I)** Female LBN mice exhibited increased probability of glutamate release in the DMS-MSN. **(H)** Representative traces of paired-pulse recordings; inter-stimulus interval was fixed at 25 ms (40 Hz) and traces were normalized to first EPSC. **(I)** Summary graph of PPR showing a decrease in ratio for female LBN mice. **(J)** Summary graph of input/output curve showing no changes of amplitudes in response to increasing stimulation intensities in the DLS-MSN of female LBN mice. **(K,L)** LBN had no effect on the relative contribution of AMPA and NMDA receptors to overall EPSC in the DLS-MSN. **(K)** Representative traces of AMPA currents (−70 mV) and NMDA currents (+40 mV); shaded area denotes the region used to measure the NMDA component of EPSCs. **(L)** Summary graph of AMPA and NMDA ratio showing no changes in ratio for female LBN mice. **(M,N)** Female LBN mice had no changes in the probability of glutamate release in the DLS-MSN. **(M)** Representative traces of paired-pulse recordings; inter-stimulus interval was fixed at 25 ms (40 Hz) and traces were normalized to first EPSC. **(N)** Summary graph of PPR showing no changes in ratio for female LBN mice. Data is represented as means ± SEM. Number of neurons/mice are listed inside the bar graphs. Each open circle in the summary graphs represents the average of each recorded cell. Statistical assessments were performed by RM two-way ANOVA **(E,J)** and unpaired two-tailed Student's *t*-test **(G,I,L,N)** by comparing female LBN to CTL mice with $*p < 0.05$.

to female LBN mice (Male LBN vs. female LBN; $t = 2.93 \pm 0.08$; $p < 0.05$; **Supplementary Figure 1B**).

For sex comparisons in the DLS, AMPA/NMDA ratio showed no significant LBN condition × sex interaction (2-way ANOVA: $F_{(1,57)} = 0.205$, $p = 0.65$) but a significant main effect of sex (2-way ANOVA: $F_{(1,57)} = 41.3$, $p < 0.0001$), suggesting that AMPA/NMDA ratio in the DLS differs between sexes but is not affected by ELA (**Supplementary Figure 1C**). Sex comparisons for PPR measures in the DLS revealed a significant LBN condition × sex interaction (2-way ANOVA: $F_{(1,64)} = 11.31$, $p < 0.01$) and a significant main effect of LBN condition (2-way ANOVA: $F_{(1,64)} = 8.08$, $p < 0.01$). Sidak's multiple comparison test revealed that PPR for male LBN mice was significantly increased compared to all other groups (**Supplementary Figure 1D**) [Male CTL vs. Male LBN ($t = 4.81 \pm 0.09$; $p < 0.0001$); Male LBN vs. Female CTL ($t = 3.24 \pm 0.09$;

$p < 0.05$); Male LBN vs. Female LBN ($t = 3.47 \pm 0.1$; $p < 0.01$)].

3.4. Fragmented maternal care early in life impaired execution of goal-directed strategy in response to outcome devaluation in male mice

It was previously shown that LBN mice relied on habitual-action strategies in response to changes in reward value upon extensive instrumental overtraining in a context that promotes goal-directedness (Xu et al., 2022). However, previous studies did not investigate the flexibility of LBN mice to alternate between goal-directed and habitual action strategies under differing schedules of reinforcement delivery. To this end, the LBN mice underwent RR (to promote goal-directedness) and RI (to promote habitual behavior) schedules of reinforcement in two separate contexts (**Figure 3A**). During the conditioning phase in the RR context, the male LBN mice did not exhibit any changes in total number of lever presses [RM 2-way ANOVA: $F_{(1,13)} = 0.7166$, $p = 0.4126$] (**Supplementary Figure 2A**), or response rate (i.e., lever presses/min) [RM 2-way ANOVA: $F_{(1,13)} = 0.9662$, $p = 0.3436$] (**Supplementary Figure 2B**), or reward rate (i.e., rewards/min) [RM 2-way ANOVA: $F_{(1,13)} = 0.2468$, $p = 0.6276$] (**Supplementary Figure 2C**) in comparison to male CTL mice, indicating normal instrumental performance in male LBN mice. There was no significant day × LBN condition interaction for either total number of lever presses [RM 2-way ANOVA: $F_{(8,104)} = 0.4029$, $p = 0.9167$) or response rate [RM 2-way ANOVA: $F_{(8,104)} = 0.5365$, $p = 0.8266$] or reward rate [RM 2-way ANOVA: $F_{(8,104)} = 0.2567$, $p = 0.9781$]. During the outcome devaluation test, repeated measures ANOVA detected a significant effect of devaluation state [RM 2-way ANOVA: $F_{(1,13)} = 11.05$, $p < 0.01$] but not that of LBN condition [RM 2-way ANOVA: $F_{(1,13)} = 2.195$, $p = 0.1623$] on lever-pressing behavior (**Figure 3B**). There was also no significant ELA condition × devaluation state interaction [RM 2-way ANOVA: $F_{(1,13)} = 0.0014472$, $p = 0.9702$] in the RR context, indicating that both male CTL and LBN mice responded similarly to the effects of outcome devaluation on lever pressing behavior. However, a one sample t-test (against chance or 0.5) of normalized lever presses between valued and devalued states in the RR context showed that male CTL (valued state = 0.67, devalued state = 0.33; $p < 0.05$; one sample t-test), but not LBN mice (valued state = 0.59, devalued state = 0.41; $p = 0.0623$; one sample t-test), exhibited a higher preference for lever-pressing in valued vs. devalued state, indicating adoption of goal-directed strategy in male CTL, but not in LBN, mice (**Figure 3C**).

During the conditioning phase in the RI context, the male LBN mice did not exhibit any changes in total number of lever presses [RM 2-way ANOVA: $F_{(1,13)} = 1.627$, $p = 0.2244$] (**Supplementary Figure 2D**), response rate [RM 2-way ANOVA: $F_{(1,13)} = 1.447$, $p = 0.2505$] (**Supplementary Figure 2E**), or reward rate [RM 2-way ANOVA: $F_{(1,13)} = 0.6728$, $p = 0.4269$] (**Supplementary Figure 2F**), in comparison to CTL mice, indicating normal instrumental performance in male LBN mice. There was no significant day × LBN condition for total number of lever presses [RM 2-way ANOVA: $F_{(8,104)} = 0.8654$, $p = 0.5482$], response rate [RM 2-way ANOVA: $F_{(8,104)} = 1.254$, $p = 0.2757$], or reward rate [RM 2-way ANOVA: $F_{(8,104)} = 0.2228$, $p = 0.9861$] in the RI context. During the outcome devaluation test, repeated measures ANOVA detected no significant effect of devaluation state [RM 2-way ANOVA: $F_{(1,13)} = 3.106$, $p = 0.1015$], but a significant effect of LBN condition on lever-pressing behavior [RM 2-way ANOVA: $F_{(1,13)} = 5.604$, $p < 0.05$], indicating that male LBN mice pressed the lever significantly more than male CTL mice (**Figure 3D**). Despite the increase in lever pressing behavior in male LBN mice, the LBN condition × devaluation state interaction was not statistically significant in the RI context [RM 2-way ANOVA: $F_{(1,13)} = 0.0002461$, $p = 0.9877$]. A one sample t-test (against chance or 0.5) of normalized lever presses between valued and devalued states in the RI context showed that both male CTL (valued state = 0.61, devalued state = 0.39; $p = 0.1092$; one sample t-test) and LBN mice (valued state = 0.54, devalued state = 0.46; $p = 0.5679$; one sample t-test) exhibited similar distribution of lever presses between valued and devalued states (**Figure 3E**), indicating that both male CTL and LBN mice adopted habitual action strategy in the RI context. For the outcome devaluation procedure, male CTL and LBN mice were able to distinguish between RI and RR schedules, as depicted by altered sensitivity to differential feedback functions produced by both these schedules (**Supplementary Figure 2G**).

3.5. Fragmented maternal care early in life did not impair alternation between goal-directed and habitual action strategies in response to outcome devaluation in female mice

During the conditioning phase in the RR context, the female LBN mice did not exhibit any significant changes in the total number of lever presses [RM 2-way ANOVA: $F_{(1,5)} = 0.5045$, $p = 0.4892$] and there was no significant day × LBN condition interaction [RM 2-way ANOVA: $F_{(8,112)} = 0.8015$, $p = 0.6025$] (**Supplementary Figure 3A**). The female LBN mice exhibited an increase in response rate [RM 2-way ANOVA: $F_{(1,14)} = 8.938$, $p < 0.01$] (**Supplementary Figure 3B**) in comparison to female CTL mice indicating increased instrumental responding in the female LBN mice in a context that promotes goal-directed behavior. There was also a significant day × LBN condition interaction for response rate [RM 2-way ANOVA: $F_{(8, 112)} = 2.262$, $p < 0.05$] with Sidak's *post-hoc* test confirming that female LBN mice exhibited an increase in response rate in RR10 on day 6 ($t = 4.097$, $p < 0.05$) and RR20 on day 11 ($t = 3.877$, $p < 0.05$; **Supplementary Figure 3B**). Female LBN mice also exhibited an increase in reward rate [RM 2-way ANOVA: $F_{(1,14)} = 6.539$, $p < 0.05$] in comparison to CTL mice without any significant day × LBN condition interaction [RM 2-way ANOVA: $F_{(8,112)} = 1.316$, $p = 0.2428$](**Supplementary Figure 3C**). During the outcome devaluation test, repeated measures ANOVA detected a significant effect of devaluation state [RM 2-way ANOVA: $F_{(1, 14)} = 20.33$, $p < 0.001$], and a non-significant

10.3389/fnsyn.2023.1128640

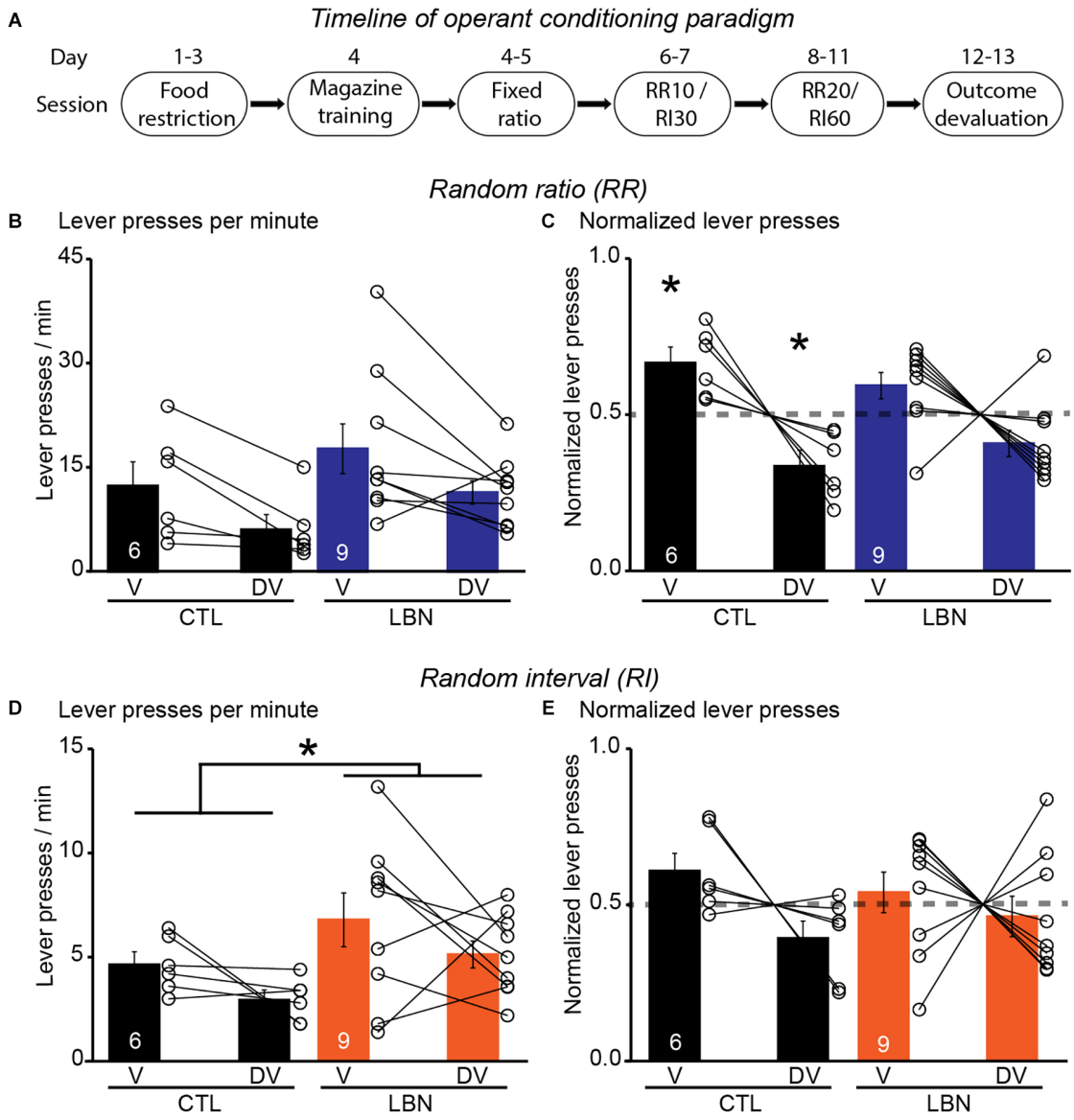

FIGURE 3
Male LBN mice failed to differentially distribute their lever presses in response to outcome devaluation in a context that promotes goal-directedness. **(A)** Experimental timeline of operant conditioning paradigm in mice. **(B,C)** Male LBN mice failed to differentially distribute their lever presses between valued (V) and devalued (DV) days in the RR context. **(B)** Summary graph of response rate (lever presses/min) on V and DV days. **(C)** Summary graph of normalized lever presses showing distribution of lever presses between V and DV days. **(D,E)** Male LBN mice exhibited normal habitual responding behavior in response to outcome devaluation in the RI context. **(D)** Summary graph of response rate (lever presses/min) on valued (V) and devalued (DV) days. **(E)** Summary graph of normalized lever presses showing distribution of lever presses between V and DV days. Data is represented as means ± SEM. Number of mice is listed inside the bar graphs. Each open circle in the summary graphs represents each mouse. Statistical assessments were performed by RM two-way ANOVA **(B,D)** by comparing male LBN to CTL mice with $*p < 0.05$ or one-sample t-test **(C,E)** by comparing normalized lever presses within each group of mice against a "no devaluation" point of 0.5 with $*p < 0.05$.

trend towards effect of LBN condition [RM 2-way ANOVA: $F_{(1,14)} = 4.053$, $p = 0.0637$] on lever-pressing behavior. There was no significant LBN condition × devaluation state interaction [RM 2-way ANOVA: $F_{(1,14)} = 0.002149$, $p = 0.9637$], indicating a similar response in female CTL and LBN mice to the effects of outcome devaluation (**Figure 4A**). A one-sample t-test (against chance or 0.5) of normalized lever presses between valued and devalued states in the RR context showed that female CTL (valued state = 0.68, devalued state = 0.32; $p < 0.05$; one sample t-test) and LBN mice (valued state = 0.63, devalued state = 0.37; $p < 0.05$; one sample t-test) exhibited differential distribution of lever presses between valued and devalued states, indicating that ELA did not impair goal-directed behavior in female mice (**Figure 4B**).

During the conditioning phase in the RI context, the female LBN mice exhibited an increase in total number of lever presses [RM 2-way ANOVA: $F_{(1,14)} = 8.471$, $p < 0.05$] in comparison to female CTL mice (**Supplementary Figure 3D**). There was a significant day × LBN condition interaction for total number of lever presses [RM 2-way ANOVA: $F_{(8,112)} = 2.979$, $p < 0.01$], with

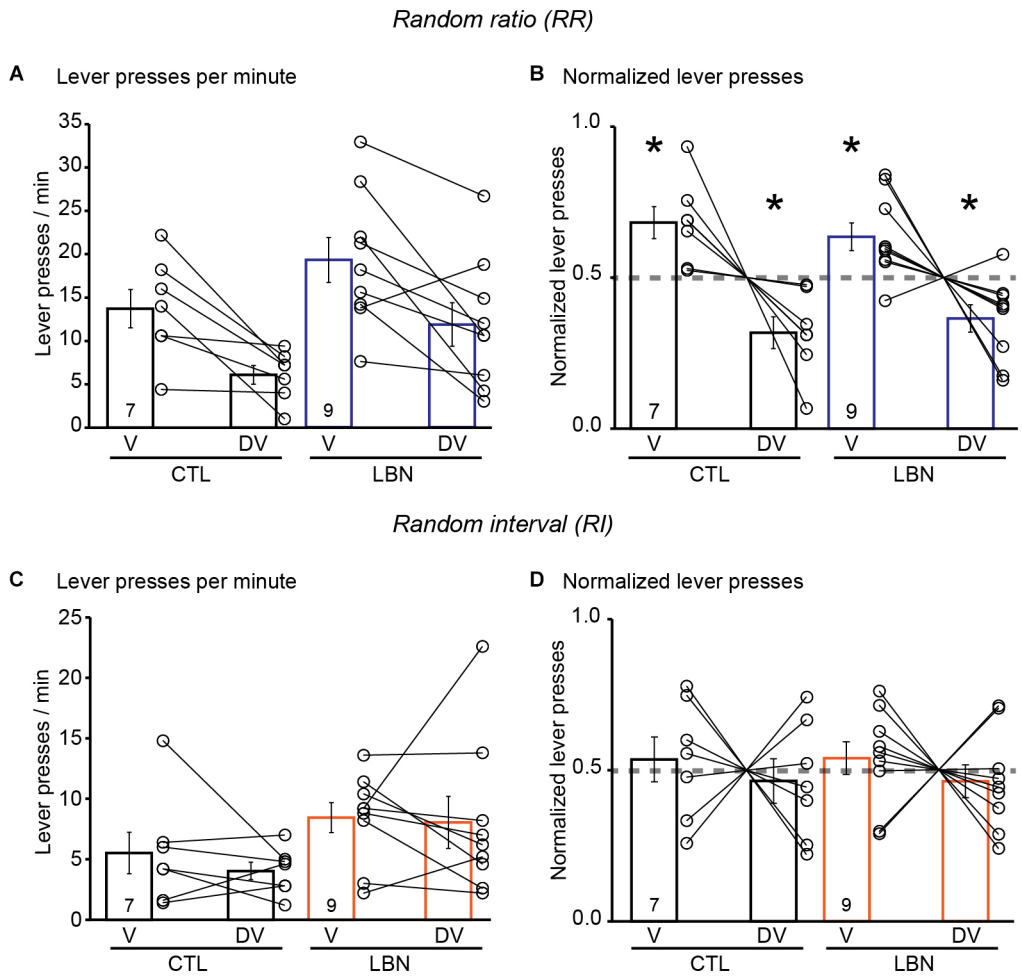

FIGURE 4
Female LBN mice did not exhibit impairments in action selection strategy in response to outcome devaluation. **(A,B)** Female LBN mice exhibited goal-directed behavior in response to outcome devaluation in the RR context. **(A)** Summary graph of response rate (lever presses/min) on V and DV days. **(B)** Summary graph of normalized lever presses showing distribution of lever presses between V and DV days. **(C,D)** Female LBN mice exhibited normal habitual responding behavior in response to outcome devaluation in the RI context. **(C)** Summary graph of response rate (lever presses/min) on valued (V) and devalued (DV) days. **(D)** Summary graph of normalized lever presses showing distribution of lever presses between V and DV days. Data is represented as means ± SEM. Number of mice is listed inside the bar graphs. Each open circle in the summary graphs represents each mouse. Statistical assessments were performed by RM two-way ANOVA **(A,C)** or one-sample t-test **(B,D)** by comparing normalized lever presses within each group of mice against a "no devaluation" point of 0.5 with $*p < 0.05$.

Sidak's *post-hoc* test confirming that female LBN mice exhibited a significant increase in total number of lever presses in RI30 on day 6 ($t = 3.368$, $p < 0.05$) and RI60 on day 11 ($t = 4.477$, $p < 0.01$; **Supplementary Figure 3D**). The female LBN mice exhibited an increase in response rate [RM 2-way ANOVA: $F_{(1,14)} = 8.911$, $p < 0.01$] in comparison to female CTL mice (**Supplementary Figure 3E**) indicating increased instrumental responding in female LBN mice in a context that promotes habitual behavior. There was also a significant day × LBN condition interaction for response rate [RM 2-way ANOVA: $F_{(8, 112)} = 3.305$, $p < 0.01$] with Sidak's *post-hoc* test confirming that female LBN mice exhibited an increase in response rate in RI30 on day 6 ($t = 3.959$, $p < 0.05$) and RI60 on day 11 ($t = 4.380$, $p < 0.01$; **Supplementary Figure 3E**). There were no significant changes in reward rate [RM 2-way ANOVA: $F_{(1,14)} = 0.4076$, $p = 0.5335$] between the female LBN and CTL mice (**Supplementary Figure 3F**). Repeated measures ANOVA detected a non-significant trend towards effect of LBN condition [RM 2-way ANOVA: $F_{(1,14)} = 3.399$, $p = 0.0865$] and no effect of devaluation state [RM 2-way ANOVA: $F_{(1,14)} = 0.5006$, $p = 0.4909$] on lever-pressing behavior (**Figure 4C**) in RI context. There was also no significant LBN condition × devaluation state interaction [RM 2-way ANOVA: $F_{(1,14)} = 0.1659$, $p = 0.6899$]. A one-sample t-test (against chance or 0.5) of normalized lever presses between valued and devalued states in the RI context showed that both the female CTL (valued state = 0.54, devalued state = 0.46; $p = 0.6349$; one sample t-test) and LBN mice (valued state = 0.54, devalued state = 0.46; $p = 0.4793$; one sample t-test) were insensitive to outcome devaluation as evidenced by their equal distribution of lever presses between valued and devalued states (**Figure 4D**). For the outcome devaluation procedure, female CTL and LBN mice were able to distinguish between RI and RR schedules, as depicted by altered sensitivity to differential feedback functions produced by both these schedules (**Supplementary Figure 3G**).

3.6. Fragmented maternal care early in life induced behavioral inflexibility in a reversal learning paradigm

During the spatial navigation phase, repeated measures ANOVA detected a significant effect of day [RM 2-way ANOVA: $F_{(1,23)} = 23.31$, $p < 0.0001$] but not that of LBN condition [RM 2-way ANOVA: $F_{(1,23)} = 2.234$, $p = 0.15$] on the number of incorrect arm entries as well as on the % of successful trials [RM 2-way ANOVA: Day: $F_{(1,23)} = 23.31$, $p < 0.0001$; LBN condition: $F_{(1,23)} = 2.234$, $p = 0.15$], indicating normal spatial navigation in LBN mice (**Figures 5A,B**). There was also no significant day × LBN condition interaction for number of incorrect arm entries [RM 2-way ANOVA: $F_{(1,23)} = 0.3357$, $p = 0.57$] or % of successful trials [RM 2-way ANOVA: $F_{(1,23)} = 0.3357$, $p = 0.57$]. The LBN mice tended to take fewer number of days to learn the task of finding the platform in comparison to CTL mice (CTL = 3.133 ± 0.31 days, LBN = 2.5 ± 0.17 days; $p = 0.08$; two-tailed Student's *t*-test; **Figure 5C**).

During the reversal learning phase, there was a significant effect of LBN condition [RM 2-way ANOVA: $F_{(1,23)} = 5.284$, $p < 0.05$] and day [RM 2-way ANOVA: $F_{(1,23)} = 71.89$, $p < 0.0001$] on number of incorrect arm entries and on % of successful trials [RM 2-way ANOVA: LBN condition: $F_{(1,23)} = 5.102$, $p < 0.05$; Day: $F_{(1,23)} = 71.00$, $p < 0.0001$] indicating reversal learning deficits in LBN mice across both the days of the test (**Figures 5D,E**). There was also no significant day × LBN condition interaction for number of incorrect arm entries [RM 2-way ANOVA: $F_{(1,23)} = 1.340$, $p = 0.26$] and % of successful trials [RM 2-way ANOVA: $F_{(1,23)} = 1.436$, $p = 0.24$], indicating that ELA impaired reversal learning throughout the entirety of the testing period. Finally, there were no significant differences in total trials to learn reversal of contingencies upon intradimensional shifts in behavior between the LBN and CTL mice (CTL = 6.8 ± 0.88 trials, LBN = 8 ± 1.39 trials; $p = 0.48$; two-tailed Student's *t*-test; **Figure 5F**). Segregation of mice for water T-maze experiments by their sexes did not show significant differences in number of incorrect arm entries or success rate (%) between CTL and LBN mice within each sex for spatial navigation and reversal learning phases (**Supplementary Data**). ANOVA analysis also did not detect any significant effects of sex on number of incorrect arm entries or success rate (%) within the CTL and LBN group for spatial navigation and reversal learning phases (**Supplementary Data**). Thus, sexes were combined for water T-maze experiments.

4. Discussion

Our investigation provides new insights into the functional impact of ELA on excitatory synaptic transmission in the dorsal striatum and behavioral adaptability in a dynamic environment. We find that ELA can impair the ability to strategize action selection or disengage from preferred behavioral patterns to learn new ones upon changes in circumstances, in order to achieve a specific goal.

Previous examinations into the impact of ELA in adult male mice showed an overall increase in dendritic spine density and immunolabeling of PSD-95 in MSNs of the DLS (Xu et al., 2022). Here, we addressed the functional impact of ELA on corticostriatal synaptic transmission. Despite morphological studies showing an increase in excitatory synapses, our data suggest that overall excitatory transmission from cortical inputs to MSNs is decreased in male mice following LBN. An important distinction between the two studies is that the current study focused on cortical inputs specifically as they are one of the major sources of glutamate to the dorsal striatum. Two possibilities arise from our current data: (i) LBN caused a decrease in glutamate release in DLS of male mice as an adaptation response to the increased excitatory synaptic connections; or (ii) LBN has opposing effects on different sources of glutamate input to the dorsal striatum (e.g., thalamus, hippocampus). If the latter is the case, then we would expect other excitatory inputs to the dorsal striatum to show increased function. A recent study found that LBN disrupts synaptic pruning mechanisms in the hippocampus, resulting in increased dendritic arborization and c-Fos activation of CA1 pyramidal cells (Dayananda et al., 2023). Future investigations are warranted to determine how LBN impacts thalamic and hippocampal inputs to the dorsal striatum.

For all electrophysiological measures, we started by measuring the relationship between EPSC amplitude and stimulation intensity of cortical inputs (I/O curve). Measures of I/O curve in voltage clamp configuration are good indicators of overall neurotransmission from a specific input. However, due to large variability in amplitude between cells, mild impairments to synaptic transmission are unlikely to be detected in I/O measures. Thus, the current study used I/O curve as a measure of overall glutamate transmission. Impairments in the DLS of male LBN mice were interpreted as a severe impact of LBN on corticostriatal transmission. I/O curve measures, however, do not indicate if synaptic impairments are pre- or post-synaptic. Thus, we measured PPR and AMPA/NMDA ratio to directly address pre- and post-synaptic alterations, respectively. The probability of glutamate release was decreased in both DLS and DMS of male LBN mice, as indicated by the increase in PPR in both regions (the interpretation of change in PPR is inverse to direction of the change in PPR, e.g., increase in PPR = decrease in release probability). Interestingly, male LBN mice showed a significant decrease of AMPA/NMDA ratio in the DMS, but not in DLS indicating a change in the relative contribution of AMPA and NMDA receptors to overall EPSC. Closer examination of these EPSCs revealed that the difference in the AMPA/NMDA ratio for the LBN mice was due to a combination of smaller AMPA currents and larger NMDA currents. It still remains uncertain whether this shift is due to changes in NMDA receptor kinetics or if density distribution of AMPA and NMDA receptors has changed. Additionally, it is well-established that long-term plasticity in MSNs of the dorsal striatum requires NMDA receptor activation (Calabresi et al., 1992; Dang et al., 2006). Thus, changes in NMDA receptor function or density could have profound consequences for striatal plasticity. Alternatively, changes in NMDA receptor subunit composition could also result in changes in AMPA/NMDA ratio. NMDA receptor subunits 2A and 2B have been shown to play critical roles in the dorsal striatum by regulating complex motor skills and reward-seeking behaviors, respectively (Lemay-Clermont et al., 2011; Gass et al., 2018).

Excitatory and inhibitory neurotransmission operate in concert within an intact circuit to determine neuronal, and subsequently,

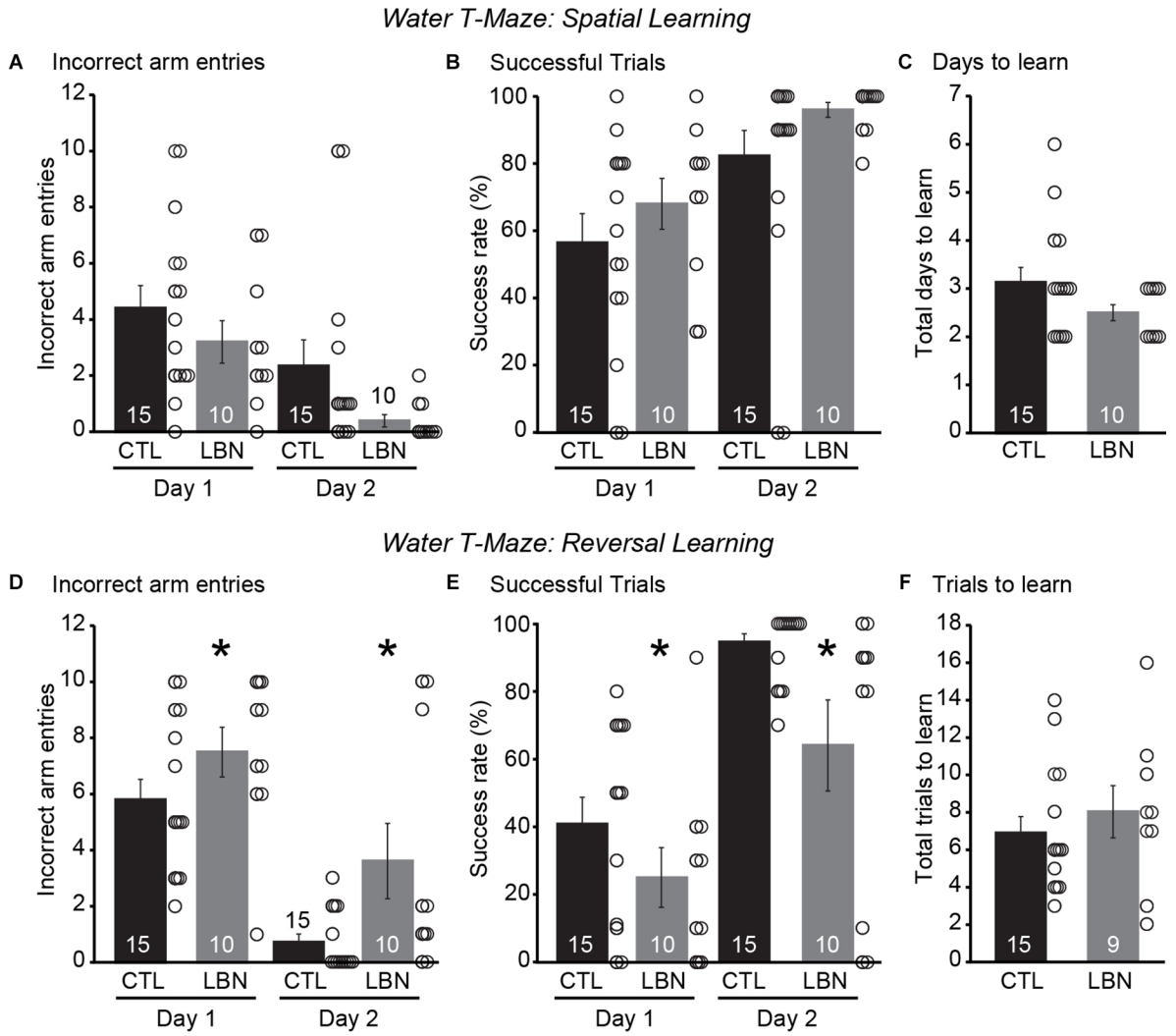

FIGURE 5
LBN mice exhibited impaired behavioral flexibility in a water T-maze reversal learning paradigm. **(A–C)** LBN mice exhibited normal spatial navigation. **(A)** Summary graph of incorrect arm entries during the spatial task on days 1 and 2. **(B)** Summary graph of percentage of successful trials during the spatial task on days 1 and 2. **(C)** Summary graph of total number of days taken to learn the spatial task. **(D–F)** LBN mice exhibited reversal learning deficits. **(D)** Summary graph of incorrect arm entries during reversal learning task on days 1 and 2. **(E)** Summary graph of percentage of successful trials during the reversal learning task on days 1 and 2. **(F)** Summary graph of total number of trials taken to learn the reversal task. Data is represented as means ± SEM. Number of mice is listed inside the bar graphs. Each open circle in the summary graphs represents each mouse. Statistical assessments were performed by RM two-way ANOVA **(A,B,D,E)** or two-tailed Student's *t*-test **(C,F)** by comparing CTL to LBN mice with $*p < 0.05$.

circuit function. Our finding of impaired glutamate transmission in male LBN mice opens the possibility of an imbalance between excitatory and inhibitory transmission in the dorsal striatum. MSNs in the dorsal striatum receive GABAergic inputs from local GABAergic interneurons and adjacent MSNs (Taverna et al., 2004; Kocaturk et al., 2022). Additionally, recent work has shown that glycine receptors containing the α2 subunit are critical for regulating excitability of striatal MSNs by controlling tonic inhibition (Molchanova et al., 2018). Future investigations into ELA-induced changes in inhibition would be necessary for a more complete understanding of the ELA-induced effects in dorsal striatum. Furthermore, it is known that expression of $GABA_A$ receptor subunits differs between D1- and D2-MSNs (Boccalaro et al., 2019). Therefore, it is possible that LBN effects to striatal inhibition are cell-type specific, which could have profound consequences to downstream processes when excitatory and inhibitory transmission are working together.

In contrast to the male data, female LBN mice had no impairments in glutamate transmission in the DLS. PPR measurements in the DMS revealed a significant decrease in ratio for female LBN mice, indicating that female LBN mice had a higher probability of glutamate release in the DMS. At present, the underlying reason for opposing results for PPR in the DMS between sexes is not clear. However, it is clear that sex is an important factor in the role of ELA on glutamate release in the DMS. This also appears to be the case for the nucleus accumbens (NAc) where sex-dependent effects of ELA on glutamate neurotransmission were also observed. ELA reduced the frequency of spontaneous excitatory postsynaptic currents (sEPSCs) in the NAc in male, but not in female rats (Ordoñes Sanchez et al., 2021). The

sex-differences in glutamate neurotransmission were attributed to unique transcriptional signature in the NAc between male and female LBN rats (Ordoñes Sanchez et al., 2021). Similar studies evaluating the effects of ELA on gene expression in the DMS would be warranted in elucidating differences in PPR between both sexes.

ELA did not affect habitual responding as evidenced by the lack of sensitivity to outcome devaluation in both sexes in the RI context. On the other hand, male (but not female) LBN mice adopted a similar action strategy (i.e., habitual action) in response to outcome devaluation in the RR context, indicating impaired goal-directed behavior. The adoption of the same action strategy under differing contingencies of reward delivery suggests the male LBN mice are unable to utilize prior knowledge of the consequences of their actions and the value of those consequences to guide action control. The generalization of habitual behavior in male LBN mice can be linked to the previously observed increase in synaptic contacts in the DLS, but not in the DMS, in male LBN mice (Xu et al., 2022). The DMS receives projections from associative cortices including the anterior cingulate cortex and the premotor cortex (Hadjas et al., 2020), and has been implicated in regulation of goal-directed behavior (Yin et al., 2005a,b; Hart et al., 2018; Terra et al., 2020). The DLS receives projections from the sensorimotor cortex (Hadjas et al., 2020) and has been linked to habitual behaviors (Yin et al., 2004, 2006; Eskenazi and Neumaier, 2011; Jenrette et al., 2019). The increase in synaptic connections in the DLS suggests a preponderance of DLS circuitry over that of DMS in the balance between goal-directed and habitual actions. This can potentially explain the over-reliance of male LBN mice on habitual actions in circumstances that warrant goal-directedness.

The ability of female LBN mice to differentiate between goal-directed and habitual action strategies under differing contingencies of reward delivery suggests normal neural circuit development and maturation. However, the effects of LBN on dendritic differentiation and spinogenesis in the dorsal striatum of female mice have not been investigated and future investigations would be warranted to confirm this hypothesis. Interestingly, the instrumental response in the RI and RR context was significantly higher in female (but not in male) LBN mice, indicating greater proficiency in encoding the incentive value of an instrumental task and faster formation of action-outcome (A-O) associations in the female LBN mice. The faster rate of habit formation in female LBN mice could potentially underlie the induction of compulsive drug-seeking habit by ELA (Levis et al., 2021). Interestingly, in the same study, the compulsive behavior induced by ELA was specific to drugs of reward (heroin) or highly palatable food (sweet banana pellets or chocolate) but not to less salient food rewards (chow pellets; Levis et al., 2021). This findings is in line with our current study in which female LBN mice did not develop habitual behavior upon devaluation of less salient food rewards. Surprisingly, the over-reliance of male LBN mice on habitual behaviors does not seem to directly apply to the effects of ELA on predisposition to drug addiction. In studies assessing the effects of ELA on rewarding properties of drug abuse, male LBN rats exhibited behavioral deficits consistent with anhedonia (Bolton et al., 2018a,b; Levis et al., 2022). In this context, we must consider animal species differences when correlating our findings with those that assess the effects of ELA on reward-seeking behavior since majority of those studies were conducted in rats and not in mice (Bolton et al., 2018a,b; Levis et al., 2021, 2022). Furthermore, habitual and drug-seeking behaviors are controlled by two different neural circuits. Habitual behavior is governed by DLS (Yin et al., 2004, 2006) while drug reward behavior is governed by NAc, amygdala, and paraventricular nucleus (Chaudhri et al., 2010; Koob and Volkow, 2010; Millan et al., 2017). The question of how the dorsal and ventral striatum regulate such behaviors in a parallel or subsequent manner remains to be explored.

The water T-maze experiment produced a different outcome, where reversal learning deficits were observed in LBN mice without any impairments in spatial memory. The normal spatial navigation in LBN mice from our study contradicts previous studies that have reported spatial memory deficits due to alterations in hippocampal neurogenesis (Naninck et al., 2015; Bath et al., 2017), synaptic plasticity (Ivy et al., 2010), and loss of dendritic spines (Xu et al., 2022). Nevertheless, previous findings on spatial memory deficits were obtained from Morris water maze tests, which require a more complex strategy for spatial navigation than the water T-maze, which requires only a simple body movement (i.e., turning right or left into the correct arm; Bardgett et al., 2003; Guariglia et al., 2011). The opposing results from these two behavioral tasks are not surprising considering that these tests measure different aspects of behavioral flexibility. Water T-maze measures intradimensional shifts in behavior that utilize a non-probabilistic reinforcement schedule, where the correct choice is reinforced 100% of the time. In contrast, the lever pressing action in the instrumental learning task delivers the reinforcer 15% of the time. Thus, it appears that LBN induced a generalized effect in flexibility tests that requires disengagement from previously learned behavioral responses and the adoption of new responses upon intradimensional shifts in A-O contingency; and a sex-dependent effect in paradigms that requires updating behavioral responses upon devaluation of the A-O contingency.

Mechanisms of synaptic signal facilitation and depression are thought to underlie synaptic temporal dynamics that are necessary for learning and cognitive function (Fortune and Rose, 2001; Zucker and Regehr, 2002). A previous study in rodents using *in vivo* electrophysiology recordings showed that action potential frequency increases significantly in the DLS and DMS during habitual and goal-directed behaviors, respectively (Gremel and Costa, 2013). In this study, a higher firing rate of DMS neurons and a lower firing rate of DLS neurons was associated with sensitivity to changes in value of outcome in the RR context vs. the RI contexts. The decrease in glutamate release in DMS and DLS in male LBN mice could potentially mean that the MSNs would be less likely to be depolarized and generate an action potential. Given the difference in magnitude of the glutamate release impairment between DLS and DMS, it is likely that cortical inputs to one or both of these regions are not able to sustain elevated levels of glutamate release that would increase the likelihood of action potentials in MSNs. This could ultimately affect the firing rate of MSNs in the DMS and DLS, thus impairing the sensitivity of mice to outcome devaluation in a context that promotes goal-directedness. A separate study using *in vivo* recordings showed that the frequency of action potentials increased in the DLS during correct runs in a T-maze task (Smith and Graybiel, 2016). Our findings on cortical glutamate release suggest that ELA disrupts synaptic mechanisms associated with short-term plasticity. In the

current study, all control mice showed paired-pulse facilitation to two electrical pulses delivered at 40 Hz. This suggests that, under normal circumstances, cortical terminals increase their glutamate release in response to elevated activation, such as what we would see during a cognitive task or learning. Additionally, all control mice showed the same magnitude of facilitation (PPR 1.2). It is likely that signal facilitation in corticostriatal synapses requires precise levels of neurotransmitter facilitation, and that impairments to short-term plasticity in either direction (increased or decreased) could result in the same cognitive impairment. Our electrophysiological results, combined with our T-maze results, agree with this observation. Future *in vivo* electrophysiological recordings of DMS and DLS in LBN mice during the instrumental learning test or T-maze would be necessary to assess a direct role for short term plasticity deficits in failure to strategize action selection. Furthermore, previous work has linked endocannabinoid signaling to the gating of strategy selection (Gremel et al., 2016), which could potentially be a candidate for a molecular mechanism of impairment in ELA. Investigations into the role of endocannabinoids in corticostriatal synaptic transmission would be warranted for future studies.

In summary, our study begins to shed light on the corticostriatal synaptic mechanisms, which are impacted by ELA, underlying the shift between goal-directed and habitual action strategies. Behavioral inflexibility in the form of impaired habitual control or deficits in goal-directedness is often associated with psychiatric disorders that are linked to ELA including schizophrenia (Morris et al., 2015), obsessive compulsive disorder (OCD; Gillan et al., 2011; Simmler and Ozawa, 2019; Dong et al., 2020), and drug addiction (Goldstein and Volkow, 2011; Belin et al., 2013). These findings will lay the foundation for the development of novel therapeutic strategies for the treatment of behavioral inflexibility in individuals who are diagnosed with ELA-associated psychiatric disorders.

Data availability statement

The original contributions presented in the study are included in the article/**Supplementary material**, further inquiries can be directed to the corresponding author.

Ethics statement

The animal study was reviewed and approved by IACUC committee, University of California, Irvine.

Author contributions

Conceptualization and design, writing and editing: SK, GC, and LYC. Methodology: SK and GC. Data analysis: SK, MH, and GC. All authors contributed to the article and approved the submitted version.

Funding

We would like to thank our funding source, NIMH-Conte UCI (P50 MH096889 Seed award FG23670) and UCI SOM startup fund (GF15247) to LYC.

Acknowledgments

We would like to thank Cristabel A. Portillo for assisting with immunohistochemistry of NeuroBiotin-filled cells. We would like to thank Jinjutha E. Cheepluesak for technical assistance with behavioral experiments. Lastly, we would like to thank Dr. Yuncai Chen for his help in teaching us how to process NeuroBiotin-filled cells with Streptavidin.

Conflict of interest

The authors declare that the research was conducted in the absence of any commercial or financial relationships that could be construed as a potential conflict of interest.

Publisher's note

All claims expressed in this article are solely those of the authors and do not necessarily represent those of their affiliated organizations, or those of the publisher, the editors and the reviewers. Any product that may be evaluated in this article, or claim that may be made by its manufacturer, is not guaranteed or endorsed by the publisher.

Supplementary material

The Supplementary Material for this article can be found online at: https://www.frontiersin.org/articles/10.3389/fnsyn.2023.1128640/full#supplementary-material.

References

Alastalo, H., von Bonsdorff, M. B., Räikkönen, K., Pesonen, A. K., Osmond, C., Barker, D. J., et al. (2013). Early life stress and physical and psychosocial functioning in late adulthood. *PLoS One* 8:e69011. doi: 10.1371/journal.pone.0069011

Arp, J. M., Ter Horst, J. P., Loi, M., den Blaauwen, J., Bangert, E., Fernández, G., et al. (2016). Blocking glucocorticoid receptors at adolescent age prevents enhanced freezing between repeated cue-exposures after conditioned fear in adult mice raised under chronic early life stress. *Neurobiol. Learn. Mem.* 133, 30–38. doi: 10.1016/j.nlm.2016.05.009

Baram, T. Z., Davis, E. P., Obenaus, A., Sandman, C. A., Small, S. L., Solodkin, A., et al. (2012). Fragmentation and unpredictability of early-life experience in mental disorders. *Am. J. Psychiatry* 169, 907–915. doi: 10.1176/appi.ajp.2012.11091347

Bardgett, M. E., Boeckman, R., Krochmal, D., Fernando, H., Ahrens, R., and Csernansky, J. G. (2003). NMDA receptor blockade and hippocampal neuronal loss impair fear conditioning and position habit reversal in C57Bl/6 mice. *Brain Res. Bull.* 60, 131–142. doi: 10.1016/s0361-9230(03)00023-6

Bath, K. G., Nitenson, A. S., Lichtman, E., Lopez, C., Chen, W., Gallo, M., et al. (2017). Early life stress leads to developmental and sex selective effects on performance in a novel object placement task. *Neurobiol. Stress* 7, 57–67. doi: 10.1016/j.ynstr.2017.04.001

Belin, D., Belin-Rauscent, A., Murray, J. E., and Everitt, B. J. (2013). Addiction: failure of control over maladaptive incentive habits. *Curr. Opin. Neurobiol.* 23, 564–572. doi: 10.1016/j.conb.2013.01.025

Boccalaro, I. L., Cristiá-Lara, L., Schwerdel, C., Fritschy, J.-M., and Rubi, L. (2019). Cell type-specific distribution of $GABA_A$ receptor subtypes in the mouse dorsal striatum. *J. Comp. Neurol.* 527, 2030–2046. doi: 10.1002/cne.24665

Bolton, J. L., Molet, J., Regev, L., Chen, Y., Rismanchi, N., Haddad, E., et al. (2018a). Anhedonia following early-life adversity involves aberrant interaction of reward and anxiety circuits and is reversed by partial silencing of amygdala corticotropin-releasing hormone gene. *Biol. Psychiatry* 83, 137–147. doi: 10.1016/j.biopsych.2017.08.023

Bolton, J. L., Ruiz, C. M., Rismanchi, N., Sanchez, G. A., Castillo, E., Huang, J., et al. (2018b). Early-life adversity facilitates acquisition of cocaine self-administration and induces persistent anhedonia. *Neurobiol. Stress* 8, 57–67. doi: 10.1016/j.ynstr.2018.01.002

Bondar, N. P., Lepeshko, A. A., and Reshetnikov, V. V. (2018). Effects of early-life stress on social and anxiety-like behaviors in adult mice: sex-specific effects. *Behav. Neurol.* 2018:1538931. doi: 10.1155/2018/1538931

Brunson, K. L., Kramár, E., Lin, B., Chen, Y., Colgin, L. L., Yanagihara, T. K., et al. (2005). Mechanisms of late-onset cognitive decline after early-life stress. *J. Neurosci.* 25, 9328–9338. doi: 10.1523/JNEUROSCI.2281-05.2005

Calabresi, P., Pisani, A., Mercuri, N. B., and Bernardi, G. (1992). Long-term potentiation in the striatum is unmasked by removing the voltage-dependent magnesium block of NMDA receptor channels. *Eur. J. Neurosci.* 4, 929–935. doi: 10.1111/j.1460-9568.1992.tb00119.x

Chaudhri, N., Sahuque, L. L., Schairer, W. W., and Janak, P. H. (2010). Separable roles of the nucleus accumbens core and shell in context- and cue-induced alcohol-seeking. *Neuropsychopharmacology* 35, 783–791. doi: 10.1038/npp.2009.187

Colich, N. L., Williams, E. S., Ho, T. C., King, L. S., Humphreys, K. L., Price, A. N., et al. (2017). The association between early life stress and prefrontal cortex activation during implicit emotion regulation is moderated by sex in early adolescence. *Dev. Psychopathol.* 29, 1851–1864. doi: 10.1017/S0954579417001444

Dang, M. T., Yokoi, F., Yin, H. H., Lovinger, D. M., Wang, Y., and Li, Y. (2006). Disrupted motor learning and long-term synaptic plasticity in mice lacking NMDAR1 in the striatum. *Proc. Natl. Acad. Sci. U S A* 103, 15254–15259. doi: 10.1073/pnas.0601758103

Davis, E. P., Stout, S. A., Molet, J., Vegetabile, B., Glynn, L. M., Sandman, C. A., et al. (2017). Exposure to unpredictable maternal sensory signals influences cognitive development across species. *Proc. Natl. Acad. Sci. U S A* 114, 10390–10395. doi: 10.1073/pnas.1703444114

Dayananda, K. K., Ahmed, S., Wang, D., Polis, B., Islam, R., and Kaffman, A. (2023). Early life stress impairs synaptic pruning in the developing hippocampus. *Brain Behav. Immun.* 107, 16–31. doi: 10.1016/j.bbi.2022.09.014

Dias-Ferreira, E., Sousa, J. C., Melo, I., Morgado, P., Mesquita, A. R., Cerqueira, J. J., et al. (2009). Chronic stress causes frontostriatal reorganization and affects decision-making. *Science* 325, 621–625. doi: 10.1126/science.1171203

Dong, C., Yang, Q., Liang, J., Seger, C. A., Han, H., Ning, Y., et al. (2020). Impairment in the goal-directed corticostriatal learning system as a biomarker for obsessive-compulsive disorder. *Psychol. Med.* 50, 1490–1500. doi: 10.1017/S0033291719001429

Ellis, S. N., and Honeycutt, J. A. (2021). Sex differences in affective dysfunction and alterations in parvalbumin in rodent models of early life adversity. *Front. Behav. Neurosci.* 15:741454. doi: 10.3389/fnbeh.2021.741454

Eskenazi, D., and Neumaier, J. F. (2011). Increased expression of $5\text{-}HT_6$ receptors in dorsolateral striatum decreases habitual lever pressing, but does not affect learning acquisition of simple operant tasks in rats. *Eur. J. Neurosci.* 34, 343–351. doi: 10.1111/j.1460-9568.2011.07756.x

Fortune, E. S., and Rose, G. J. (2001). Short-term synaptic plasticity as a temporal filter. *Trends Neurosci.* 24, 381–385. doi: 10.1016/s0166-2236(00)01835-x

Frodl, T., Reinhold, E., Koutsouleris, N., Reiser, M., and Meisenzahl, E. M. (2010). Interaction of childhood stress with hippocampus and prefrontal cortex volume reduction in major depression. *J. Psychiatr. Res.* 44, 799–807. doi: 10.1016/j.jpsychires.2010.01.006

Gass, N., Becker, R., Sack, M., Schwarz, A. J., Reinwald, J., Cosa-Linan, A., et al. (2018). Antagonism at the NR2B subunit of NMDA receptors induces increased connectivity of the prefrontal and subcortical regions regulating reward behavior. *Psychopharmacology (Berl)* 235, 1055–1068. doi: 10.1007/s00213-017-4823-2

Gasser, J., de Vasconcelos, A. P., Cosquer, B., Boutillier, A. L., and Cassel, J.-C. (2020). Shifting between response and place strategies in maze navigation: effects of training, cue availability and functional inactivation of striatum or hippocampus in rats. *Neurobiol. Learn. Mem.* 167:107131. doi: 10.1016/j.nlm.2019.107131

Gershon, A., Sudheimer, K., Tirouvanziam, R., Williams, L. M., and O'Hara, R. (2013). The long-term impact of early adversity on late-life psychiatric disorders. *Curr. Psychiatry Rep.* 15:352. doi: 10.1007/s11920-013-0352-9

Gillan, C. M., Papmeyer, M., Morein-Zamir, S., Sahakian, B. J., Fineberg, N. A., Robbins, T. W., et al. (2011). Disruption in the balance between goal-directed behavior and habit learning in obsessive-compulsive disorder. *Am. J. Psychiatry* 168, 718–726. doi: 10.1176/appi.ajp.2011.10071062

Gilles, E. E., Schultz, L., and Baram, T. Z. (1996). Abnormal corticosterone regulation in an immature rat model of continuous chronic stress. *Pediatr. Neurol.* 15, 114–119. doi: 10.1016/0887-8994(96)00153-1

Glynn, L. M., and Baram, T. Z. (2019). The influence of unpredictable, fragmented parental signals on the developing brain. *Front. Neuroendocrinol.* 53:100736. doi: 10.1016/j.yfrne.2019.01.002

Goldstein, R. Z., and Volkow, N. D. (2011). Dysfunction of the prefrontal cortex in addiction: neuroimaging findings and clinical implications. *Nat. Rev. Neurosci.* 12, 652–669. doi: 10.1038/nrn3119

Gremel, C. M., Chancey, J. H., Atwood, B. K., Luo, G., Neve, R., Ramakrishnan, C., et al. (2016). Endocannabinoid modulation of orbitostriatal circuits gates habit formation. *Neuron* 90, 1312–1324. doi: 10.1016/j.neuron.2016.04.043

Gremel, C. M., and Costa, R. M. (2013). Orbitofrontal and striatal circuits dynamically encode the shift between goal-directed and habitual actions. *Nat. Commun.* 4:2264. doi: 10.1038/ncomms3264

Guariglia, S. R., and Chadman, K. K. (2013). Water T-maze: a useful assay for determination of repetitive behaviors in mice. *J. Neurosci. Methods* 220, 24–29. doi: 10.1016/j.jneumeth.2013.08.019

Guariglia, S. R., Jenkins, E. C., Chadman, K. K., and Wen, G. Y. (2011). Chlorination byproducts induce gender specific autistic-like behaviors in CD-1 mice. *Neurotoxicology* 32, 545–553. doi: 10.1016/j.neuro.2011.06.008

Gunn, B. G., Sanchez, G. A., Lynch, G., Baram, T. Z., and Chen, Y. (2019). Hyper-diversity of CRH interneurons in mouse hippocampus. *Brain Struct. Funct.* 224, 583–598. doi: 10.1007/s00429-018-1793-z

Hadjas, L. C., Schartner, M. M., Cand, J., Creed, M. C., Pascoli, V., LÃijscher, C., et al. (2020). Projection-specific deficits in synaptic transmission in adult Sapap3-knockout mice. *Neuropsychopharmacology* 45, 2020–2029. doi: 10.1038/s41386-020-0747-3

Hall, F. S. (1998). Social deprivation of neonatal, adolescent and adult rats has distinct neurochemical and behavioral consequences. *Crit. Rev. Neurobiol.* 12, 129–162. doi: 10.1615/critrevneurobiol.v12.i1-2.50

Hart, G., Bradfield, L. A., and Balleine, B. W. (2018). Prefrontal corticostriatal disconnection blocks the acquisition of goal-directed action. *J. Neurosci.* 38, 1311–1322. doi: 10.1523/JNEUROSCI.2850-17.2017

He, Y., Xu, B., Chen, Y., Liu, L., Xu, L., Chen, Y., et al. (2021). Early-life adversity selectively interrupts the dendritic differentiation of dorsolateral striatal neurons in male mice. *Brain Struct. Funct.* 226, 397–414. doi: 10.1007/s00429-020-02183-7

Hunnicutt, B. J., Jongbloets, B. C., Birdsong, W. T., Gertz, K. J., Zhong, H., and Mao, T. (2016). A comprehensive excitatory input map of the striatum reveals novel functional organization. *eLife* 5:e19103. doi: 10.7554/eLife.19103

Ivy, A. S., Brunson, K. L., Sandman, C., and Baram, T. Z. (2008). Dysfunctional nurturing behavior in rat dams with limited access to nesting material: a clinically relevant model for early-life stress. *Neuroscience* 154, 1132–1142. doi: 10.1016/j.neuroscience.2008.04.019

Ivy, A. S., Rex, C. S., Chen, Y., Dubé, C., Maras, P. M., Grigoriadis, D. E., et al. (2010). Hippocampal dysfunction and cognitive impairments provoked by chronic early-life stress involve excessive activation of CRH receptors. *J. Neurosci.* 30, 13005–13015. doi: 10.1523/JNEUROSCI.1784-10.2010

Jenrette, T. A., Logue, J. B., and Horner, K. A. (2019). Lesions of the patch compartment of dorsolateral striatum disrupt stimulus-response learning. *Neuroscience* 415, 161–172. doi: 10.1016/j.neuroscience.2019.07.033

Kessler, R. C., McGonagle, K. A., Zhao, S., Nelson, C. B., Hughes, M., Eshleman, S., et al. (1994). Lifetime and 12-month prevalence of DSM-III-R psychiatric disorders in the United States. Results from the National Comorbidity Survey. *Arch. Gen. Psychiatry* 51, 8–19. doi: 10.1001/archpsyc.1994.03950010008002

Kocaturk, S., Guven, E. B., Shah, F., Tepper, J. M., and Assous, M. (2022). Cholinergic control of striatal GABAergic microcircuits. *Cell Rep.* 41:111531. doi: 10.1016/j.celrep.2022.111531

Koob, G. F., and Volkow, N. D. (2010). Neurocircuitry of addiction. *Neuropsychopharmacology* 35, 217–238. doi: 10.1038/npp.2009.110

Korosi, A., Shanabrough, M., McClelland, S., Liu, Z. W., Borok, E., Gao, X. B., et al. (2010). Early-life experience reduces excitation to stress-responsive hypothalamic neurons and reprograms the expression of corticotropin-releasing hormone. *J. Neurosci.* 30, 703–713. doi: 10.1523/JNEUROSCI.4214-09.2010

Ladd, C. O., Huot, R. L., Thrivikraman, K. V., Nemeroff, C. B., Meaney, M. J., and Plotsky, P. M. (2000). Long-term behavioral and neuroendocrine adaptations to adverse early experience. *Prog. Brain Res.* 122, 81–103. doi: 10.1016/s0079-6123(08)62132-9

Lapp, H. E., Bartlett, A. A., Zup, S. L., Hunter, R. G., and Moore, C. L. (2020). Early experience alters developmental trajectory of central oxytocin systems involved in hypothalamic-pituitary-adrenal axis regulation in Long-Evans rats. *Horm. Behav.* 126:104822. doi: 10.1016/j.yhbeh.2020.104822

Lemay-Clermont, J., Robitaille, C., Auberson, Y. P., Bureau, G., and Cyr, M. (2011). Blockade of NMDA receptors 2A subunit in the dorsal striatum impairs the learning of a complex motor skill. *Behav. Neurosci.* 125, 714–723. doi: 10.1037/a0025213

Levis, S. C., Bentzley, B. S., Molet, J., Bolton, J. L., Perrone, C. R., Baram, T. Z., et al. (2021). On the early life origins of vulnerability to opioid addiction. *Mol. Psychiatry* 26, 4409–4416. doi: 10.1038/s41380-019-0628-5

Levis, S. C., Birnie, M. T., Bolton, J. L., Perrone, C. R., Montesinos, J. S., Baram, T. Z., et al. (2022). Enduring disruption of reward and stress circuit activities by early-life adversity in male rats. *Transl. Psychiatry* 12:251. doi: 10.1038/s41398-022-01988-w

Merrick, M. T., Ford, D. C., Ports, K. A., Guinn, A. S., Chen, J., Klevens, J., et al. (2019). Vital signs: estimated proportion of adult health problems attributable to adverse childhood experiences and implications for prevention - 25 states, 2015-2017. *MMWR Morb. Mortal. Wkly. Rep.* 68, 999–1005. doi: 10.15585/mmwr.mm6844e1

Millan, E. Z., Ong, Z., and McNally, G. P. (2017). Paraventricular thalamus: gateway to feeding, appetitive motivation and drug addiction. *Prog. Brain Res.* 235, 113–137. doi: 10.1016/bs.pbr.2017.07.006

Molchanova, S. M., Comhair, J., Karadurmus, D., Piccart, E., Harvey, R. J., Rigo, J.-M., et al. (2018). Tonically active α2 subunit-containing glycine receptors regulate the excitability of striatal medium spiny neurons. *Front. Mol. Neurosci.* 10:442. doi: 10.3389/fnmol.2017.00442

Molet, J., Heins, K., Zhuo, X., Mei, Y. T., Regev, L., Baram, T. Z., et al. (2016). Fragmentation and high entropy of neonatal experience predict adolescent emotional outcome. *Transl. Psychiatry* 6:e702. doi: 10.1038/tp.2015.200

Morris, R. W., Quail, S., Griffiths, K. R., Green, M. J., and Balleine, B. W. (2015). Corticostriatal control of goal-directed action is impaired in schizophrenia. *Biol. Psychiatry* 77, 187–195. doi: 10.1016/j.biopsych.2014.06.005

Naninck, E. F. G., Hoeijmakers, L., Kakava-Georgiadou, N., Meesters, A., Lazic, S. E., Lucassen, P. J., et al. (2015). Chronic early life stress alters developmental and adult neurogenesis and impairs cognitive function in mice. *Hippocampus* 25, 309–328. doi: 10.1002/hipo.22374

Oomen, C. A., Girardi, C. E., Cahyadi, R., Verbeek, E. C., Krugers, H., Joëls, M., et al. (2009). Opposite effects of early maternal deprivation on neurogenesis in male versus female rats. *PLoS One* 4:e3675. doi: 10.1371/journal.pone.0003675

Ordoñes Sanchez, E., Comhair, J., Karadurmus, D., Piccart, E., Harvey, R. J., Rigo, J. M., et al. (2021). Early life adversity promotes resilience to opioid addiction-related phenotypes in male rats and sex-specific transcriptional changes. *Proc. Natl. Acad. Sci. U S A* 118:e2020173118. doi: 10.1073/pnas.2020173118

Rice, C. J., Sandman, C. A., Lenjavi, M. R., and Baram, T. Z. (2008). A novel mouse model for acute and long-lasting consequences of early life stress. *Endocrinology* 149, 4892–4900. doi: 10.1210/en.2008-0633

Ruigrok, S. R., Kotah, J. M., Kuindersma, J. E., Speijer, E., van Irsen, A. A. S., la Fleur, S. E., et al. (2021a). Adult food choices depend on sex and exposure to early-life stress: underlying brain circuitry, adipose tissue adaptations and metabolic responses. *Neurobiol. Stress* 15:100360. doi: 10.1016/j.ynstr.2021.100360

Ruigrok, S. R., Stöberl, N., Yam, K. Y., de Lucia, C., Lucassen, P. J., Thuret, S., et al. (2021b). Modulation of the hypothalamic nutrient sensing pathways by sex and early-life stress. *Front. Neurosci.* 15:695367. doi: 10.3389/fnins.2021.695367

Russell, P. A. (1973). Effects of maternal separation and maternal disturbance on offspring growth and behavior in rats. *J. Gen. Psychol.* 88, 127–133. doi: 10.1080/00221309.1973.9920718

Simmler, L. D., and Ozawa, T. (2019). Neural circuits in goal-directed and habitual behavior: implications for circuit dysfunction in obsessive-compulsive disorder. *Neurochem. Int.* 129:104464. doi: 10.1016/j.neuint.2019.104464

Smith, K. S., and Graybiel, A. M. (2016). Habit formation coincides with shifts in reinforcement representations in the sensorimotor striatum. *J. Neurophysiol.* 115, 1487–1498. doi: 10.1152/jn.00925.2015

Taverna, S., van Dongen, Y. C., Groenewegen, H. J., and Pennartz, C. M. A. (2004). Direct physiological evidence for synaptic connectivity between medium-sized spiny neurons in rat nucleus accumbens *in situ*. *J. Neurophysiol.* 91, 1111–1121. doi: 10.1152/jn.00892.2003

Tepper, J. M., Sharpe, N. A., Koós, T. Z., and Trent, F. (1998). Postnatal development of the rat neostriatum: electrophysiological, light- and electron-microscopic studies. *Dev. Neurosci.* 20, 125–145. doi: 10.1159/000017308

Terra, H., Bruinsma, B., Pattij, T., and Mansvelder, H. D. (2020). Prefrontal cortical projection neurons targeting dorsomedial striatum control behavioral inhibition. *Curr. Biol.* 30, 4188–4200.e5. doi: 10.1016/j.cub.2020.08.031

van Hasselt, F. N., Boudewijns, Z. S., van der Knaap, N. J. F., Krugers, H. J., and Joëls, M. (2012). Maternal care received by individual pups correlates with adult CA1 dendritic morphology and synaptic plasticity in a sex-dependent manner. *J. Neuroendocrinol.* 24, 331–340. doi: 10.1111/j.1365-2826.2011.02233.x

Wang, L., Jiao, J., and Dulawa, S. C. (2011). Infant maternal separation impairs adult cognitive performance in BALB/cJ mice. *Psychopharmacology (Berl)* 216, 207–218. doi: 10.1007/s00213-011-2209-4

Xu, B., Zhang, X., He, Y., Liu, C., Li, L., Liu, Q., et al. (2022). The impacts of early-life adversity on striatal and hippocampal memory functions. *Neuroscience* 490, 11–24. doi: 10.1016/j.neuroscience.2022.02.029

Yin, H. H., and Knowlton, B. J. (2004). Contributions of striatal subregions to place and response learning. *Learn. Mem.* 11, 459–463. doi: 10.1101/lm.81004

Yin, H. H., Knowlton, B. J., and Balleine, B. W. (2004). Lesions of dorsolateral striatum preserve outcome expectancy but disrupt habit formation in instrumental learning. *Eur. J. Neurosci.* 19, 181–189. doi: 10.1111/j.1460-9568.2004.03095.x

Yin, H. H., Knowlton, B. J., and Balleine, B. W. (2005a). Blockade of NMDA receptors in the dorsomedial striatum prevents action-outcome learning in instrumental conditioning. *Eur. J. Neurosci.* 22, 505–512. doi: 10.1111/j.1460-9568.2005.04219.x

Yin, H. H., Knowlton, B. J., and Balleine, B. W. (2006). Inactivation of dorsolateral striatum enhances sensitivity to changes in the action-outcome contingency in instrumental conditioning. *Behav. Brain Res.* 166, 189–196. doi: 10.1016/j.bbr.2005.07.012

Yin, H. H., Ostlund, S. B., Knowlton, B. J., and Balleine, B. W. (2005b). The role of the dorsomedial striatum in instrumental conditioning. *Eur. J. Neurosci.* 22, 513–523. doi: 10.1111/j.1460-9568.2005.04218.x

Zoladz, P., Reneau, K., Weiser, J., Cordes, C., Virden, E., Helwig, S., et al. (2022). Childhood maltreatment in females is associated with enhanced fear acquisition and an overgeneralization of fear. *Brain Sci.* 12:1536. doi: 10.3390/brainsci12111536

Zucker, R. S., and Regehr, W. G. (2002). Short-term synaptic plasticity. *Annu. Rev. Physiol.* 64, 355–405. doi: 10.1146/annurev.physiol.64.092501.114547

frontiers | Frontiers in Synaptic Neuroscience

TYPE Original Research
PUBLISHED 06 April 2023
DOI 10.3389/fnsyn.2023.1042858

OPEN ACCESS

EDITED BY
Lu Chen,
Stanford University, United States

REVIEWED BY
Peng Cao,
National Institute of Biological Sciences (NIBS), China
José M. Delgado-García,
Universidad Pablo de Olavide, Spain

*CORRESPONDENCE
Wei Xu
✉ wei.xu1@utsouthwestern.edu

RECEIVED 13 September 2022
ACCEPTED 09 March 2023
PUBLISHED 06 April 2023

CITATION
Chen Y-T, Arano R, Guo J, Saleem U, Li Y and Xu W (2023) Inhibitory hippocampus-medial septum projection controls locomotion and exploratory behavior.
Front. Synaptic Neurosci. 15:1042858.
doi: 10.3389/fnsyn.2023.1042858

Inhibitory hippocampus-medial septum projection controls locomotion and exploratory behavior

Yuh-Tarng Chen, Rachel Arano, Jun Guo, Uzair Saleem, Ying Li and Wei Xu*

Department of Neuroscience, The University of Texas Southwestern Medical Center, Dallas, TX, United States

Although the hippocampus is generally considered a cognitive center for spatial representation, learning, and memory, increasing evidence supports its roles in regulating locomotion. However, the neuronal mechanisms of the hippocampal regulation of locomotion and exploratory behavior remain unclear. In this study, we found that the inhibitory hippocampal synaptic projection to the medial septum (MS) bi-directionally controls the locomotor speed of mice. The activation of the MS-projecting interneurons in the hippocampus or the activation of the hippocampus-originated inhibitory synaptic terminals in the MS decreased locomotion and exploratory behavior. On the other hand, the inhibition of the hippocampus-originated inhibitory synaptic terminals in the MS increased locomotion. Unlike the septal projecting interneurons, the activation of the hippocampal interneurons projecting to the retrosplenial cortex did not change animal locomotion. Therefore, this study reveals a specific long-range inhibitory synaptic output from the hippocampus to the medial septum in the regulation of animal locomotion.

KEYWORDS

hippocampus, septum, GABAergic interneuron, inhibitory synapse, locomotion, exploratory behavior

Introduction

Moving and exploring freely in an environment are essential skills for constructing a neuronal representation of the world and hence survival. Locomotion is regulated by brain motor systems consisting of brain regions such as the motor cortex, basal ganglia, thalamus, and spinal cord (Ferreira-Pinto et al., 2018). Normally, the hippocampus is considered not a component of this system but rather a cognitive center that integrates multi-modal sensory information and spatial/temporal relations to construct a representation and memory of the world (Eichenbaum, 2004; Buzsaki and Moser, 2013). However, accumulating evidence indicates a direct role of the hippocampus in regulating locomotion.

First, hippocampal neuronal activities, especially those in the dorsal hippocampus, are associated with locomotion. Most noticeably, the activity level of some hippocampal neurons directly reflects the speed of animals (McNaughton et al., 1983; Geisler et al., 2007; Gois and Tort, 2018; Iwase et al., 2020). Interestingly, many of these "speed cells" are found to be inhibitory GABAergic "interneurons" (Gois and Tort, 2018; Iwase et al., 2020). Second, lesions or pathogenic damages to the hippocampus are frequently accompanied by alterations in locomotion (Sams-Dodd et al., 1997; Katsuta et al., 2003; Godsil et al., 2005; White et al., 2006). Third, direct functional manipulations of the hippocampal neuronal

activities with optogenetic or pharmacogenetic stimuli altered animal locomotion (Bender et al., 2015; Wolff et al., 2018). However, many studies reported the opposite results. For example, the electrolytic lesion of the hippocampus caused hyperlocomotion (Douglas and Isaacson, 1964) and enhanced the locomotion-stimulating effect of amphetamine (Swerdlow et al., 2001), while the aspiration lesion of the hippocampus did not produce similar impacts (Douglas and Isaacson, 1964). Furthermore, unlike in the study mentioned earlier, some pharmacological, optogenetic, or pharmacogenetic treatments of the hippocampus failed to change animal locomotion (Zhang et al., 2002; Degoulet et al., 2008; Goshen et al., 2011; Lopez et al., 2016; Bian et al., 2019).

The contradictory results may arise from the anatomical and functional heterogeneity of the hippocampus. The hippocampus has multiple functional divisions along its longitudinal and transversal axis (Soltesz and Losonczy, 2018). It consists of numerous neuronal types including both excitatory glutamatergic principal neurons and inhibitory GABAergic interneurons (Pelkey et al., 2017). It is possible that different divisions or cell types were preferentially impacted in the aforementioned studies and generated different behavioral phenotypes. To test this possibility, we focused on the GABAergic outputs from the hippocampus to examine their specific contributions to the regulation of locomotion. We found that among hippocampal GABAergic outputs, those to the medial septum (MS) were particularly engaged in locomotion regulation. Consistent with earlier studies showing the importance of the hippocampus-to-lateral septum pathway (Bender et al., 2015), this study reveals a new hippocampal mechanism for locomotion regulation.

Materials and methods

Animals

8- to 12-week-old C57BL/6J (B6J) male mice were obtained from UT Southwestern animal breeding core or The Jackson Laboratory. We used heterozygotes (±) NDNF-Cre transgenic male mice and maintained them on a C57BL/6J background (The Jackson Laboratory). Animal work was approved and conducted under the oversight of the UT Southwestern Institutional Animal Care and Use Committee and complied with the Guide for the Care and Use of Laboratory Animals by the National Research Council.

AAV vectors

AAV-Dlx-SynaptoTAG was made by switching the Synapsin promoter to the Dlx promoter in the SynaptoTAG2 AAV vector (Li et al., 2021). We also added the coding sequence of GAP43 palmitoylation sequence "MLCCMRRTKQVEKNDEDQKIE" to the 5′ of the tdTomato coding sequence. Construction of the other AAV vectors, packaging, and tittering of AAVs was the same as previously described (Guo et al., 2021). The titers of the AAVs for stereotaxic intracranial injections were in the range of 1E13 to 3E13 copies/ml.

Stereotaxic surgery and adeno-associated virus injection

Mice were anesthetized with an intraperitoneal (i.p.) injection of tribromoethanol (Avertin) (125–250 mg/kg) before the stereotaxic surgery or anesthetized with 1–3% isoflurane and placed on a stereotaxic instrument (Kopf Instruments). To identify the septum-projecting hippocampal GABAergic interneurons, AAV-Dlx-SynaptoTAG (0.5 μl) was injected into the CA1 (coordinates A/P −1.95 mm, M/L ±1.25 mm, and D/V 1.25 mm). To manipulate the septum-projecting hippocampal GABAergic interneurons, AAV2-retro-Cre (0.75 μl) was injected into the septum (coordinates: A/P 0.80 mm, M/L ±0.00 mm, and D/V 4.20 mm) and infused slowly over 7.5 min (rate: 0.1 μl/min), and then AAV-dlx-DIO-hM3Dq-mCherry was injected into the CA1 (coordinates A/P −1.95 mm, M/L ± 1.25 mm, and D/V 1.25 mm).

To optogenetically activate the hippocampal inhibitory output to the septum, AAV-Dlx-DIO-ChIEF-EGFP and AAV-Syn-Cre were mixed in the ratio of 4:1 (to optically inhibit the hippocampal inhibitory output to the septum, we used the virus mixture of AAV-Dlx-DIO-Jaws-EGFP and AAV-Syn-Cre). Viruses (0.5 μl for each target) were infused slowly over 5 min (rate: 0.1 μl/min) into the CA1 (coordinates A/P −1.95 mm, M/L ±1.25 mm, and D/V 1.25 mm) bilaterally using a microdriver with a 10 μl Halmiton syringe connected to a glass pipette; after the virus injection, flat-cut 400 μm diameter optic fiber with ferrule (Ø 400 μm; CFM14U-20, Thorlabs) was implanted on the top of the medial septum (A/P 0.60 mm, M/L 0.00 mm, and D/V 2.50 mm) and cemented in place using dental cement and CandB-Metabond (Patterson Dental, MN).

To pharmacogenetically manipulate the hippocampal output to the septum, the viruses, AAV-dlx-DIO-hM3Dq-mCherry and AAV-Syn-Cre, were mixed in the ratio of 4:1 (0.5 μl for each target) using the same stereotaxic coordinates to target the CA1. After the virus injection, a gauge 28 guide-cannula was implanted on the top of the medial septum (A/P 0.60 mm, M/L 0.00 mm, and D/V 2.50 mm) and cemented in place using dental cement and CandB-Metabond (Patterson Dental, MN).

To pharmacogenetically manipulate the NDNF-expressing interneurons in the hippocampus, we bilaterally injected 0.5 μl of AAV hDlx-DIO-hM3Dq-mCherry in the dorsal hippocampus (A/P: −1.95, mm, M/L: +1.25 mm, and D/V: 1.45 mm) of NDNF-Cre+ and Cre− littermates.

Brain slice electrophysiology

After >8 weeks of injection of AAVs (AAV-Dlx-DIO-ChIEF-EGFP and AAV-Syn-Cre mixed in the ratio of 4:1), coronal slices of the septum (300 μm) were prepared with a vibratome (Leica VT1200) in an ice-cold cutting solution containing (in mM) 75 sucrose, 85 NaCl, 2.5 KCl, 1.3 NaH_2PO4, 4 $MgSO_4$, 0.5 $CaCl_2$, 24 $NaHCO_3$, and 25 D-glucose, saturated with 95% O_2/5% CO_2. The slices were incubated for 30 min in artificial cerebrospinal fluid (ACSF) containing (in mM) 124 NaCl, 5 KCl, 1.2 NaH2PO4, 26 NaHCO3, 10 D-glucose, 1.3 MgCl2, and 2.5 CaCl2 at 32°C and then incubated for at least 1 h at room temperature. The cutting

solution and ACSF were adjusted to a pH of 7.3–7.4, 290–300 mOsm, and constantly aerated with 95% O_2/5% CO_2. The whole-cell patch-clamp recording was performed in a recording chamber perfused (∼1 ml/min) with oxygenated ACSF at 26–28°C. The recording pipettes (2.2–3 MΩ) were filled with an internal solution containing (in mM) 120 CsCl, 5 NaCl, 10 HEPES, 10 EGTA, 1 MgCl2, 3 Mg-ATP, 0.3 GTP, and 10 QX-314, adjusted to a pH of 7.3–7.4 and 310 mOsm. For optogenetic experiments, blue light (473 nm) was delivered by an LED coupled with a 40× water objective. Some of the recordings were conducted with Picrotoxin (50 μM) and CGP55845 (10 μM) in the ACSF.

Optogenetic and pharmacogenetic manipulation

For optogenetics in the ChIEF experiment, a blue laser was delivered through a fiber optic cord using a DPSS Blue 473 nm laser source (MBL-III-473/1–100 mW, Opto Engine LLC). A train of blue laser pulses (10 mW, 20 Hz, 10 ms duration, and 40 ms interval) was generated and controlled by an Optogenetics Pulser (Prizmatix). In Jaw's experiments, continuous orange-red LED was delivered through a fiber optic cord using a high-power orange-red ∼625 nm LED module at 10 mW (Prizmatix). The light intensity was calibrated with the PM100D Console (Thorlabs). For pharmacogenetic experiments, i.p. injections of clozapine (0444, Tocris Bioscience) (0.1 mg/kg) or control vehicle saline (0.9% NaCl) were administered 30 min before the behavioral test. For terminal manipulation experiments, intracranial injections of 300 nl clozapine (0.001 mg/ml) or control vehicle saline (0.9% NaCl) were administered 15 min before the behavioral test.

Open-field test

Animals were handled for 1–2 min a day for 7 days before the open-field test. The open-field apparatus was a custom-made 50 × 50 cm testing chamber. A video camera was placed above the open field, and mice traces were tracked using the ANY-maze video tracking system. Mice were placed in the center of the open-field area prior to the initiation of tracking. The center of the open field was defined as 20 × 20 cm square in the geometric center of the arena. Each chamber was cleaned between individual animal testing. To calculate the percentage of the open-field area each mouse explored, the open-field arena was divided into 100 grids (5 × 5 cm). If the mouse passed through the corresponding grid, then the grid would be counted as being explored. The exploration percentage of the open field ranges from 1 to 100%.

Elevated plus maze

Animals used in the elevated plus maze (EPM) were tested in the open field before. The EPM apparatus was elevated 38.7 cm above the floor and consisted of two open arms (30.5 cm in length and 5 cm in width) and two closed arms (30.5 cm in length; 6 cm high wall; and 5 cm in width). Open arms and closed arms were all connected to a center platform in the middle (5 cm in length and width). The behavior was recorded and analyzed by the ANY-maze video tracking system.

Tissue processing, immunohistochemistry, and cell counting

For regular preparation with no need to do immunohistochemical staining, mice were anesthetized by an intraperitoneal (i.p.) injection of tribromoethanol (Avertin) or anesthetized with 1–3% isoflurane and were perfused with phosphate-buffered saline (PBS) followed by 4% paraformaldehyde (PFA) in PBS. Brains were post-fixed in 4% PFA overnight and were cryoprotected in 30% sucrose. Brains were cut into 40 μm sections on a cryostat (Leica CM1950) and were collected in PBS and stored at 4°C. Finally, sections were then mounted on slides and stained with DAPI. Sections were imaged on a Zeiss LSM 880 confocal microscope with a 5×, 10×, and 20× objective under the control of Zen software.

For c-Fos immunohistochemistry staining, mice were injected with clozapine (0.1 mg/kg) and then transferred to a new clean cage and singly housed for 1 h before the perfusion. Brains were post-fixed in 4% PFA overnight and were cryoprotected in 30% sucrose. Brains were cut into 30 μm sections on a cryostat (Leica CM1950) and were collected in PBS. Sections were washed in PBS and blocked in 10% horse serum, 0.2% bovine serum albumin (BSA), and 0.5% Triton X-100 in PBS for 2 h at room temperature. For immunohistochemistry staining, sections were incubated overnight in primary antibodies [anti-cFos antibody: 1:1,000, catalog # 226 003, Synaptic Systems (SYSY)] with 1% horse serum, 0.2% BSA, and 0.5% Triton X-100 in PBS at 4°C. Sections were washed in PBS and reacted with fluorescent secondary antibodies (goat anti-rabbit Alexa Fluor 488, 1:500, Invitrogen, catalog # A-11034) in 1% horse serum, 0.2% BSA, and 0.5% Triton X-100 in PBS for 2 h at room temperature. Sections were then mounted on slides and stained with DAPI. Sections were imaged on the Zeiss LSM 880 confocal microscope with a 5×, 10×, and 20× objective under the control of Zen software.

To quantify the number of activated hM3Dq expressing septum-projecting inhibitory cells in the hippocampus, the hippocampus was outlined as a region of interest (ROI), and the colocalization ratio was calculated as [($cFos^+$ and $mCherry^+$)/($mCherry^+$)] × 100. To quantify the fluorescence intensity of the hippocampal projections in each innervated region, the mean intensity of each ROI was acquired using ZEISS ZEN Microscope Software. The normalized fluorescence intensity was calculated as (mean fluorescence intensity)/(average mean fluorescence intensity of the medial septum).

Statistical analysis

Data are presented as mean ± SEM, and all statistical analyses of the data were performed using GraphPad Prism software (GraphPad Software Inc., La Jolla, USA). Student's unpaired *t*-test

was used to analyze two independent samples and the paired *t*-test was used to analyze two dependent samples. To test the optical stimulation effects in two groups, open-field results were analyzed by two-way repeated measures ANOVA with "Order" and "Light" as within-subject factors followed by multiple comparisons tests. A 1 h (5-min bin) open field was analyzed by two-way repeated measure ANOVA with time (minutes) as a within-subject factor and "Group" as a between-subject factor followed by multiple comparisons tests. The Kolmogorov–Smirnov test was used to compare the speed distribution of the two groups. The Mann–Whitney *U*-test was used to compare c-Fos activity (Figure 3B) and speed latency (Figure 4H). A p-value of <0.05 was considered statistically significant.

Results

GABAergic hippocampus-septum projections

Although commonly referred to as "interneurons," many GABAergic inhibitory neurons in the hippocampus send long-range projections to extrahippocampal regions (Klausberger and Somogyi, 2008). In this study, we focused on the role of these hippocampal inhibitory outputs in regulating locomotion. We first examined the distribution of the long-range hippocampal GABAergic projections. We constructed an adeno-associated virus (AAV) vector (AAV-Dlx-SynaptoTAG) to trace from GABAergic neurons (Figure 1A). This AAV expresses a green fluorescent protein, EGFP, fused with synaptic vesicle protein, Synaptobrevin-2, to label synaptic terminals, and tdTomato to fill the soma and axons, under the control of GABAergic neuron-specific Dlx promoter (Dimidschstein et al., 2016). The tdTomato is fused to the palmitoylation sequence of GAP43 to increase the axonal targeting of the fusion protein (Palm-tdTomato). We injected this AAV into the CA1 region of the dorsal hippocampus. In CA1, we observed the soma of labeled interneurons and densely distributed perisomatic synapses in the pyramidal layer, and less dense synaptic terminals in the other layers (Figures 1B, C). Inside the hippocampal formation (but outside CA1), the subiculum (SUB) had the highest density of EGFP-positive boutons. Outside the hippocampus, tdTomato and EGFP were detected in limited brain regions, including the medial septum (MS), the nucleus of the diagonal band (NDB), the superficial portion of layer 1 of the retrosplenial area (RSP), and to a much less degree, the transition area between the perirhinal cortex (PRC) and entorhinal cortex (EC), consistent with earlier studies (Gulyas et al., 2003; Jinno et al., 2007; Muller and Remy, 2018) (Figures 1B–E).

To confirm that the traced synaptic boutons at the MS are functional synapses, we expressed excitatory channelrhodopsin ChIEF in the CA1 GABAergic interneurons so that we can activate these neurons by light. We locally injected two AAVs into the CA1: one expressing recombinase Cre and the other ChIEF-tdTomato under the Dlx promoter in a Cre-dependent manner. Cre's expression would turn on the expression of ChIEF-tdTomato. Approximately 2 months after the AAV injection, we prepared acute brain slices containing the MS for whole-cell patch-clamp recordings (Figure 2A). We recorded neurons close to the midline of the septum either in the middle of or right next to the dense axonal bundles running in the midline. Among the 11 neurons from three mice recorded in the absence of antagonists of GABA receptors, optical stimuli elicited postsynaptic currents (PSCs) in nine neurons (Figures 2B, C). A total of eight out of the nine showed success rates (the possibility of each light pulse to evoke PSCs) of 100%, and one neuron had a lower success rate of 56.6%. To determine if the optically evoked PSCs were inhibitory synaptic currents, we recorded neurons in the presence of GABA receptor antagonists, including the GABA-A receptor blocker picrotoxin and the GABA-B receptor antagonist CGP55845. With these antagonists, optical stimuli did not elicit PSCs in the 13 neurons we recorded from two mice although some spontaneous synaptic activities (presumably excitatory postsynaptic currents) could still be observed, indicating that the optically elicited PSCs were GABAergic.

Activation of septum-projecting hippocampal interneurons decreases locomotion

To functionally control these septum-projecting hippocampal GABAergic interneurons, we injected AAV2-retro-Cre into the MS and injected Cre-dependent AAV (AAV-Dlx-DIO-hM3Dq-mCherry) into CA1 (Figure 3A). AAV2-retro-Cre can enter the synaptic terminals that lie in the MS but originate from the hippocampal neurons and is transported back to the soma in CA1 (Tervo et al., 2016). At CA1, the expression of Cre turns on the expression of hM3Dq that only occurs in interneurons due to the Dlx promoter. hM3Dq is an excitatory Designer Receptors Exclusively Activated by Designer Drugs (DREADD) effector that can be activated by its ligand clozapine or clozapine N-oxide (CNO) (Roth, 2016; Gomez et al., 2017). With immunostaining of c-Fos, an immediate early gene reporting neuronal activities, we confirmed that a low dose of clozapine (0.1 mg/kg, intraperitoneal injection) increased the activity of hM3Dq-positive hippocampal GABAergic interneurons, which project to the septum (Figure 3B). We then examined the mice in behavioral tests. In an open field, the mice decreased the speed of locomotion and exploratory behavior with the injection of clozapine (Figure 3C; Supplementary Figure 1) without any change in the time spent in the center of the open-field arena, a parameter frequently used to monitor the anxiety level (Figure 3D). Similarly, the mice did not show a phenotype in an elevated-plus maze test, another frequently used assay for anxiety (Figure 3D). In addition to anxiety, the septum is known to be involved in the expression of other emotional or motivational behaviors. We did not observe other apparent behavioral abnormalities in these mice after the treatments. These results indicate that septum-projecting hippocampal GABAergic interneurons negatively regulate mouse locomotion.

Activation of hippocampal inhibitory synapses in the MS decreases locomotion

The septum-projecting hippocampal GABAergic interneurons may regulate locomotion by inhibiting the local hippocampal network or through their actions in the MS. To determine if

10.3389/fnsyn.2023.1042858

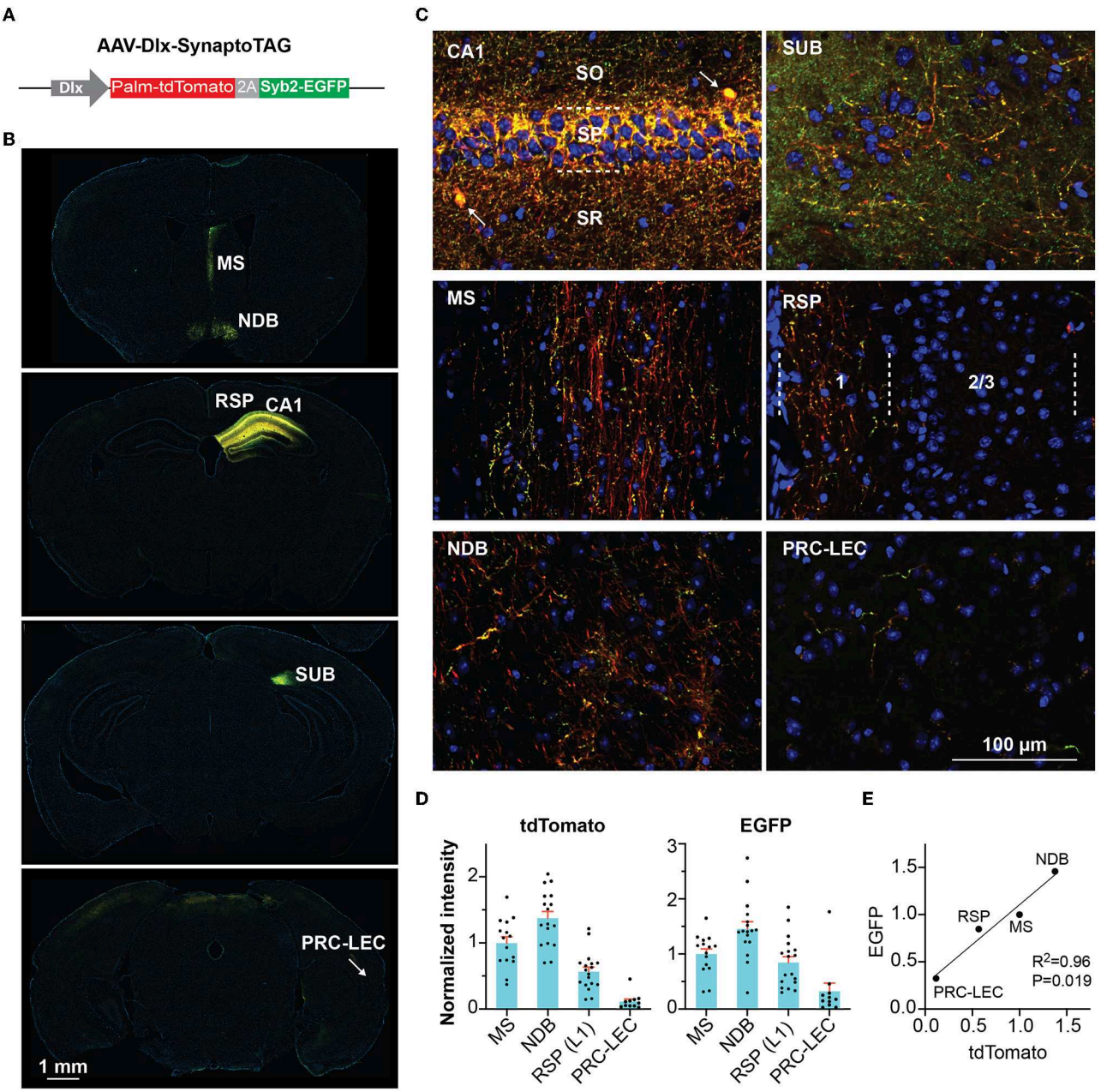

FIGURE 1
Tracing GABAergic outputs from the hippocampal CA1 region. **(A)** Design of AAV-Dlx-SynaptoTAG. **(B, C)** Low- and high-resolution representative images showing the Palm-tdTomato-positive axons and EGFP-positive boutons in the respective brain regions. The axons and boutons from CA1 GABAergic neurons were detected at the hippocampus, subiculum (SUB), medial septum (MS), and nucleus of the diagonal band (NDB), and the superficial portion of layer 1 of the retrosplenial area (RSP), and the transition area between the perirhinal cortex and the entorhinal cortex (PRC-EC). **(D)** Quantification of the fluorescence intensities in the different brain regions. The intensities were measured from 11 to 17 sections for each region from four mice. Data are represented as mean ± SEM **(E)** Correlation between the averaged intensities of EGFP and tdTomato measured in the brain regions.

their synapses in the MS are sufficient to regulate locomotion, we stimulated these synaptic terminals with locally injected CNO through cannula implanted into the MS to activate hM3Dq (Figure 4A). The injection of CNO into the MS decreased locomotion (Figure 4B), similar to the effects produced by activating the septum-projecting hippocampal GABAergic interneurons (Figure 3C), suggesting that through the direct inhibition of axons in the MS, the septum-projecting hippocampal GABAergic interneurons negatively regulate locomotion.

To temporally precisely control the projections to the MS, we expressed ChIEF in hippocampal interneurons and delivered light to the MS to stimulate the GABAergic hippocampal axons there (Figure 4C). Optical stimulation acutely decreased mouse locomotor activities measured by multiple parameters including

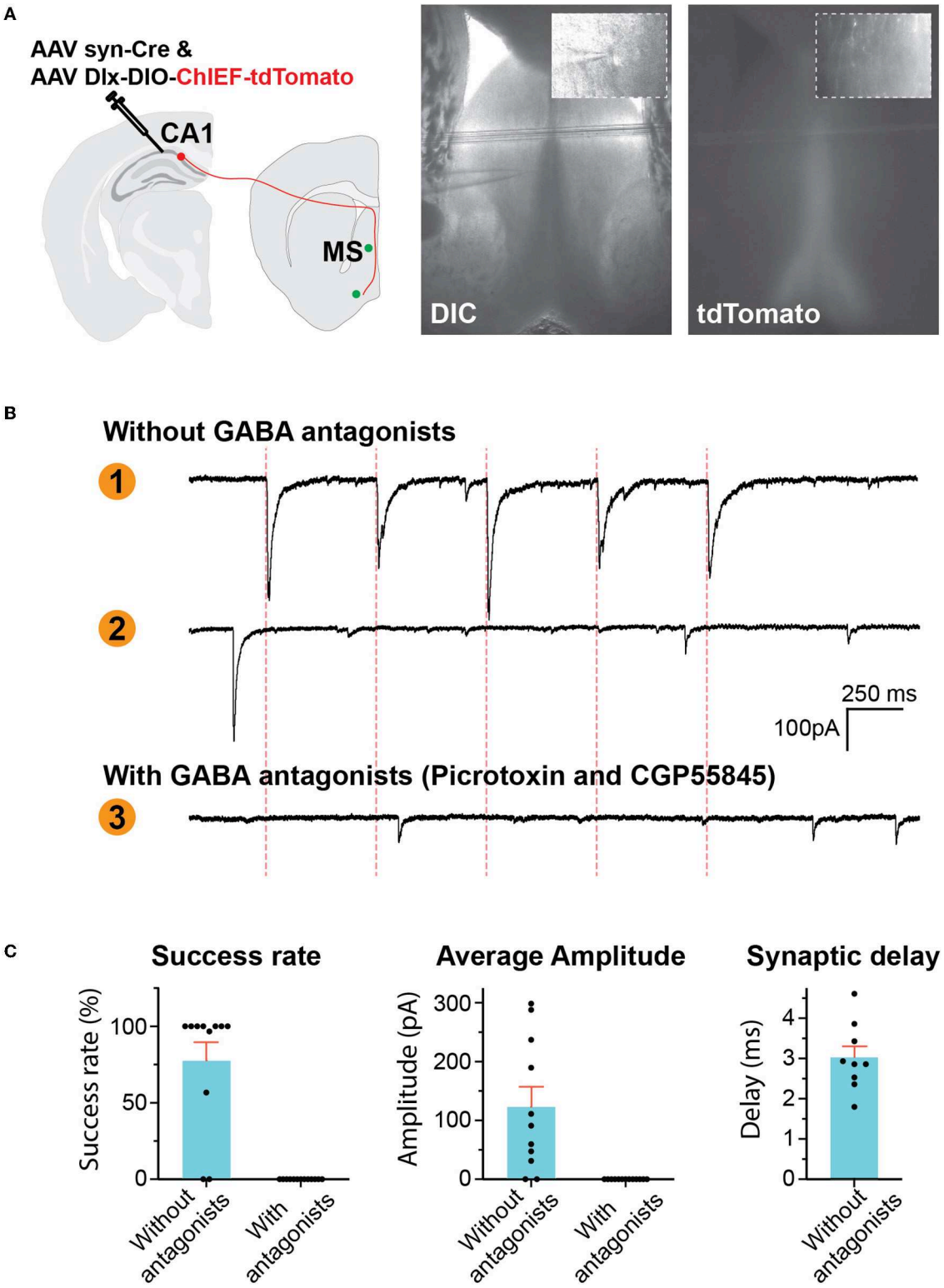

FIGURE 2
GABAergic hippocampus–septum projections. **(A)** AAV injection scheme (left). Representative photos of brain slice (right) showing the location of tdTomato-positive axons in the MS and the location of whole-cell patch-clamp recording. The inserts are high-resolution images of the location of the pipette tip. **(B)** Representative traces of voltage-clamp recording of postsynaptic currents (PSCs). Traces 1 and 2 were recorded in the absence of GABA antagonists, showing a neuron reacting to optical stimulation (Trace 1) and another neuron not responding (Trace 2). Trace 3 was recorded in the presence of picrotoxin and CGP55845. The red dashed lines indicate the time of optical stimuli. **(C)** Quantification of the PSCs.

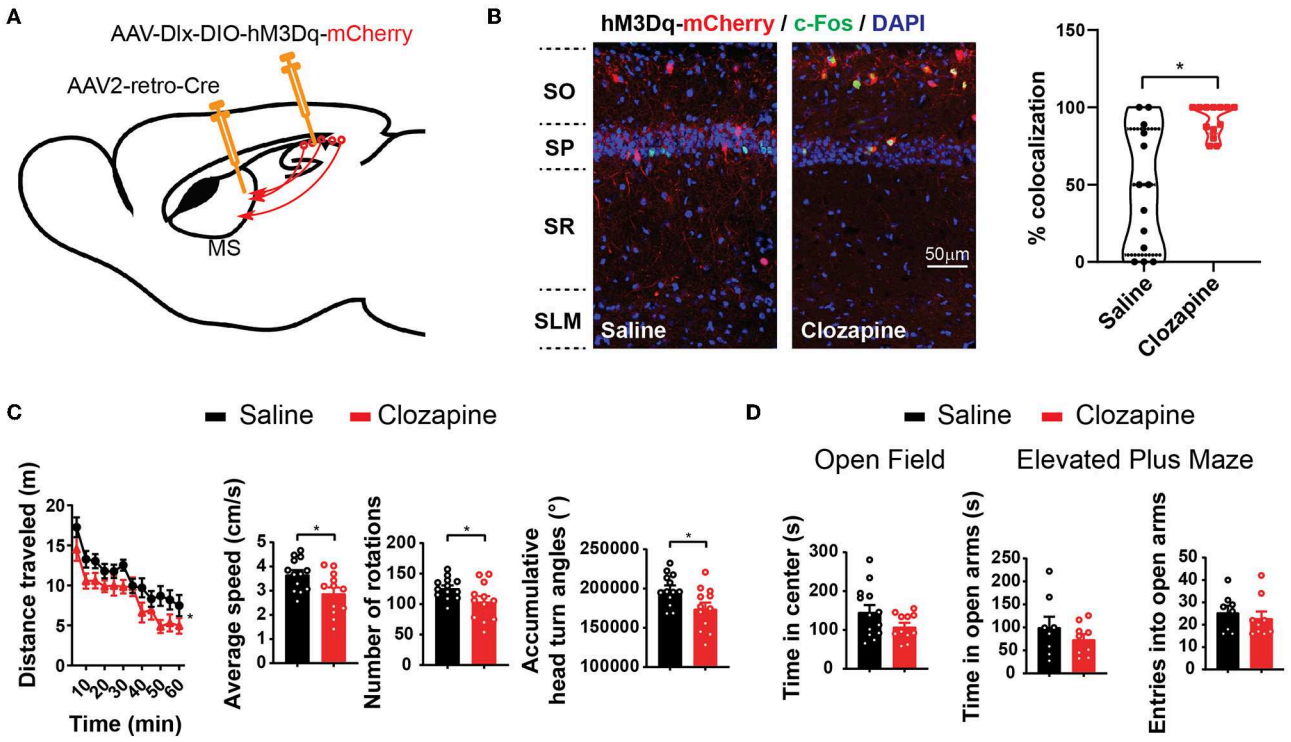

FIGURE 3
Activation of septum-projecting interneurons reduces locomotion. **(A)** Expression of hM3Dq in septum-projecting hippocampal GABAergic interneurons by AAV injections. **(B)** Intraperitoneal injections of clozapine (0.1 mg/kg), a ligand of hM3Dq, increased activity of septum-projecting hippocampal GABAergic interneurons measured by double labeling of c-Fos (green) and mCherry (red) (saline, $n = 13$ sections, total 62 cells from two mice; clozapine, $n = 13$ sections, total 73 cells from two mice) (Mann–Whitney U-test, $^*p < 0.05$). **(C)** Activation of the septum-projecting hippocampal GABAergic interneurons with clozapine decreased mouse locomotion measured by the distance traveled in the open field, number of rotations, and accumulative head turn angles [two-way ANOVA, $F_{(1,23)} = 6.35$, $p < 0.05$; Two-tailed t-test, $^*p < 0.05$]. **(D)** Activation of the septum-projecting hippocampal GABAergic interneurons did not change time spent in the center of the open-field test (two-tailed t-test, $p = 0.1$), time spent in the open arms (two-tailed t-test, $p = 0.31$), and the number of entries into the open arms of the elevated plus maze test (two-tailed t-test, $p = 0.55$) (open field: saline: $n = 13$; clozapine: $n = 11$. Elevated plus maze: saline: $n = 8$; clozapine: $n = 9$).

the distance traveled (Figure 4D), the area of the open field that the animals explored (Figure 4E), immobility time (Figure 4F), and accumulative head turn angles in the open field (Figure 4G). The stimulation also decreased the latency to reach a low speed (Figure 4H). The decreased locomotion was reversible (Figure 4D) and was not accompanied by a change in the anxiety level (Supplementary Figure 2). Consistent with the aforementioned pharmacogenetic findings, these results indicate that the activation of the GABAergic septal projections from the hippocampus decreases animal locomotion and exploratory behavior.

Inhibiting hippocampo-septal inhibitory synaptic projections increases locomotion

Next, to test if the inhibitory hippocampal outputs to the MS could bi-directionally regulate locomotion, we expressed an inhibitory opsin, Jaws (Chuong et al., 2014), in the hippocampal interneurons and delivered light to the MS to silence the GABAergic axons originating from the hippocampus (Figure 5A). This optical inhibition increased mouse locomotor activity measured by the maximum locomotor speed, accumulative head turn angles (Figures 5B, C), and the number of rearing and habituation (Supplementary Figure 3). Nevertheless, the increased locomotion and exploratory behavior were not accompanied by changes in the anxiety level measured by the time spent in the center of the open field or time spent in the open arms of the elevated plus maze (Supplementary Figure 3). Together, the results demonstrate that the activities of the GABAergic septum projection from the hippocampus bi-directionally regulate mouse locomotion and exploratory behavior.

Retrosplenial cortex-projecting hippocampal interneurons does not change locomotion

In addition to the MS, the RSP receives a significant amount of GABAergic inputs from the hippocampus (Klausberger and Somogyi, 2008; Witter, 2010) (Figure 1). Recently, we found that a group of GABAergic interneurons at stratum lacunosum-moleculare (SLM) of the hippocampus, which expresses a marker gene, neuron-derived neurotrophic factor (NDNF), sends long-ranged projection exclusively to the RSP (Figures 6A, B). To

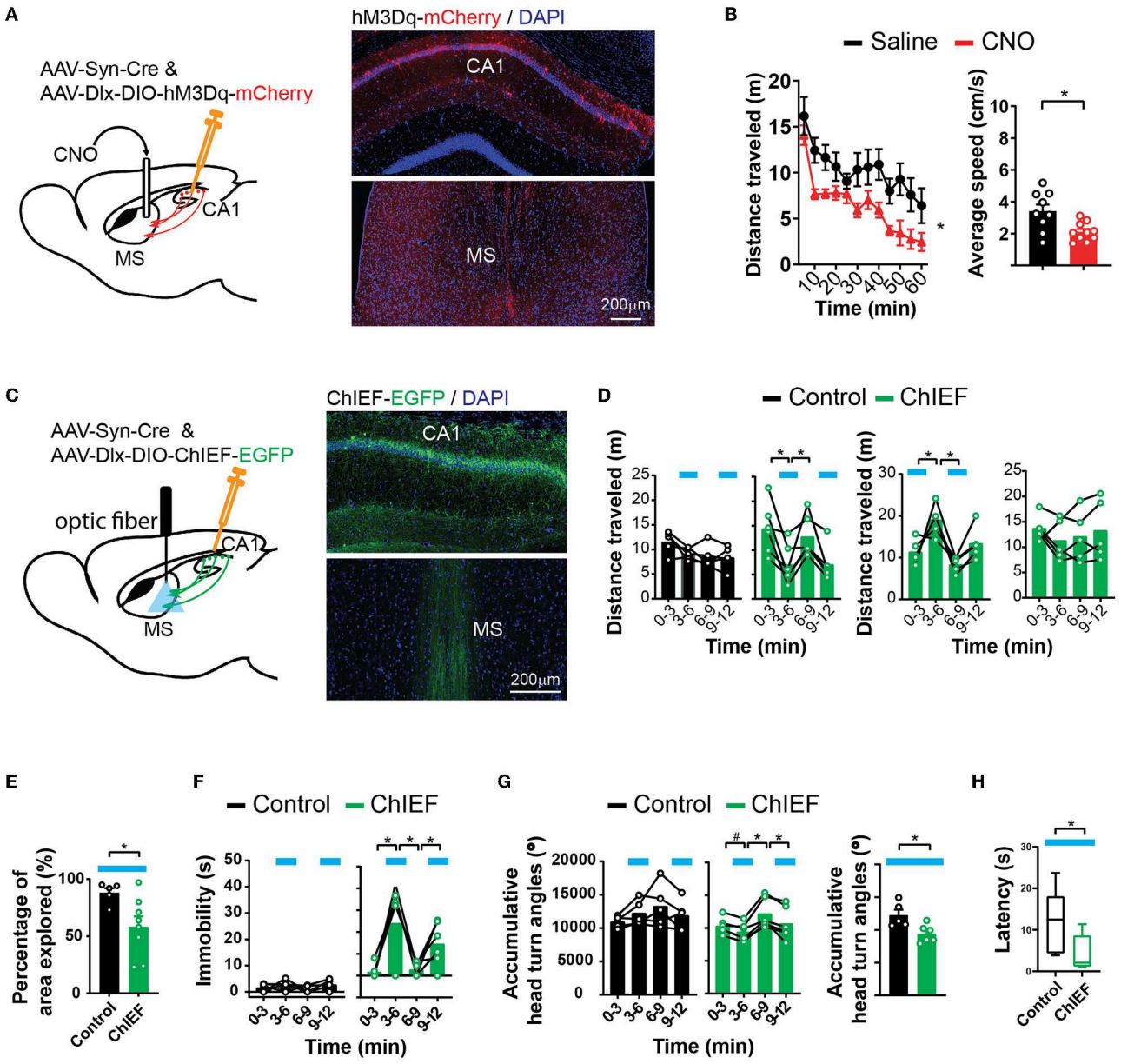

FIGURE 4
Activation of hippocampal inhibitory projections to the MS reduces locomotion. **(A)** Pharmacogenetic activation of the hippocampal inhibitory inputs to the MS with local infusion of CNO in the MS. **(B)** CNO decreased locomotion in the open field as measured by distance traveled [two-way ANOVA, $F_{(1,17)} = 9.00$, $^*p < 0.05$] and average speed (two-tailed *t*-test, $^*p < 0.05$) (saline, $n = 9$ mice; CNO, $n = 10$ mice). **(C)** Optogenetic activation of the hippocampal inhibitory inputs to the MS by light. An excitatory channelrhodopsin, ChIEF, was expressed in the hippocampal GABAergic neurons with AAVs in the "ChIEF" mice. Control mice received AAVs expressing EGFP only. **(D–H)** Light delivered to the MS (indicated by blue bars) decreased mouse locomotion measured by distance traveled **(D)**, percentage of the open-field area the mice explored **(E)**, immobility **(F)**, accumulative angles of head turns **(G)**, and latency to reach a low speed **(H)**. [**(D)** Two-way ANOVA. Left ChIEF group, light, $F_{(1,5)} = 30.42$, $p < 0.05$; Right ChIEF group, light, $F_{(1,4)} = 10.15$, $p < 0.05$; Tukey's multiple comparison test, $^*p < 0.05$. **(E)** Two-tailed *t*-test, $^*p < 0.05$. **(F)** Left two-way ANOVA. Control group, light, $F_{(1,4)} = 5.409$, $p = 0.08$; ChIEF group, light, $F_{(1,5)} = 10.57$, $p < 0.05$; Tukey's multiple comparison test, $^*p < 0.05$. **(G)** Left two-way ANOVA. Control group, Light, $F_{(1,4)} = 0.03$, $p = 0.86$; ChIEF group, light, $F_{(1,5)} = 22.01$, $p < 0.05$; Tukey's multiple comparison test, $^*p < 0.05$; Right two-tailed *t*-test, $^*p < 0.05$. **(H)** Mann–Whitney *U*-test, $^*p < 0.05$.] (Control, $n = 5$ mice; ChIEF, $n = 6$ mice).

determine if the RSP-projecting hippocampal interneurons also regulate locomotion, we expressed hM3Dq selectively in these NDNF-expressing interneurons by injecting the Cre-dependent AAV into the hippocampus of the NDNF-Cre mouse line. Although pharmacogenetic stimulation of these NDNF-cells by an i.p. injection of clozapine significantly changed learning and memory behaviors (Guo et al., 2021), this treatment did not alter mouse locomotion (Figure 6C). It is possible that not enough interneurons were activated in this experiment to significantly alter locomotion. Nevertheless, these results demonstrate the functional heterogeneity of the hippocampal interneurons in the regulation of locomotion and that hippocampal interneurons' impact on

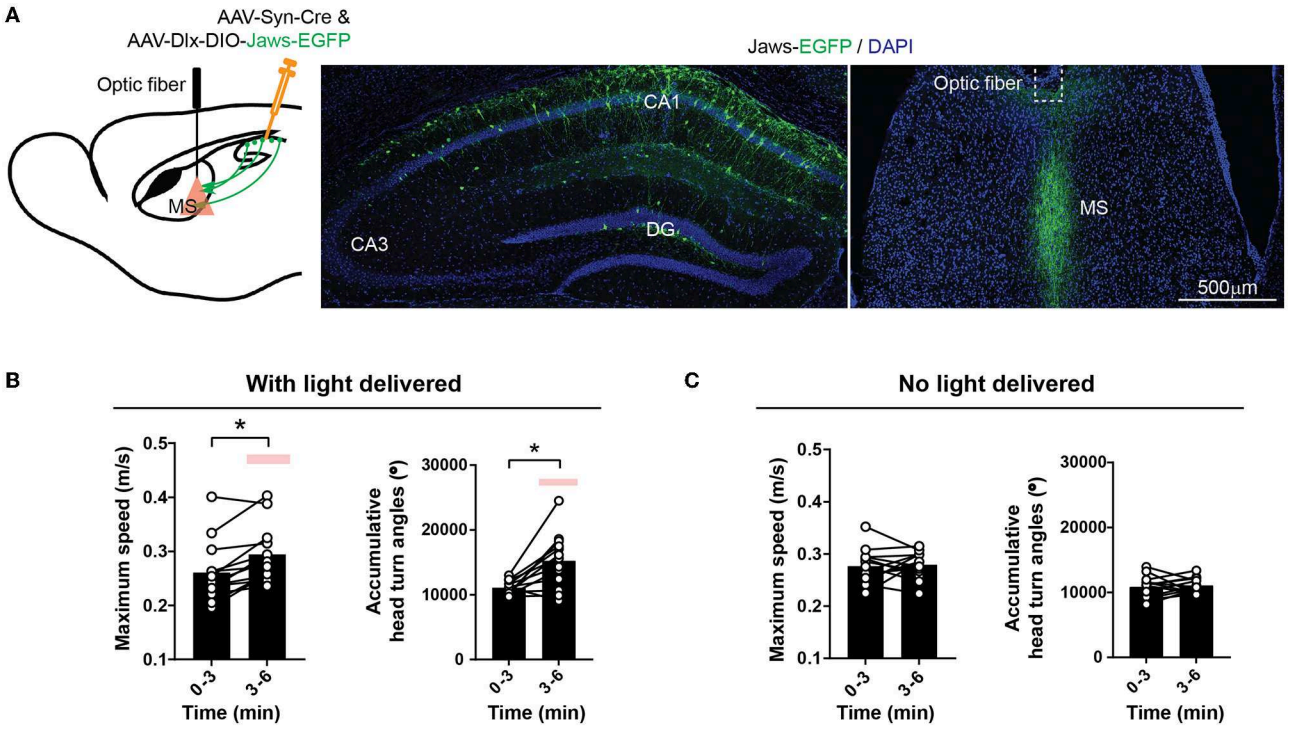

FIGURE 5
Inhibiting inhibitory hippocampal output to the MS increases locomotion. **(A)** Optogenetic inhibition of the hippocampal inhibitory inputs to the MS by light delivered into the MS. An inhibitory opsin, Jaws, was expressed in the hippocampal GABAergic neurons with AAVs. **(B)** Red light delivered to the MS increased mouse locomotion measured by maximum speed and accumulative head turn angles in the open field. (Two-tailed paired *t*-test, $*p < 0.05$) (Dlx-Jaws, $n = 13$ mice). The red bars indicate the delivery of optostimulation. **(C)** No change in maximum speed (left) or accumulative head turn angles (right) occurred when the optical stimulation was not delivered (Left: Two-tailed paired *t*-test, $p = 0.77$; Right: Two-tailed paired *t*-test, $p = 0.71$) (Dlx-Jaws, $n = 13$ mice).

locomotion can be separated from their regulation of other behaviors to a certain degree.

Discussion

In brain systems, the hippocampus lies at the top of the hierarchy of sensory information processing (Squire et al., 2004). The associative cortices feed multi-modal sensory information to the hippocampus to construct an integrated representation and record of the world that includes the "where, when, and what" information about our experiences (Eichenbaum, 2004). The information about an animal's own locations and actions is essential for constructing and updating this neuronal representation (Gois and Tort, 2018). It is therefore not surprising that hippocampal neuronal activities closely correlate with locomotion. However, it was not clear if and how the hippocampus directly regulates locomotion by interacting with brain motor systems and what the functional importance of this regulation may be.

Knowing how the hippocampus directly regulates locomotion will help us to understand not only the neuronal control of locomotion but also the pathogenesis and treatment of neuropsychiatric disorders involving functional abnormalities in the hippocampal circuits. One prominent example is schizophrenia. Schizophrenia patients consistently show anatomical, biochemical, and functional alterations in the hippocampus (Tamminga et al., 2010). In addition to cognitive symptoms, the patients frequently show motor symptoms of either dyskinesia or parkinsonism (Walther and Strik, 2012) and deficits in sensory-motor gating (Braff and Geyer, 1990; Mena et al., 2016). In animal models of schizophrenia, including both pharmacological and genetic models, hyperlocomotion is the most common behavioral phenotype and is commonly considered as a correlate of the positive symptoms (van den Buuse, 2010). The reduction of hyperlocomotion is frequently used as a behavioral readout for screening antipsychotic medicines (Powell and Miyakawa, 2006; Peleg-Raibstein et al., 2008; van den Buuse, 2010; Wolff et al., 2018). Determining the hippocampal mechanisms in locomotion regulation will elucidate the origin of the locomotor symptoms in patients and help us to determine the predictive value of the locomotor parameters in animal models for therapeutic treatments of patients.

In this study, we identified the inhibitory hipocampo-septal projection as a key pathway for locomotion regulation. The pharmacogenetic and optogenetic techniques allowed us to isolate this pathway for precise and reversible functional manipulations. The results indicate that the GABAergic hippocampo-septal projection bi-directionally and reversibly regulates locomotor activities. This reveals a new function of the extrahippocampal projection of the hippocampal interneurons and builds a

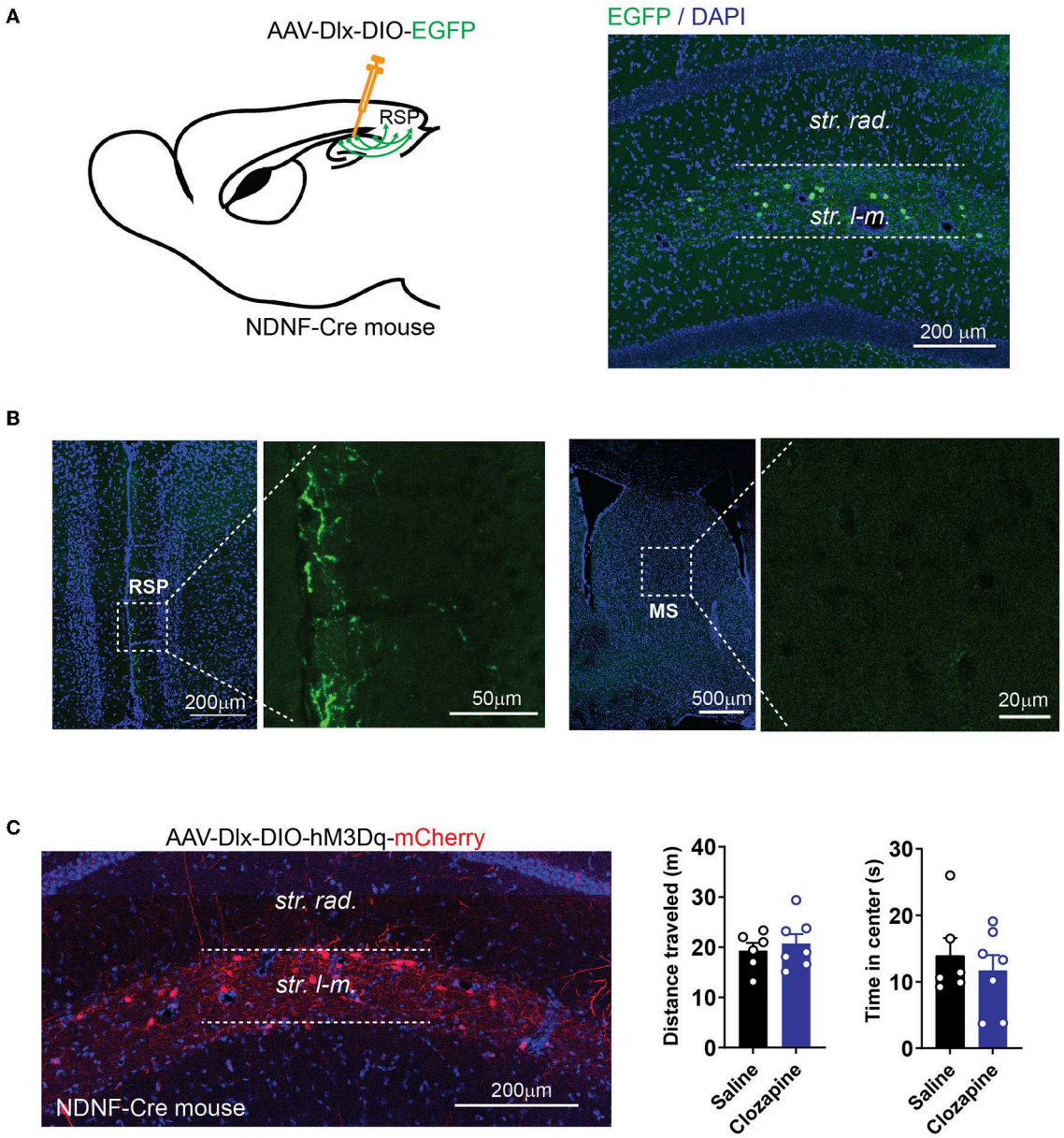

FIGURE 6
Activation of cortex-projecting hippocampal interneurons does not change locomotor activity. **(A)** Expression of EGFP in NDNF-positive interneurons in NDNF-Cre mice by injecting AAV-Dlx-DIO-EGFP into the hippocampus. **(B)** NDNF-positive interneurons in the hippocampus project to the RSP but not MS. **(C)** Expression of hM3Dq in NDNF-positive interneurons in the hippocampus (left). Pharmacogenetic activation of NDNF-positive interneurons with clozapine did not alter the distance traveled or time spent in the center of the open field (distance traveled: two-tailed *t*-test, $p = 0.58$; time in the center: two-tailed *t*-test, $p = 0.53$; data are represented as mean ± SEM; $n = 6$ mice for the saline group; $n = 7$ mice for the clozapine group).

foundation for further elucidation of hippocampal regulation of motor activities. The MS is innervated by and projects to multiple brain regions. It is engaged in learning, memory, emotional reaction, defensive behaviors, and sensorimotor gating (Tsanov, 2017, 2018; Jin et al., 2019). However, anatomically and functionally, it is most closely coupled with the hippocampus (Muller and Remy, 2018; Iyer and Tole, 2020). The hippocampo-septal loop is particularly critical for generating hippocampal oscillations arising from locomotion and active exploration in the environment (O'keefe and Nadel, 1978; Buzsaki, 2002; Drieu and Zugaro, 2019). MS also plays a pacemaker role in hippocampal theta oscillation (Buzsaki, 2002; Tsanov, 2017). These GABAergic projections to the septum may exert their locomotion regulation effects by altering the functions of the hippocampo-septal loop or acting on the motor structures downstream of the septum.

MS contains GABAergic, cholinergic, and glutamatergic neurons (Huh et al., 2010; Takeuchi et al., 2021). The cholinergic and glutamatergic neurons are mainly in the lateral zones of the

MS, while GABAergic neurons are predominantly in the midline zone. Our tracing of the GABAergic axons from the hippocampus shows that these axons and their synapses are largely confined to the midline of MS where GABAergic neurons dominate. An earlier study, which characterized the inhibitory projections from the hippocampus to the MS with optogenetics, showed that ∼24% of MS neurons, mainly fast-spiking cells, showed fast IPSCs in response to the optostimulation of hippocampal outputs, while another ∼19% of MS cells, such as cholinergic cells, showed synaptic responses to the optical stimulation (Mattis et al., 2014). In the current study, a higher percentage (nine out of 11 recorded cells) of neurons reacted to the optogenetic stimulation of the hippocampal projection with fast IPSCs. This discrepancy may be explained by the differences in the two experimental conditions. In the earlier study, AAV with the somatostatin (SST) promoter was used to express opsins in the rat hippocampus; we used the Dlx enhancer/promoter, which may allow us to express opsins in broader GABAergic neuronal types in the hippocampus. In addition, we conducted the recordings in the neurons close to the axonal bundles at the midline, where neurons responsive to hippocampal projections are enriched. Considering that GABAergic neurons are the predominant cell type in the MS (especially in the midline region) and that >80% of cells we recorded responded to the optical stimulation of the hippocampal projections, we can speculate that the majority of the neurons in the MS innervated by the hippocampal GABAergic neurons are also GABAergic. It is known that the GABAergic neurons in the MS project to the hippocampus and form synapses on the GABAergic interneurons there (Freund and Antal, 1988). The GABAergic neurons in the MS and those in the hippocampus may therefore form a bi-neuronal dis-inhibitory loop. This loop may serve as a positive-feedback mechanism for the GABAergic neurons in the MS to enhance their own activities. The activity of the GABAergic septum-to-hippocampus projection correlates with locomotion (Kaifosh et al., 2013). Consistent with this finding, we saw a decrease in locomotion with the activation of the hippocampus-to-septum GABAergic projections and vice versa. We can speculate that in a behaving animal, the excitatory inputs into the hippocampus may generate an oscillatory activation of the GABAergic interneuron in the hippocampus, which in turn acts on the MS GABAergic neurons to promote or reduce locomotion and exploratory behaviors.

Multiple types of GABAergic neurons exist in the MS, including those expressing calbindin (CaBP), calretinin (CR), or parvalbumin (PV). The PV neurons are more concentrated in the midline and are the projection neurons. These PV neurons are most likely the postsynaptic neurons to the hippocampal GABAergic projections due to their location. The CaBP and CR neurons are local interneurons interacting with the cholinergic and glutamatergic neurons in the MS (Ang et al., 2017). The PV neurons and cholinergic send broad efferent projections to innervate brain regions including the hippocampus, cortex, thalamus, hypothalamus, and brain stem structures. Many of these brain regions, such as the motor cortex, the lateral habenula in the thalamus, and the lateral hypothalamus, have been shown to interact with the septum in regulating locomotion (Bender et al., 2015; Zhang et al., 2018). Therefore, determining the cell types in the MS receiving hippocampal inhibitory innervation and their synaptic projections to other locomotion-related brain regions will be essential for us to draw a complete picture of how the hippocampo-septum system regulates locomotion and how this regulation is coupled to the cognitive functions of this circuit. Recently, we developed techniques for stepwise polysynaptic tracing and genetic control (Du et al., 2021; Li et al., 2021). These techniques allow us to trace and selectively control the septal neurons innervated by the hippocampal GABAergic outputs and their postsynaptic neurons in other brain regions. With these techniques, we may be able to identify the next stage of the hippocampo-septal pathway in regulating locomotion.

Data availability statement

The original contributions presented in the study are included in the article/Supplementary material, further inquiries can be directed to the corresponding author.

Ethics statement

The animal study was reviewed and approved by UT Southwestern Institutional Animal Care and Use Committee.

Author contributions

Y-TC and WX designed this study. Y-TC, RA, JG, US, YL, and WX conducted the experiments, collected data, and plotted the figures. Y-TC wrote the first draft of this paper. All authors contributed to the writing and approved the submitted version.

Funding

This study was supported by a grant from NIH/NINDS (NS104828 to WX).

Acknowledgments

We would like to thank Elizabeth Li and Wenqin Du for helping with AAV construction and preparation and Dr. Brad Pfeiffer, Dr. Julian Meeks, and Dr. Carol Tamminga for their valuable comments and suggestions.

Conflict of interest

The authors declare that the research was conducted in the absence of any commercial or financial relationships that could be construed as a potential conflict of interest.

Publisher's note

All claims expressed in this article are solely those of the authors and do not necessarily represent those of

their affiliated organizations, or those of the publisher, the editors and the reviewers. Any product that may be evaluated in this article, or claim that may be made by its manufacturer, is not guaranteed or endorsed by the publisher.

Supplementary material

The Supplementary Material for this article can be found online at: https://www.frontiersin.org/articles/10.3389/fnsyn.2023.1042858/full#supplementary-material

References

Ang, S. T., Ariffin, M. Z., and Khanna, S. (2017). The forebrain medial septal region and nociception. *Neurobiol. Learn. Mem.* 138, 238–251. doi: 10.1016/j.nlm.2016.07.017

Bender, F., Gorbati, M., Cadavieco, M. C., Denisova, N., Gao, X., Holman, C., et al. (2015). Theta oscillations regulate the speed of locomotion via a hippocampus to lateral septum pathway. *Nat. Commun.* 6, 8521. doi: 10.1038/ncomms9521

Bian, X. L., Qin, C., Cai, C. Y., Zhou, Y., Tao, Y., Lin, Y. H., et al. (2019). Anterior cingulate cortex to ventral hippocampus circuit mediates contextual fear generalization. *J. Neurosci.* 39, 5728–5739. doi: 10.1523/JNEUROSCI.2739-18.2019

Braff, D. L., and Geyer, M. A. (1990). Sensorimotor gating and schizophrenia. Human and animal model studies. *Arch. Gen. Psychiatry* 47, 181–188. doi: 10.1001/archpsyc.1990.01810140081011

Buzsaki, G. (2002). Theta oscillations in the hippocampus. *Neuron* 33, 325–340. doi: 10.1016/S0896-6273(02)00586-X

Buzsaki, G., and Moser, E. I. (2013). Memory, navigation and theta rhythm in the hippocampal-entorhinal system. *Nat. Neurosci.* 16, 130–138. doi: 10.1038/nn.3304

Chuong, A. S., Miri, M. L., Busskamp, V., Matthews, G. A., Acker, L. C., Sorensen, A. T., et al. (2014). Noninvasive optical inhibition with a red-shifted microbial rhodopsin. *Nat. Neurosci.* 17, 1123–1129. doi: 10.1038/nn.3752

Degoulet, M., Rouillon, C., Rostain, J. C., David, H. N., and Abraini, J. H. (2008). Modulation by the dorsal, but not the ventral, hippocampus of the expression of behavioural sensitization to amphetamine. *Int. J. Neuropsychopharmacol.* 11, 497–508. doi: 10.1017/S146114570700822X

Dimidschstein, J., Chen, Q., Tremblay, R., Rogers, S. L., Saldi, G. A., Guo, L., et al. (2016). A viral strategy for targeting and manipulating interneurons across vertebrate species. *Nat. Neurosci.* 19, 1743–1749. doi: 10.1038/nn.4430

Douglas, R. J., and Isaacson, R. L. (1964). Hippocampal lesions and activity. *Psychon. Sci.* 1, 187–188. doi: 10.3758/BF03342856

Drieu, C., and Zugaro, M. (2019). Hippocampal sequences during exploration: mechanisms and functions. *Front. Cell. Neurosci.* 13, 232. doi: 10.3389/fncel.2019.00232

Du, W. R., Li, E., Guo, J., Chen, Y.-T., Oh, S. J., Samuel, A., et al. (2021). Hippocampus-striatum wiring diagram revealed by directed stepwise polysynaptic tracing. *bioRxiv*. doi: 10.1101/2021.10.12.464132

Eichenbaum, H. (2004). Hippocampus: cognitive processes and neural representations that underlie declarative memory. *Neuron* 44, 109–120. doi: 10.1016/j.neuron.2004.08.028

Ferreira-Pinto, M. J., Ruder, L., Capelli, P., and Arber, S. (2018). Connecting circuits for supraspinal control of locomotion. *Neuron* 100, 361–374. doi: 10.1016/j.neuron.2018.09.015

Freund, T. F., and Antal, M. (1988). GABA-containing neurons in the septum control inhibitory interneurons in the hippocampus. *Nature* 336, 170–173. doi: 10.1038/336170a0

Geisler, C., Robbe, D., Zugaro, M., Sirota, A., and Buzsaki, G. (2007). Hippocampal place cell assemblies are speed-controlled oscillators. *Proc. Natl. Acad. Sci. U. S. A.* 104, 8149–8154. doi: 10.1073/pnas.0610121104

Godsil, B. P., Stefanacci, L., and Fanselow, M. S. (2005). Bright light suppresses hyperactivity induced by excitotoxic dorsal hippocampus lesions in the rat. *Behav. Neurosci.* 119, 1339–1352. doi: 10.1037/0735-7044.119.5.1339

Gois, Z., and Tort, A. B. L. (2018). Characterizing speed cells in the rat hippocampus. *Cell Rep.* 25, 1872-84.e4. doi: 10.1016/j.celrep.2018.10.054

Gomez, J. L., Bonaventura, J., Lesniak, W., Mathews, W. B., Sysa-Shah, P., Rodriguez, L. A., et al. (2017). Chemogenetics revealed: DREADD occupancy and activation via converted clozapine. *Science* 357, 503–507. doi: 10.1126/science.aan2475

Goshen, I., Brodsky, M., Prakash, R., Wallace, J., Gradinaru, V., Ramakrishnan, C., et al. (2011). Dynamics of retrieval strategies for remote memories. *Cell* 147, 678–689. doi: 10.1016/j.cell.2011.09.033

Gulyas, A. I., Hajos, N., Katona, I., and Freund, T. F. (2003). Interneurons are the local targets of hippocampal inhibitory cells which project to the medial septum. *Eur. J. Neurosci.* 17, 1861–1872. doi: 10.1046/j.1460-9568.2003.02630.x

Guo, J., Oliveros, H. C., Oh, S. J., Liang, B., Li, Y., Kavalali, E. T., et al. (2021). Stratum lacunosum-moleculare interneurons of the hippocampus coordinate memory encoding and retrieval. *bioRxiv*. doi: 10.21203/rs.3.rs-310894/v1

Huh, C. Y., Goutagny, R., and Williams, S. (2010). Glutamatergic neurons of the mouse medial septum and diagonal band of Broca synaptically drive hippocampal pyramidal cells: relevance for hippocampal theta rhythm. *J. Neurosci.* 30, 15951–15961. doi: 10.1523/JNEUROSCI.3663-10.2010

Iwase, M., Kitanishi, T., and Mizuseki, K. (2020). Cell type, sub-region, and layer-specific speed representation in the hippocampal-entorhinal circuit. *Sci. Rep.* 10, 1407. doi: 10.1038/s41598-020-58194-1

Iyer, A., and Tole, S. (2020). Neuronal diversity and reciprocal connectivity between the vertebrate hippocampus and septum. *Wiley Interdiscip. Rev. Dev. Biol.* 9, e370. doi: 10.1002/wdev.370

Jin, J., Cheng, J., Lee, K. W., Amreen, B., McCabe, K. A., Pitcher, C., et al. (2019). Cholinergic neurons of the medial septum are crucial for sensorimotor gating. *J. Neurosci.* 39, 5234–5242. doi: 10.1523/JNEUROSCI.0950-18.2019

Jinno, S., Klausberger, T., Marton, L. F., Dalezios, Y., Roberts, J. D., Fuentealba, P., et al. (2007). Neuronal diversity in GABAergic long-range projections from the hippocampus. *J. Neurosci.* 27, 8790–8804. doi: 10.1523/JNEUROSCI.1847-07.2007

Kaifosh, P., Lovett-Barron, M., Turi, G. F., Reardon, T. R., and Losonczy, A. (2013). Septo-hippocampal GABAergic signaling across multiple modalities in awake mice. *Nat. Neurosci.* 16, 1182–1184. doi: 10.1038/nn.3482

Katsuta, K., Umemura, K., Ueyama, N., and Matsuoka, N. (2003). Pharmacological evidence for a correlation between hippocampal CA1 cell damage and hyperlocomotion following global cerebral ischemia in gerbils. *Eur. J. Pharmacol.* 467, 103–109. doi: 10.1016/S0014-2999(03)01573-5

Klausberger, T., and Somogyi, P. (2008). Neuronal diversity and temporal dynamics: the unity of hippocampal circuit operations. *Science* 321, 53–57. doi: 10.1126/science.1149381

Li, E., Guo, J., Oh, S. J., Luo, Y., Oliveros, H. C., Du, W., et al. (2021). Anterograde transneuronal tracing and genetic control with engineered yellow fever vaccine YFV-17D. *Nat. Methods* 18, 1542–1551. doi: 10.1038/s41592-021-01319-9

Lopez, A. J., Kramar, E., Matheos, D. P., White, A. O., Kwapis, J., Vogel-Ciernia, A., et al. (2016). Promoter-specific effects of DREADD modulation on hippocampal synaptic plasticity and memory formation. *J. Neurosci.* 36, 3588–3599. doi: 10.1523/JNEUROSCI.3682-15.2016

Mattis, J., Brill, J., Evans, S., Lerner, T. N., Davidson, T. J., Hyun, M., et al. (2014). Frequency-dependent, cell type-divergent signaling in the hippocamposeptal projection. *J. Neurosci.* 34, 11769–11780. doi: 10.1523/JNEUROSCI.5188-13.2014

McNaughton, B. L., Barnes, C. A., and O'Keefe, J. (1983). The contributions of position, direction, and velocity to single unit activity in the hippocampus of freely-moving rats. *Exp. Brain Res.* 52, 41–49. doi: 10.1007/BF00237147

Mena, A., Ruiz-Salas, J. C., Puentes, A., Dorado, I., Ruiz-Veguilla, M., and De la Casa, L. G. (2016). Reduced prepulse inhibition as a biomarker of schizophrenia. *Front. Behav. Neurosci.* 10, 202. doi: 10.3389/fnbeh.2016.00202

Muller, C., and Remy, S. (2018). Septo-hippocampal interaction. *Cell Tissue Res.* 373, 565–575. doi: 10.1007/s00441-017-2745-2

O'keefe, J., and Nadel, L. (1978). *The Hippocampus as a COGNITIVE MAP*: Oxford: Clarendon Press.

Peleg-Raibstein, D., Knuesel, I., and Feldon, J. (2008). Amphetamine sensitization in rats as an animal model of schizophrenia. *Behav. Brain Res.* 191, 190–201. doi: 10.1016/j.bbr.2008.03.037

Pelkey, K. A., Chittajallu, R., Craig, M. T., Tricoire, L., Wester, J. C., and McBain, C. J. (2017). Hippocampal GABAergic inhibitory interneurons. *Physiol. Rev.* 97, 1619–1747. doi: 10.1152/physrev.00007.2017

Powell, C. M., and Miyakawa, T. (2006). Schizophrenia-relevant behavioral testing in rodent models: a uniquely human disorder? *Biol. Psychiatry* 59, 1198–1207. doi: 10.1016/j.biopsych.2006.05.008

Roth, B. L. (2016). DREADDs for neuroscientists. *Neuron* 89, 683–694. doi: 10.1016/j.neuron.2016.01.040

Sams-Dodd, F., Lipska, B. K., and Weinberger, D. R. (1997). Neonatal lesions of the rat ventral hippocampus result in hyperlocomotion and deficits in social behaviour in adulthood. *Psychopharmacology* 132, 303–310. doi: 10.1007/s002130050349

Soltesz, I., and Losonczy, A. (2018). CA1 pyramidal cell diversity enabling parallel information processing in the hippocampus. *Nat. Neurosci.* 21, 484–493. doi: 10.1038/s41593-018-0118-0

Squire, L. R., Stark, C. E., and Clark, R. E. (2004). The medial temporal lobe. *Annu. Rev. Neurosci.* 27, 279–306. doi: 10.1146/annurev.neuro.27.070203.144130

Swerdlow, N. R., Halim, N., Hanlon, F. M., Platten, A., and Auerbach, P. P. (2001). Lesion size and amphetamine hyperlocomotion after neonatal ventral hippocampal lesions: more is less. *Brain Res. Bull.* 55, 71–77. doi: 10.1016/S0361-9230(01)00492-0

Takeuchi, Y., Nagy, A. J., Barcsai, L., Li, Q., Ohsawa, M., Mizuseki, K., et al. (2021). The medial septum as a potential target for treating brain disorders associated with oscillopathies. *Front. Neural Circ.* 15, 701080. doi: 10.3389/fncir.2021.701080

Tamminga, C. A., Stan, A. D., and Wagner, A. D. (2010). The hippocampal formation in schizophrenia. *Am. J. Psychiatry* 167, 1178–1193. doi: 10.1176/appi.ajp.2010.09081187

Tervo, D. G., Hwang, B. Y., Viswanathan, S., Gaj, T., Lavzin, M., Ritola, K. D., et al. (2016). A designer AAV variant permits efficient retrograde access to projection neurons. *Neuron* 92, 372–382. doi: 10.1016/j.neuron.2016.09.021

Tsanov, M. (2017). Speed and oscillations: medial septum integration of attention and navigation. *Front. Syst. Neurosci.* 11, 67. doi: 10.3389/fnsys.2017.00067

Tsanov, M. (2018). Differential and complementary roles of medial and lateral septum in the orchestration of limbic oscillations and signal integration. *Eur. J. Neurosci.* 48, 2783–2794. doi: 10.1111/ejn.13746

van den Buuse, M. (2010). Modeling the positive symptoms of schizophrenia in genetically modified mice: pharmacology and methodology aspects. *Schizophr. Bull.* 36, 246–270. doi: 10.1093/schbul/sbp132

Walther, S., and Strik, W. (2012). Motor symptoms and schizophrenia. *Neuropsychobiology* 66, 77–92. doi: 10.1159/000339456

White, I. M., Whitaker, C., and White, W. (2006). Amphetamine-induced hyperlocomotion in rats: hippocampal modulation of the nucleus accumbens. *Hippocampus* 16, 596–603. doi: 10.1002/hipo.20189

Witter, M. P. (2010). "Connectivity of the hippocampus," in *Hippocampal Microcircuits: A Computational Modeler's Resource Book*, eds V. Cutsuridis, B. Graham, S. Cobb, and I. Vida (New York, NY: Springer New York, 5–26.

Wolff, A. R., Bygrave, A. M., Sanderson, D. J., Boyden, E. S., Bannerman, D. M., Kullmann, D. M., et al. (2018). Optogenetic induction of the schizophrenia-related endophenotype of ventral hippocampal hyperactivity causes rodent correlates of positive and cognitive symptoms. *Sci. Rep.* 8, 12871. doi: 10.1038/s41598-018-31163-5

Zhang, G. W., Shen, L., Zhong, W., Xiong, Y., Zhang, L. I., and Tao, H. W. (2018). Transforming sensory cues into aversive emotion via septal-habenular pathway. *Neuron* 99, 1016-28.e5. doi: 10.1016/j.neuron.2018.07.023

Zhang, W. N., Bast, T., and Feldon, J. (2002). Effects of hippocampal N-methyl-D-aspartate infusion on locomotor activity and prepulse inhibition: differences between the dorsal and ventral hippocampus. *Behav. Neurosci.* 116, 72–84. doi: 10.1037/0735-7044.116.1.72

Frontiers in
Synaptic Neuroscience

Synthesizing knowledge on various aspects of synapses

Part of a popular neuroscience journal series which advances our understanding of the synaptic structure, function, plasticity and alterations in disease.

Discover the latest Research Topics

See more →

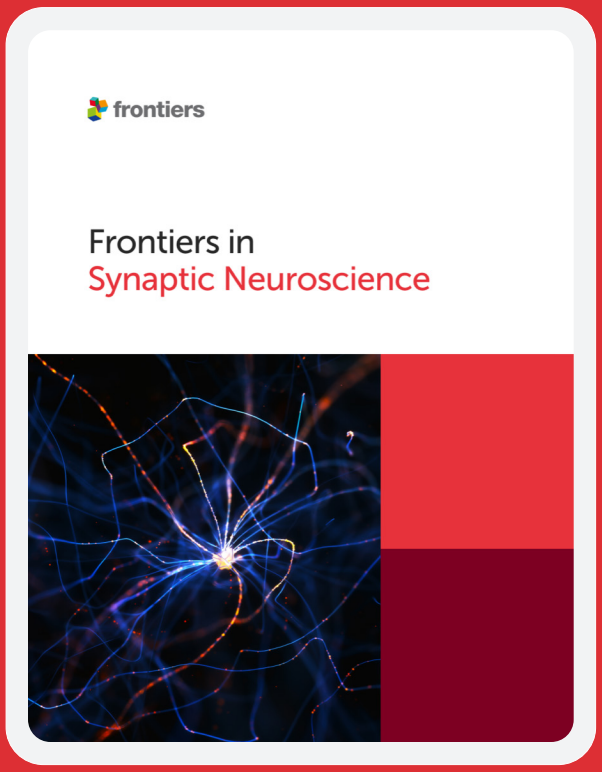

Frontiers

Avenue du Tribunal-Fédéral 34
1005 Lausanne, Switzerland
frontiersin.org

Contact us

+41 (0)21 510 17 00
frontiersin.org/about/contact